ADVANCES IN TREATMENT OF SINONASAL AND SKULL BASE TUMORS

EDITED BY: Xicai Sun, Juan C. Fernandez-Miranda, Lin Kong and Varun R. Kshettry

PUBLISHED IN: Frontiers in Oncology

frontiers Research Topics

ISSN 1664-8714
ISBN 978-2-88974-993-5
DOI 10.3389/978-2-88974-993-5

About Frontiers

Frontiers is more than just an open-access publisher of scholarly articles: it is a pioneering approach to the world of academia, radically improving the way scholarly research is managed. The grand vision of Frontiers is a world where all people have an equal opportunity to seek, share and generate knowledge. Frontiers provides immediate and permanent online open access to all its publications, but this alone is not enough to realize our grand goals.

Frontiers Journal Series

The Frontiers Journal Series is a multi-tier and interdisciplinary set of open-access, online journals, promising a paradigm shift from the current review, selection and dissemination processes in academic publishing. All Frontiers journals are driven by researchers for researchers; therefore, they constitute a service to the scholarly community. At the same time, the Frontiers Journal Series operates on a revolutionary invention, the tiered publishing system, initially addressing specific communities of scholars, and gradually climbing up to broader public understanding, thus serving the interests of the lay society, too.

Dedication to Quality

Each Frontiers article is a landmark of the highest quality, thanks to genuinely collaborative interactions between authors and review editors, who include some of the world's best academicians. Research must be certified by peers before entering a stream of knowledge that may eventually reach the public - and shape society; therefore, Frontiers only applies the most rigorous and unbiased reviews.
Frontiers revolutionizes research publishing by freely delivering the most outstanding research, evaluated with no bias from both the academic and social point of view. By applying the most advanced information technologies, Frontiers is catapulting scholarly publishing into a new generation.

What are Frontiers Research Topics?

Frontiers Research Topics are very popular trademarks of the Frontiers Journals Series: they are collections of at least ten articles, all centered on a particular subject. With their unique mix of varied contributions from Original Research to Review Articles, Frontiers Research Topics unify the most influential researchers, the latest key findings and historical advances in a hot research area! Find out more on how to host your own Frontiers Research Topic or contribute to one as an author by contacting the Frontiers Editorial Office: frontiersin.org/about/contact

ADVANCES IN TREATMENT OF SINONASAL AND SKULL BASE TUMORS

Topic Editors:
Xicai Sun, Fudan University, China
Juan C. Fernandez-Miranda, Stanford University Medical Center, United States
Lin Kong, Fudan University, China
Varun R. Kshettry, Cleveland Clinic, United States

Citation: Sun, X., Fernandez-Miranda, J. C., Kong, L., Kshettry, V. R., eds. (2022). Advances in Treatment of Sinonasal and Skull Base Tumors. Lausanne: Frontiers Media SA. doi: 10.3389/978-2-88974-993-5

Table of Contents

frontiers in Oncology

SYSTEMATIC REVIEW
published: 29 April 2021
doi: 10.3389/fonc.2021.649958

A Potential Concomitant Sellar Embryonic Remnant-Associated Collision Tumor: Systematic Review

Mingdong Wang[1], Qianhui Fu[2], Mingjing Song[3], Zongmao Zhao[4], Renzhi Wang[5], John Zhang[6], Wenbin Ma[5] and Zhanxiang Wang[1]**

[1] Department of Neurosurgery, The First Affiliated Hospital of Xiamen University, School of Medicine, Xiamen University, Xiamen, China, [2] School of Pharmacy, Minzu University of China, Beijing, China, [3] Institute of Laboratory Animal Science, Chinese Academy of Medical Science and Comparative Medical Center, Peking Union Medical College, Beijing, China, [4] Department of Neurosurgery, The Second Hospital of Hebei Medical University, Hebei, China, [5] Department of Neurosurgery, Peking Union Medical College Hospital, Beijing, China, [6] Physiology Program, Department of Anesthesiology, Neurosurgery, Neurology, and Physiology, Center for Neuroscience Research, Loma Linda, CA, United States

OPEN ACCESS

Edited by:
Xicai Sun, Fudan University, China

Reviewed by:
Marco Artico, Sapienza University of Rome, Italy
Hamid Borghei-Razavi, Cleveland Clinic Florida, United States

****Correspondence:***
Wenbin Ma
mwb2020@hotmail.com
Zhanxiang Wang
xmdxsjwk@163.com

Specialty section:
This article was submitted to Surgical Oncology, a section of the journal Frontiers in Oncology

Received: *06 January 2021*
Accepted: *25 March 2021*
Published: *29 April 2021*

Citation:
Wang M, Fu Q, Song M, Zhao Z, Wang R, Zhang J, Ma W and Wang Z (2021) A Potential Concomitant Sellar Embryonic Remnant-Associated Collision Tumor: Systematic Review. Front. Oncol. 11:649958. doi: 10.3389/fonc.2021.649958

Background: Diagnosing the well-known concomitant Rathke's cleft cyst (RCC) and differentiating it from other sellar lesions are difficult because RCC is and other sellar lesions are closely related and represent a continuum from simple RCCs to more complex lesions. The purpose of this study is to better understand the adeno- and neurohypophysis adjacent to the par intermedia remnants and their role in the origin of the coexistence of these two distinct tumor neoplasias; to assess the incidence in different age groups; to categorize the pathohistological subtype, which can be incorporated in predictive/prognostic models; and finally, to evaluate the current evidence on collision tumors of the sellar embryonic remnant tract in terms of their biological behavior and pathology.

Methods: Utilizing the PubMed database, data were collected from 1920 to 2019. Information about demographics, clinical characteristics, and age was summarized and analyzed by using univariable and multivariable models. The same cell type was observed regardless of whether the tumor was only one type or mixed types, and their histologic patterns were assessed.

Results: The incidence rates were similar among patients stratified into three age subgroups: 40–49 years (24.57%), 50–59 years (19.54%), and older than 60 years (22.98%). We found that various types of sellar lesions, namely, squamous metaplasia (SM) + goblet cells (GC) (HR 46.326), foamy macrophages (FM) (HR 39.625), epithelial cells and multinucleated giant cells or cholesterin (EM) (HR 13.195), a cavernous portion of the right internal carotid artery (CP-ICA) (HR 9.427), epithelial cells with ciliated cuboidal (EC-CC) (HR 8.456), were independently associated with RCC pathological status. These divergent AUCs (0.848 for Hypo as RCC, 0.981 for RCC co PA, 0.926 for CD and CP co RCC) and subtypes of PA (HR 4.415, HR 2.286), Hypo (HR 3.310), CD and CP (HR 2.467), EC and DC and PG and SGR (HR 1.068), coexisting with the risk of a comorbid RCC lesion, may reflect the etiologic heterogeneity of coderivation and the different effects of some risk factors on tumor subtypes. Our analyses suggested that the greatest accuracy was observed for the pituitary adenoma subtype, with an AUC of 0.981 (95% confidence interval [CI]: 0.959–1.005), while the poorest accuracy was observed for aneurysms, with an AUC of 0.531 (95% CI: 0.104–0.958). We separately analyzed and confirmed the above results. Sensitivity analysis revealed no evidence of systematic bias due to missing data.

Conclusion: This study showed that the histopathological changes in patients with sellar embryonic remnant-associated collision tumors showed highly consistent epithelial cell replacement (renewal) (ciliated columnar epithelium to ciliated squamous epithelium to squamous epithelium) or accumulation, and the RCC cyst wall was similar in structure to the tracheobronchial airway epithelium, with progenitor cell characteristics. The collision accuracy between RCC and other tumors (PAs, craniopharyngioma, chordoma, etc.) is different; these characteristics constitute the theoretical basis for the postmigration development of the pharyngeal bursa.

Keywords: collision sellar lesions, Rathke cleft cyst, solid sellar lesion, sellar embryonic-remnants lesions, cystic sellar lesions

BACKGROUND

The anterior limb of Rathke's pouch contributes to the anterior lobe and forms the posterior lobe of the hypophysis, which is derived from two components: neuroectodermal evagination and oral ectoderm invagination (1, 2). Embryonic remnants of the diverticulum of Rathke's pouch at the junction between the anterior and posterior lobes (in the area representing the vestigial intermediate lobe) normally regresses and is less distinct in humans but almost always contains small cysts, namely, Rathke's cleft cysts (RCCs), and the cells lining the cleft are thought to be the origin of various cystic lesions. These cysts are lined with one or multiple layers of epithelial cells; some cysts are lined with cuboidal or columnar ciliated cells, while others are lined with flattened cells (3–5). Consequently, this category of tumor displays considerable variation in cytology, encompassing a range of primitive homologous cells in the midline ectoderm. However, the nature of sellar embryonic remnant-associated collision tumors (S-ErACTs) is not well understood.

A diversity of S-ErACT occurs in humans, including RCC, chordomas (CD), craniopharyngiomas (CPs), dermoid cyst (DC), epidermoid cyst (EC), salivary gland remnants (SGR), and atypical teratoid rhabdoid tumor (AT/RT), which can occur individually or concomitantly. One of the hallmarks of S-ErACT is its sellar neuroendocrine clinical and biological heterogeneity. Previous work has suggested that another variant of RCC elements is nested within a typical papillary or adamantinomatous lesion (6). This is consistent with the basic definition of collision tumors (CTs), which are composed of two neighboring independent neoplasms that coexist with little or no interaction between them (7). It is unclear whether these concomitant tumors arise from remnants of Rathke's pouch, embryonic remnant cells that exhibit metaplasia in the sellar region, or a possible common origin or other association, such as the induction of stratified squamous epithelial progenitor cells. Most RCCs are within the sellar region between the anterior and posterior lobes, but some extend to the optic chiasm. Strikingly, the dysembryogenetic conditions of the sellar and suprasellar regions are probably underrecognized (8). This persisting embryonal infundibular recess (PEIR) can be misdiagnosed as a sellar lesion; however, it is relatively rare.

The origin of RCCs is unclear, and no systematic genetic and pathology research has been conducted in humans. Rathke's pouch remnants, an ectodermal diverticulum arising from the foregut, may give rise to Rathke's cysts. To date, it is still unclear whether these cysts are incidental. However, a high rate of cystic lesions has been noted in autopsy cases (13–33%) (4, 9). Cysts are hypothesized to arise from oral ectoderm cells of the pharyngeal duct that fail to degenerate. This idea is supported by the ability of the oral epithelium or pharyngeal bursa to grow (4, 10). RCC was observed in 1.2% of patients between the ages of 1 and 4 years (11). These patients are different when compared with

Abbreviations: Acro, acromegaly; AComA, anterior communicating artery; AUC, areas under curves; AT/RT, atypical teratoid rhabdoid tumor; CA-ccc, ciliated columnar cell or monolayer of cuboidal; CP-ICA, cavernous portion of the right internal carotid artery; CD, chordoma; CP, craniopharyngioma; CT, computerized tomography; CTA, computerized tomographic angiography; CI, confidence interval; CTs, collision tumors; DC, dermoid cyst; DI, diabetes insipidus; DSA, digital subtraction angiography; EC, epidermoid cyst; EC-CC, epithelial cells with ciliated cuboidal; EM, epithelial cells and multinucleated giant cells or cholesterin; FM, foamy macrophages; KM, Kaplan-Meier; Hypo, hypophysitis, HR, hazard ratio; IR, incidence rates; GA, gonadotroph adenomas; GC, goblet cells; MRI, magnetic resonance imaging; MRA, magnetic resonance angiography; NFPA, non-functioning pituitary adenomas; OS, overall survival; PA, pituitary adenomas; PEIR, persisting embryonal infundibular recess; PIA, plurihormonal and double adenomas; PitNET, pituitary neuroendocrine tumor; PG, pituitary granulomatosis; ROC, receiver operating characteristic; RCTs, randomized controlled trials; RCCs, Rathke's cleft cysts; RFS, relapse free survival; SA, somatotroph adenoma; S-ErCT, sellar embryonic-remnants associated collision tumors; SGR, salivary gland remnants; SM, squamous metaplasia; SSEC, stratified squamous epithelium cell; TSS, trans-sphenoidal surgery; TCT, transitional cell tumor.

children of the same age or adult. RCC patients display a slow-growing in adulthood (12). The incidence of concomitant occurrence is unclear, but estimates range from 0.51 to 3.55% of intrasellar lesions (13). Some RCC patients have prolactinoma, Cushing's disease, Pluri-hormonal and double adenoma (PIA), non-functioning pituitary adenoma (NFPA), or transitional cell tumor (TCT) of the pituitary or pituitary oncocytoma (14).

We propose that pharyngeal bursa migration and stratified squamous epithelial progenitor cells can be caused by the continued growth of the nasopharynx, a pharyngeal bursa appearing at the anchoring point of the notochord and overlying endoderm, and stromal cell-derived induction activity in residual embryonic tissue that could induce subsequent development of the remnant diverticulum of Rathke's pouch. Although RCC and pituitary neuroendocrine tumors (PitNETs) or other benign sellar lesions rarely occur together, the origin and histopathology remain controversial in the literature. However, many factors affect the pathogenic process of concomitant disease due to the risk of recurrence. These embryological changes prompted us to examine the histopathological and clinical presentation of pituitary function to determine whether coderivation (the identification of continually changing pathological tissues with potential stem cell characteristics) was concomitantly associated (continuum) with both diseases in the sellar region.

This study aimed to clarify the correlation between the stratified squamous epithelium cells of RCC and the characteristics of pluripotent stem cells (stratified squamous epithelial progenitor cells) and coexisting sellar lesions with a focus on the relationship between the main factors affecting the development and growth of residual embryo tissue and pathological changes.

METHODS

We performed a literature search of the MEDLINE databases, Wiley online library, Science Direct, and Web of Science from March 1, 1920, through April 1, 2019. Searches of PubMed over the past 99 years were conducted using terms related to RCC. We included case series (case reports) on patient characteristics, interventions and comparisons, and randomized controlled trials (RCTs) in English or Chinese. All authors reviewed the abstracts to assess eligibility. The included studies fulfilled the following requirement: All studies reporting RCC were included. The systematic review followed preferred reporting items for systematic reviews and meta-analyses (PRISMA) guidelines (see **Supplementary Appendix-1** pp 1).

Patient and Study Eligibility

We included patients and studies that met the following inclusion criteria (**Supplementary Appendix-1**: The diagnosis standard of pituitary adenoma): 1) We included observational and treatment (surgery plus radiotherapy) studies on coexisting RCC and sellar region lesions that contain data about the population-based prevalence of symptomatic RCC coexisting with the sellar lesion (the cooccurrence of the two diseases is the basic feature). 2) We included patients with a diagnosis of RCC coexisting with sellar lesion based on suggestions from qualified neurosurgeons and radiologists, confirmatory imaging evidence from CT, MRI, DSA, CTA, and MRA, observations during operation, and histological examinations. 3) Cross-checking of references was performed until no new articles were identified. Available full-text articles written in English or Chinese. The study had to be retrospective by definition. 4) For an explanation of cases without modern imaging in the 1920s and 1970s and the primary basis of pathological diagnosis, see the appendix (pp 4). For the classification of tumors of the pituitary gland, see the **Supplementary Information** (pp 7,8).

We excluded studies based on the following: 1) abstracts from conferences, full texts without raw data, duplicate publications, letters, or reviews (no case reports); or 2) RCC coexisting with sellar lesions that was diagnosed based on objective imaging, observations in operation, histological examinations, and medical records but only by imaging examination (lack of laboratory or endocrinology examination or self-reported cases).

Data Analysis (Data Extraction, Quality Assessment)

Two investigators independently extracted relevant data using a standardized from: publication year, origin of study (first author), type of study (study design, prospective, retrospective, single-center, multi-center), size of study population, mean age, rang of patients, hormone level, clinical imaging, pituitary function, Clinical diagnosis, surgical treatment, histopathological subtypes, following-up time, survival and died. Two authors cross-checked the results. Based on these data included 67 articles, 7-by-8 tables were constructed from each study based on raw data. Each study was rated with regard to the following domains: patient selection, pituitary function, hormone level, therapeutic method, following-up, reference standard, timing, the risk of bias, and the results were discussed by all authors.

Risk of Bias Assessment

The Cochrane risk of bias tool was used to assess the construct validity for preclinical studies, the clinical generalizability of the experimental conditions, and the seven domains involved.

Statistical Analysis

We first used R version 3.4 (statistic package studio) to implement the random forest algorithm and obtain the important categorical variable score (see the **Appendix—**67meta-analyses were identified, pp 10). The association between unitary factors and clinical surgery was regarded as the outcome. Next, we performed several *post hoc* sensitivity analyses. A Cox proportional hazards model and Bayesian analysis for multivariable analysis were applied to the variables. The Kaplan-Meier (KM) method for overall survival (OS) and relapse-free survival (RFS) analysis was performed for six subgroups of patients.

The receiver operating characteristic (ROC) curve was used to evaluate the performance of the constructed models. ROC comparison analysis was performed to assess significant differences in AUCs by using the method developed by DeLong et al. (15).

RESULT

Patient Demographics

Sixty-seven studies met our pre-established inclusion criteria (for our case, see supplementary, pp 10) (**Supplementary Data-Figure S1**). Patient demographic, clinical and histopathological data are shown in **Tables 1**, **2**, **3**, and **4**. Among the 118 studied patients (including our own patients), 43 (36.44%) were male, and 75 (63.55%) were female. The age characteristics of patients with RCC concomitant with various sellar lesions are summarized in **Table 1**. The rates of various sellar lesions were (male, female) (36.78%, 63.21%), (31.25%, 68.75%), (50%, 50%), and (20%, 80%).

Clinical Presentation and Risk Parameters

The clinical and biologic characteristics at diagnosis of the 118 patients in the analytic cohort with an assigned primary lesion site are listed in **Table 4**. Among them, 45.76% had hormone hypersecretion, 5.93% had hypo-TSH/FSH/LH, 15.25% had diabetes insipidus hypopituitarism/panhypopituitarism, 22.88% had diabetes insipidus (DI) or hypopituitarism postoperatively, and 1.69% had new-onset disease after tumor resection.

A total of 102 (86.44%) of the 118 patients in the six subgroups underwent transsphenoidal surgery (TSS): 11.86% underwent craniotomy, 1.69% received replacement therapy, and 1.69% received conservative therapy. A total of 2.98% of the patients experienced recurrence, 46.61% completed a clearly

TABLE 1 | The age characteristic of RCC concomitance sellar lesion.

Parameter (No. Cases)	RCC co PA Subtypes—other and Acromegaly N = 87	RCC as Hypophysitis N = 16	RCC co Aneurysm N = 4	RCC co Chordoma and Cran and other lesion N = 11	Total: N = 118
Gender (%)					
Male	32 (36.78%)	5 (31.25%)	2 (50%)	4 (20%)	43 (36.44%)
Female	55 (63.21%)	11 (68.75%)	2 (50%)	7 (80%)	75 (63.55%)
Age (%)					
0–11y	1 (1.14%)	1 (6.25%)	0	1 (9%)	3 (2.54%)
12–19y	2 (2.29%)	2 (12.5%)	0	3 (27.27%)	7 (5.93%)
20–29y	16 (18.39%)	3 (18.75%)	0	–	19 (16.10%)
30–39y	21 (24.13%)	2 (12.5%)	0	–	23 (19.49%)
40–49y	20 (22.98%)	4 (25%)	1(25%)	4 (36.36%)	29 (24.57%)
50–59y	14 (16.09%)	2 (12.5%)	0	1 (9%)	17 (19.54%)
≥60y	13 (14.94%)	2 (12.5%)	3(75%)	2 (18.18%)	20 (22.98%)
F*	7.606	12.714	5.581	2.245	
P Value*	0	–	0	0.044	

RCC, Rathke's cleft cysts; PA, pituitary adenoma; co, co-existent; as, associated with. Other: include Lactotroph adenoma, Plurihormonal adenoma, non-functioning pituitary adenoma, adrenocorticotropin adenoma, Thyrotroph adenoma. Other lesion: include Epidermoid Cyst, Dermoid Cyst, pituitary granulomatosis, Salivary, Salivary gland remnants. F P*: P value from post-hoc test for categorical variables. Hypop, Hypophysitis; Chor, Chordoma; Acro, Acromegaly; Cran, Craniopharyngioma.*

TABLE 2 | RCC coexistent pituitary adenoma subtype and histopathological features and immunohistochemistry.

Adenoma type (No. Cases)	Morphological (%)	Immunohistochemistry (IHC) (%)	HR (95% CI) *P**	*P**
Total PA co RCC n=87				
LA+ CA-CCC	29 (33.33%)	31 (47.69%)	2.118 (1.311–3.422)	0.002
TA+ CA-CCC	1 (1.14%)	4 (6.15%)	1.763 (0.243–12.805)	0.575
PIA+ CA-CCC/SSEC	6 (6.89%)	7 (10.76%)	1.524 (0.651–3.564)	0.332
NFPA+ CA-CCC/CIC	14 (16.09%)	18 (27.69%)	2.049 (1.101–3.814)	0.024
ACTHA+ CA-CCC	8 (9.19%)	8 (12.3%)	2.652 (1.235–5.696)	0.012
Other + CA-CCC	9 (10.34%)	11 (16.92%)	2.719 (1.314–5.626)	0.007
SA(DG)+ CA-CCC	2 (10%)	–	0.902 (0.125–6.485)	0.918
SA+ CA-CCC	17 (85%)	–	2.448 (1.441–4.158)	0.001
Gangl	1 (5%)	–	0.506 (0.070–3.651)	0.499

Neg, negative; Co, coexistent; As, associated with; DG, densely granulated. SG, Sparsely granulated. SA, Somatotroph adenoma; TA, Thyrotroph adenoma; LA, Lactotroph adenoma; PIA, Plurihormonal adenoma; NFPA, non-functioning pituitary adenoma; ACTHA, adrenocorticotropin adenoma; CA-CCC, ciliated columnar cell or monolayer of cuboidal; SSEC, stratified squamous epithelium cell; CIC, chronic inflammatory cells; IC, inflammatory cells (mainly lymphocytes and plasma); HR, hazard ratio; CI, indicates confidence interval; Gangl, gangliocytomas; Other, gonadotroph adenoma with craniopharyngioma, Null-cell adenoma. P: P value. Other: include gonadotroph.*

TABLE 3 | RCC coexistent various type other sellar lesion and histopathological features and immunohistochemistry.

Coexistence sellar lesion category (No. Cases)	Morphological (%)	Immunohistochemistry (IHC) (%)	HR (95% CI) *P**
RCC as Hypophysitis n = 16			
SM+GC/FM +CA-CCC+IC	4(25%)	–	46.326 (8.080–265.600) 0.000
No-FM+CA-CCC+IC	3(18.75%)	–	39.625 (6.369–246.521) 0.000
EM+CA-CCC+IC	9(56.25%	–	13.195 (2.152–80.917) 0.005
–	-	–	
RCC co Aneurysm n = 4			
CP-ICA+ CA-CCC/SSEC	1 (25%)	1 (25%)	9.427 (1.225–72.555) 0.031
ACA+ CA-CCC/SSEC	1 (25%)	1 (25%)	9.427 (1.225–72.555) 0.031
A-A1-C A+ CA-CCC/SSEC	1 (25%)	1 (25%)	9.427 (1.225–72.555) 0.031
A-com A+ CA-CCC/SSEC	1 (25%)	1 (25%)	3.111 (0.425–22.772) 0.264
RCC co Chordoma and Craniopharyngioma n = 5			
EITC+CA-CCC/SSEC	3 (60%)	3 (60%)	0.728 (0.230–2.304) 0.589
mMC+CA-CCC	2 (40%)	2 (40%)	3.244 (0.782–13.466) 0.105
EMA	–	–	–
RCC co Other sellar lesion n = 6			
EC-CC+ CA-CCC/SSEC	1 (16.66%)	1 (16.66%)	8.456 (1.108–64.522) 0.039
RTE+ CA-CCC/SSEC	1 (16.66%)	1 (16.66%)	–
Xantho+CA-CCC/SSEC	1 (16.66%)	1 (16.66%)	3.275 (0.447–24.008) 0.243
CIC + CA-CCC/SSEC	1 (16.66%)	1 (16.66%)	5.194 (0.698–38.679) 0.108
SGR+ CA-CCC/SSEC	1 (16.66%)	1 (16.66%)	2.560 (0.351–18.666) 0.354
HA+ CA-CCC/SSEC	1 (16.66%)	1 (16.66%)	0.633 (0.88–4.560) 0.650

CA-CCC, ciliated columnar cell or monolayer of cuboidal; SSEC, stratified squamous epithelium cell; EITC, epithelioid-like tumor cells; SM, squamous metaplasia; GC, goblet cells; MC, mucous cells and basal cells; EC-CC, epidermoid cyst with ciliated cuboidal; FM, foamy macrophages; EM, epithelial cells and multinucleated giant cells or cholesterin; RTE, respiratory type epithelium; Xantho, xanthogranulomatous, CIC, chronic inflammatory cells; SGR, salivary gland remnants; HA, hematoma; CP-ICA, cavernous portion of the right internal carotid artery; ACA, anterior cerebral artery; AcomA, anterior communicating artery aneurysm; IC, inflammatory cells (mainly lymphocytes and plasma); HR, hazard ratio; CI, confidence interval. Other sellar lesion: include Epidermoid Cyst, Dermoid Cyst, pituitary granulomatosis, Salivary, Salivary gland remnants. P: P value.*

outlined follow-up period, 53.39% were considered to have an unclear/uncertain follow-up time or follow-up was not described, 1.69% patients died, and 98.31% patients survived.

Patients in with coexisting disease in different age subgroups and with different pathological characteristics have a higher degree of risk than other patients.

Stratified Identification Analysis of the Incidence of RCC Associated With Various Types of Sellar Lesions

The incidence of RCC associated with various types of sellar lesions across different age subgroups are summarized in **Table 1**. The rates of coexistence with RCC were 5.93% in the 12- to 19-year-old age groups and a mere 2.54% in the 0- to 11-year-old age groups. The 40–49-year-old, 50–59-year-old, and ≥60-year-old subgroups had rates of coexistence of 24.57, 19.54, and 22.98%, respectively.

Notably, the univariate subgroup analysis for age showed that most patients in the 20- to 59-year-old group had the highest incidence rates among all age groups, with tumors that develop over time and remain subclinical until later in life (3). The validation of the three prediction models was performed by assessing the differences in the age groups in terms of the cooccurrence of various types of diseases, along with categorical data (**Table 1**). **Figure 1** displays the most significant hazard of various types of sellar lesions associated with high *vs.* low exposure by age. The association between age and the cooccurrence of various types of sellar diseases varied across age groups and residual embryonic tissues. Regarding age variation, the coexisting risk among patients in the 30–39-year-old, 50–59-year-old, 12–19-year-old, and ≥60-year-old subtypes was greatest for the PA subtype, somatotroph (acromegaly acro) subgroup, Hypo subgroup, and aneurysm subgroup.

Among the other sellar subtypes, the histologic evaluation revealed two types of lesions: respiratory-type epithelium and stratified squamous epithelium cells and ciliated columnar cells (**Table 3**).

Clinicopathologic Features of Lesion Tissue From Patients With S-ErACT

Tables 2 and **3** show the significance of each clinicopathologic factor used to identify RCC and various sellar lesions in the 118 patients with the corresponding HR. It is worth noting that the incidence rates (IRs) of squamous metaplasia (SM)/or stratified squamous epithelium cells (SSECs) show different ranges (1.46–22.46%) for different subtypes (RCCs with various sellar lesions and aneurysms) and an increased risk of recurrence.

These lesions (RCC co PA) have been found to contain ciliated columnar cells or monolayers of cuboidal cells and show different incidence rates (IRs), ranging from 0.02 to 27.62%, suggesting that the resected lesion met the criteria of RCC, with extensive squamous metaplasia possessing apical ciliated columnar epithelium and interspersed goblet cells (16). There were inconsistencies in the surgical modalities due to the long treatment era studied.

The analysis of 31 patients with various coexisting types of sellar lesions is presented in **Table 3**. Here, SM+ goblet cells (GC) (HR 46.326, 95% CI 8.080–265.600 P = 0.000), foamy macrophages (FM) (HR 39.625, 95% CI 6.369–246.521 P = 0.000), epithelial cells, and multinucleated giant cells (EM)

TABLE 4 | Total surgical data and follow-up sellar lesion and pituitary adenoma subtype.

Factors parameters	RCC co PA Subtypes—other and Acromegaly N = 87		RCC as Hypophysitis N = 16	RCC co Aneurysm N = 4	RCC co Other sellar lesion-N = 11	
	RCC co Subtype PA—other N = 67	RCC co Subtype PA—Acromegaly N = 20			Chordoma and Craniopharyngioma N = 5	Other sellar lesions N = 6
HR (95% CI)	4.415 (1.803–10.808)	2.286 (0.886–5.898)	3.31 (1.230–8.907)	0.937 (0.263–3.340)	2.467 (0.736–8.269)	1.068 (0.299–3.807)
*P**	0.001	0.087	0.018	0.92	0.143	0.92
AUC (95% CI)	0.981 (0.959–1.005)		0.848 (0.687–1.008)	0.531 (0.104–0.958)	0.926 (0.806–1.046)	
Preoperative-PF (%)						
PRL↑	32 (47.76%)	–	–	–	1 (20%)	–
GH↑	4 (5.97%)	10 (50%)	–	–	–	–
ACTH↑	5 (7.46%)	–	1 (6.25%)	–	1 (20%)	–
DI/+Hypo	–	1 (5%)	3 (18.75%)	–	–	–
FSH/LH/T TSH/FSH	2 (2.98%)	–	–	–	1 (20%)	–
Unknown	2 (2.98%)	–	1 (6.25%)	–	–	1 (20%)
Hypo/PHP	6 (8.95%)	9 (45%)	–	–	3 (60%)	4 (60%)
Normal	2 (2.98%)		10 (62.5%)		1 (20%)	1 (20%)
	14 (20.89%)		2 (12.5%)		1 (20%)	
Postoperative-PF (%)						
DI/+Hypo/+AI	6 (8.95%)	2 (10%)	5 (31.25%)	–	1 (20%)	1 (20%)
Hypo/+TD	-	–	–	1 (25%)	–	1 (20%)
PHP	3 (4.47%)	–	4 (25%)	–	1 (20%)	2 (30%)
Normal	56 (83.58%)	13 (65%)	6 (37.5%)	3 (75%)	3 (60%)	2 (30%)
Unknown	2 (2.98%)	5 (25%)	1 (6.25%)			
Therapeutics (%)						
TSS	60 (89.55%)	19 (95%)	15 (93.75%)	–	4 (66.67%)	4*(70%)
Cr/ ± CE	5 (7.46%)	–	1 (6.25%)	4 (100%)	2 (33.33%)	2 (30%)
Conservative	1 (1.49%)	1 (5%)	–	–	–	–
REPL-T	2 (2.98%)	–	–	–	–	–
Follow-up time (%)						
3–12 months	9(14.43%)	5 (25%)	–	3 (75%)	–	1 (20%)
1–3 years	13 (19.40%)	2 (10%)	5 (31.25%)	1 (25%)	1 (20%)	2 (30%)
3–7 years	7 (10.44%)	1 (5%)	1 (6.25%)	–	–	–
Uncertain	34 (50.75%)	12 (60%)	10 (62.5%)		4 (80%)	3 (50%)
Recurrence	2 (2.98%)					
Died	2 (2.98%)					

PF, Pituitary Function; co, coexistent; as, associated with; other, pituitary adenomas of other types except growth hormone adenomas type; Hypo, Hypopituitarism; AI, adrenal insufficiency; TSS, trans-sphenoidal surgical; CCC, Ciliated columnar cells; SSC, stratified squamous cells; DI, diabetes insipidus; PHP, panhypopituitarism; TD, thyroid dysfunction; Cr, Craniotomy; CE, coil embolization. Other sellar lesion : Epidermoid+ Dermoid+Salivary gland remnants+granulomatosis+pituitary abscess+pituitary apoplexy. 4, one of the1case had 5time TSS; HR, hazard ratio; CI, indicates confidence interval; REPL-T, Replacement therapy. P*, P value. AUC, area under the curve. Uncertain, include lost follow-up; follow-up time.*

(HR 13.195, 95% CI 2.152–80.917 P = 0.005), epithelial cells with ciliated cuboidal (EC-CC) (HR 8.456, 95% CI 1.108–64.522 P = 0.039), and CP-ICA (HR 9.427, 95% CI 1.225–72.555 P = 0.031) had a highly significant association. A high-risk pathological type can increase the risk of coexistent RCC and was found to be independently associated with RCC pathological status to various degrees.

Validation of the Collision Accuracy of Different Subtypes by ROC Curve Analysis in an Independent Cohort of S-ErACT

The AUCs derived from this analysis equaled 0.848 (95% CI 0.687–1.008) for the hypophysis associated with RCC, 0.981 (95% CI 0.959–1.005) for subtype PA, and 0.926 (95% CI 0.806–1.046) for other sellar lesions (**Figure 2**), and there were marginally significant differences among the six sellar lesion subtypes. The results of the S-ErCT subtype prediction by the ROC curve analysis model with existing unique clinicopathologic features are shown in **Table 4**. The accuracy rate of subtype diagnosis was 89.83%, with the highest accuracy rate achieved for the PA subtype (93.94%). The accuracy rates for hypophysitis, aneurysm, and other sellar lesions were 82, 75.75, and 81.82%, respectively.

To assess the utility of these clinicopathologic feature parameters as diagnostic tools, we performed ROC curve analysis. The ROC curve shows [ciliated columnar cell or

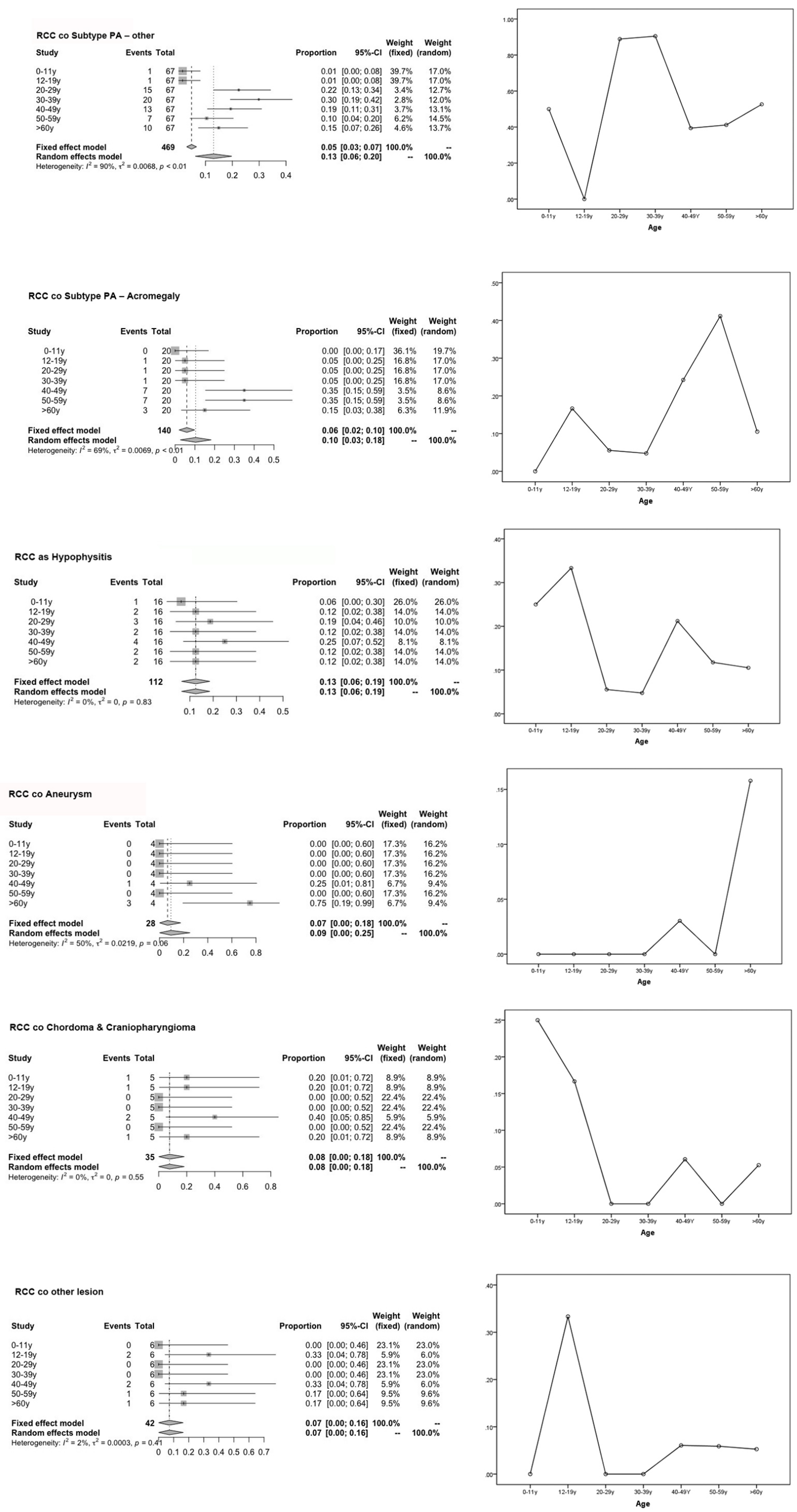

FIGURE 1 | Forest plot for the subgroup analysis of various population-based age groups and risk of age graph. This graph compares the risk of various subgroups (represented by combined RCC with sellar lesion) in each age group and the degree of merger risk within the age group (30–39 y, 50–59 y) calculated using our predictive model.

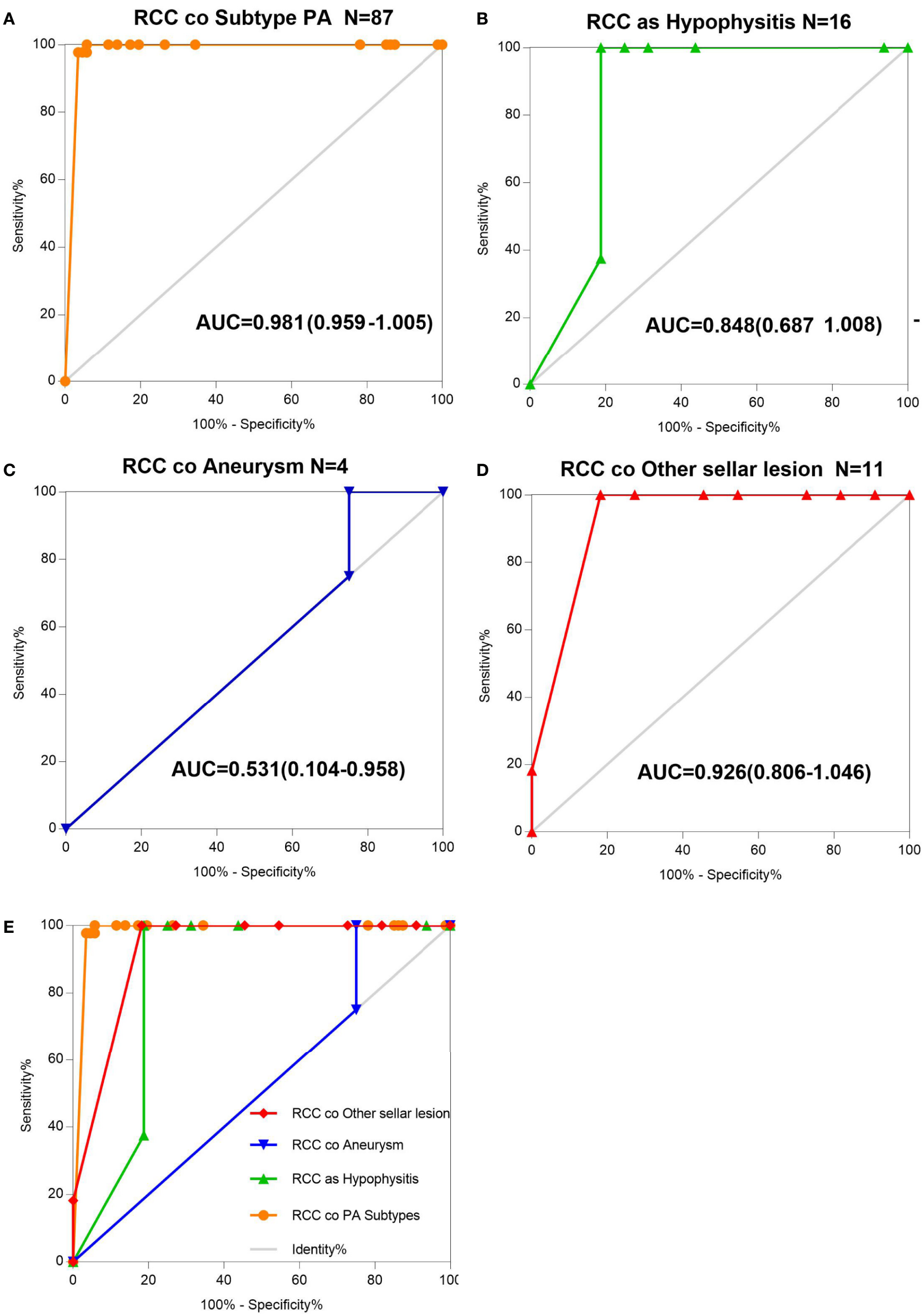

FIGURE 2 | AUC determination using receiver operating characteristic (ROC) curves. **(A)** Information on the results of age group value markers and RCC coexisting with pituitary adenoma subtype, assessed by the AUC. **(B)** Information on the age group value markers and RCC coexisting with hypophysitis, assessed by the AUC. **(C)** Information on the age group value markers and RCC coexisting with aneurysm, assessed by the AUC. **(D)** Information on the age group value markers and RCC coexisting with other sellar lesions, assessed by the AUC. **(E)** RCC and various sellar lesions in 118 patients classified into five groups according to different sellar lesions. Total ROC plot.

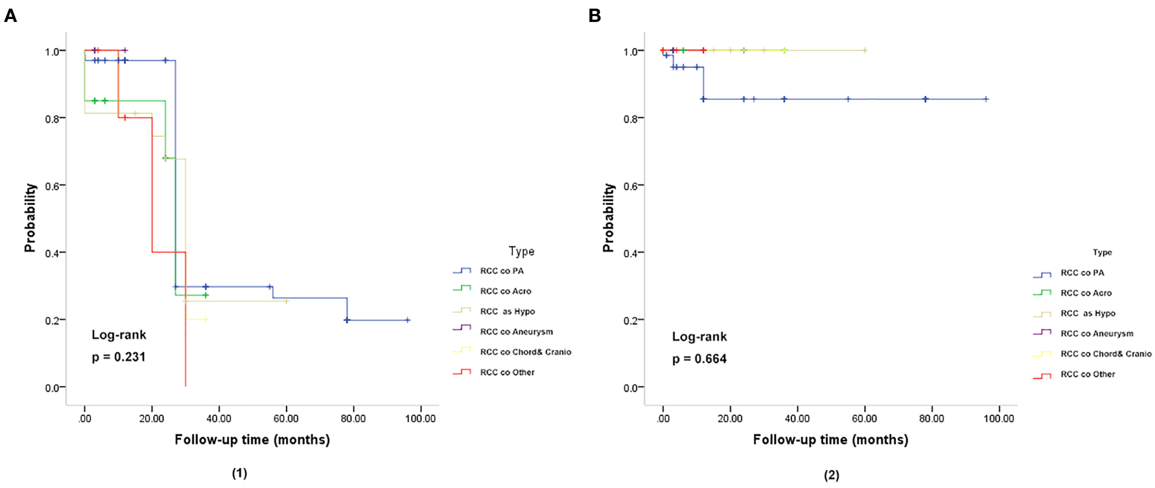

FIGURE 3 | Kaplan-Meier plot for overall survival (OS) **(A)** and relapse-free survival (RFS) **(B)** in patients with RCC coexisting with various sellar lesions. (**A**, 1): Kaplan-Meier plot for overall survival in patients. The solid blue line represents patients with the coexistence of RCC and PA (n = 67). The solid green line represents patients with the coexistence of RCC and somatotroph adenoma (acromegaly) (n = 20). The solid yellow line represents patient with the coexistence of RCC and hypophysitis (n = 16). The solid purple line represents patients with the coexistence of RCC and aneurysm (n = 4). The solid yellow line represents patients with the coexistence of RCC and chordoma and craniopharyngioma (n = 5). The solid red line represents patients with the coexistence of RCC and other sellar lesions (n = 6) (epidermoid cyst, dermoid cyst, pituitary granulomatosis, salivary tumor, salivary gland remnants). There was no significant difference in OS and RFS between the six subgroups of patients (*P* = 0.231). (**B**, 2): Kaplan-Meier plot showing the relapse-free survival (RFS) of patients. There was no significant difference in OS and RFS among the six subgroups of patients (*P* = 0.664). The *P*-values were obtained by the log-rank (Mantel-Haenszel) test.

monolayer of cuboidal (CA-ccc)] a sensitivity of 89.93% and a specificity of 100%.

Factors Associated With S-ErACT Formation Included RCC and Various Sellar Lesions and Clinical Characteristics

As presented in **Table 4**, all four subtypes of S-ErACT were significantly associated with RCCs and with all types of PAs (HR 4.415, 95% CI 1.803–10.808, P = 0.001, HR 2.286, 95% CI 0.886–5.898, P = 0.087), Hypo (HR 3.310, 95% CI 1.230–8.907, P = 0.018), CD and CP (HR 2.467, 95% CI 0.736–8.269, P = 0.143), EC and DC and PG and SGR (HR 1.068, 95% CI 0.299–3.807, P = 0.920) coexisting with RCC. An additional analysis was performed to assess the correlations between the clinical features and embryonic remnant-associated tumors of the sellar region in patients with collision lesions. As indicated in **Table 4**, concerning the association of RCC coexisting with all types of sellar lesions by specific subtypes, no difference was observed, regardless of whether CA-ccc and SSEC or GA and SA were present. Among embryonic remnant-related lesions, intermediate lobe-located lesions were associated with the pituitary and CP compared with the suprasellar septum or posterior lobe. RCC and sellar lesions showed an association with coexisting lesions.

In the follow-up analysis, various subgroups showed no difference in overall survival (OS), and relapse-free survival (RFS) ($P = 0.231$, $P = 0.664$) (**Figure 3**). The Median overall survival period was 22.93 months. The 3- and 5-year OS rates were 95.50 and 95.77%, respectively, which did not differ based on imaging evidence. In this group, 2 (2.98%) patients experienced recurrence.

Risk of Bias (Methodological Quality)

The risk of bias in the included case series/case-control original studies is shown in **Figure 4**. The bias risk of all studies in the literature was evaluated in seven domains; 50 studies (case series) and 17 studies (case controls) were at risk of unbiased data (attrition bias) and were considered low risk in terms of bias. In terms of bias in measuring the results, only one study in the case series had incomplete outcome data (attrition bias).

Disease Model Validation

A 23-year-old Chinese man presented to the clinic 2 days following sudden onset of headache and vomiting. Neurological examination revealed no focal deficit include oculomotor palsy or visual field defect. Computerized tomography (CT) and MRI image showed 2.5 × 2.4 × 2.3 cm cystic-solid lesion in the sellar and suprasellar regions, which had low signal intensity on T1-weight image and high signal intensity on T2-weighted image. The cystic mass located between the anterior and posterior pituitary lobes, and no evidence of SAH (**Case illustrate - Figure 1A**). A disease was suspected. Endocrinological evaluation revealed a serum prolactin level of 12.0 ng/mL (reference range, normal 2.1–11.7 ng/mL), testosterone level of 255.9 ng/dL (reference range, normal 358–1217 pg/dL), and estradiol level of 0.0 pg/mL (reference range, normal 19.9–47.9 pg/dL), adrenocorticotrophic hormone, follicle stimulating hormone, luteinizing hormone, growth hormone, insulin-like growth factor, thyroid stimulating hormone, free T3, free T4, and cortisol were within normal limits.

The patient underwent microsurgical resection using the trans-sphenoidal surgery (TSS) approach under general

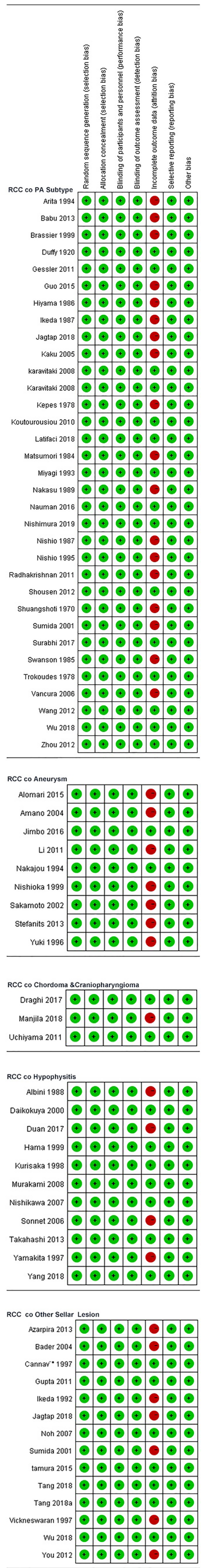

FIGURE 4 | Review author's judgements about each risk of bias item for each included case series /case-control.

anesthesia. Intraoperatively, the cyst was found to contain whitish yellow free-flowing mucus (**Case illustrate - Figure 1**) the pathology was consistent with that of an RCC (**Case illustrate - Figure 3**). Gross total resection (complete cyst and wall excision) was performed without intraoperative tearing of the arachnoid membrane or subsequent cerebrospinal fluid (CSF) leakage and massive hemorrhage.

The patient's level of arousal at postoperative 24 hours decreased to somnolence. The pupils were equal and reactive to light bilaterally. The visual fields were full, and the extraocular eye movements were intact. Laboratory test results were normal. Postoperative CT (postoperative day 1) revealed Fisher grade IV SAH (**Case illustrate - Figure 1**). Computerized tomographic angiography (CTA) demonstrated a 5 mm AComA aneurysm with diffuse perfusion delay in the anterior longitudinal fissure and bilateral sylvian fissures (**Case illustrate - Figure 2**). The patient underwent a right frontotemporal craniotomy to treat the aneurysm (postoperative day 3). When the dura mater was opened, the brain was found to be swollen and the SAH was clearly observed. Intraoperative findings were consistent with that of a ruptured AComA aneurysm (**Case illustrate - Figure 2**). The patient recovered well following craniotomy and clipping of the aneurysm and was discharged home 5 days following the clipping. There was no symptomatic cerebral vasospasm or hydrocephalus. At 6 months follow-up, visual field acuity had fully recovered to the preoperative level, and physical examination findings remained unchanged. A repeat CT and MRI of the brain with gadolinium showed no residual tumor or cyst recurrence.

DISCUSSION

S-ErACT is a rare entity that consists of two distinct neoplasms that have an embryological ancestry (or share common embryologic ancestry), develop in juxtaposition to one another and have no or varying degrees of involvement intermingling between them; moreover, one of the tumors may exhibit characteristics of pluripotent stem cells (stratified squamous epithelial progenitor cells) (7). The use of preoperative MRI/CT diagnosis to distinguish both lesions is challenging, as they share similarities in radiological appearance and are often incidental. However, the presence of both lesions significantly alters the biological behavior of tumors and can be mistaken for cystic sellar lesions (17, 18), and postoperative pathological diagnosis is the only main basis for distinguishing the two.

Whereas the results of analyses on the outcomes of RCC coexisting with sellar lesions in adults are available, there are no such studies on different age groups and the clinicopathology of sellar collision lesions. Thus far, it is known from the MEDLINE database that embryonic remnants are significant risk factors for sellar tumors. In this study, the incidence rates of concomitant sellar lesions were influenced by the presence of RCC, PA, age, and S-ErACTs but not by location. The risk of coexistence was most significant in patients aged 30–39 years (PA), 50–59 years (SA), 12–19 years (Hypo), and ≥60 years (aneurysm), compared

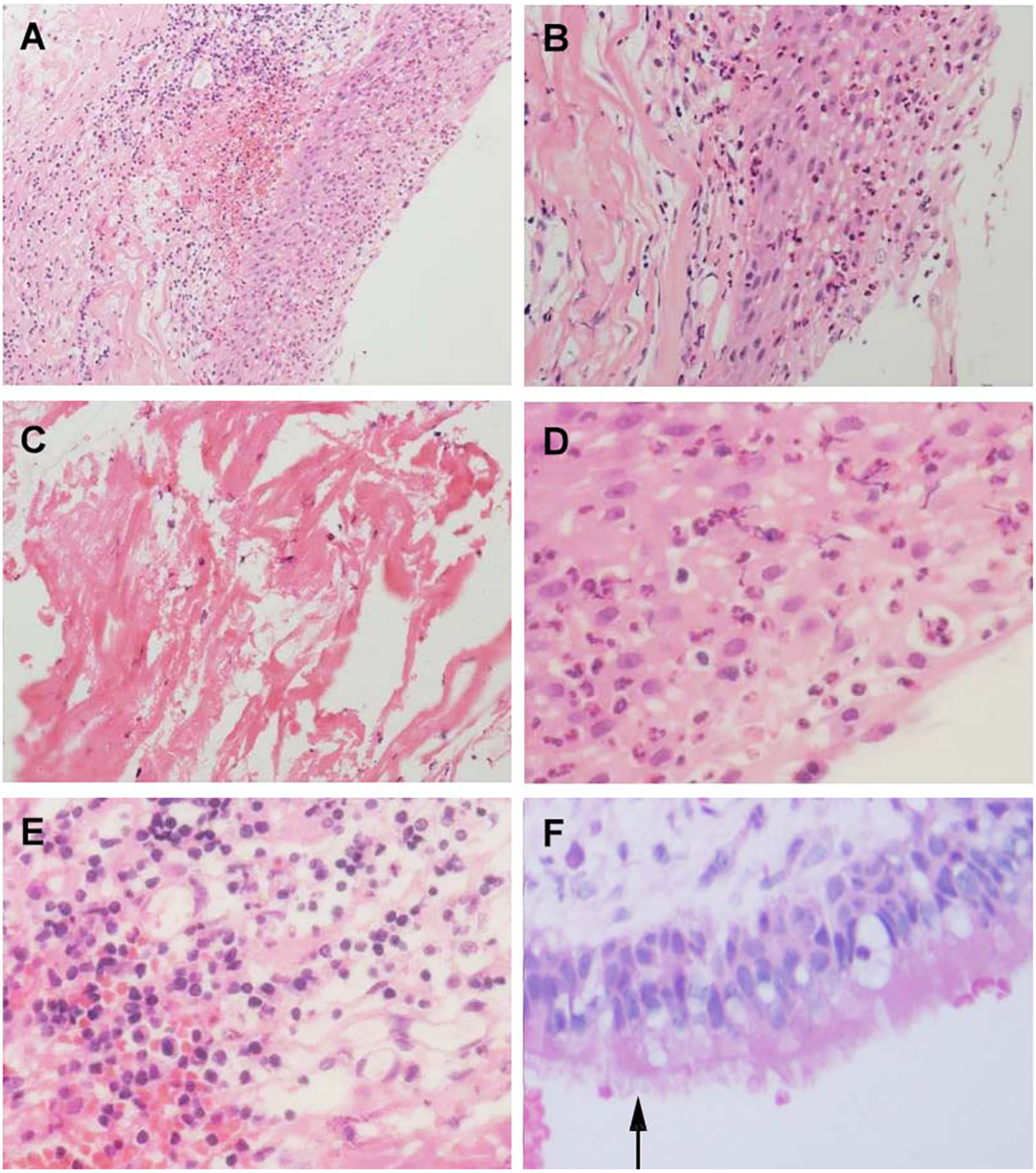

FIGURE 5 | Histological feature of Aneurysm with Rathke's cleft cyst, H&E stained section. **(A)** Shows the histological features of simple partial covered squamous epithelium with fibrous connective tissue presents acute and chronic inflammation (×150). **(B)** Squamous epithelial mucosa (×300). **(C)** The keratin in the cyst wall. **(D)** cystic wall lined by a squamous epithelium (×400). **(E)** Groups of inflammation cells (400×). **(F)** cuboidal ciliated epithelium cells(arrows) (×400).

with those who were in other age groups (various sellar lesions). Women had a higher prevalence of the coexistence of RCC with sellar lesions than men. Patients with coexisting PA and Hypo or CD and CP had a higher prevalence than those with coexisting aneurysm. The coexistence of RCCs and AComA aneurysms has rarely been reported, and systematic reviews of just four cases (including our one case) have been published from 1920 to 2018 (19–22).

We calculated that in a population of people with collision lesions consisting of men and females of various ages, the incidence rates of RCC coexisting with PA ranged from 0.02 to 57.91%. This is higher than that in previous studies, which reported a range of 1.7–1.9%. This difference can be explained by adjustments for age and sex in retrospective studies. Our present findings are probably more accurate because we included approximately several times more studies than previous works,

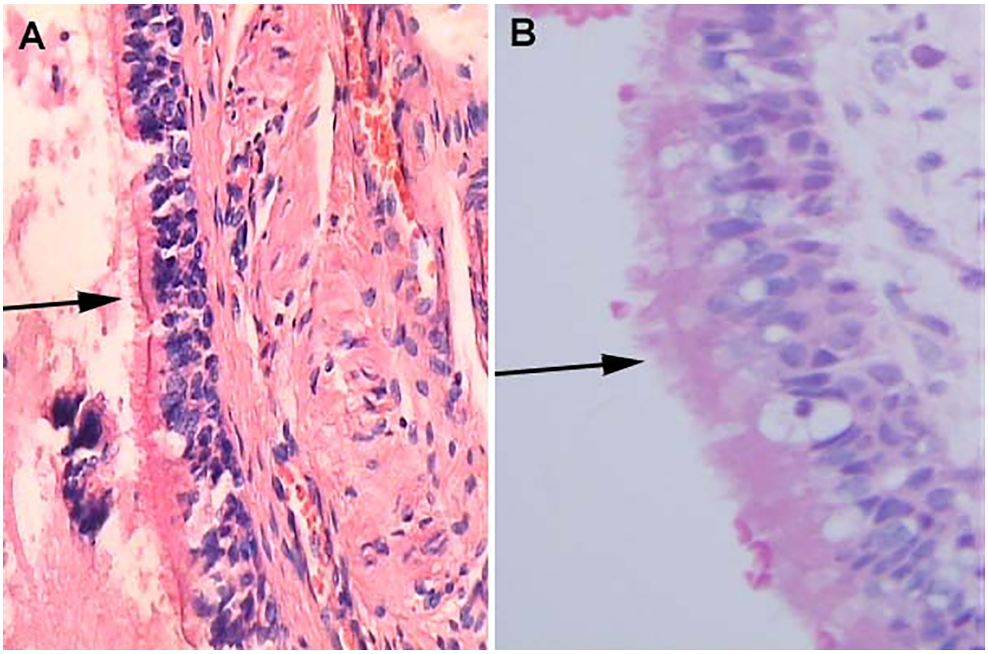

FIGURE 6 | Histological features of Human bronchial epithelium and Rathke's cleft cyst epithelium, H&E stained section. **(A)** Ciliated bronchial epithelium (arrows) (×100). **(B)** Cuboidal ciliated epithelium (arrows) (×400).

and more importantly, we were able to adjust IR for different age groups.

Different age groups and histopathological characteristics are major risk factors for RCC coexisting with various sellar lesions, and patients who have sellar embryonic remnants are at increased risk of developing this disease over time. Owing to abundant data, we could separately assess the incidence of concomitance (RCC and various sellar lesions) in different age groups and patients with various subtypes of coexistence of sellar lesions. For patients who are in different age groups and have sellar embryonic remnant-associated disease, there may be a clear association. This means that these embryonic residues, which should have disappeared after birth or with development, are affected by acquired factors, such as hormone axes and changes in the developmental environment.

Although collision lesions of the sellar region are incidentally found at the clinic or on imaging, the rate of asymptomatic cystic lesions identified at autopsy is as high as 33% (9). The cell distribution of the various embryonic remnants in histopathological patterns is as follows: ciliated columnar cells or monolayers of cuboidal, stratified squamous epithelium, inflammatory cells, respiratory type epithelium, cilia, and mucous secreting goblet cells, and some were squamous metaplasia (see **Figure 5**). They have a similar location in the sellar and suprasellar regions and show overlapping histopathologic features, namely, ciliated columnar epithelium to ciliated squamous epithelium to squamous epithelium. This reflects the process of lesion development; the changes in these pathological cells are similar to embryonic esophageal epithelial replacement during the embryonic period. These pathological changes in the respiratory-type epithelium (see **Table 3**) prompted us to examine the bronchial epithelial structure. In contrast, the pathological structure of the RCC cyst wall was surprisingly similar to that of bronchial epithelial cells (see **Figure 6**), suggesting that the presence of squamous metaplasia or pseudostratified cuboidal cells in the cyst wall was regenerative and revealing that this layer of cells has the characteristics of progenitor cells or stem cells. Recent experimental studies have also confirmed this view (23). Another study suggested that squamous metaplasia and isointensity on T2-weighted MRI were independent predictors of cyst recurrence (24).

The changes in RCC pathological cells and the similarity between the pathological structures and the bronchial epithelium structure support the theory of the development of the pharyngeal bursa after migration (25). There is compelling evidence to show that a proportion of stem cells around the pituitary cleft and marginal zone in the pituitary or epithelial cells in Rathke's pouch wall formed by mesenchyme accumulation may undergo further differentiation in response to some growth (23, 26–28). Under different inducing factors, these progenitor cells behave similarly to the transition cells proposed by Kepes (29). This finding illustrates the replacement/ or renewal process to transitional and accumulation of epithelial cells (30). In a more recent report published in 2018, four cases of previously diagnosed RCC were reclassified as papillary craniopharyngioma because they were

$BRAF^{V600E}$ positive, implying the transformation of RCC into papillary craniopharyngioma (16).

This evidence supports our study as the basis for the theory of the postmigration development of the pharyngeal bursa. However, evidence of a common origin remains controversial. To our knowledge, PA is the independent risk factor with the highest risk (minimal difference in collision accuracy) according to the pathological graded risk for association with RCC. Interestingly, we found that gonadotroph hormone adenoma (HR 2.719) and corticotrophin hormone adenoma (HR 2.652) had the highest risk of merging with RCC among the pathological subtypes of PA (**Table 2**). Evaluations of both age and pathology for sellar lesions may provide meaningful information to determine whether there are pathological structures and cells with potential stem cell characteristics in constantly changing pathological tissues and concomitant/ associated diseases in the sellar region.

In fact, we observed differentiated epithelial cells in RCC, from single columnar epithelium to ciliated epithelium, and GC (HR 13.195, P = 0.005) and/or stratified epithelium had a significantly higher risk of replacement/renewal to transitional/ accumulation. This finding shows the process of replacement/ renewal or transition and accumulation of epithelial cells, which may arise from Rathke's pouch parietal cells, as they are composed of progenitor cells, which directly differentiate from stem cells. These lesions (RCC co PA) have been found to contain ciliated columnar cells or monolayers of cuboidal cells and show different incidence rates (IR) ranging from 0.02 to 27.62%, suggesting an intermediate entity between RCC and sellar lesions, and this evidence lends support to this idea (13).

Our data also demonstrated that the different sellar embryonic remnants associated with tumor progression represent a multistep process that involves age and the accumulation of heterogeneous genetic mutations. Previous studies have reported that the pathological findings of various diseases in the sellar region are consistent with RCC embryology and elements (6, 31). However, it has recently been asserted that the persistence of the embryonal morphology of the infundibular recess might then be the result of dysembryogenesis in humans. No data have yet confirmed the neoplastic nature of the lesion (8). In addition, evaluating RCCs and sellar lesions is useful because it yields information on RCCs and the pathological tissue in sellar lesions. However, its role in pathogenesis remains unclear.

This study has several limitations. First, it was a retrospective study, so unknown biases could be present, and any biases would affect positive results. Another limitation is the small sample size. We only provide pooled data for patients who had reported morbidities, but those who were already sick and reported were not included (patients not included because of incomplete full-text retrieval or inconsistent data). Thus, more studies are needed to focus on such patients. The unknown heterogeneity of the included studies in terms of study design, regions of study, time of onset, age at diagnosis, living environment, and other factors made it difficult to achieve valid and stable meta-analysis.

CONCLUSIONS

These pathological changes represent crucial information on sellar embryonic remnant-associated collision tumors and provide necessary clinical observation data to these tumors. Exploratory traceability studies have shown that our clinical observation data verify the accumulation process from ciliated columnar epithelium to ciliated squamous epithelium to squamous epithelium and that the RCC cyst wall has tracheobronchial airway epithelium with similar characteristics to progenitor cells. It is necessary to further expand this work to find more evidence.

DATA AVAILABILITY STATEMENT

The datasets presented in this study can be found in online repositories. The names of the repository/repositories and accession number(s) can be found in the article/**Supplementary Material**.

ETHICS STATEMENT

The study was approved by the ethics committee in Peking Union Medical College Hospital, China. Written informed consent was obtained from the legal representatives of all participants before inclusion (approval date. 2011-0831).

AUTHOR CONTRIBUTIONS

Conception and design: MW and WM. Acquisition of data: MW, ZW, ZZ, MS, and WM. Analysis and interpretation of data: MW and MS. Drafting the article: MW, WM, and ZZ. Critically revising the article: ZW, WM, and ZZ. Reviewed submitted version of manuscript: all authors. Approved the final version of the manuscript on behalf of all authors: WM and ZW. Statistical analysis: MW, MS, and QF. Administrative/ technical/material support: ZZ, ZW, JZ, RW, and WM. Study supervision: ZW, JZ, RW, WM, and ZZ. All authors contributed to the article and approved the submitted version.

FUNDING

This research did not receive any specific grant from funding agencies in the public, commercial, or not-for-profit sectors.

SUPPLEMENTARY MATERIAL

The Supplementary Material for this article can be found online at: https://www.frontiersin.org/articles/10.3389/fonc.2021.649958/full#supplementary-material

REFERENCES

1. Pérez-Pomares JM, Foty RA. Tissue fusion and cell sorting in embryonic development and disease: biomedical implications. *Bioessays* (2006) 28:809–21. doi: 10.1002/bies.20442
2. Smith CJ, Bensing S, Maltby VE, Zhang MD, Scott RJ, Smith R, et al. Intermediate lobe immunoreactivity in a patient with suspected lymphocytic hypophysitis. *Pituitary* (2014) 17(1):22–9. doi: 10.1007/s11102-013-0461-9
3. Han SJ, Rolston JD, Jahangiri A, Aghi MK. Rathke's cleft cysts: review of natural history and surgical outcomes. *J Neurooncol* (2014) 117(2):197–203. doi: 10.1007/s11060-013-1272-6
4. Brinkmeier ML, Bando H, Camarano AC, Fujio S, Yoshimoto K, de Souza FSJ, et al. Rathke's cleft-like cysts arise from Isl1 deletion in murine pituitary progenitors. *J Clin Invest* (2020) 130(8):4501–15. doi: 10.1172/JCI136745
5. Akita S, Readhead C, Stefaneanu L, Fine J, Tampanaru-Sarmesiu A, Kovacs K, et al. Pituitary-directed Leukemia Inhibitory Factor Transgene Forms Rathke's Cleft Cysts and Impairs Adult Pituitary Function A Model for Human Pituitary Rathke's Cysts. *J Clin Invest* (1997) 99(10):2462–9. doi: 10.1172/JCI119430
6. Manjila S, El Asmar N, Vidalis BM, Alonso F, Singh G, Vadamalai K, et al. Intratumoral Rathke's Cleft Cyst Remnants Within Craniopharyngioma, Pituitary Adenoma, Suprasellar Dermoid, and Epidermoid Cysts: A Ubiquitous Signature of Ectodermal Lineage or a Transitional Entity. *Neurosurgery* (2018) 0:1–9. doi: 10.1093/neuros/nyy285
7. Schizas D, Katsaros I, Michalinos A, Damaskos C, Garmpis N, Ntomi V, et al. Collision Tumors of the Gastrointestinal Tract: A Systematic Review of the Literature. *Anticancer Res* (2018) 38:6047–57. doi: 10.21873/anticanres.12955
8. Belotti F, Lupi I, Cosottini M, Ambrosi C, Gasparotti R, Bogazzi F, et al. Persisting Embryonal Infundibular Recess (PEIR): Two Case Reports and Systematic Literature Review. *J Clin Endocrinol Metab* (2018) 103(7):2424–9. doi: 10.1210/jc.2018-00437
9. Osborn AG, Preece MT. Intracranial cysts: radiologic-pathologic correlation and imaging approach. *Radiology* (2006) 239(3):650–64. doi: 10.1148/radiol.2393050823
10. Weissman JL. Thornwaldt cysts. *Am J Otolaryngol* (1992) 13:381–5. doi: 10.1016/0196-0709(92)90080-D
11. Takanashi J, Tada H, Barkovich AJ, Saeki N, Kohno Y. Pituitary cysts in childhood evaluated by MR imaging. *AJNR Am J Neuroradiol* (2005) 26:2144–7.
12. Larkin S, Karavitaki N, Ansorge O. Rathke's cleft cysts. In: *Handbook of Clinical Neurology*, E Fliers, M Korbonite, JA Romijin, editors. Amsterdam, The Netherlands: Elsevier BV. (2014). p. 255–69. doi: 10.1016/B978-0-444-59602-4.00017-4
13. Chaudhry NS, Raber MR, Cote DJ, Laws ERJr. Spontaneous pituitary adenoma occurring after resection of a Rathke's cleft cyst. *J Clin Neurosci* (2016) 33:247–51. doi: 10.1016/j.jocn.2016.05.018
14. Pearl GS, Takei Y, Kurisaka M, Seyama S, Tindall GT. Cystic prolactinoma. A variant of "transitional cell tumor" of the pituitary. *Am J Surg Pathol* (1981) 5:85. doi: 10.1097/00000478-198101000-00012
15. DeLong ER, DeLong DM, Clarke-Pearson DL. Comparing the areas under two or more correlated receiver operating characteristic curves: a nonparametric approach. *Biometrics* (1988) 44(3):837–45. doi: 10.2307/2531595
16. Schlaffer S-M, Buchfelder M, Stoehr R, Buslei R, Hölsken A. Rathke's Cleft Cyst as Origin of a Pediatric Papillary Craniopharyngioma. *Front Genet* (2018) 9:49. doi: 10.3389/fgene.2018.00049
17. Minaya-Bravo AM, Garcia Mahillo JC, Mendoza Moreno F, Noguelares Fraguas F, Granell J. Large cell neuroendocrine- Adenocarcinona mixed tumour of colon: Collision tumour with peculiar behaviour. What do we know about these tumours? *Ann Med Surg* (2015) 4:399–403. doi: 10.1016/j.amsu.2015.10.004
18. de Almeida Verdolin A, Baranski Lamback E, Ventura N, Guasti A, da Mata Pereira PJ, Gadelha MR, et al. Collision sellar lesions: coexistence of pituitary adenoma and Rathke cleft cyst—a single-center experience. *Endocrine* (2020) 68:174–81. doi: 10.1007/s12020-019-02149-8
19. Yamamoto M, Takara E, Imanaga H, Jimbo M, Kubo O. Rathke's cleft cyst. Report of two cases. *No Shinkei Geka* (1984) 12(5):609–16.
20. Yuki K, Katsuzo K, Ikawa F, Takeshita S, Hamasaki O, Tohru U. A case of Rathke's cleft cyst in association with anterior communicating artery aneurysm presenting a rare visual field defect. *No To Shinkei* (1996) 48 (5):482–5.
21. Sakamoto S, Ikawa F, Kawamoto H, Ohbayashi N, Sakoda E, Hidaka T, et al. case of Rathke's cleft cyst in association with a ruptured aneurysm of the anterior cerebral artery mimicking pituitary apoplexy. *No Shinkei Geka* (2002) 30(2):199–203.
22. Amano T, Kajiwara K, Harada K, Yoshikawa K, Akimura T, Kato S, et al. A case of Rathke's cleft cyst in association with bilateral unruptured aneurysms of internal carotid artery. *No Shinkei Geka* (2004) 32(1):49–54.
23. Yoshida S, Yasuda M, Miyashita H, Ogawa Y, Yoshida T, Matsuzaki Y, et al. Generation of Stratified Squamous Epithelial Progenitor Cells from Mouse Induced Pluripotent Stem Cells. *PloS One* (2011) 6(12):e28856. doi: 10.1371/journal.pone.0028856
24. Chotai S, Liu Y, Pan J, Qi S. Characteristics of Rathke's cleft cyst based on cyst location with a primary focus on recurrence after resection. *J Neurosurg* (2015) 122:1380–9. doi: 10.3171/2014.12.JNS14596
25. Nikolić MZ, Sun D, Rawlins EL. Human lung development: recent progress and new challenges. *Development* (2018) 145:dev163485. doi: 10.1242/dev.163485
26. Goldsmith S, Lovell-Badge R, Rizzoti K. SOX2 is sequentially required for progenitor proliferation and lineage specification in the developing pituitary. *Development* (2016) 143:2376–88. doi: 10.1242/dev.137984
27. Pérez Millán MI, Brinkmeier ML, Mortensen AH, Camper SA. PROP-1 triggers epithelial- mesenchymal transition-like proces in pituitary stem cells. *Elife* (2016) 5:e14470. doi: 10.7554/eLife.14470
28. Jacobson AG, Miyamoto DM, Mai SH. Rathke's puoch morphogenesis in the chick embryo. *J Exp Zool* (1979) 207:351–66. doi: 10.1002/jez.1402070303
29. Kepes JJ. Transitional cell tumor of the pituitary gland developing from a Rathke's cleft cyst. *Cancer* (1978) 41(1):337–43. doi: 10.1002/1097-0142(197801)41:1<337::AID-CNCR2820410145>3.0.CO;2-T
30. Ogawa Y, Watanabe M, Tominaga T. Prognostic factors of operated Rathke's cleft cysts with special reference to re-accumulation and recommended surgical strategy. *Acta Neurochir* (2011) 153:2427–33. doi: 10.1007/s00701-011-1072-8
31. Geddes JF, Jansen GH, Robinson SF, Gömöri E, Holton JL, Monson JP, et al. "Gangliocytomas" of the pituitary. A heterogeneous group of lesion with differing histogenesis. *Am J Surg Pathol* (2000) 24:607–13. doi: 10.1097/00000478-200004000-00017

Conflict of Interest: The authors declare that the research was conducted in the absence of any commercial or financial relationships that could be construed as a potential conflict of interest.

frontiers in Oncology

ORIGINAL RESEARCH
published: 26 May 2021
doi: 10.3389/fonc.2021.676683

Check for updates

Clinical Factors and Outcomes of Atypical Meningioma: A Population-Based Study

Gui-Jun Zhang[†], *Xiao-Yin Liu*[†] *and Chao You**

Department of Neurosurgery, West China Hospital, Sichuan University, Chengdu, China

Objective: Atypical meningioma is a non-benign tumor, and its prognostic factors and treatment strategies are unclear.

Methods: Patients with atypical meningioma, between 2004 and 2016, were collected from the Surveillance, Epidemiology, and End Results database. Then, we randomly divided patients into a training set and a validation set at a ratio of 8:2. The nomogram was constructed based on the multivariate Cox regression analyses. And the concordance index, calibration curves, and receiver operating character were used to assess the predictive ability of the nomogram. We divided the patient scores into three groups and constructed a survival curve using Kaplan–Meier analysis.

Results: After our inclusion and exclusion criteria, 2358 patients were histologically diagnosed of atypical meningioma. The prognostic nomogram comprised factors of overall survival, including age, tumor size and surgery. The concordance index was 0.715 (95%CI=0.688-0.742) for overall survival in the training set and 0.688 (95%CI=0.629-0.747) for overall survival in the validation set. The calibration curves and receiver operating character also indicated the good predictability of the nomogram. Risk stratification revealed a statistically significant difference among the three groups of patients according to quartiles of risk score.

Conclusion: Gross total resection is an independent factor for survival, and radiation after non-gross total resection potentially confers a survival advantage for patients with atypical meningioma.

Keywords: atypical meningioma, prognostic factor, treatment, SEER database, nomogram

Edited by:
Xicai Sun,
Fudan University, China

Reviewed by:
Chuzhong Li,
Capital Medical University, China
Ye Gu,
Fudan University, China

***Correspondence:**
Chao You
chaoyou1991@163.com

[†]*These authors have contributed equally to this work*

Specialty section:
This article was submitted to Surgical Oncology, a section of the journal Frontiers in Oncology

Received: *05 March 2021*
Accepted: *06 May 2021*
Published: *26 May 2021*

Citation:
Zhang G-J, Liu X-Y and You C (2021) Clinical Factors and Outcomes of Atypical Meningioma: A Population-Based Study. Front. Oncol. 11:676683. doi: 10.3389/fonc.2021.676683

INTRODUCTION

Meningiomas constitute the most prevalent primary intracranial tumor, with an annual incidence of around 5 per 100,000 individuals, which account for approximately 30% of central nervous system, ranging from World Health Organization (WHO) grade I benign to WHO grade III malignant meningioma (1, 2). Atypical meningioma, as grade II, belongs to a distinctive category with a typical behavior, accounting for 8% of all meningiomas (3).

For treatment strategy in the atypical meningioma, an increasing number of reports advocated the critical importance of extensive resection as initial therapy (4, 5), which indicated the extent of resection affected prognosis. But some scholars suspected the role of aggressive resection on survival. On the other hand, limited literature existed over whether radiotherapy should be added into standard therapy regardless of the extent of resection for this non-benign tumor (6–9).

Given the controversy in the literature, and undetailed enunciation about prognostic factors for atypical meningioma from small series (10–12), we aimed to identify the prognostic factors to modify treatment strategies so as to improve the survival of patients with this tumor. Meanwhile, a nomogram model was established and validated for reliable estimation of 3-, 5-, and 8-year survival.

MATERIAL AND METHODS

The National Cancer Institute's Surveillance, Epidemiology and End Results (SEER) database includes incidence, patient demographics, clinic-pathological, treatment, and survival data from approximately 28% of the US cancer cases. This study cohort included adult patients more than 18 years old with histologically confirmed atypical meningioma. The extracted clinical information included in the following: patient ID, age at diagnosis, sex, race, year of diagnosis, primary site, laterality, tumor size, diagnostic confirmation, surgery at the primary site, radiation code, survival months, and vital status. The exclusion criteria were as follows (**Supplementary Figure 1**): 1) missing critically clinical patient information; 2) not confirmed histologically atypical meningioma; 3) patient survival time equally to 0 month; 4) not primary sequence only; 5) patients without surgical resection.

After filtering the data, additional classification was performed: sex (female *vs*. male), location (cerebral menings *vs*. non-cerebral menings), laterality (left *vs*. right *vs*. bilateral *vs*. others), surgery (gross total resection (GTR) *vs*. non-GTR), and radiation (yes *vs*. no). The age and tumor size were divided into subgroups using the receiver operating character (ROC). For the extent of resection, "radical resection" was considered GTR; "biopsy", "subtotal resection", and "partial resection" were considered non-GTR. The endpoint was defined as overall survival (OS).

Construction and Validation of the Nomogram

The enrolled patients were randomly divided into training and validation sets at a ratio of 8:2, and the clinical information of two groups were described. Survival analysis were performed using univariate and multivariate proportional hazard models. Univariate analysis was performed first and variables were inclusion for multivariate analysis if the univariate p value<0.15.

The nomogram was established to estimate 3-, 5-, and 8-year OS rates for patients with atypical meningioma, and then nomogram models were internally validated. To verify the discrimination ability of the nomogram, we used concordance index (C-index) and ROC in the training and validation sets. In addition, calibration curve was performed to assess the consistency between actual prognosis and predicted survival.

Categorical variables were compared with the Chi-square or Fisher's exact test, and continue variables were compared with the independent-samples student's t-test. In addition, we calculated the scores of each patient in the training cohorts based on the nomogram models. Then, we divided the training set into three groups according to the total score of each patient, and constructed the survival curve and log-rank test to compare the OS of patients in the different groups.

Statistical Analysis

Statistical analysis was performed using R statistical software (version 3.6.3) and SPSS software (version 25.0; IBM Corp, Armonk, NY, USA), p<0.05 was considered statistically significant.

RESULTS

After our inclusion and exclusion criteria, 2358 patients with histologically-identified atypical meningioma in the SEER database and were included in our further analysis. The best cut-off value for the age and the tumor size were determined to be 67.5 years and 52.5 mm, respectively. The clinical variables of patients were in the training and validation sets (**Table 1**).

The Training Set

Of 1888 patients in the training set, there was 1105 (58.5%) female patients and 783 (41.5%) male patients, with a female-male ratio of 1.4. The median age at diagnosis was 61 years, with an age range of 20-93 years. The majority of patients (n=1110, 58.8%) were diagnosed after year 2011. The 3-, 5-, and 8-year OS for all patients by Kaplan-Meier analysis were 87.1%, 78.9%, and 67.7%, respectively. GTR was achieved in 1098 (58.2%) patients, and non-GTR was achieved in 790 (41.8%) patients. Most patients (n=1375, 72.8%) declined adjuvant radiotherapy.

Using univariate analysis, factors significantly predicting worse OS included age more than 67.5 years (HR=4.219, 95% CI=3.454-5.153; p<0.001) (**Figure 1A**), and tumor size more than 52.5mm (HR=1.752, 95% CI=1.441-2.130; p<0.001) (**Figure 1B**); factors trending toward a better OS included male (HR=1.193, 95%CI=0.981-1.450; p=0.077) and GTR (HR=0.825, 95%CI=0.678-1.003; p=0.053) (**Figure 1C**). By multivariate analysis, older age (HR=4.184, 95%CI=3.417-5.124; p<0.001), larger tumor size (HR=1.692, 95%CI=1.389-2.061; p<0.001) significantly predicted worse OS, and GTR (HR=0.818, 95% 220 CI=0.673-0.995; p=0.045) was an independent favorable factor of better OS (**Figure 2**).

The prognostic nomogram (**Figure 3A**) comprised all significant factors of OS based on the multivariate analysis. The C-index for OS was 0.715 (95%CI=0.688-0.742). AUCs for ROC curves (**Figure 3B**) and the calibration plot (**Figures 3C–E**) for the probability of survival at 3, 5, and 8 years displayed an ideal agreement between the prediction and actual observations

Abbreviations: C-index, concordance index; GTR, gross total resection; OS, overall survival; PFS, progression-free survival; ROC, receiver operating characteristic; SEER, Surveillance, Epidemiology and End Results; STR, subtotal resection; WHO, World Health Organization.

TABLE 1 | Demographic characteristics of included 2358 cases with atypical meningioma.

Variable	Total n (%)	Training set n (%)	Validation set n (%)	P value
	2358	1888 (80.1)	470 (19.9)	
Sex				0.239*
Male	992 (42.1)	783 (41.5)	209 (44.5)	
Female	1366 (57.9)	1105 (58.5)	261 (55.5)	
Race				0.554*
White	1738 (73.7)	1385 (73.4)	353 (75.1)	
Black	325 (13.8)	258 (13.7)	67 (14.3)	
Other	275 (11.7)	229 (12.1)	46 (9.8)	
Unknown	20 (0.8)	16 (0.8)	4 (0.9)	
Age, years				0.192†
Range	20-93	20-93	21-90	
Mean	59.2 ± 15.0	59.4 ± 15.1	58.4 ± 14.8	
Median	60	61	60	
Location				0.981*
Cerebral meninges	2165 (91.8)	1731 (91.6)	434 (92.3)	
Meninges, NOS	165 (7.0)	132 (7.0)	33 (7.0)	
Cerebrum	2 (0.1)	2 (0.1)	0	
Frontal lobe	13 (0.6)	11 (0.6)	2 (0.4)	
Temporal lobe	2 (0.1)	2 (0.1)	0	
Parietal lobe	2 (0.1)	2 (0.1)	0	
Occipital lobe	2 (0.1)	2 (0.1)	0	
Cerebellum	2 (0.1)	2 (0.1)	0	
Brain, NOS	2 (0.1)	1 (0.1)	1 (0.2)	
Overlapping lesion of brain	2 (0.1)	2 (0.1)	0	
Pineal gland	1 (0)	1 (0.1)	0	
Year of diagnosis				0.846*
2004-2010	974 (41.3)	778 (41.2)	196 (41.7)	
2011-2016	1384 (58.7)	1110 (58.8)	274 (58.3)	
Laterality				0.164*
Bilateral	51 (2.2)	36 (1.9)	15 (3.2)	
Left	1072 (45.5)	868 (46.0)	204 (43.4)	
Right	1032 (43.8)	820 (43.4)	212 (45.1)	
Not a paired site	97 (4.1)	78 (4.1)	19 (4.0)	
Only one side	3 (0.1)	1 (0.1)	2 (0.4)	
Paired site	103 (4.4)	85 (4.5)	18 (3.8)	
Tumor size, mm				0.078†
Range	5-145	6-145	5-120	
Mean	49.3 ± 17.2	49.6 ± 17.2	48.0 ± 16.9	
Median	49	49	47	
Surgery				0.540*
Non-GTR	994 (42.2)	790 (41.8)	204 (43.4)	
GTR	1364 (57.8)	1098 (58.2)	266 (56.6)	
Radiation				0.076*
Yes	660 (28.0)	513 (27.2)	147 (31.3)	
None	1698 (72.0)	1375 (72.8)	323 (68.7)	

*Chi-square test.

†Independent t-test.

by nomogram, which suggested that the best discriminative ability of nomogram models.

The Validation Set

A total of 470 patients were included in the validation set. The median age at diagnosis was 60 years (range, 21-90 years), and the sex distribution showed a slight female predominance (n=261, 55.5%). 75.1% of patients (n=353) were white, 14.3% of patients (n=67) were black, and 10.7% of patients (n=50) were others and unknown. The median tumor size was 47mm, ranging from 5 to 120mm. Therapeutically, 266 (56.6%) patients underwent GTR and 147 (31.3%) patients received adjuvant radiation. We did not get the median OS. The 3, 5-, and 8-year OS rates were 87.5%, 80.3% and 69.0%, respectively, ranging from 1 to 155 months.

Univariate analysis revealed that age more than 67.5 years (HR=3.336, 95%CI=2.218-5.020; p<0.001) (**Figure 4A**), and tumor size more than 52.5 mm (HR=1.524, 95%CI=1.013-2.293; p=0.043) were significantly associated with worse survival (**Figure 4B**). GTR (HR=0.680, 95%CI=0.452-1.024; p=0.065) trending toward a better survival (**Figure 4C**). Multivariate analysis revealed that age more than 67.5 years (HR=3.474, 95%CI=2.304-5.239; p<0.001) and tumor size more than 52.5mm (HR=1.619, 95%CI=1.075-2.439; p=0.021) remained statistical significance (**Figure 5**).

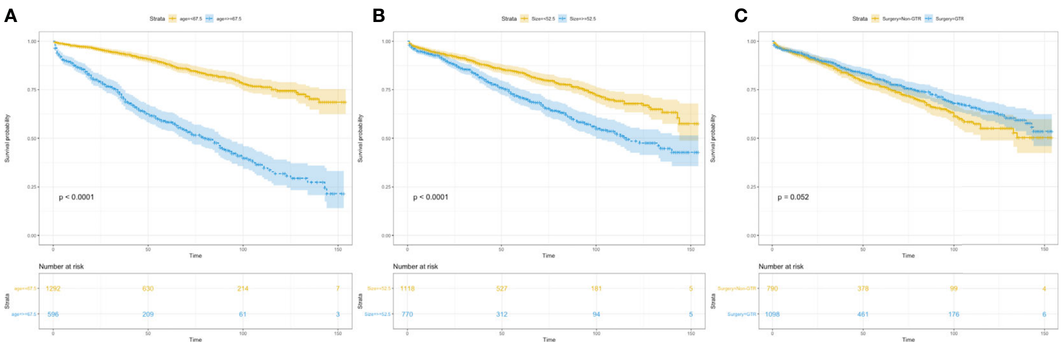

FIGURE 1 | Kaplan–Meier estimated overall survival in patients with atypical meningioma that were: age<67.5 years *vs*. age≥67.5 years **(A)** tumor size<52.5mm *vs*. tumor size≥52.5mm **(B)** non-gross total resection *vs*. gross total resection **(C)**.

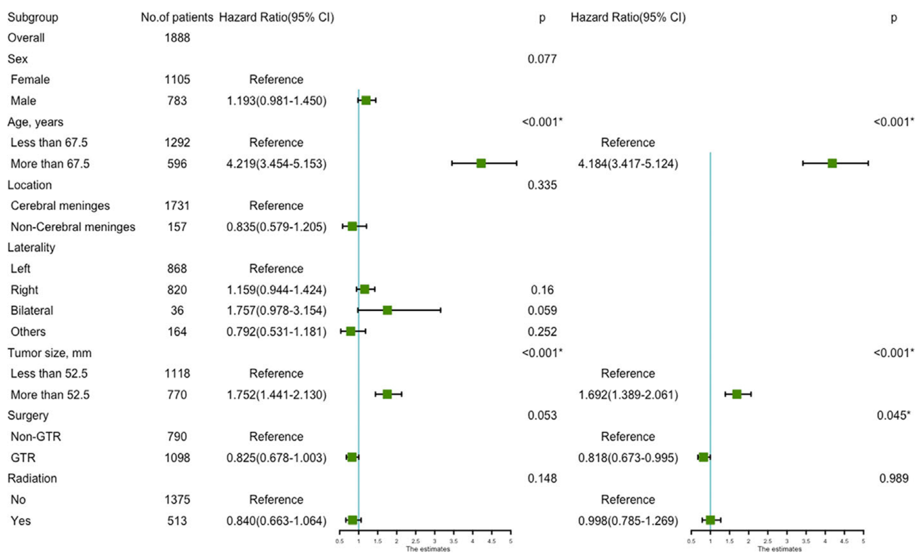

FIGURE 2 | The forest map of Cox regression analysis. Univariate and multivariate Cox regression analyses and estimating the risk factors for overall survival in the training set. *Means $P < 0.05$.

The prognostic nomogram (**Figure 6A**) comprised two significant factors (age and tumor size) and one therapeutic factor (surgery, p=0.051). The C-index was 0.688 (95%CI=0.629-0.747) for OS, the AUCs for ROC curves indicated that nomogram models had best risk discriminative ability (**Figure 6B**), and the predicted calibration curves were closed to the standard curves for 3-, 5-, and 8-year survival for OS (**Figures 6C–E**).

Risk Stratification

The total score was calculated for each patient in the training and validation sets, and the scores were divided into three subgroups for OS (0-14.1, 14.1-52, 52-152, training set; 0, 33-71.7, 71.7-171.7, validation set) to display different outcomes (**Supplementary Figure 2A** and **Figure 2B**).

To explore the role of adjuvant radiotherapy in addition to STR in survival, the entire cohort was divided into GTR and non-GTR groups. In the both GTR and non-GTR groups, there was no significant difference in survival between surgery alone and surgery with radiation. (Chi-square=0.018, p=0.893, log rank; GTR group). But, in the non-GTR group, surgery with radiation toward reaching a significantly increased survival compared with surgery alone (111.7 *vs*. 107.2 months) (Chi-square=2.363, p=0.124, log-rank; non-GTR group).

DISCUSSION

Prior to this study, to our best knowledge, there was no nomogram model for atypical meningioma, and because of

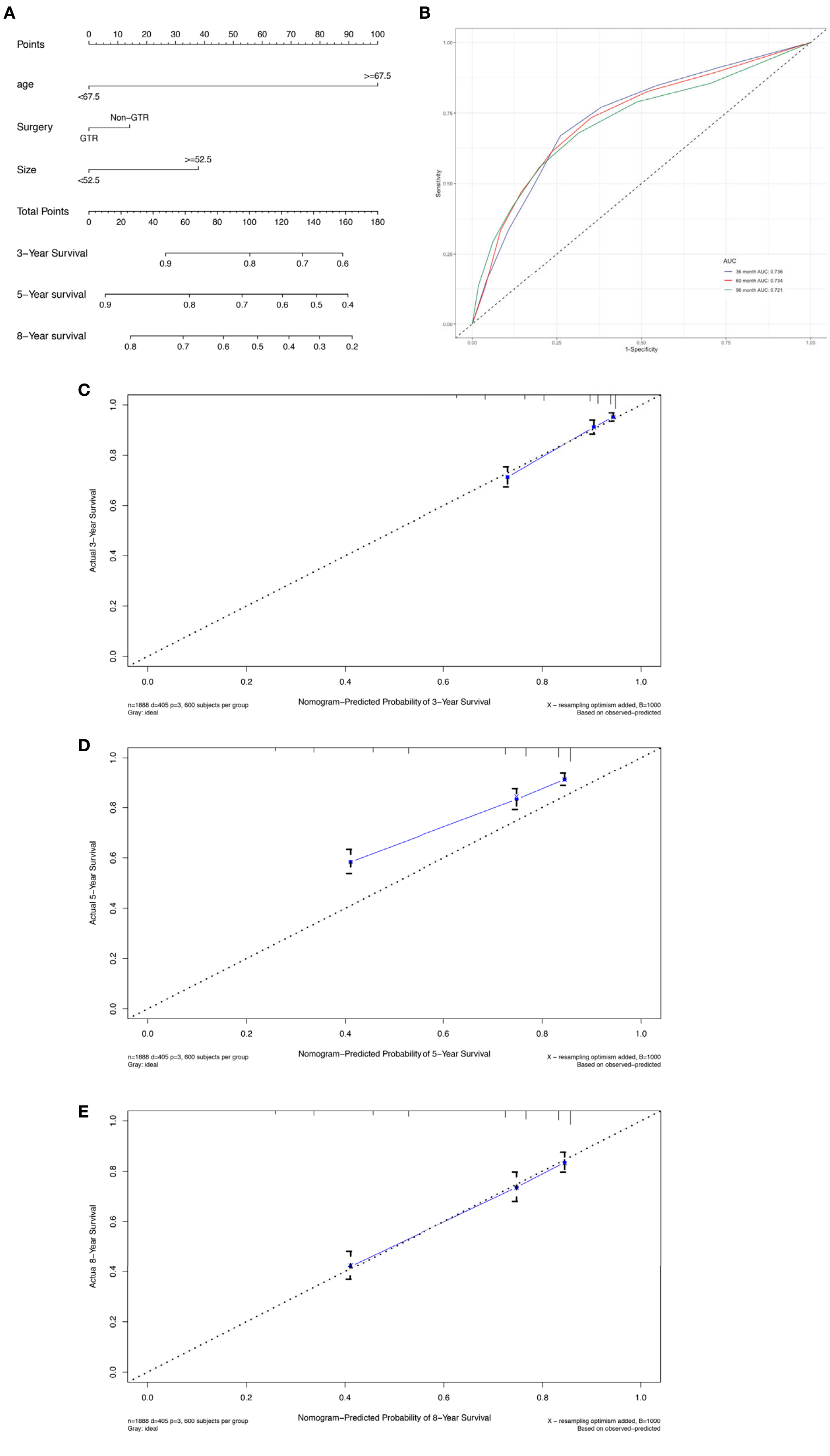

FIGURE 3 | Nomogram used to predict the 3-, 5- and 8-year OS rates of patients with atypical meningioma **(A)**. AUC curve of receiver operating character of the nomogram for predicting the 3-, 5- and 8- year overall rates of patients with atypical meningioma from the training set **(B)**. Calibration curve of the nomogram for predicting the 3- **(C)**, 5- **(D)** and 8- **(E)** year OS rates of patients with atypical meningioma from the training set.

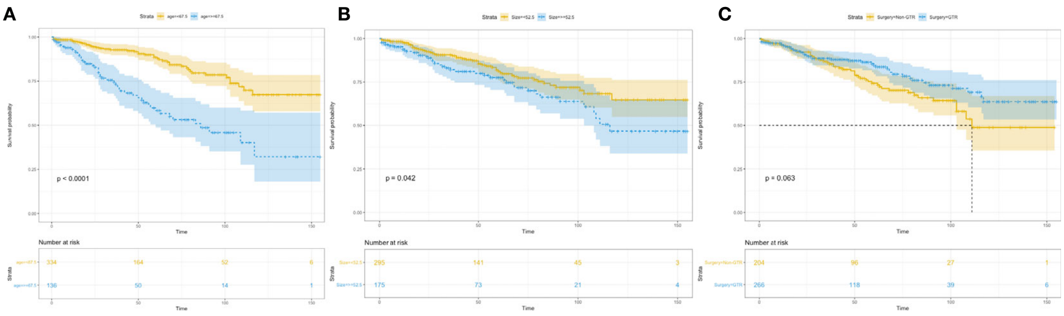

FIGURE 4 | Kaplan–Meier estimated overall survival in patients with atypical meningioma that were: age<67.5 years *vs*. age≥67.5 years **(A)** tumor size<52.5mm *vs*. tumor size≥52.5mm **(B)** non-gross total resection *vs*. gross total resection **(C)**.

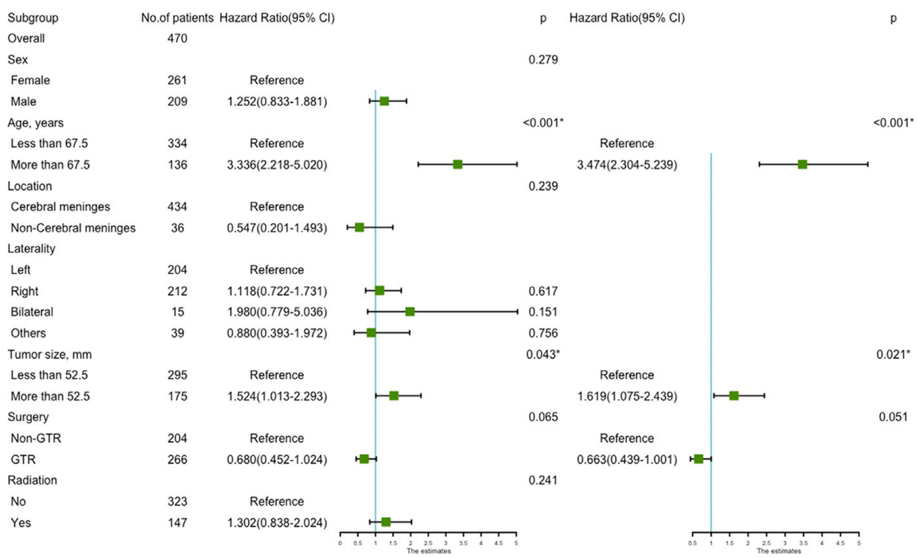

FIGURE 5 | The forest map of Cox regression analysis. Univariate and multivariate Cox regression analyses and estimating the risk factors for overall survival in the validation set. *Means $P < 0.05$.

this, a nomogram was developed based on a SEER database in this study. We identified the age, tumor size and surgical treatment as significant prognostic factors of OS. The nomogram established in this study not only was of high predictive power but also significant for clinical treatment.

Female sex showed a predominance in terms of incidence, and it conferred a toward OS advantage in univariate analysis. We were aware that most benign meningioma had slight prediction to affect female patients. But the potential relation between sex and survival in atypical meningioma need to be further explored. Older patients more than 67.5 years had an increased risk of mortality, in our study, compared with those who were under 67.5 years, which was consistent with previous studies (13–15).

A larger tumor size was found to be a paramount consideration associated with worse survival, which has been rarely reported by others. Larger tumor size had greater mass effect and more non-tumor tissues were involved at a high risk, which caused a difficulty for total resection.

Zaher et al. (13) reported on 44 patients with atypical meningioma who were surgically treated between 2009 and 2012, GTR was achieved in 16 cases and subtotal resection (STR) was achieved in 22 cases. A significant difference in OS between GTR and STR was observed in their study. Also, in a large series of 302 cases with atypical meningioma (16), the 3- and 5-year OS rates for GTR were 94.0% and 83.9%, respectively, and the 3- and 5- year OS rates for STR were 84.5% and 70.0%, respectively. Our study confirmed the findings of previous literature regarding complete resection statistically associated with increase in survival, which indicated that extent of resection was the most significant factor for outcome. On the contrary to us, some studies did not support the role of GTR in OS, although they demonstrated that GTR as a favorable factor of better progression-

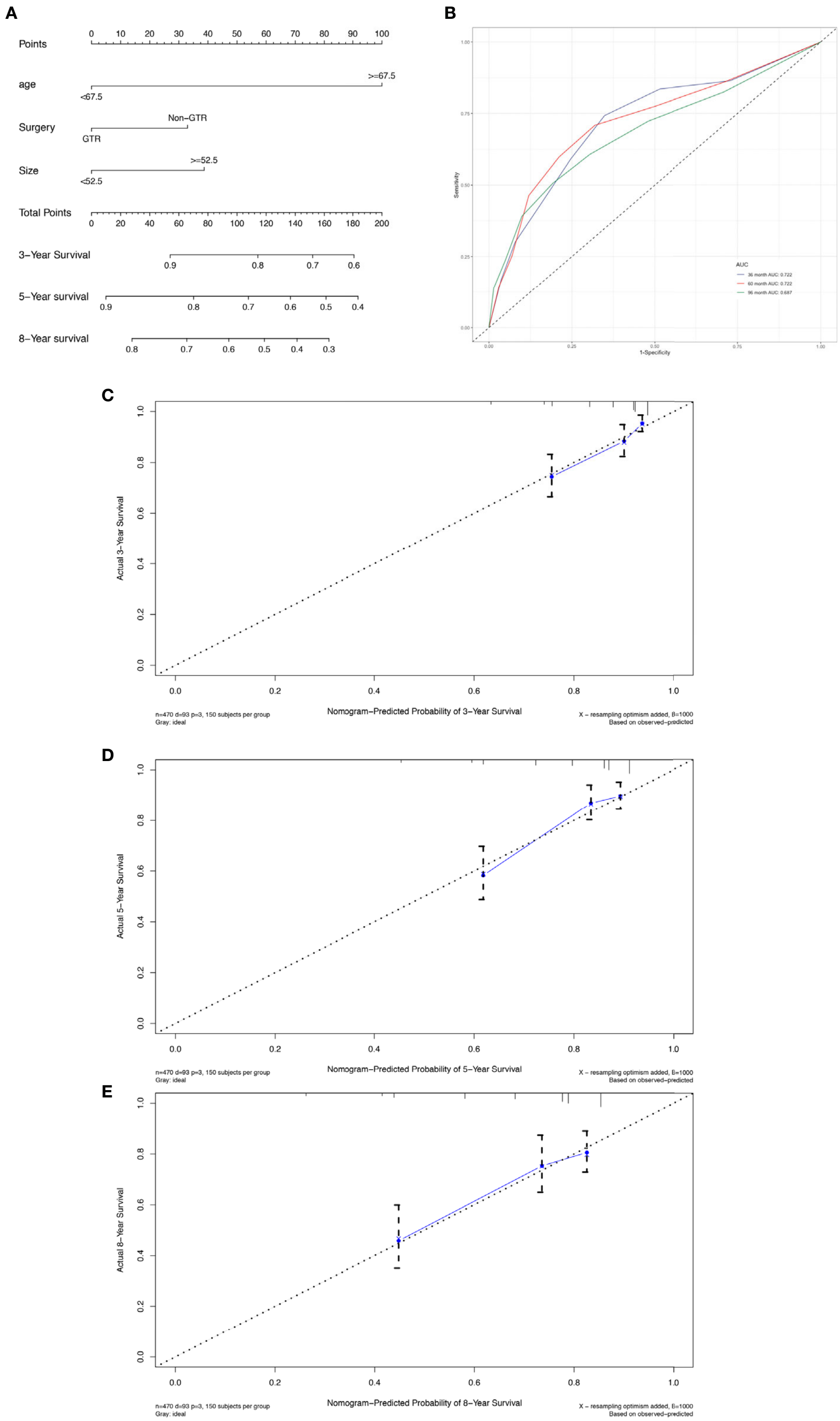

FIGURE 6 | Nomogram used to predict the 3-, 5- and 8-year OS rates of patients with atypical meningioma **(A)**. AUC curve of receiver operating character of the nomogram for predicting the 3-, 5- and 8- year overall rates of patients with atypical meningioma from the validation set **(B)**. Calibration curve of the nomogram for predicting the 3- **(C)**, 5- **(D)** and 8- **(E)** year OS rates of patients with atypical meningioma from the validation set.

free survival (PFS) (17). Moreover, many studies assessed the effect of surgery on PFS following surgery, rather than OS after surgery (7, 18). Our studies made up for the lack of association between surgery and OS in the historical process.

The effect of adjuvant radiotherapy on survival of patients with atypical meningioma remained controversial (14). In our study, adjuvant radiation was not statistically related to increased OS. A multi-institutional study of 166 patients with grade II meningioma (atypical meningioma, n=149) by Purand et al. (19) over 14 years showed radiation did not affect OS. In another series of 99 cases with atypical meningioma, 72.7% patients received adjuvant radiotherapy. A significant difference, between surgery alone and surgery with radiotherapy, was not observed in either PFS or OS (20). In addition, there was an observe trend toward reduced risk of mortality with non-GTR+ radiotherapy compared with non-GTR alone, but it did not reach a significance. Despite a large sample size, we failed to prove the significant role of radiation in addition to non-GTR in survival. While some studies showed benefits to adjuvant radiation only in patients who underwent STR, rather than GTR (21–23). But in MK et al. and HP et al. studies, they found that radiation after even GTR could contribute to an improvement in PFS (24, 25).

There were several limitations of this study. The nomogram was established based on SEER database in the United States, which was probably not representation of patients worldwide with atypical meningioma. Moreover, considering a retrospective study, some critical prognostic factors were not included in our study due to the limitations of SEER database, such as the clinical presentation, bone/brain invasion and tumor markers, which might affect survival. Additionally, it was unable to stratify for Simpson grades and tumor location (convexity *vs*. non-convexity) that might be potential factors of survival.

CONCLUSION

The proposal nomogram in this study accurately predicted the OS. Accordingly, GTR is an independent factor for survival, and radiation after non-GTR potentially confers a survival advantage for patients with atypical meningioma.

DATA AVAILABILITY STATEMENT

The original contributions presented in the study are included in the article/**Supplementary Material**. Further inquiries can be directed to the corresponding author.

AUTHOR CONTRIBUTIONS

Conception and experimental design: all authors. Acquisition of data: G-JZ and X-YL. Analysis and interpretation of data: all authors. Drafting the article: G-JZ. Critically revising the article: all authors. Study supervision: all authors. All authors contributed to the article and approved the submitted version.

FUNDING

Supported by 1.3.5 project for disciplines of excellence, West China Hospital, Sichuan University (NO. 2018HXFH010).

SUPPLEMENTARY MATERIAL

The Supplementary Material for this article can be found online at: https://www.frontiersin.org/articles/10.3389/fonc.2021.676683/full#supplementary-material

Supplementary Figure 1 | Study flow diagram

Supplementary Figure 2 | Kaplan–Meier curves of risk group stratifications within the training set for OS **(A)** and validation set for OS **(B)**.

REFERENCES

1. Apra C, Peyre M, Kalamarides M. Current Treatment Options for Meningioma. *Expert Rev Neurother* (2018) 18:241–9. doi: 10.1080/14737175.2018.1429920
2. Riemenschneider MJ, Perry A, Reifenberger G. Histological Classification and Molecular Genetics of Meningiomas. *Lancet Neurol* (2006) 5:1045–54. doi: 10.1016/S1474-4422(06)70625-1
3. Huffmann BC, Reinacher PC, Gilsbach JM. Gamma Knife Surgery for Atypical Meningiomas. *J Neurosurg* (2005) 102 Suppl:283–6. doi: 10.3171/sup.2005.102.s_supplement.0283
4. Yang SY, Park CK, Park SH, Kim DG, Chung YS, Jung HW. Atypical and Anaplastic Meningiomas: Prognostic Implications of Clinicopathological Features. *J Neurol Neurosurg Psychiatry* (2008) 79:574–80. doi: 10.1136/jnnp.2007.121582
5. Aizer AA, Bi WL, Kandola MS, Lee EQ, Nayak L, Rinne ML, et al. Extent of Resection and Overall Survival for Patients With Atypical and Malignant Meningioma. *Cancer* (2015) 121:4376–81. doi: 10.1002/cncr.29639
6. Endo T, Narisawa A, Ali HS, Murakami K, Watanabe T, Watanabe M, et al. A Study of Prognostic Factors in 45 Cases of Atypical Meningioma. *Acta Neurochir (Wien)* (2016) 158:1661–7. doi: 10.1007/s00701-016-2900-7
7. Park HJ, Kang HC, Kim IH, Park SH, Kim DG, Park CK, et al. The Role of Adjuvant Radiotherapy in Atypical Meningioma. *J Neurooncol* (2013) 115:241–7. doi: 10.1007/s11060-013-1219-y
8. Liu X, Shan B, Wang M, Xu J. World Health Organization Grade Ii Meningiomas: The Role of Adjuvant/Salvage Gamma Knife Surgery After Initial Surgery and Prognostic Factor Assessment. *World Neurosurgery* (2018) 109:e352–62. doi: 10.1016/j.wneu.2017.09.178
9. Hemmati SM, Ghadjar P, Grün A, Badakhshi H, Zschaeck S, Senger C, et al. Adjuvant Radiotherapy Improves Progression-Free Survival in Intracranial Atypical Meningioma. *Radiat Oncol* (2019) 14:160. doi: 10.1186/s13014-019-1368-z
10. Klinger DR, Flores BC, Lewis JJ, Hatanpaa K, Choe K, Mickey B, et al. Atypical Meningiomas: Recurrence, Reoperation, and Radiotherapy. *World Neurosurgery* (2015) 84:839–45. doi: 10.1016/j.wneu.2015.04.033
11. Zhang M, Ho AL, D'Astous M, Pendharkar AV, Choi CY, Thompson PA, et al. Cyberknife Stereotactic Radiosurgery for Atypical and Malignant Meningiomas. *World Neurosurgery* (2016) 91:574–81. doi: 10.1016/j.wneu.2016.04.019
12. Wang WH, Lee CC, Yang HC, Liu KD, Wu HM, Shiau CY, et al. Gamma Knife Radiosurgery for Atypical and Anaplastic Meningiomas. *World Neurosurg* (2016) 87:557–64. doi: 10.1016/j.wneu.2015.10.021

13. Zaher A, Abdelbari MM, Zayed DH, Ellatif RA, Ashamallah SA. Atypical Meningioma: A Study of Prognostic Factors. *World Neurosurgery* (2013) 80:549–53. doi: 10.1016/j.wneu.2013.07.001
14. Barthélemy E, Loewenstern J, Konuthula N, Pain M, Hall J, Govindaraj S, et al. Primary Management of Atypical Meningioma: Treatment Patterns and Survival Outcomes by Patient Age. *J Cancer Res Clin Oncol* (2018) 144:969–78. doi: 10.1007/s00432-018-2618-4
15. Streckert E, Hess K, Sporns PB, Adeli A, Brokinkel C, Kriz J, et al. Clinical, Radiological, and Histopathological Predictors for Long-Term Prognosis After Surgery for Atypical Meningiomas. *Acta Neurochir (Wien)* (2019) 161:1647–56. doi: 10.1007/s00701-019-03956-8
16. Li H, Zhang YS, Zhang GB, Zhang GJ, Wang B, Li D, et al. Treatment Protocol, Long-Term Follow-Up, and Predictors of Mortality in 302 Cases Of Atypical Meningioma. *World Neurosurgery* (2019) 122:e1275–84. doi: 10.1016/j.wneu.2018.11.032
17. Nanda A, Bir SC, Konar S, Maiti T, Kalakoti P, Jacobsohn JA, et al. Outcome of Resection of WHO Grade II Meningioma and Correlation of Pathological and Radiological Predictive Factors for Recurrence. *J Clin Neurosci* (2016) 31:112–21. doi: 10.1016/j.jocn.2016.02.021
18. Mair R, Morris K, Scott I, Carroll TA. Radiotherapy for Atypical Meningiomas. *J Neurosurg* (2011) 115:811–9. doi: 10.3171/2011.5.JNS11112
19. Durand A, Labrousse F, Jouvet A, Bauchet L, Kalamaridès M, Menei P, et al. WHO Grade II and III Meningiomas: A Study of Prognostic Factors. *J Neurooncol* (2009) 95:367–75. doi: 10.1007/s11060-009-9934-0
20. Zhu H, Bi WL, Aizer A, Hua L, Tian M, Den J, et al. Efficacy of Adjuvant Radiotherapy for Atypical and Anaplastic Meningioma. *Cancer Med* (2019) 8:13–20. doi: 10.1002/cam4.1531
21. Kaur G, Sayegh ET, Larson A, Bloch O, Madden M, Sun MZ, et al. Adjuvant Radiotherapy for Atypical and Malignant Meningiomas: A Systematic Review. *Neuro Oncol* (2014) 16:628–36. doi: 10.1093/neuonc/nou025
22. Simon M, Boström J, Koch P, Schramm J. Interinstitutional Variance of Postoperative Radiotherapy and Follow Up for Meningiomas in Germany: Impact of Changes of the WHO Classification. *J Neurol Neurosurg Psychiatry* (2006) 77:767–73. doi: 10.1136/jnnp.2005.077974
23. Weber DC, Lovblad KO, Rogers L. New Pathology Classification, Imagery Techniques and Prospective Trials for Meningiomas: The Future Looks Bright. *Curr Opin IN Neurol* (2010) 23:563–70. doi: 10.1097/WCO.0b013e328340441e
24. Bagshaw HP, Burt LM, Jensen RL, Suneja G, Palmer CA, Couldwell WT, et al. Adjuvant Radiotherapy for Atypical Meningiomas. *J Neurosurg* (2017) 126:1822–8. doi: 10.3171/2016.5.JNS152809
25. Aghi MK, Carter BS, Cosgrove GR, Ojemann RG, Amin-Hanjani S, Martuza RL, et al. Long-Term Recurrence Rates of Atypical Meningiomas After Gross Total Resection With or Without Postoperative Adjuvant Radiation. *Neurosurgery* (2009) 64:56–60, 60. doi: 10.1227/01.NEU.0000330399.55586.63

Conflict of Interest: The authors declare that the research was conducted in the absence of any commercial or financial relationships that could be construed as a potential conflict of interest.

frontiers in Oncology

ORIGINAL RESEARCH
published: 21 June 2021
doi: 10.3389/fonc.2021.693063

Check for updates

Outcomes and Complications of Aggressive Resection Strategy for Pituitary Adenomas in Knosp Grade 4 With Transsphenoidal Endoscopy

Taohui Ouyang[1†], Na Zhang[2†], Shenhao Xie[1], Bin Tang[1], Junjun Li[3], Limin Xiao[1], Fabao Zhang[4], Bowen Wu[1], Dongwei Zhou[1], Meihua Li[1] and Tao Hong[1]*

[1] *Department of Neurosurgery, the First Affiliated Hospital of Nanchang University, Nanchang, China,* [2] *Department of Neurology, the First Affiliated Hospital of Nanchang University, Nanchang, China,* [3] *Department of Neurosurgery, Wuhan Union Hospital, Wuhan, China,* [4] *Department of Radiology, the First Affiliated Hospital of Nanchang University, Nanchang, China*

OPEN ACCESS

Edited by:
Xicai Sun,
Fudan University, China

Reviewed by:
Tomasz Dziedzic,
Medical University of Warsaw, Poland
Ye Gu,
Fudan University, China
Renzhi Wang,
Peking Union Medical College Hospital (CAMS), China

***Correspondence:**
Tao Hong
ht2000@vip.sina.com

†These authors have contributed equally to this work

Specialty section:
This article was submitted to Surgical Oncology, a section of the journal Frontiers in Oncology

Received: 09 April 2021
Accepted: 20 May 2021
Published: 21 June 2021

Citation:
Ouyang T, Zhang N, Xie S, Tang B, Li J, Xiao L, Zhang F, Wu B, Zhou D, Li M and Hong T (2021) Outcomes and Complications of Aggressive Resection Strategy for Pituitary Adenomas in Knosp Grade 4 With Transsphenoidal Endoscopy. Front. Oncol. 11:693063. doi: 10.3389/fonc.2021.693063

Surgery for pituitary adenomas (PAs) with cavernous sinus (CS) invasion in Knosp grade 4 is a great challenge and whether to adopt a conservative or aggressive surgical strategy is controversial. The aim of this study is to provide the outcomes and complications of an aggressive resection strategy for Knosp grade 4 PAs with transsphenoidal endoscopic surgery. Outcomes and complications were retrospectively analyzed in 102 patients with Knosp grade 4 PAs. Among them, primary PAs were seen in 60 patients and recurrent PAs were seen in 42 cases. Gross total resection (GTR) of the entire tumor was achieved in 72 cases (70.6%), subtotal tumor resection (STR) in 18 cases (17.6%), and partial tumor resection (PTR) in 12 cases (11.8%). Additionally, GTR of the tumor within the CS was achieved in 82 patients (80.4%), STR in 17 patients (16.7%), and PTR in 3 patients (2.9%). Statistical analyses showed that both recurrent tumors and firm consistency tumors were adverse factors for complete resection ($P<0.05$). Patients with GTR of the entire tumor were more likely to have favorable endocrine and visual outcomes than those with incomplete resection ($P<0.05$). Overall, the most common surgical complication was new cranial nerve palsy (n=7, 6.8%). The incidence of internal carotid artery (ICA) injury and postoperative cerebrospinal fluid (CSF) leakage was 2.0% (n=2) and 5.9% (n=6), respectively. Six patients (5.9%) experienced tumor recurrence postoperatively. For experienced neuroendoscopists, an aggressive tumor resection strategy *via* transsphenoidal endoscopic surgery may be an effective and safe option for Knosp grade 4 PAs.

Keywords: endoscopic, cavernous sinus, pituitary adenoma, outcome, surgery

INTRODUCTION

Pituitary adenomas (PAs) are the third most common primary intracranial tumor, following meningiomas and gliomas, accounting for about 10% to 25% of intracranial tumors (1, 2). Some PAs invade surrounding structures such as the diaphragma sellae, the sphenoid sinus, and the cavernous sinus (CS), with approximately 10% involving the CS (3, 4). PAs invading the CS are particularly surgically challenging due to their close proximity to critical neurovascular structures and their deep intracranial location.

For PAs with CS invasion, surgical approaches include transcranial microscopy, transsphenoidal microscopy, and transsphenoidal endoscopy. Transcranial microscopy is a "lateral to medial" approach that basically entails entering from the lateral wall of the CS where multiple cranial nerves are located (5, 6). In addition, surgical visualization when utilizing the transcranial microscopy approach is often insufficient. These disadvantages support the argument that transcranial microscopic surgery is not an ideal approach for the removal of PAs with CS invasion. Since its introduction, the transsphenoidal approach has been continuously refined and popularized, and to date is the most common approach for PAs. Transsphenoidal approach is a "medial to lateral" approach that enters the CS through the medial CS wall, thereby avoiding direct obstruction by the cranial nerves within the lateral CS wall. Moreover, PAs invade the CS in a medial to lateral direction, often pushing the CS contents medially to laterally. Therefore, the transsphenoidal approach is an excellent and logical route for the removal of PAs within the CS through the medial CS wall. However, certain limitations such as a narrow surgical corridor and insufficient visualization, confine use of the transsphenoidal microscopic approach to those PAs with mild CS invasion (Knosp grades 1-2) (7). Compared with transsphenoidal microscopy, transsphenoidal endoscopic surgery not only improves surgical visualization, but also provides greater exposure to the lateral CS extension of tumors (7, 8). Consequently, transsphenoidal endoscopic surgery is the preferred choice for PAs with severe CS invasion (Knosp grades 3-4) (9, 10).

For PAs with severe CS invasion, especially grade 4 PAs, gross total resection (GTR) with transsphenoidal endoscopic surgery still presents a great challenge. To illustrate, Hwang et al. (11) retrospectively examined data on 275 patients with non-functional PAs with CS invasion from 2000-2012, and reported a GTR rate of 5.9% in transsphenoidal endoscopy for grade 4 PAs. This low GTR rate reflects the conservative strategy regarding tumor resection, but it also indicates that in some cases with grade 4 PAs, GTR can be achieved by transsphenoidal endoscopic surgery. Of note, these cases occurred a decade ago when transsphenoidal endoscopic technology was still in its infancy.

With the recent, rapid development in transsphenoidal endoscopic techniques and advances made through in-depth study of the endoscopic anatomy of the CS (12, 13), as well as the availability of intraoperative neuronavigation, doppler ultrasonography, and cranial nerve monitoring, it is worth reconsidering whether it is best to adopt a conservative or aggressive surgical strategy for grade 4 PAs. The current study provides the outcomes and complications of an aggressive surgical strategy for 102 patients with grade 4 PAs treated by transsphenoidal endoscopic surgery performed by the same surgeon.

MATERIALS AND METHODS

Clinical Materials

Between January 2014 and August 2020, 908 consecutive patients undergoing transsphenoidal endoscopic surgery for PAs were evaluated. A total of 102 patients were included in this study according to the following criteria: 1) Knosp grade 4 PAs identified jointly by a neuroradiologist and two neurosurgeons; 2) Complete preoperative and postoperative magnetic resonance imaging (MRI) data and follow-up data; and 3) All operations performed by the same neurosurgeon (Tao Hong). A total of 4 cases were excluded due to lack of complete follow-up data. Hospital review board approval was obtained from the Institutional Ethics Committee of the First Affiliated Hospital of Nanchang University.

Neuroradiological Evaluation

MRI examination was performed for all patients to evaluate tumor size and volume. Tumors with a maximum diameter (MD) of more than 1 cm were defined as macroadenomas, and tumors with a MD of more than 4 cm were defined as giant PAs. Tumor volume was approximated by calculations using the sphericity formula $(A \times B \times C) \times \pi/6$, where A, B and C represent the maximum length in three dimensions of the PA. Extent of resection for the entire tumor and tumors within the CS were analyzed and the extent of resection was then classified into categories: gross-total resection (GTR) (no residual enhancing lesion), subtotal tumor resection (STR) (residual enhancing lesion $\leq$ 20%) and partial tumor resection (PTR) (residual enhancing lesion >20%).

Evaluation of the Internal Carotid Artery (ICA)

A preoperative balloon occlusion test was used to evaluate the contralateral compensatory capability of the ICA in case of injury. Although the anatomy of the ICA was generally consistent, the shape of the ICA under the influence of the tumor was inconsistent and individualized depending on the tumor location. Preoperatively, three-dimensional (axial, coronal, and sagittal) MRI was used to individually analyze the spatial relationship between the ICA and the CS tumor, and further, to determine the size of the space for each compartment within the CS. For example, when the horizontal ICA was inferior to the tumor, it caused the horizontal ICA to sink due to the depression of the tumor, resulting in a larger posterosuperior compartment and a smaller anteroinferior compartment within the CS. When the horizontal ICA was superior to the tumor, it caused the horizontal ICA to be raised by the tumor, leading to a smaller posterosuperior compartment and a larger anteroinferior compartment within the CS. When the horizontal ICA was in the middle of the tumor, the result was a combination of the above two conditions, leaving large posterosuperior and anteroinferior compartments.

Endoscopic Surgery of PA in Knosp Grade 4

For PAs invading the CS, transsphenoidal endoscopic surgery mainly included medial (transsphenoidal transsellar) and lateral (transmaxillary transpterygoidal) approaches. The medial approach was used to remove tumors in the posterosuperior and lateral compartments of the CS. The lateral approach, including an anteroinferior approach and a lateral-superior approach, was used to open the pterygopalatine fossa to obtain more exposure, and to remove tumors in the anteroinferior and lateral compartments of the CS. These approaches were shown in **Figure 1**. An angular endoscope was used to obtain different angles of surgical field visualization, and various other angular instruments were used to

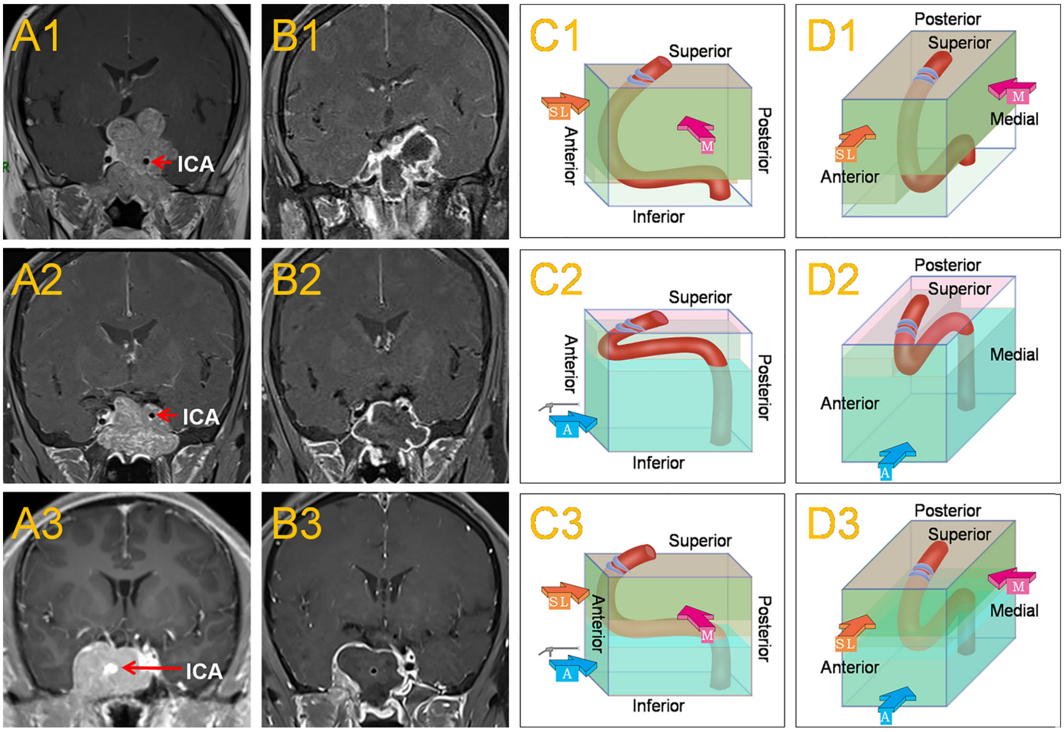

FIGURE 1 | This shows the common location of the horizontal ICA in Knosp grade 4 PAs and the main surgical approaches. When the horizontal ICA was inferior to the tumor **(A1)**, it caused the horizontal ICA to sink due to the oppression of the tumor, resulting in a larger posterosuperior compartment and a smaller anteroinferior compartment within the CS. The medial approach, often combined with the superior-lateral approach was mainly used to remove the tumor **(C1, D1)**. Postoperative MRI revealed a subtotal resection of the tumor **(B1)**.When the horizontal ICA was superior to the tumor **(A2)**, it caused the horizontal ICA to be raised by the tumor, leading to a smaller posterosuperior compartment and a larger anteroinferior compartment within the CS. The anteroinferior approach was mainly used to remove the tumor **(C2, D2)**. Postoperative MRI revealed a total resection of the tumor **(B2)**. When the horizontal ICA was in the middle of the CS tumor **(A3)**, which was a combination of the two conditions, then the medial, superior-lateral, and anteroinferior approaches could be used **(C3, D3)**. Postoperative MRI revealed a total resection of the tumor **(B3)**. The red, thick arrow 'M' represents the medial approach, the orange-yellow, thick arrow 'SL' represents the superior-lateral approach, and the blue, thick arrow 'A' represents the anteroinferior approach.

assist with the medial and lateral approaches. In many cases, a combination of medial and lateral approaches was required to radically remove the tumor. Intraoperative navigation and doppler ultrasonography were used to assist in determining the exact position and shape of the ICA. Before entering the CS to remove the tumor, the proximal end (paraclivus segment) of the ICA was exposed in order to temporarily block the proximal end in the event of injury to the ICA. Based on these analyses above, the individual spatial relationship among the ICA, the CS tumor, and various compartments of the CS were evaluated in order to determine the point of entry to the CS and the type of surgical approach to take within the CS. For example, when the horizontal ICA was inferior to the tumor, first, the medial wall of the CS was opened into the posterosuperior compartment of the CS, and then a combination of angle endoscopy and the medial approach was used to remove the tumor in the posterosuperior and lateral compartments. With this approach, the tumor extending into the oculomotor nerve triangle of the posterosuperior compartment might remain unresectable; in this case, a combination of the lateral-superior approach and the medial approach was required. When the horizontal ICA was superior to the tumor, first, the anterior wall of the CS was opened and then the anteroinferior approach was used to remove the tumor in the anteroinferior compartment and a lateral-superior approach was used for removing the tumor in the lateral compartment. When the horizontal ICA was in the middle of the CS tumor, which is a combination of the two conditions, then various approaches could be used. Particularly, in some special cases, such as when the ICA was medial to the tumor, which was common in recurrent tumors, a lateral approach was used to remove the tumor. When the ICA was lateral to the tumor, a medial approach alone was used. During tumor resection, any adhesion between the ICA and the abducens nerve requires sharp dissection to avoid injury to the abducens nerve. Care also needs to be taken to avoid injury to the oculomotor nerve in the removal of tumors within the posterosuperior compartment of the CS or even when extending to the temporal lobe through the oculomotor nerve triangle.

After tumor removal, the multilayered method of fat + artificial dura + fascia lata + pedicled mucosal flap + biological glue was used to reconstruct the sellar floor. For patients at high risk of cerebrospinal fluid (CSF) leakage, a lumbar puncture catheter drainage system was used to release CSF to prevent CSF leakage after surgery.

Endocrinological Assessment

Endocrinological results of all the patients were evaluated preoperatively and at 3 months postoperatively. Hormone remission was based on the following criteria (14–17): for prolactin (PRL)-secreting adenomas, serum PRL <20 ng/mL in female patients or, <15 ng/mL in male patients; for adrenocorticotropic hormone (ACTH)-secreting adenomas, a serum cortisol nadir of < 2 mg/dL or normal 24-hour urinary free cortisol test at 3 months; and for growth hormone (GH)-secreting tumors, normalization of serum insulin-like growth factor-1 level (IGF-1), basal serum GH <2.5 ng/mL, or an oral glucose tolerance test of 0.4 ng/mL. During the test, IGF-1 levels were expressed relative to the upper limit of the patient's normal values for the patient's age and sex. The first choice for the treatment of PRL-secreting adenomas was drugs, and surgical indications were mainly drug-resistant tumors and drug intolerance, and rarely, patient choice.

Visual Assessment

All patients received preoperative and postoperative formal visual function examinations. During follow-up, a visual examination was performed at 3 months, postoperatively.

Statistical Analysis

Statistical analyses comparing categorical variables were performed using X^2 tests or Fisher's exact tests. A two-tailed $P<0.05$ was considered to be statistically significant. Data were analyzed using SPSS version 25.0 (IBM Corporation, Armonk, New York).

TABLE 1 | Demographic and clinical characteristics of the 102 patients with pituitary adenomas invading the CS.

Variables	Value
Mean age, years (range)	39.1 (24~71)
Females (%)	53 (52.0)
Preoperative manifestation	
High hormone level (%)	40 (39.0)
Headache (%)	33 (32.4)
Visual dysfunction (%)	38 (37.3)
Cranial nerve palsy (%)	6 (5.9)
Incidental discovery (%)	8 (7.8)
Endocrinological types	
Non-functional (%)	62 (60.8)
GH (%)	13 (12.7)
GH/PRL mixed (%)	10 (9.8)
PRL (%)	9 (8.8)
ACTH (%)	5 (4.9)
FSH (%)	2 (2.0)
TSH (%)	1 (1.0)
Direction of invasion	
Bilateral (%)	36 (35.3)
Unilateral (%)	66 (64.7)
Left (%)	35 (53.0)
Right (%)	31 (47.0)
Contralateral (%)	
Knosp 0 (%)	19 (28.8)
Knosp 1 (%)	17 (25.8)
Knosp 2 (%)	14 (21.2)
Knosp 3 (%)	16 (24.2)
Size of tumor	
Giant pituitary adenoma	39 (38.2)
Macroadenoma	63 (61.8)
Volume of tumor (V, cm^3)	
V<15	22 (21.6)
15≤V ≤ 30	37 (36.3)
>30	43(42.1)
Previous treatment	
No surgery (%)	60 (58.8)
Craniotomy (%)	5 (4.9)
Transnasal microscopy (%)	12 (11.8)
Transnasal endoscopic (%)	15 (14.7)
Mixed surgery (%)	10 (9.8)
Radiotherapy (%)	16 (15.7)

RESULTS

Patient Population and Clinical Presentation

The 102 patients in the final analysis included 53 females and 49 males, of mean age 39.1 years (range 24-71 years). Primary PAs were seen in 60 patients and recurrent PAs were seen in 42 cases. Preoperative headache symptoms were seen in 33 patients (32.4%), visual dysfunction in 38 patients (37.3%), incidental discovery in 8 patients (7.8%), and cranial nerve palsy in 6 patients (5.9%). The detailed results are shown in **Table 1**.

Neuroradiological Outcomes

Of the 102 cases, 39 patients had giant PAs and 63 patients had macroadenomas. The median tumor volume in all patients was 23.8 cm^3, ranging from 1.63~182 cm^3. In 36 patients, bilateral CS invasion was in grade 4, while unilateral CS invasion in grade 4 was observed in 66 patients (**Table 1**).

Extent of Resection

GTR of the entire tumor was achieved in 72 cases (70.6%), STR in 18 cases (17.6%), and PTR in 12 cases (11.8%). **Figure 2** illustrated the GTR of the entire tumor. For tumors within the CS, GTR was achieved in 82 patients (80.4%), STR in 17 patients (16.7%), and PTR in 3 patients (2.9%). The GTR rates of the entire lesion and the CS lesion in the primary tumor were 80% and 91.7%, respectively, while the GTR rates of the entire lesion and the CS lesion in recurrent tumors were 57.1% and 64.3%, respectively. These results are shown in **Tables 2** and **3**. Statistical analyses showed that recurrent tumors and firm consistency tumors had lower GTR rates ($p<0.05$). However, no statistical differences were found between tumor size or tumor volume and the extent of resection ($p>0.05$). Additionally, there was no statistically significant relationship between extent of resection and postoperative CSF leakage or cranial nerve palsy ($p>0.05$). These results are shown in **Tables 3** and **4**.

Surgical Complications

Surgical complications were uncommon. Overall, the most common complications were new cranial nerve palsy (n=7,

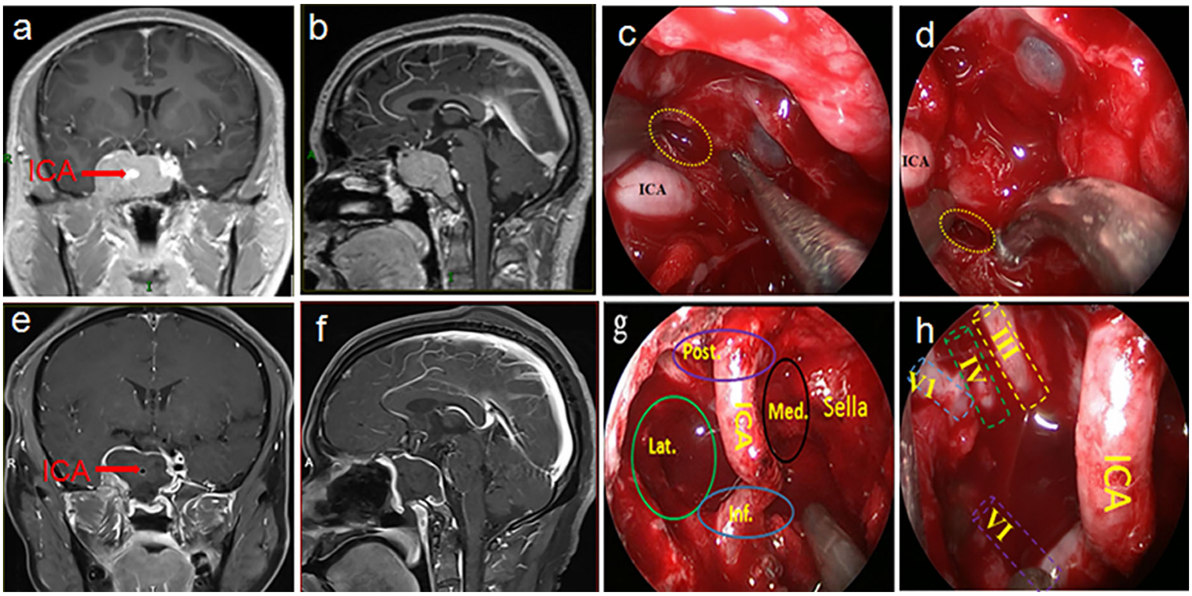

FIGURE 2 | This was a 32-year-old male patient who was admitted to hospital after the accidental discovery of a pituitary tumor due to trauma. The preoperative visual examination was normal, and the preoperative PRL and ACTH hormones were increased. A preoperative MRI **(A, B)** showed that the tumor was in Knosp grade 4 and was mainly distributed in both posterosuperior and anteroinferior compartments of the CS. Intraoperatively, various compartments **(G)** and nerves **(H)** in the CS could be observed after total tumor resection. Postoperative MRI **(E, F)** also confirmed total tumor resection. The yellow dotted circle indicated entry into the CS from above **(C)** and below **(D)** the horizontal ICA. The pathological examination of the tumor was mixed pituitary adenoma. The visual and endocrine function of the patient were all normal three months after the operation. Post., posterior compartment; Med., medial compartment; Lat., lateral compartment; Inf., inferior compartment; ICA, internal carotid artery; III, oculomotor nerve; IV, trochlear nerve; V1, first branch of the trigeminal nerve; VI, abducens nerve.

6.8%) (**Table 5**), followed by postoperative CSF leakage (n=6, 5.9%), intracranial infection (n=5, 4.9%), and ICA injury (n=2, 2.0%). New cranial nerve palsy consisted of oculomotor nerve and abducens nerve palsy, with an incidence of 3.9% and 2.9%, respectively. For the two patients with ICA injury, the injured ICA was completely clipped in one patient, and the ICA wall was electrocoagulated in the other patient. During the follow-up period, both patients underwent cerebral angiography; no pseudoaneurysm formation was found, and no obvious symptoms were observed. CSF leakage occurred in 6 patients and was managed by lumbar puncture catheter drainage in 2 patients and endoscopic repair surgery in the remaining 4 cases. Of the 5 patients with intracranial infection, 4 patients recovered through the use of antibiotics and lumbar puncture catheter drainage, and the remaining 1 patient died of infection.

Endocrinological Outcomes

Of the 102 patients, 40 cases (39.2%) were classified as functional PAs, and hormone remission was seen in 29 of these 40 patients (72.5%), postoperatively. Statistical analysis showed no statistical differences between endocrine outcomes and tumor size, tumor recurrence, or extent of CS lesion (p>0.05). However, for the entire tumor, patients with GTR had better endocrine outcomes than those with incomplete resection, and the difference was statistically significant (p=0.028). These results are shown in **Table 6**.

Visual Outcomes

Preoperative visual dysfunction was found in 38 patients, of which 28 patients (73.7%) improved postoperatively. For the entire tumor, the visual improvement rate was 90.9% in the GTR group, compared with 63.6% in the STR group and 20.0% in the PTR group. The difference between the three groups was statistically significant (p=0.003). However, preoperative visual function, extent of resection of CS lesion, tumor size, tumor volume, tumor recurrence or tumor consistency were not significantly associated with postoperative visual outcomes (p>0.05). These results are shown in **Table 7**.

Follow-Up Results

The follow-up period was 7-87 months, with an average of 46 months. Postoperatively, of the 30 patients with incomplete tumor resection, 5 patients with functional PAs received medical treatment and 12 patients (1 patient with functional PA and 11 patients with non-functional PAs) received radiotherapy. Among the 7 patients with postoperative new cranial nerve palsy, improvement was observed in 3 patients. For the 6 patients with preoperative cranial nerve palsy, improvement was seen in 4 patients. Six patients, including four patients with PTR, one with STR and one with GTR, experienced tumor recurrence and accepted reoperation. The follow-up methods were conducted through outpatient visits and telephone calls.

TABLE 2 | Surgical results and postoperative complications in the 102 patients who underwent transsphenoidal endoscopic surgery for pituitary adenomas in Knosp Grade 4.

Variable	Value
Extent of resection	
GTR (%)	72 (70.6)
STR (%)	18 (17.6)
PTR (%)	12 (11.8)
Extent of CS resection	
GTR (%)	82 (80.4)
STR (%)	17 (17.6)
PTR (%)	3 (2.0)
Intraoprative variables	
Mean operation time (min)	158.5
Mean intraoperative hemorrhage (ml)	456.7
Firm consistency (%)	31 (30.4)
ICA rupture (%)	2 (2.0)
CSF leakage (%)	11 (10.8)
Postoperative variables	
Headache	33
Better (%)	22 (66.7)
No change (%)	11 (33.3)
Visual dysfunction	38
Better (%)	28 (73.7)
No change (%)	10 (26.3)
Hormone remission	40
Yes (%)	29 (72.5)
No (%)	11 (27.5)
Postoperative complications	
abducens nerve palsy (%)	3 (2.9)
oculomotor nerve palsy (%)	4 (3.9)
CSF leakage (%)	6 (5.9)
CNS infection (%)	5 (4.9)
Monocular blindness (%)	2 (2.0)
Panhypopituitarism (%)	3 (2.9)
Permanent diabetes insipidus (%)	2 (2.0)
Follow-up treatments	
Radiotherapy (%)	12 (11.8)
Medical therapy (%)	5 (4.9)
Recurrence (%)	6 (5.9)

GTR, gross total resection; STR, subtotal tumor resection; PTR, partial tumor resection; CS, cavernous sinus; CSF, cerebrospinal fluid; CNS, Central Nervous System; ICA, Internal carotid artery.

DISCUSSION

Outcomes of Aggressive Tumor Resection

Extent of Resection

This study outlines the surgical outcomes and experiences of 102 patients with grade 4 PAs who underwent endoscopic transsphenoidal surgery. To date, this is the largest study conducted on grade 4 PAs, and is the first study to specifically focus on functional and non-functional grade 4 PAs. One of the study's strengths is that all of the surgeries in this study were performed by the same surgeon, eliminating variability and rendering more credibility to the study results. Management of the intracavernous ICA contributes to some of the challenges surrounding the surgical removal of grade 4 PAs. To address this, individual spatial relationships among the ICA, the CS tumor, and various compartments of the CS were evaluated in detail preoperatively, and different CS approaches were adopted, accordingly. For example, when the horizontal ICA was superior to the tumor, the anterior wall of the CS was opened, and then an anteroinferior approach was used to remove the tumor from within the anteroinferior compartment, while a lateral-superior approach was used to remove the tumor from within the lateral compartment. This study represents the first time that these methods were carried out for grade 4 PAs. In this study, an aggressive resection strategy was adopted, not only for tumors in the medial CS, but also for tumors in the lateral CS. This approach differs from the previous surgical resection strategies of Woodworth et al. (18) and Toda et al. (19). Their surgical concept included using an aggressive strategy for tumors in the medial CS and a conservative strategy for tumors in the lateral CS. Both reported GTR rates for grade 4 PAs of no more than 10%. However, our study reported a GTR rate of 70.6%, which is significantly higher than the GTR rates (from 0 to 53.8%) reported in the previous literature (19–27) (**Table 8**). Of note, while we adopted an aggressive tumor resection strategy to obtain a considerable GTR rate, the incidence of surgical complications was still within an acceptable range. This indicates the feasibility and efficacy of aggressive resection strategy *via* transsphenoidal endoscopic surgery for grade 4 PAs.

Factors Influencing the Extent of Resection

The factors that influence the extent of resection for grade 4 PAs are unclear, because no previous study has ever specifically examined these potential factors. Any previous studies that did report on potential factors influencing the extent of resection included common PAs without CS invasion, or invasive PAs with varying extents of CS involvement. Chabot et al. (28) found that factors influencing the extent of resection included tumor recurrence, preoperative hormone replacement therapy, and Knosp grade. Bao et al. (24) also found that tumor recurrence and high Knosp grade were adverse factors affecting the extent of resection. In our study, we analyzed various potential factors, including tumor recurrence, tumor size, tumor volume, and tumor consistency, and found that tumor recurrence and consistency affected the extent of resection, while the other factors did not. In addition, we also found that there was no statistical correlation between the extent of tumor resection and the occurrence of CSF leakage and postoperative cranial nerve palsy ($P > 0.05$).

Visual Outcome

In a 2012 systematic review by Komotar et al. (29), those patients who underwent transsphenoidal microscopic approach showed that the rate of visual improvement after PA surgery was 34.8%. Kalinin et al. (25) reported on a transsphenoidal endoscopic study of 97 patients with PAs invading CS in 2016, and vision improvement was achieved in 41.4% of cases. In a study of 39 patients with transsphenoidal endoscopic surgery, Chabot et al. (28) reported that 31 had CS invasion and the improvement rates of visual acuity and visual field were 73.9% and 72.4%, respectively. In our study, of the 38 patients who had visual impairment before surgery, visual improvement was achieved in 28 patients (73.7%), postoperatively. The visual results in our study were better than those reported for transsphenoidal

TABLE 3 | Surgical results and postoperative complications stratified by primary and recurrent pituitary adenomas.

Variables	Primary	Recurrent	P value
No. of patients (%)	60 (58.8)	42 (41.2)	
Extent of resection			
GTR (%)	48 (80.0)	24(57.1)	**0.013**
STR (%)	8 (13.3)	10 (23.8)	0.172
PTR (%)	4 (6.7)	8 (19.1)	0.056
Extent of CS resection			
GTR (%)	55 (91.7)	27 (64.3)	**0.001**
STR (%)	4 (6.7)	13 (31.0)	**0.001**
PTR (%)	1 (1.6)	2 (4.7)	0.363
Intraoprative variables			
ICA rupture (%)	0 (0.0)	2 (4.8)	0.088
CSF leakage (%)	4 (6.7)	7 (16.7)	0.109
Firm consistency (%)	14 (23.3)	17 (40.5)	0.064
Postoperative complications			
CSF leakage (%)	2 (3.3)	4 (9.5)	0.191
CNS infection (%)	2 (3.3)	3 (7.1)	0.380
Monocular blindness (%)	1 (1.7)	1 (2.4)	0.798
Panhypopituitarism (%)	1 (1.7)	2 (4.8)	0.363
Permanent diabetes insipidus (%)	1 (1.7)	1 (2.4)	0.798
Follow-up treatments			
Radiation therapy (%)	5 (8.3)	7 (16.7)	0.199
Medical therapy (%)	2 (33.3)	3 (7.1)	0.380

CS, cavernous sinus; CSF, cerebrospinal fluid; GTR, gross total resection; STR, subtotal tumor resection; PTR, partial tumor resection; CNS, central nervous system; ICA: internal carotid artery.
In bold: represent statistical significance.

TABLE 4 | Extent of resection correlated with multiple potential variables.

Variables	Within the CS			Entire tumor		
	GTR of CS	STR of CS	P value	GTR	STR	P value
Size of tumor						
Giant PA	31 (37.8)	7 (41.2)		28 (38.9)	9 (50.0)	
Macroadenoma	51 (62.2)	10 (58.8)	0.795	44 (61.1)	9 (50.0)	0.391
Volume of tumor(V, cm^3)						
V<15	19 (23.2)	3 (17.6)		16 (22.2)	4 (22.2)	
15≤V ≤ 30	32 (39.0)	4 (23.5)		29 (40.3)	6 (33.3)	
>30	31 (37.8)	10 (58.9)	0.269	27 (37.5)	8 (44.5)	0.836
Firm consistency						
Yes	19 (23.2)	12 (70.6)		16 (22.2)	10 (55.6)	
No	63 (76.8)	5 (29.4)	**<0.001**	56 (77.8)	8 (44.4)	**0.005**
Postoperative CSF leak						
Yes	4 (4.9)	2 (11.8)		3 (4.2)	3 (16.7)	
No	78 (95.1)	15 (88.2)	0.279	69 (95.8)	15 (83.3)	0.057
Postoperative cranial nerve palsy						
Yes	4 (4.9)	3 (17.6)		4 (5.6)	3 (16.7)	
No	78 (95.1)	14 (82.4)	0.062	68 (94.4)	15 (83.3)	0.115

PA, pituitary adenoma; CS, cavernous sinus; CSF, cerebrospinal fluid; GTR, gross total resection; STR, subtotal tumor resection.
In bold: represent statistical significance.

TABLE 5 | Complications of cranial nerve palsy.

	Postoperative			Improvement during follow-up		
	Total	Primary	Recurrent	Total	Primary	Recurrent
CN III	4	1	3	2	1	1
CN IV	0	0	0	0	0	0
CN V	0	0	0	0	0	0
CN VI	3	1	2	1	1	0

CN III, oculomotor nerve, CN IV, trochlear nerve, CN V, trigeminal nerve, CN VI, abducens nerve.

TABLE 6 | Endocrine outcomes correlated with multiple potential variables.

Variables	Hormone remission Yes	Hormone remission No	P Value
Size of tumor			
Giant PA	13 (76.5)	4 (23.5)	
Macroadenoma	16 (69.6)	7 (30.4)	0.629
Volume of tumor(V, cm3)			
V<15	6 (75.0)	2 (25.0)	
15≤V ≤ 30	11 (78.6)	3 (21.4)	
>30	12(66.7)	6 (33.3)	0.744
Extent of resection			
GTR	16 (88.9)	2 (11.1)	
STR	11 (68.7)	5 (31.3)	
PTR	2 (33.3)	4 (66.7)	**0.028**
Extent of CS resection			
GTR	18 (75.0)	6 (25.0)	
STR	10 (71.4)	4 (28.6)	
PTR	1 (50.0)	1 (50.0)	0.744
Tumor characteristics			
Primary	19 (76.0)	6 (24.0)	
Recurrent	10 (66.7)	5 (33.3)	0.522

GTR, gross total resection; STR, subtotal tumor resection; PTR, partial tumor resection; CS, cavernous sinus.
In bold: represent statistical significance.

TABLE 7 | Visual outcomes correlated with multiple potential variables.

Variables	Improved	Unchanged	P value
Preoperative visual symptoms			
Unilateral	17(70.8)	7(29.2)	
Bilateral	11(78.6)	3(21.4)	0.601
Size of tumor			
Giant PA	19(79.2)	5(20.8)	
Macroadenoma	9(64.3)	5(35.7)	0.315
Volume of tumor(V, cm^3)			
V<15	12(80.0)	3(20.0)	
15≤V ≤ 30	9(69.2)	4(31.8)	
>30	7(70.0)	3(30.0)	0.774
Firm consistency			
Yes	9(60.0)	6(40.0)	
No	19(82.6)	4(17.4)	0.122
Extent of resection			
GTR	20(90.9)	2(9.1)	
STR	7(63.6)	4(36.4)	
PTR	1(20.0)	4(80.0)	**0.003**
Extent of CS resection			
GTR	20(83.3)	4(16.7)	
STR	7(58.3)	5(41.7)	
PTR	1(50.0)	1(50.0)	0.203
Tumor characteristics			
Primary	18(85.7)	3(14.3)	
Recurrent	10(58.8)	7(41.2)	0.061

PA, pituitary adenoma; GTR, gross tumor resection; STR, subtotal tumor resection; PTR, partial tumor resection.
In bold: represent statistical significance.

microscopy, and this is broadly consistent with the results of previously published endoscopic studies. The superior visual outcomes of endoscopic endonasal surgery reflect the ability of the endoscope to visualize and protect the optic apparatus and its blood supply in the subarachnoid space, which these tumors can sometimes invade. In our study, patients with a total resection were more likely to have visual improvement than those with incomplete resection.

Endocrine Outcome

In addition to removal of the tumor, hormone remission is an important indicator of surgical outcome for functional PAs.

TABLE 8 | Comparison with similar studies of pituitary adenomas involving cavernous sinus published in the last decade.

Author	Year	No. of cases	Grade 1	Grade 2	Grade 3	Grade 4 (GTR %)	GTR (%)	Mean follow-up(m)
Ceylan et al. (20)	2010	19	0	0	9	10 (NR)	63.2	26
Zhao et al. (21)	2010	61	0	0	21	40 (47.5)	62.0	38
Paluzzi et al. (22)	2013	403	105	142	81	75 (0.0)	64.1	NR
Taniguchi et al. (23)	2015	25	0	0	23	2 (0.0)	56.0	36
Ferreli et al. (27)	2015	56	0	0	28	28 (17.8)	30.3	61
Bao et al. (24)	2015	52	0	0	13	39 (53.8)	63.5	24
Kalinin et al. (25)	2016	97	11	22	23	41 (NR)	50.5	NR
Toda et al. (19)	2018	30	0	0	0	30 (10.0)	10.0	NR
Kosugi et al. (26)	2019	23	0	0	7	16 (6.3)	8.7	NR
Total		766	116	164	205	281		
Present study	2020	102	0	0	0	102 (70.6)	70.6	46

NR, not reported; GTR, gross total resection.

Hofstetter et al. (30) reviewed 86 consecutive functional PAs (18 cases with CS invasion and 68 cases without CS invasion) by transsphenoidal endoscopy and the overall hormone remission rate was 60%. Bao et al. (24) reported a study of 52 cases of PAs that had invaded the CS, including 25 cases of functional PAs. Among the functional PAs, the hormone remission rate was 76%. In our study, among the 40 cases of functional PAs, the rate of hormone remission was 72.5%, which is consistent with previous studies. Patients with GTR of the entire tumor were more likely to experience hormone remission than those with incomplete resection ($P<0.05$). Of note, in our study, the endocrine outcomes were difficult to compare with previous endoscopic studies, which included tumors that did not invade the CS or different extents of CS invasion, whereas our study only included grade 4 PAs.

PRL-secreting adenomas with CS invasion present a significant challenge to pharmacologic treatment. In our study, indications for surgery mainly included drug-resistant tumors and patients who experienced drug intolerance due to side effects. Residual tumors in the CS can continue to cause endocrinological symptoms, and tumors with CS invasion are more likely to develop drug resistance. In some patients, residual CS lesions may remain even after continued medical treatment (31, 32).

Tumor Recurrence

PAs are benign tumors, although they often invade surrounding structures such as the CS and the sphenoid sinus. For benign tumors, patients have a good prognosis if the tumor can be completely removed; on the contrary, incomplete tumor resection may result in tumor recurrence. Prior studies have reported that incomplete tumor resection leads to a high recurrence rate, as high as 40-70% (33, 34). In contrast, the recurrence rate after GTR is significantly lower, with a 6-21% recurrence rate reported in the literature (33, 35). Notably, these studies include both invasive and non-invasive PAs, not just PAs invading the CS. Recently, Hwang et al. reported that up to 25% of cases with severe CS invasion recurred after total resection or near-total resection *via* a transsphenoidal endoscopic approach with long-term follow-up (11). In our study, 6 patients (5.9%), including 4 patients with PTR, 1 with STR and 1 with GTR, experienced tumor recurrence. Compared with the results reported in previous literature, the tumor recurrence rate in our study was relatively low. It is more difficult to achieve GTR in recurrent tumors, due to the formation of tissue adhesion and scar tissue, and changes that can occur in the normal anatomical structure after the initial operation. Additionally, the possibility of intraoperative injury to the ICA and surrounding cranial nerves is significantly increased (36). This was also confirmed in our study. Therefore, it is particularly important to completely remove the tumor during the first operation.

The Safety of Aggressive Tumor Resection

Complications—ICA Injury

ICA injury is the most serious complication of transsphenoidal endoscopic surgery and is the main obstacle to GTR within the CS. Because of this, many tumors within the CS are not aggressively removed. In practice, however, it is not impossible to avoid ICA injury. Accumulated evidence has shown that the incidence of ICA injury by the transsphenoidal approach to PAs is low, reportedly 0-1.6% (22, 37–39). However, these studies include PAs with or without CS invasion. In one study, Raithatha et al. reported 41 cases of PAs involving CS that utilized transsphenoidal endoscopic surgery, and the incidence of ICA injury was 2.4% (40). In our study, among the 102 cases of grade 4 PAs, ICA injury occurred in 2 patients (1.9%). Given the severity of risk with CS invasion, the incidence of ICA injury in our study appears to be favorable, compared with what has been previously reported. In our experience, the risk of ICA injury can be reduced by the following: 1) Performing a preoperative cerebral angiography balloon occlusion test to evaluate the compensatory capacity of the contralateral ICA in case of ipsilateral ICA injury; 2) Utilizing intraoperative navigation and doppler ultrasonography to assist in determining the position of the ICA in advance; 3) Exposing the proximal end of the ICA before entering the CS to remove the tumor; and 4) Using three-dimensional MRI to individually analyze the spatial relationship between the ICA and the CS tumor, and further, to determine the size of each compartment in the CS. After following these steps, and, according to the individual spatial relationship, it is possible to then decide the point of entry to the CS and the type of surgical approach to take within the CS. If the above four objectives are achieved, and intraoperative ICA injury still occurs, then it is imperative to restore it intraoperatively in the best way possible. Once injury occurs to the ICA, various methods, such as electrocoagulation of the vessel wall, clipping the proximal end of the ICA with an aneurysm clamp, or interventional therapy, can be adopted to manage the injury according to the extent of injury. For the 2 patients with ICA injury in our study, the injured ICA was completely clipped in one patient, and the ICA wall was electrocoagulated in the other patient. During the follow-up period, cerebral angiography was performed on the 2 patients, and for both, no pseudoaneurysm formation occurred, and no obvious symptoms were observed. Of note, both of these patients with intraoperative ICA injury had undergone previous operations for PAs. This also further demonstrates the importance of GTR at the first operation.

Complications—Cranial Nerve Palsy

Cranial nerve palsy is a common surgical complication of PAs with CS invasion, especially in the transcranial microscopic resection of CS tumors, because in traditional craniotomy, the CS is entered from the lateral wall of the CS, which is the exact location of multiple cranial nerves. In current transsphenoidal endoscopic surgical procedures, the CS is entered through the medial or anterior wall of the CS, which has no nerve structures. Therefore, the incidence of cranial nerve palsy is low by transsphenoidal endoscopy for the removal of PAs from the CS. Toda et al. reported a study of 30 patients who underwent transsphenoidal endoscopic surgery; the GTR rate of grade 4 PAs was 10% and the complication rate of cranial nerve palsy was 6.7% (19). Similarly, another transsphenoidal endoscopic study of 52 patients included 13 patients with grade 3 PAs and 39 patients with grade 4 PAs, and the incidence of cranial nerve palsy was 9.6% (24). These studies both show that cranial nerve palsy occurred mainly in the oculomotor and abducens nerves. In contrast, trochlear and trigeminal nerve palsy rarely occurred. In our study, new postoperative cranial nerve palsy was found in 7 cases (6.8%), including 3 cases of abducens nerve palsy and 4 cases of oculomotor nerve palsy, which is consistent with the findings of previous literature. During the follow-up, improvement was observed in 3 of the 7 patients, including 1 case with abducens nerve palsy and 2 cases with oculomotor nerve palsy. As the oculomotor nerve is located in the oculomotor nerve triangle of the CS, damage to the oculomotor nerve can occur when removing the tumor from this area, especially a tumor that is invading the temporal lobe through the oculomotor nerve triangle. Of note, the oculomotor nerve triangle is often referred to as the blind area of transsphenoidal endoscopic surgery (41). Unlike the oculomotor nerve, the abducens nerve is not located on the lateral wall of the CS, but rather within the space of the CS and has adhesion connections with the ICA (12). During tumor resection, it is necessary to be familiar with the shape of the abducens nerve in the CS and to sharply separate adhesions from the ICA to reduce the incidence of injury to the abducens nerve. In our study, cranial nerve palsy occurred in 2 of the 60 patients (3.3%) with primary PAs, compared with 5 of the 42 patients (11.9%) with recurrent PAs. In order to avoid cranial nerve palsy for PAs with CS invasion, especially for recurrent PAs, it is necessary to monitor craniocerebral nerves, such as the oculomotor nerve and the abducens nerve, by means of intraoperative electrophysiological detection of extraocular muscle movement (42).

Reasons for Aggressive Removal of Grade 4 PAs

In our study, the GTR rate of Knosp grade 4 PAs was significantly higher than any previously published study. Additionally, patients maintained favorable visual function and endocrine outcomes, and had low recurrence rates. Far more importantly, for an experienced endoscopist, such an aggressive tumor resection strategy did not significantly increase the incidence of complications. This favorable surgical outcome is due to the recent significant improvement in the understanding of Knosp grade 4 PAs. A preoperative analysis of the individual spatial relationship among the ICA, the CS tumor, and various compartments of the CS, coupled with intraoperative assistive techniques such as neuronavigation, doppler ultrasonography and cranial nerve monitoring, have enabled us to aggressively pursue GTR. However, it is important to emphasize that a successful procedure requires extensive experience in transsphenoidal endoscopic surgery.

CONCLUSIONS

For experienced neuroendoscopists, an aggressive tumor resection strategy *via* transsphenoidal endoscopic surgery may be an effective and safe option for Knosp grade 4 PAs.

DATA AVAILABILITY STATEMENT

The original contributions presented in the study are included in the article/supplementary material. Further inquiries can be directed to the corresponding author.

ETHICS STATEMENT

The studies involving human participants were reviewed and approved by the Institutional Ethics Committee of the First Affiliated Hospital of Nanchang University. The patients/participants provided their written informed consent to participate in this study.

AUTHOR CONTRIBUTIONS

Conception and design: TO and TH. Acquisition of data: JL, FZ, and LX. Analysis and interpretation of data: NZ, SX, and BW. Drafting the article: TO. Critically revising the article: DZ and BT. Reviewed submitted version of manuscript: TH. Approved the final version of the manuscript on behalf of all authors: TH. Statistical analysis: SX. Study supervision: TH, DZ, and ML. All authors contributed to the article and approved the submitted version.

FUNDING

The present study was supported by the National Natural Science Foundation of China (grant no. 81760447; grant no. 81960247, grant no. 82060246), Project of Science and Technology Department of Jiangxi Province (grant no. 20192BBG70026, grant no. S2019QNJJB1056), and Jiangxi Provincial Education Department Project (grant no. GJJ180054; grant no. GJJ180116).

REFERENCES

1. Ostrom QT, Gittleman H, Farah P, Ondracek A, Chen Y, Wolinsky Y, et al. CBTRUS Statistical Report: Primary Brain and Central Nervous System Tumors Diagnosed in the United States in 2006-2010. *Neuro Oncol* (2013) 15 Suppl 2(Suppl 2):ii1–56. doi: 10.1093/neuonc/not151. Erratum in: *Neuro Oncol* (2014) 16(5):760.
2. Aflorei ED, Korbonits M. Epidemiology and Etiopathogenesis of Pituitary Adenomas. *J Neurooncol* (2014) 117:379–94. doi: 10.1007/s11060-013-1354-5
3. Knosp E, Steiner E, Kitz K, Matula C. Pituitary Adenomas With Invasion of the Cavernous Sinus Space: A Magnetic Resonance Imaging Classification Compared With Surgical Findings. *Neurosurgery* (1993) 33:610–617; discussion 617-618. doi: 10.1227/00006123-199310000-00008
4. Cottier JP, Destrieux C, Brunereau L, Bertrand P, Moreau L, Jan M, et al. Cavernous Sinus Invasion by Pituitary Adenoma: MR Imaging. *Radiology* (2000) 215:463–9. doi: 10.1148/radiology.215.2.r00ap18463
5. Pontius AT, Ducic Y. Extended Orbitozygomatic Approach to the Skull Base to Improve Access to the Cavernous Sinus and Optic Chiasm. *Otolaryngol Head Neck Surg* (2004) 130:519–25. doi: 10.1016/j.otohns.2004.01.013
6. Spallone A, Vidal RV, Gonzales JG. Transcranial Approach to Pituitary Adenomas Invading the Cavernous Sinus: A Modification of the Classical Technique to be Used in a Low-Technology Environment. *Surg Neurol Int* (2010) 1:25. doi: 10.4103/2152-7806.65054
7. Dallapiazza R, Bond AE, Grober Y, Louis RG, Payne SC, Oldfield EH, et al. Retrospective Analysis of a Concurrent Series of Microscopic Versus Endoscopic Transsphenoidal Surgeries for Knosp Grades 0-2 Nonfunctioning Pituitary Macroadenomas at a Single Institution. *J Neurosurg* (2014) 121:511–7. doi: 10.3171/2014.6.jns131321
8. Fathalla H, Cusimano MD, Di Ieva A, Lee J, Alsharif O, Goguen J, et al. Endoscopic Versus Microscopic Approach for Surgical Treatment of Acromegaly. *Neurosurg Rev* (2015) 38:541–548; discussion 548-549. doi: 10.1007/s10143-015-0613-7
9. Gaillard S. The Transition From Microscopic to Endoscopic Transsphenoidal Surgery in High-Caseload Neurosurgical Centers: The Experience of Foch Hospital. *World Neurosurg* (2014) 82:S116–120. doi: 10.1016/j.wneu.2014.07.033
10. Koutourousiou M, Gardner PA, Fernandez-Miranda JC, Paluzzi A, Wang EW, Snyderman CH. Endoscopic Endonasal Surgery for Giant Pituitary Adenomas: Advantages and Limitations. *J Neurosurg* (2013) 118:621–31. doi: 10.3171/2012.11.jns121190
11. Hwang J, Seol HJ, Nam DH, Lee JI, Lee MH, Kong DS. Therapeutic Strategy for Cavernous Sinus-Invading Non-Functioning Pituitary Adenomas Based on the Modified Knosp Grading System. *Brain Tumor Res Treat* (2016) 4:63–9. doi: 10.14791/btrt.2016.4.2.63
12. Fernandez-Miranda JC, Zwagerman NT, Abhinav K, Lieber S, Wang EW, Snyderman CH, et al. Cavernous Sinus Compartments From the Endoscopic Endonasal Approach: Anatomical Considerations and Surgical Relevance to Adenoma Surgery. *J Neurosurg* (2018) 129:430–41. doi: 10.3171/2017.2.JNS162214
13. Wu X, Xie SH, Tang B, Yang YQ, Yang L, Ding H, et al. Pituitary Adenoma With Posterior Area Invasion of Cavernous Sinus: Surgical Anatomy, Approach, and Outcomes. (2020). doi: 10.1007/s10143-020-01404-1
14. Casanueva FF, Molitch ME, Schlechte JA, Abs R, Bonert V, Bronstein MD, et al. Guidelines of the Pituitary Society for the Diagnosis and Management of Prolactinomas. *Clin Endocrinol* (2006) 65:265–73. doi: 10.1111/j.1365-2265.2006.02562.x
15. Katznelson L, Laws ERJr., Melmed S, Molitch ME, Murad MH, Utz A, et al. Acromegaly: An Endocrine Society Clinical Practice Guideline. *J Clin Endocrinol Metab* (2014) 99:3933–51. doi: 10.1210/jc.2014-2700
16. Nieman LK, Biller BM, Findling JW, Murad MH, Newell-Price J, Savage MO, et al. Treatment of Cushing's Syndrome: An Endocrine Society Clinical Practice Guideline. *J Clin Endocrinol Metab* (2015) 100:2807–31. doi: 10.1210/jc.2015-1818
17. Melmed S, Bronstein MD, Chanson P, Klibanski A, Casanueva FF, Wass JAH, et al. A Consensus Statement on Acromegaly Therapeutic Outcomes. *Nat Rev Endocrinol* (2018) 14:552–61. doi: 10.1038/s41574-018-0058-5
18. Woodworth GF, Patel KS, Shin B, Burkhardt JK, Tsiouris AJ, McCoul ED, et al. Surgical Outcomes Using a Medial-to-Lateral Endonasal Endoscopic Approach to Pituitary Adenomas Invading the Cavernous Sinus. *J Neurosurg* (2014) 120:1086–94. doi: 10.3171/2014.1.jns131228
19. Toda M, Kosugi K, Ozawa H, Ogawa K, Yoshida K. Surgical Treatment of Cavernous Sinus Lesion in Patients With Nonfunctioning Pituitary Adenomas Via the Endoscopic Endonasal Approach. *J Neurol Surg Part B Skull Base* (2018) 79:S311–5. doi: 10.1055/s-0038-1667123
20. Ceylan S, Koc K, Anik I. Endoscopic Endonasal Transsphenoidal Approach for Pituitary Adenomas Invading the Cavernous Sinus. *J Neurosurg* (2010) 112:99–107. doi: 10.3171/2009.4.jns09182
21. Zhao B, Wei YK, Li GL, Li YN, Yao Y, Kang J, et al. Extended Transsphenoidal Approach for Pituitary Adenomas Invading the Anterior Cranial Base, Cavernous Sinus, and Clivus: A Single-Center Experience With 126 Consecutive Cases. *J Neurosurg* (2010) 112:108–17. doi: 10.3171/2009.3.JNS0929
22. Paluzzi A, Fernandez-Miranda JC, Tonya Stefko S, Challinor S, Snyderman CH, Gardner PA. Endoscopic Endonasal Approach for Pituitary Adenomas: A Series of 555 Patients. *Pituitary* (2014) 17:307–19. doi: 10.1007/s11102-013-0502-4
23. Taniguchi M, Hosoda K, Akutsu N, Takahashi Y, Kohmura E. Endoscopic Endonasal Transsellar Approach for Laterally Extended Pituitary Adenomas: Volumetric Analysis of Cavernous Sinus Invasion. *Pituitary* (2015) 18:518–24. doi: 10.1007/s11102-014-0604-7
24. Bao X, Deng K, Liu X, Feng M, Chen CC, Lian W, et al. Extended Transsphenoidal Approach for Pituitary Adenomas Invading the Cavernous Sinus Using Multiple Complementary Techniques. *Pituitary* (2016) 19:1–10. doi: 10.1007/s11102-015-0675-0
25. Kalinin PL, Sharipov OI, Pronin IN, Kutin MA, Fomichev DV, Kadashev BA, et al. Endoscopic Transsphenoidal Resection of Pituitary Adenomas Invading the Cavernous Sinus. *Zh Vopr Neirokhir Im N N Burdenko* (2016) 80:63–74. doi: 10.17116/neiro201680463-74
26. Kosugi K, Tamura R, Mase T, Tamura H, Jinzaki M, Yoshida K, et al. Relationship Between Pneumatization of Lateral Recess in the Sphenoid Sinus and Removal of Cavernous Sinus Invasion in Pituitary Adenomas by Endoscopic Endonasal Surgery. *Surg Neurol Int* (2019) 10:222. doi: 10.25259/SNI_169_2019
27. Ferreli F, Turri-Zanoni M, Canevari FR, Battaglia P, Bignami M, Castelnuovo P, et al. Endoscopic Endonasal Management of non-Functioning Pituitary Adenomas With Cavernous Sinus Invasion: A 10- Year Experience. *Rhinology* (2015) 53:308–16. doi: 10.4193/Rhin14.309
28. Chabot JD, Chakraborty S, Imbarrato G, Dehdashti AR. Evaluation of Outcomes After Endoscopic Endonasal Surgery for Large and Giant Pituitary Macroadenoma: A Retrospective Review of 39 Consecutive Patients. *World Neurosurg* (2015) 84:978–88. doi: 10.1016/j.wneu.2015.06.007
29. Komotar RJ, Starke RM, Raper DM, Anand VK, Schwartz TH. Endoscopic Endonasal Compared With Microscopic Transsphenoidal and Open Transcranial Resection of Giant Pituitary Adenomas. *Pituitary* (2012) 15:150–9. doi: 10.1007/s11102-011-0359-3
30. Hofstetter CP, Shin BJ, Mubita L, Huang C, Anand VK, Boockvar JA, et al. Endoscopic Endonasal Transsphenoidal Surgery for Functional Pituitary Adenomas. *Neurosurg Focus* (2011) 30:E10. doi: 10.3171/2011.1.FOCUS10317
31. Hamilton DK, Vance ML, Boulos PT, Laws ER. Surgical Outcomes in Hyporesponsive Prolactinomas: Analysis of Patients With Resistance or Intolerance to Dopamine Agonists. *Pituitary* (2005) 8:53–60. doi: 10.1007/s11102-005-5086-1

32. Wu ZB, Su ZP, Wu JS, Zheng WM, Zhuge QC, Zhong M. Five Years Follow-Up of Invasive Prolactinomas With Special Reference to the Control of Cavernous Sinus Invasion. *Pituitary* (2008) 11:63–70. doi: 10.1007/s11102-007-0072-4
33. Santoro A, Minniti G, Ruggeri A, Esposito V, Jaffrain-Rea ML, Delfini R. Biochemical Remission and Recurrence Rate of Secreting Pituitary Adenomas After Transsphenoidal Adenomectomy: Long-Term Endocrinologic Follow-Up Results. *Surg Neurol* (2007) 68:513–518. doi: 10.1016/j.surneu.2007.05.057
34. Cappabianca P, Solari D. The Endoscopic Endonasal Approach for the Treatment of Recurrent or Residual Pituitary Adenomas: Widening What to See Expands What to do? *World Neurosurg* (2012) 77:455–6. doi: 10.1016/j.wneu.2011.08.047
35. Chang EF, Zada G, Kim S, Lamborn KR, Quinones-Hinojosa A, Tyrrell JB, et al. Long-Term Recurrence and Mortality After Surgery and Adjuvant Radiotherapy for Nonfunctional Pituitary Adenomas. *J Neurosurg* (2008) 108:736–45. doi: 10.3171/JNS/2008/108/4/0736
36. Chang EF, Sughrue ME, Zada G, Wilson CB, Blevins LSJr., Kunwar S. Long Term Outcome Following Repeat Transsphenoidal Surgery for Recurrent Endocrine-Inactive Pituitary Adenomas. *Pituitary* (2010) 13:223–9. doi: 10.1007/s11102-010-0221-z
37. Dehdashti AR, Ganna A, Karabatsou K, Gentili F. Pure Endoscopic Endonasal Approach for Pituitary Adenomas: Early Surgical Results in 200 Patients and Comparison With Previous Microsurgical Series. *Neurosurgery* (2008) 62:1006–15. doi: 10.1227/01.neu.0000325862.83961.12
38. Frank G, Pasquini E, Farneti G, Mazzatenta D, Sciarretta V, Grasso V, et al. The Endoscopic Versus the Traditional Approach in Pituitary Surgery. *Neuroendocrinology* (2006) 83:240–8. doi: 10.1159/000095534
39. Gondim JA, Schops M, de Almeida JP, de Albuquerque LA, Gomes E, Ferraz T, et al. Endoscopic Endonasal Transsphenoidal Surgery: Surgical Results of 228 Pituitary Adenomas Treated in a Pituitary Center. *Pituitary* (2010) 13:68–77. doi: 10.1007/s11102-009-0195-x
40. Raithatha R, McCoul ED, Woodworth GF, Schwartz TH, Anand VK. Endoscopic Endonasal Approaches to the Cavernous Sinus. *Int Forum Allergy Rhinol* (2012) 2:9–15. doi: 10.1002/alr.20097
41. Goel A, Nadkarni T, Muzumdar D, Desai K, Phalke U, Sharma P. Giant Pituitary Tumors: A Study Based on Surgical Treatment of 118 Cases. *Surg Neurol* (2004) 61:436–45. doi: 10.1016/j.surneu.2003.08.036
42. Kitano M, Taneda M, Shimono T, Nakao Y. Extended Transsphenoidal Approach for Surgical Management of Pituitary Adenomas Invading the Cavernous Sinus. *J Neurosurg* (2008) 108:26–36. doi: 10.3171/jns/2008/108/01/0026

Conflict of Interest: The authors declare that the research was conducted in the absence of any commercial or financial relationships that could be construed as a potential conflict of interest.

frontiers in Oncology

ORIGINAL RESEARCH
published: 25 June 2021
doi: 10.3389/fonc.2021.689943

Invasive Corridor of Clivus Extension in Pituitary Adenoma: Bony Anatomic Consideration, Surgical Outcome and Technical Nuances

Xiao Wu[1†], *Han Ding*[1†], *Le Yang*[1†], *Xuan Chu*[2†], *Shenhao Xie*[1], *Youyuan Bao*[1], *Jie Wu*[1], *Youqing Yang*[1], *Lin Zhou*[1], *Minde Li*[1], *Shao Yang Li*[1], *Bin Tang*[1], *Limin Xiao*[1], *Chunlong Zhong*[3], *Liang Liang*[2*] and *Tao Hong*[1*]

[1] *Department of Neurosurgery, The First Affiliated Hospital of Nanchang University, Nanchang, China,* [2] *Department of Anatomy, School of Basic Medical Sciences, Anhui Medical University, Hefei, China,* [3] *Department of Neurosurgery, Shanghai East Hospital, Tongji University School of Medicine, Shanghai, China*

Edited by:
Xicai Sun,
Fudan University, China

Reviewed by:
Ye Gu,
Fudan University, China
Tomasz Dziedzic,
Medical University of Warsaw, Poland
Tao Xie,
Fudan University, China

***Correspondence:**
Tao Hong
ht2000@vip.sina.com
Liang Liang
liangliang@ahmu.edu.cn

†*These authors have contributed equally to this work*

Specialty section:
This article was submitted to Surgical Oncology, a section of the journal Frontiers in Oncology

Received: *01 April 2021*
Accepted: *28 May 2021*
Published: *25 June 2021*

Citation:
Wu X, Ding H, Yang L, Chu X, Xie S, Bao Y, Wu J, Yang Y, Zhou L, Li MD, Li SY, Tang B, Xiao L, Zhong C, Liang L and Hong T (2021) Invasive Corridor of Clivus Extension in Pituitary Adenoma: Bony Anatomic Consideration, Surgical Outcome and Technical Nuances. Front. Oncol. 11:689943. doi: 10.3389/fonc.2021.689943

Background: It is well known that the clivus is composed of abundant cancellous bone and is often invaded by pituitary adenoma (PA), but the range of these cancellous bone corridors is unknown. In addition, we found that PA with clivus invasion is sometimes accompanied by petrous apex invasion, so we speculated that the petrous apex tumor originated from the clivus cancellous bone corridor. The aim of this study was to test this hypothesis by investigating the bony anatomy associated with PA with clival invasion and its clinical significance.

Methods: Twenty-two cadaveric heads were used in the anatomical study to research the bony architecture of the clivus and petrous apex, including six injected specimens for microsurgical dissection and sixteen cadavers for epoxy sheet plastination. The surgical videos and outcomes of PA with clival invasion in our single center were also retrospectively reviewed.

Results: The hypoglossal canal and internal acoustic meatus are composed of bone canals surrounded by cortical bone. The cancellous corridor within clivus starts from the sellar or sphenoid sinus floor and extends downward, bypassing the hypoglossal canal and finally reaching the occipital condyle and the medial edge of the jugular foramen. Interestingly, we found that the cancellous bone of the clivus was connected with that of the petrous apex through petroclival fissure extending to the medial margin of the internal acoustic meatus instead of a separating cortical bone between them as it should be. It is satisfactory that the anatomical outcomes of the cancellous corridor and the path of PA with clival invasion observed intraoperatively are completely consistent. In the retrospective cohort of 49 PA patients, the clival component was completely resected in 44 (89.8%), and only five (10.2%) patients in the early-stage had partial residual cases in the inferior clivus.

Conclusion: The petrous apex invasion of PA is caused by the tumor invading the clivus and crossing the petroclival fissure along the cancellous bone corridor. PA invade the clivus along the cancellous bone corridor and can also cross the hypoglossal canal to the occipital condyle. This clival invasion pattern presented here deepens our understanding of the invasive characteristics of PA.

Keywords: pituitary adenoma, clival invasion, endonasal endoscopic approach, epoxy sheet plastination, corridor, cancellous bone, anatomy

INTRODUCTION

Pituitary adenoma (PA) is a common benign tumor, but it has the biological characteristics of malignant tumors that invade adjacent structures, such as the sphenoid sinus (SS), cavernous sinus, suprasellar region, nasopharynx, and clivus (1). Cavernous sinus invasion is considered to be almost equivalent to the invasiveness of PA, until recently, still considered to be surgically challenging (2–5). Nevertheless, tumor invasiveness has many aspects, and clival invasion is also worthy of our attention.

The clivus used to be considered an unusual location for PA invasion, and most of the reported cases involving the clivus were ectopic PA cases (6–9). However, Chen et al. analyzed clival invasion with multidetector CT in 390 pituitary macroadenomas, and 32 (8.21%) patients had clival invasion (10). It is common knowledge that the clivus has a cancellous bone that is often invaded by PA. However, there are few studies on the clivus corridor of PA, including how the tumor extends into the clivus and the extent of cancellous bone involvement. In some cases, PA invading the clivus may be accompanied by petrous apex invasion, while petrous apex invasion is rarely seen in cases without clivus involvement. Therefore, we hypothesize that tumors in the petrous apex originate from the cancellous bone corridor within the clivus.

In this study, we studied the bony architecture of the clivus and petrous apex, including the extent and characteristics of the cancellous bone, by performing microsurgical dissection and a recently developed epoxy sheet plastination technique. We also reviewed 49 cases of PA involving the clivus treated by the endoscopic endonasal approach (EEA) in our institution. Finally, information useful for eventual clinical applications, including surgical techniques and outcomes, were discussed.

MATERIALS AND METHODS

Microsurgical Dissection

The research was authorized by the Ethics Committee of Nanchang University. Six injected adult cadaveric specimens (12 sides) were used to dissect the bony architectures of the clivus and petrous apex (magnification ×4–40, surgical microscopes by Zeiss). The heads were fixed in a Mayfield head holder to maintain a stable position for navigation (Brainlab, Germany) and drilling (NSK, Japan). The specimens were bisected axially using a high-speed electric saw for stepwise superior-to-inferior and medial-to-lateral dissection in the clivus.

Epoxy Sheet Plastination

Sixteen cadaveric heads with thirty-two sides underwent epoxy sheet plastination. The cadavers were donated for anatomic education and research to the Department of Anatomy at Anhui Medical University. The skull base tissue blocks were removed from the cadaver and plastinated by the E12/E6/E600 resin (Biodur, Heidelburg, Germany) ultrathin plastination technique (11). These undecalcified resin blocks were serially sectioned in the axial (eight sets), coronal (eight sets), and sagittal (16 sets) planes with the Exakt 310 CP cutting system (Exakt, Norderstedt, Germany). All sections stained with Stevenel's blue and Alisarin red S were examined and photographed by a Leica DM6 B light microscope (Leica, Bensheim, Germany). This step was performed to better understand the relationship between the bony architectures of the clivus and the surrounding important neurovascular structures, including the internal carotid artery, petrous apex, hypoglossal nerve canal, and occipital condyle.

Patient Population

The data of 49 PAs with clival invasion who underwent EEA between July 2015 and May 2020 in our single center were retrospectively reviewed, including 31 females and 18 males, with an average age of 49.1 years. The collection of medical records and surgical videos was authorized by the Institutional Review Board of Nanchang University. The patient's age, sex, Knosp grade, pathological type, and extent of tumor resection were obtained from the medical records. Because the corridor of PA with upper clivus (dorsum sellae) invasion is not consistent with the middle and inferior clivus, it often directly invades the bony structures of the posterior clinoid process and dorsum sellae. In our study, we will not discuss this type of invasive PA.

Preoperative Evaluation

All patients underwent conventional T1- and T2-weighted MRI scans and T1-weighted 3D MP-RAGE sequence scans before the operation. Moreover, CT scans were performed to obtain detailed information on the bony structures. In the preoperative radiological evaluation, we evaluated the upper, middle, and lower thirds of the clivus in the sagittal plane. The upper clivus extends from the posterior clinoid process to the sellar floor, the middle clivus extends from the sellar floor to the roof of the choana, and the lower clivus extends from the roof of the choana to the foramen magnum, corresponding to the nasopharyngeal clivus (12).

Preoperative Preparation

In addition to routine examinations for PAs (visual acuity, visual field, endocrine examination), evaluations of the paraclival and petrous segments of the internal carotid artery (ICA) were performed. Under exceptional circumstances, evaluations of collateral circulation were also performed, and a balloon occlusion test was performed when necessary. Moreover, for PA with extensive clival invasion, we paid attention to cranial nerve-related symptoms such as abducens, acoustic and hypoglossal nerve-related symptoms.

Assessment of the Path of PA Invading Clivus

The CT bone window was used to evaluate the type of SS pneumatization. The type of SS pneumatization was determined by the method proposed by Hammer et al. (13). A surgical video was used to further confirm the type of SS pneumatization and assess the relationship between SS pneumatization and clival invasion.

Postoperative Imaging Evaluation

All patients were reexamined with MRI on the 3rd day after the operation. To minimize interrater variability, the extent of resection was assessed by two independent neurosurgeons in the First Affiliated Hospital of Nanchang University according to the postoperative enhanced MRI and CT thin-section data. We defined gross total resection as the absence of a residual tumor, subtotal resection as ≥80% of the tumor being resected, and partial resection as <80% of the tumor being resected.

RESULTS

Microsurgical Dissection

Cancellous bone within clivus is composed of irregular grids, which are separated by bony septa and resemble honeycomb-like structures. The bony septa separating these grids are very thin and weak and are easily penetrated by the spatula into the next grid. These characteristics are obviously beneficial for the extension of the clival corridor in PA. However, we observed that the bony canal of hypoglossal nerve is composed of cortical bone. Therefore, the extent of cancellous bone within the clivus extend across the hypoglossal canal and reach the occipital condyle and the medial edge of the jugular foramen.

The bony architecture of the petrous apex is similar to that of the clivus. Interestingly, we found that the cancellous bones of the clivus and petrous apex were connected through petroclival fissure, and no tough cortical bone between them was found. Due to the bony canals of the acoustic nerve is composed of cortical bone, the cancellous bone corridor of the petrous apex only reached the medial edge of the internal acoustic meatus (**Figure 1**).

Epoxy Sheet Plastination

Most of the microanatomy results are consistent with those of plastination anatomy studies. The bony surface of the clivus and petrous apex is composed of dense cortical bone, while the inner part is composed of loose cancellous bone separated by numerous thin bony septa. Dense cortical bone was not found between the petrous apex and the clivus, which indicated that PA can easily extend to the petrous apex through the clival cancellous corridor. Moreover, the bone canal of the petrous ICA surrounded by cancellous bone is relatively thin and weak, thereby careful manipulation is needed to protect the petrous ICA during tumor resection of the petrous apex component

Clivus is formed by the synostosis of the sphenoid bone and the basilar part of occipital bone. It was found that the bony structure of spheno-ocipital synchondrosis was similar to petroclival fissure, and there was no dense cortical bone to separate it, but communicated through cancellous bone, which also became the anatomical corridor for PA to enter the lower clivus. The bony structure of upper clivus is relatively complex, which can be mainly composed of cortical bone, or the outer layer is surrounded by cortical bone, while the inner part is full of cancellous bone (**Figure 2**).

Relationship Between SS Pneumatization and Clival Invasion

The CT bone window can be used to determine the type of SS and the corridors of the invading clivus. Conchal-type SS was not found in our case series due to its rarity. For patients with medium SS pneumatization, that is, the presellar type, PA can directly invade the clivus through the sellar floor (**Figure 3A**). In other cases, clival invasion may be accompanied by SS invasion, and PA can also invade the clivus through the SS floor (**Figure 4A**).

For patients with sufficient SS pneumatization, that is, the sellar type, the tumor can break through the sellar floor into the SS and then further invade the bone within the clivus through the SS corridor (**Figure 5A**).

Surgical Techniques

All operations were performed under intraoperative electrophysiological monitoring. The surgical approach and preparation process are described in a previous report (14). Two surgeons (four hands) performed the surgery *via* the binostril EEA. A wide bilateral sphenoidotomy was performed to provide more access for better observation of the tumor invasion corridors. Intraoperatively, the tumor was found to be hidden and mixed in the honeycomb-like structure formed by the cancellous bone within the clivus. The extent of tumor invasion was consistent with the distribution of cancellous bone found in our microanatomy and epoxy sheet plastination study. Tumor resection cannot be performed with only the double suction technique. Tumors mixed with the cancellous bone should be removed together with a power drill or a curette. The cortical bone surrounding the clival surface often indicate the boundary of total tumor resection.

For patients with medium SS pneumatization, the cortical bone in front of the clivus was exposed as much as possible. Then, we looked for defects in the sellar floor after drilling the cortical bone in front of the clivus and removing the tumor along the natural corridor. This type of procedure is relatively safe because the tumor can be completely resected without exposing the ICA (**Figure 3**). If the patient also exhibits SS invasion, ICA protection should be taken seriously due to the risk of the erosion of bone covering the paraclival ICA (**Figure 4**).

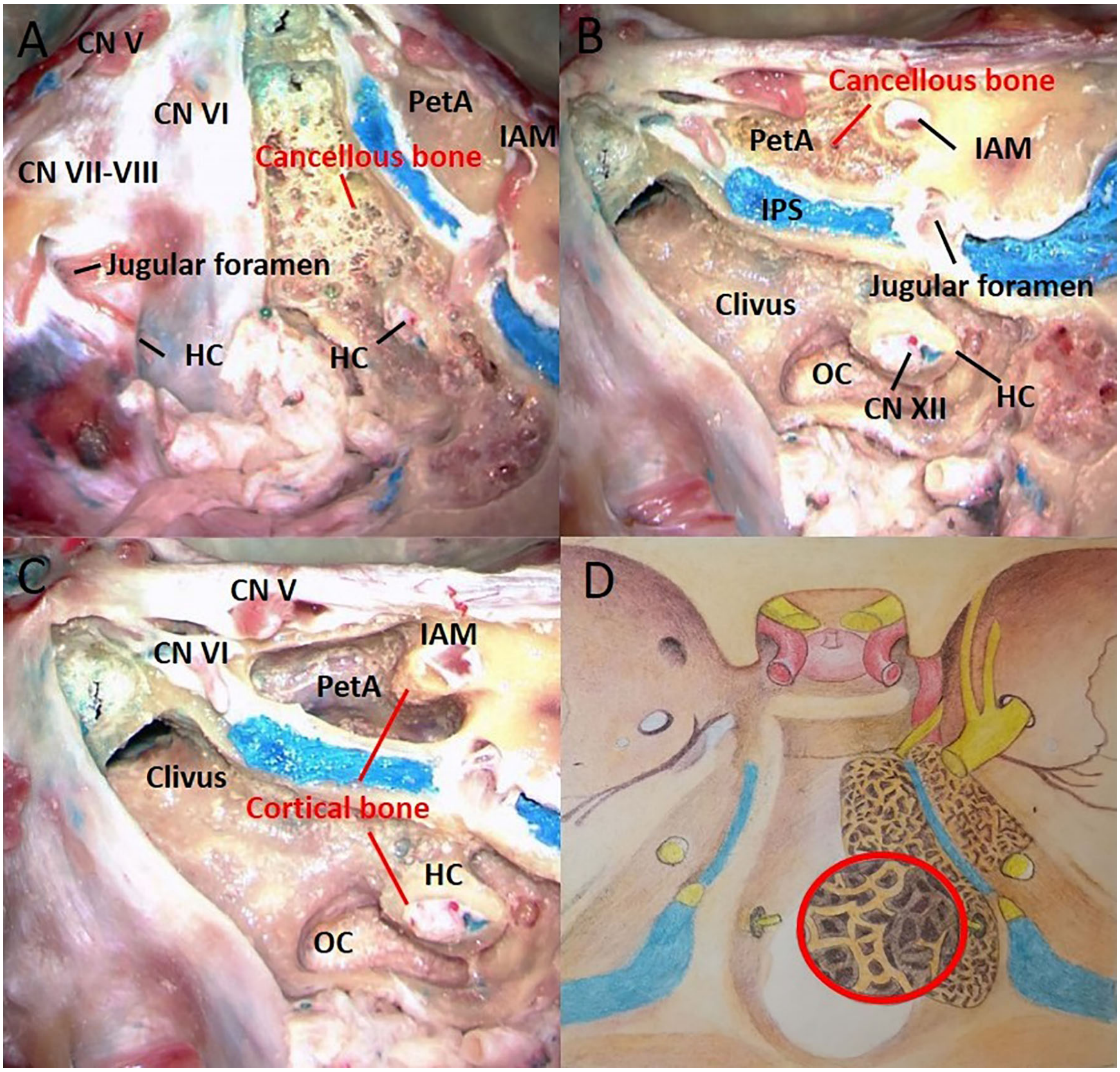

FIGURE 1 | The right half of the cortical bone was removed, and the left half was used as the control. The bony architecture in the clivus and petrous apex includes the cancellous bone and cortical bone. **(A)** The clivus is made of loose cancellous bone beneath the cortical bone. **(B)** The cancellous bone within the clivus extends downward to the occipital condyle. The petrous apex is also made of loose cancellous bone beneath the cortical bone. **(C)** The bony canals of the acoustic and hypoglossal nerves are composed of cortical bone. **(D)** Artistic illustration demonstrating the shape and extent of cancellous bone in the clivus and petrous apex. The red circle represents the enlarged view of the cancellous bone structure. CN, cranial nerve; HC, hypoglossal canal; IPS, inferior petrous sinus; IAM, internal acoustic meatus; OC, occipital condyle; PetA, Petrous apex.

However, in cases of tumors invading the clivus after breaking through the anterior sellar wall or sellar floor to enter the SS, paraclival ICA protection should be considered carefully during tumor resection. When tumors near the paraclival ICA (SS component) were resected, the ICA was often exposed in the SS. At this time, stripper should be used to carefully separate the boundary between ICA and PA to avoid blindly pulling tumor. In these cases, Doppler ultrasound or neuronavigation should be used to accurately locate the ICA (**Figure 5**).

Different landmarks may be used for tumors with varying extents of invasion in varying directions. The isolated hypoglossal canal was observed when a PA extended to the inferior clivus after the tumor was completely resected (**Figure 4G**). PAs can even cross the hypoglossal canal and reach the occipital condyle or the medial margin of the jugular foramen. Moreover, the medial edge of the internal acoustic meatus can be seen when PAs cross the petroclival fissure to reach the petrous apex, and special attention should be paid to protect the abducens nerve and petrous ICA during tumor resection. A sign of total tumor resection is total removal of the PA and cancellous bone within the clivus. Except for the bone canal of the hypoglossal nerve, an empty clivus was observed (**Figure 4H**). In fact, the endoscopic endonasal anatomy of these anatomical structures has been reported in the literature (15–17).

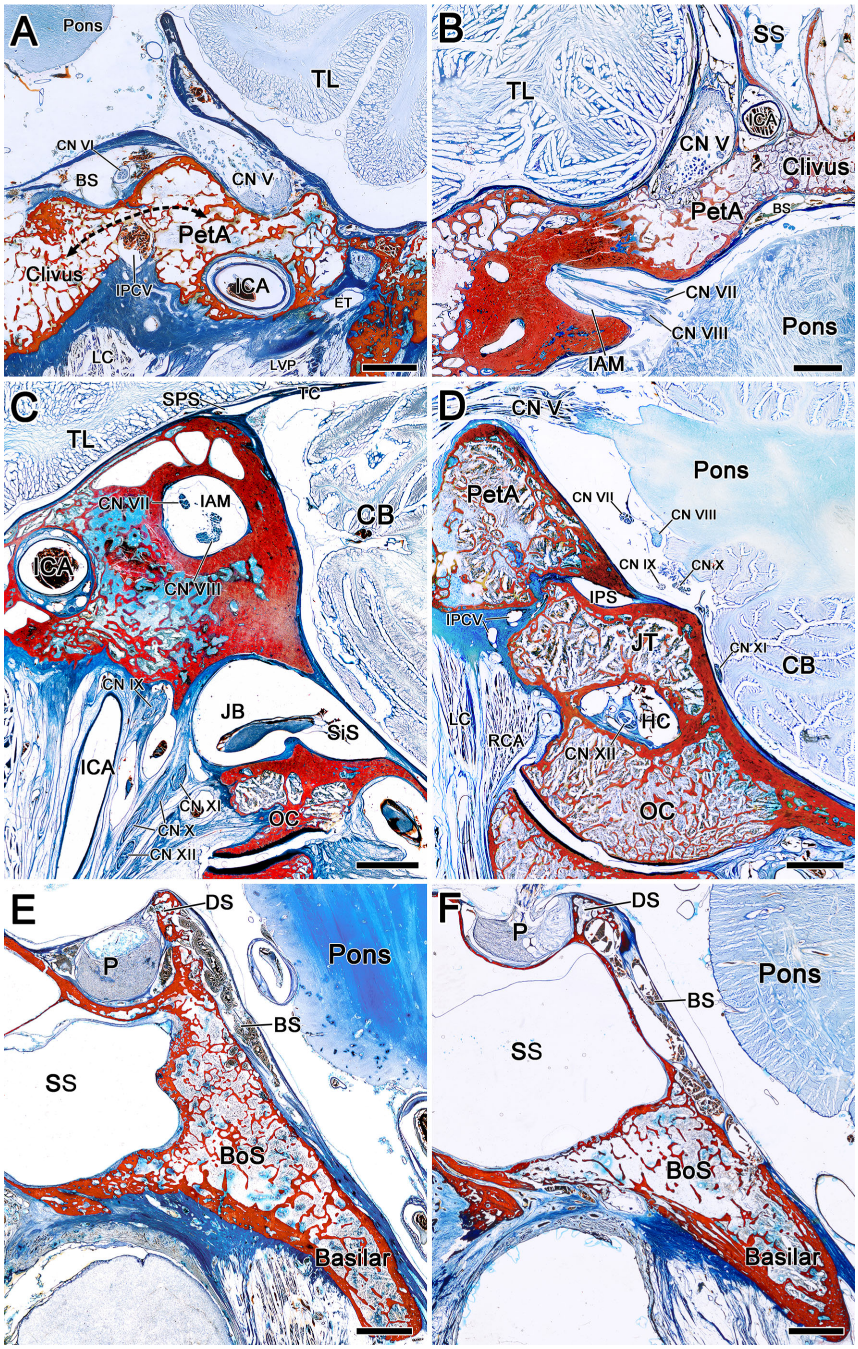

FIGURE 2 | The composition and connection of bony architecture around the clivus were observed by epoxy sheet plastination. **(A)** Coronal sections of a right clivus and petrous apex. The bony surface of the clivus and petrous apex is composed of dense cortical bone, while the inner part is composed of loose cancellous bone separated by numerous thin bony septa. The bone canal of the petrous ICA surrounded by cancellous bone is relatively thin and weak. The black arrow indicates the communication of cancellous bone between the clivus and petrous apex. **(B)** Axial sections of a left clivus and petrous apex. The cancellous bone of the clivus communicates with that of the petrous apex to the medial margin of the IAM. **(C)** Sagittal sections of a right IAM. There is high density cortical bone around the IAM. **(D)** Sagittal sections of a right HC. The bony canal of the hypoglossal nerve is composed of cortical bone. **(E, F)** Sagittal section of clivus and sella turcica. There is no dense cortical bone between the body of sphenoid bone and the basilar part of occipital bone, and communicate through cancellous bone. The bony structure of upper clivus (dorsum sellae) can be mainly composed of cortical bone **(E)**, or the outer layer is surrounded by cortical bone, while the inner part is full of cancellous bone **(F)**. BS, basilar sinus; Basilar, basilar part of occipital bone; BoS, body of sphenoid bone; CB, cerebellum; DS, dorsum sellae; ET, eustachian tube; ICA, internal carotid artery; IPCV, inferior petroclival vein; IPS, inferior petrosal sinus; JB, jugular bulb; JT, jugular tubercle; LVP, levator veli palatini; LC, Longus capitis; MA, maxillary artery; NP, nasopharynx; PP, pterygoid plexus; P, pituitary; RCA, rectus capitis anterior; SPS, superior petrosal sinus; SiS, sigmoid sinus; SS, sphenoidal sinus; TC, tentorium cerebelli; TJ, temporomandibular joint. TL, temporal lobe. Bar = 5 mm.

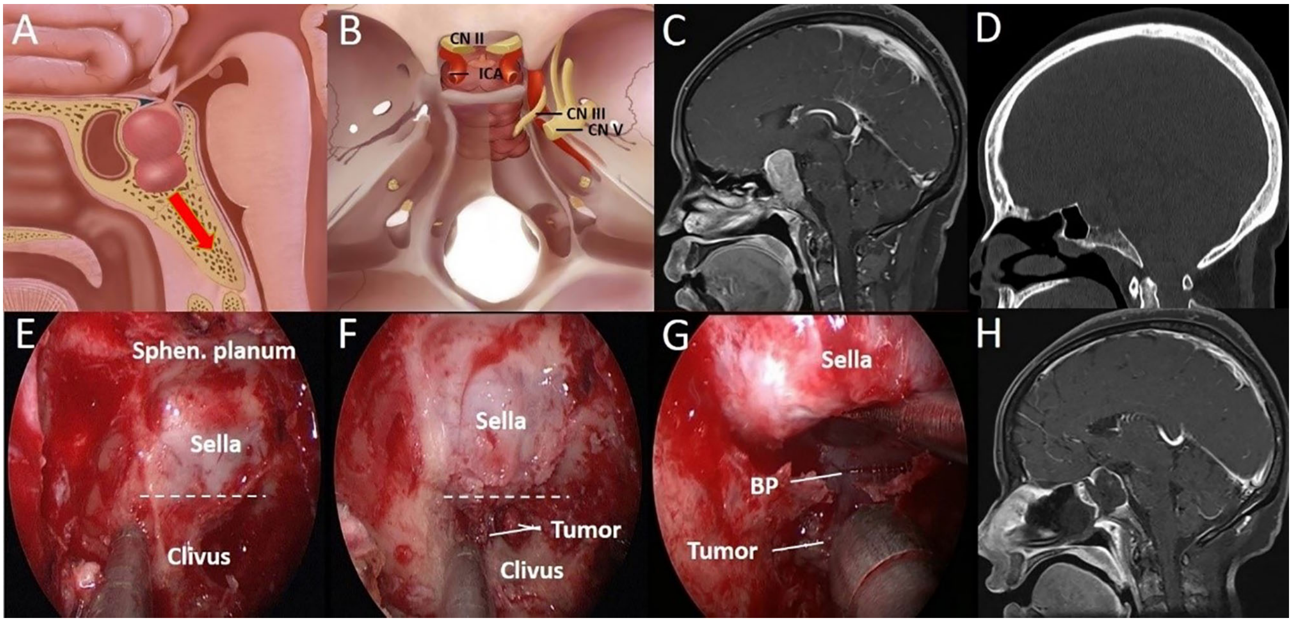

FIGURE 3 | A 44-year-old woman with binocular vision blurred and headache for 2 years was aggravated for 10 days. **(A)** Artistic illustration demonstrating that the tumor directly invades the clivus through the sellar floor on sagittal view. **(B)** Intracranial view of PA with clival invasion. **(C)** Preoperative sagittal T1-weighted MRI shows PA with a daughter tumor in the clivus. **(D)** The CT bone window shows a presellar SS. The bony structure was destroyed to the middle clivus by tumor invasion. **(E)** After completion of the sphenoidotomy, SS is confirmed as presellar type under an endoscopic view. **(F)** The daughter tumor was exposed after drilling off the bony structure in the clivus recess. **(G)** Through the sellar floor, the breakthrough point of tumor invasion to the clivus can be seen directly under a close-up view. **(H)** Postoperative T1-weighted MRI shows complete resection of the tumor in the clivus. The dotted line indicates the location of the sellar floor. BP, Breakthrough point; CN, Cranial nerve; ICA, Internal carotid artery; Sphen, Sphenoid.

It is necessary to be familiar with these anatomical characteristics to completely remove the tumor without neurovascular injury.

Surgical Outcomes

The mean follow-up time was 29.5 months (range 5–58 months). Of the 49 tumors, 35 (71.4%) were nonfunctional adenomas, and 14 (28.6%) were functional adenomas. According to the Knosp classification system (18), 33 (67.3%) cases were classified as grade 4 cases, and 16 (32.7%) cases were classified as grade 1–3 cases.

Thirty-one (63.3%) patients had presellar SS with clival invasion, including eight (16.3%) patients without SS invasion and 23 (46.9%) patients with SS invasion. Ten (20.4%) patients had sellar SS. In addition, SS was difficult to identify in 8 patients, mainly due to the patient having a history of endoscopic surgery or extensive skull base destruction caused by giant PA invasion.

Regarding the extent of clival invasion, 22 (44.9%) patients had middle clival invasion, and 27 (55.1%) had inferior clival invasion. The intraoperative assessment and postoperative MRI findings on the extent of tumor resection showed that 31 (63.3%) patients underwent gross total resection, 15 (30.6%) patients underwent subtotal resection, and three (6.1%) patients underwent partial resection. In 44 (89.8%) PA patients, the clival component was completely resected, and only five (10.2%) patients in the early stage had partial residual cases in the inferior clivus (**Table 1**).

Two patients had transient abducens nerve palsy, and no complications, such as auditory nerve or hypoglossal nerve injury, occurred. One (1/31) of the patients with total resection had recurrence at the last follow-up. Of the 18 patients who underwent subtotal or partial resection, nine underwent postoperative radiotherapy, and five underwent reoperation. At the last follow-up, there were five cases of recurrence.

DISCUSSION

According to the biological behavior of the tumor, PAs can be considered noninvasive PAs, invasive PAs or pituitary cancer. The concept of invasive PA was first proposed by Jefferson in 1940 and refers to the condition in which PA cells invade the surrounding structures and destroy corresponding tissues (19). Among the types of invasive PA, clival invasion is easily ignored, but it is worthy of further study.

Characteristics of PA With Clival Invasion

The clivus is an endochondral bone; its progression involves cartilaginous formation followed by reabsorption preceding bone deposition (20, 21). At birth, the clivus is composed of partially ossified basioccipital and basisphenoid parts separated by the spheno-occipital synchondrosis. PA with clival involvement has been reported for many years (10, 22, 23); however, the growth corridors of clival invasion and corresponding surgical techniques have not been delineated. With exploration of clival invasion corridors, a high total resection rate has been achieved in our center.

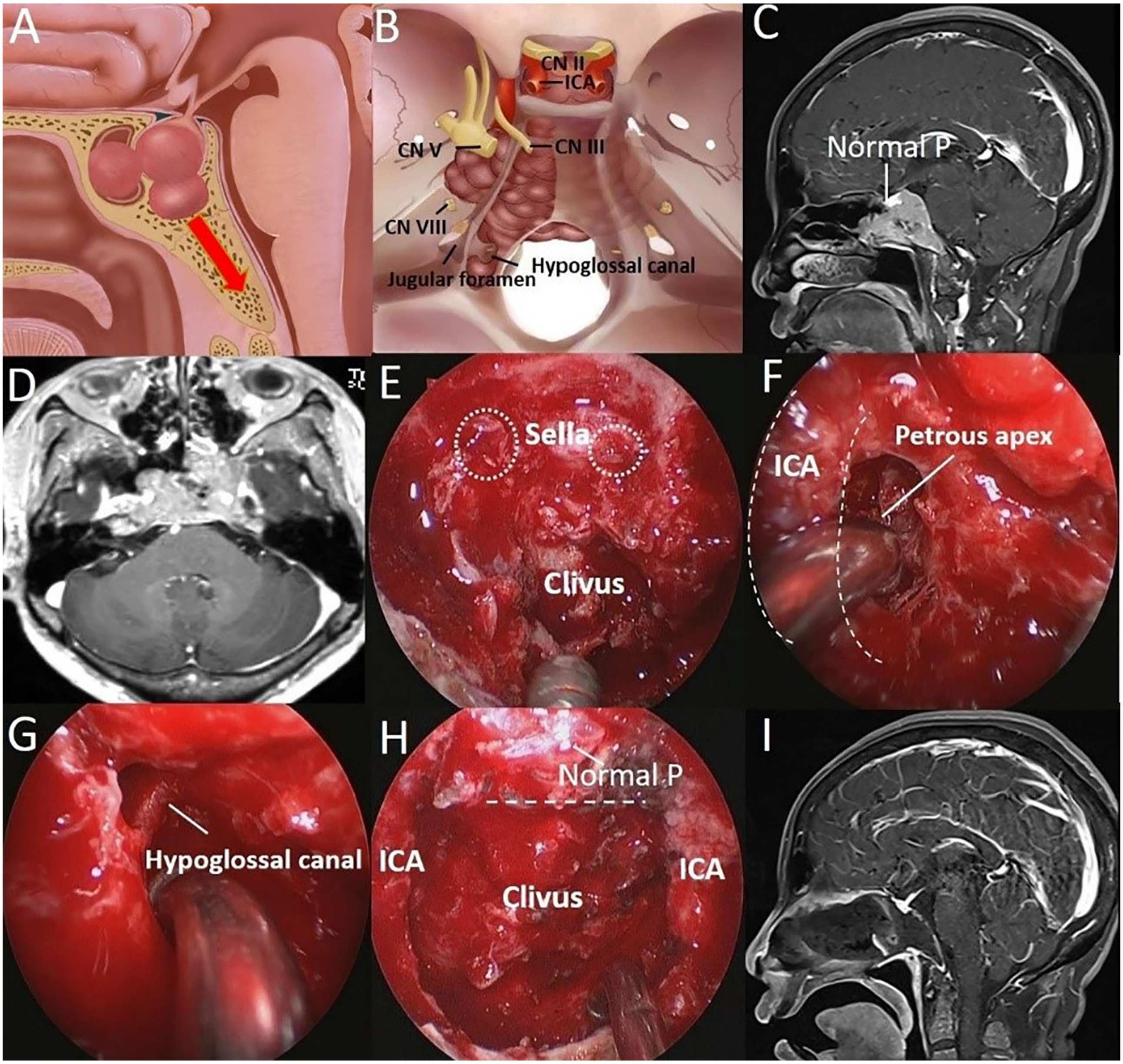

FIGURE 4 | A 51-year-old woman was hospitalized 8 years after surgery for PA, and tumor recurrence was found for 1 year. **(A)** Artistic illustration demonstrating PA with clival and SS invasion simultaneously in presellar SS on sagittal view. **(B)** Intracranial view of PA extending laterally to the petrous apex and downward to the hypoglossal canal. **(C)** Preoperative sagittal T1-weighted MRI shows a PA extending to the inferior clivus, and the normal pituitary can be seen above the tumor. **(D)** Preoperative axial T1-weighted MRI shows a tumor with bilateral petrous apex extension. **(E)** After completion of the sphenoidotomy, SS is confirmed as presellar type under an endoscopic view. The breakthrough point of the PA from the anterior sellar wall into the SS can be seen. (white dotted circle). **(F)** The tumor (petrous apex component) was resected through the posterior space of the paraclival ICA (dotted curved line) under a 30° endoscope. **(G)** The tumor around the hypoglossal canal was resected under a 30° endoscope. **(H)** The tumor was completely resected, and the normal pituitary was well protected. The dotted line indicates the location of the sellar floor. **(I)** Postoperative T1-weighted MRI shows complete resection of the tumor in the clivus.

The characteristics of clival invasion in PA are obvious and unique. Because PAs often extends along the loose cancellous corridor without cortical bone erosion, tumor growth in the clivus remains within the bone cavity and is restricted by tough cortical bone. Therefore, the configuration of the clivus bone in radiological images does not appear abnormal, whereas other tumors such as chordoma and osteogenic tumors are often accompanied by cortical bone invasion and distort the appearance of the clivus bone.

The clival component is different from any other invasive region. Intraoperatively, we found that PA in the sellar, SS, suprasellar region and cavernous sinus were easily aspirated as a whole by a

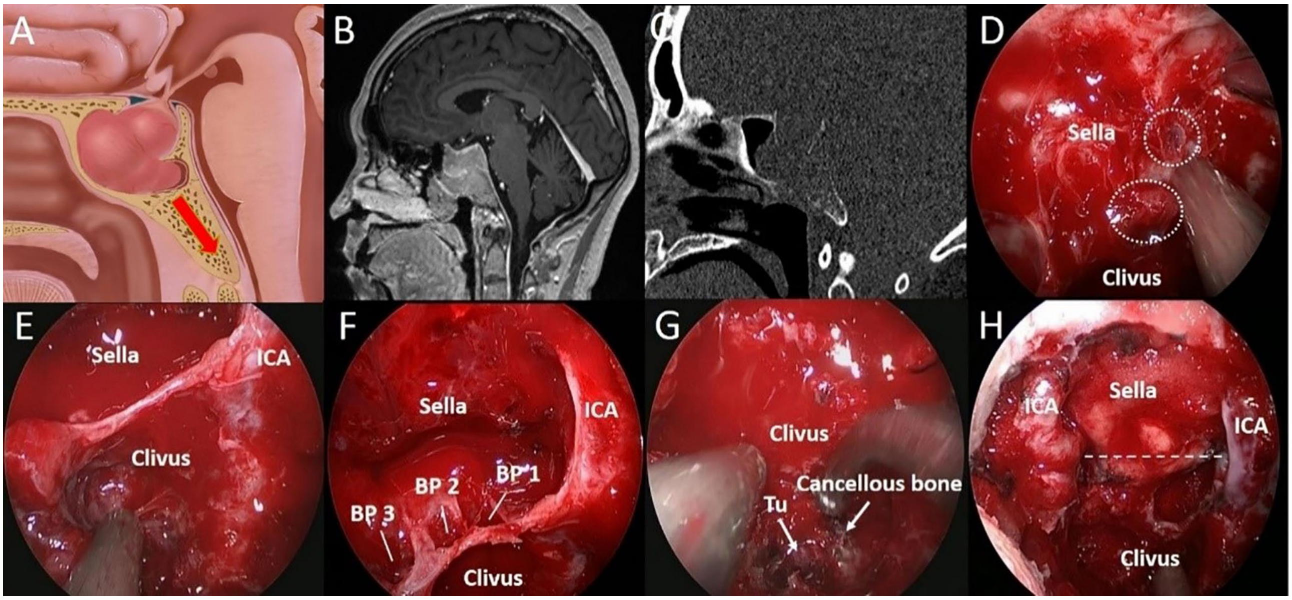

FIGURE 5 | A 37-year-old woman with binocular vision blurred for 3 months. **(A)** Artistic illustration demonstrating that the PA invades the clivus through the SS floor with sufficient pneumatization on sagittal view. **(B)** Preoperative sagittal T1-weighted MRI shows PA with SS and clival invasion. **(C)** The bone window image of CT shows that SS pneumatization is sellar type. The bony structure was destroyed to the inferior clivus by tumor invasion. **(D)** After resecting the SS component, the breakthrough point of the PA from the anterior sellar wall into the SS can be seen. (white dotted circle). **(E)** Intraoperative observation confirmed that the SS was sellar type. In addition, the tumors in the middle clivus on MRI were all in the SS. **(F)** After tumor resection in the sellar region, it was found that there were three breakthrough points in the sellar floor, which led to downward invasion. **(G)** Intraoperative observation showed that the tumor (Tu) was hidden in the honeycomb-like structure formed by the cancellous bone within the clivus. **(H)** The tumor was completely resected, and the bilateral ICAs were exposed in the surgical field. The dotted line indicates the location of the sellar floor.

TABLE 1 | Clinical characteristics of 49 PA with clival invasion.

Variables	No. of Patients
Gender	
Female	31 (63.3%)
Male	18 (36.7%)
Age (years)	49.1
Pathological types	
Nonfunctional	35 (71.4%)
Functional	14 (28.6%)
Knosp grade	
4	33 (67.3%)
1–3	16 (32.7%)
Extent of clival invasion	
Middle	22 (44.9%)
Inferior	27 (55.1%)
Extent of resection (Entire PA)	
GTR	31 (63.3%)
STR	15 (30.6%)
PR	3 (6.1%)
Extent of resection (Clival component)	44 (89.8%)
GTR	5 (10.2%)
STR	29.5 (5–58) M
Mean follow-up time (Range)	

GTR, gross-total resection; STR, sub-total resection; PR, partial resection; M, month.

suction device. In contrast, the tumors in the clivus were separated and mixed by numerous tiny and paper-like bone septa and hidden in the honeycomb-like cancellous bone. Therefore, it was difficult to achieve complete resection because it was difficult to aspirate the tumors by a suction device alone. Residual tumors can cause recurrence and a wider extent of invasion, leading to the need for more complex treatment.

Clivus–Petrous Apex Corridor for PA Invasion

In this study, we researched the relationship between the cancellous bone corridor and PA invasion using microsurgical dissection and the recently developed epoxy sheet plastination technique. The plastination technique uses durable and transparent resin to replace water and fat in tissues and cells, thus keeping all the neural and vascular structures in their natural state *in situ* without decalcification (11, 24, 25). The combination of plastination and microsurgical dissection is a good way to explore the extent of cancellous bone within the clivus. In contrast to other anatomical studies on the clivus, we studied the bony architecture, which helped us better understand the characteristics of PA invasion.

Structurally, cancellous bone is composed of numerous grids of different shapes and sizes, separated by paper-like bony septa and partially communicated, which promotes PA extension. The cancellous bone within cortical bone extends downward from the sellar or SS floor to the occipital condyle and to the medial edge of the jugular foramen. Laterally, the cancellous bone of the clivus and petrous apex are connected through petroclival fissure extending to the medial edge of the internal acoustic meatus. Fortunately, the extent of cancellous bone found in the anatomical study mentioned above was almost the same as that of clival tumor invasion observed during the operation. Obviously, the petrous apex invasion of PA is caused by the tumor invading the clivus and crossing the petroclival fissure along the cancellous bone corridor. Therefore, the results support our hypothesis that the PA with petrous apex invasion is originate from the corridor of cancellous bone within the clivus. This finding is of great significance for selecting the appropriate surgical techniques because it is difficult to achieve total resection with craniotomy or the EEA if the petrous apex corridor is considered to be a separate corridor.

However, because the medial edge of the internal acoustic meatus is composed of tough and dense cortical bone, the petrous apex corridor does not cross it and extend laterally. For downward clival invasion, although the tumor can reach the occipital condyle, it will not erode the bone canal of the hypoglossal nerve. Our anatomic results showed that cortical bone formed around those two bone canals, which explains our intraoperative findings.

SS Pneumatization Affects Clival Invasion

PA extending into the bony structure within the clivus is related to the pneumatization of SS. The SS is located in the body of sphenoid bone, and its pneumatization forms the main sinus cavity occupying the sphenoid body. In cases of well pneumatization, it can extend to the dorsum sellae and clivus, and even to greater and lesser wings, anterior clinoid process and pterygoid process (26).

According to the degree of pneumatization, there are various classification for the types of SS. Hammer et al. classified in the sagittal plane as three types: conchal, presellar, and sellar (13). Based on the correlation of endoscopic skull base surgery, Vaezi et al. classified SS pneumatization into three types: previdian, intercanal, and postrotundum (27). Wang et al. classified SS into the six basic types based on the direction of pneumatization: sphenoid body, lateral, clival, lesser wing, anterior, and combined (26). The most widely adopted classification is proposed by Hammer, which is also used in this study.

Different types of SS require different surgical techniques and intraoperative precautions. For conchal-type SS, we believe that the corridor of clival invasion directly extends into the clivus without SS invasion. Among the cases in our study, pressellar SS with both clivus and SS invasion was the most common type (46.9%, 23/49). This kind of tumor invades the clivus extensively, reaching all longitudinal regions of the cancellous bone within the clivus.

In patients with sellar SS, PAs can extend to the SS first and then erode the clivus through the SS floor. However, this phenomenon is relatively rare because the tumor always grows along the direction of the least resistance, and tumors more commonly fill the SS and then protrude into the nasal cavity. Most importantly, according to our experience, this type of tumor often invades the bony structure, which covers the paraclival ICA, so the operation should be performed carefully.

Furthermore, cases of sufficient SS pneumatization that extends to the inferior clivus can be mistaken as cases of clivus invasion preoperatively, but in fact, these tumors are located in the SS without clival bony erosion. Therefore, we should carefully determine whether the cortical bone of the SS floor is invaded by a PA with preoperative CT bone window imaging (**Figure 6**).

Surgical Approaches

In traditional craniotomy, the upper clivus can be approached through the orbitozygomatic route or the variant approach; the middle clivus can be reached through the transpetrosal approach; and the lower clivus can be accessed through the far-lateral approach. Due to the proximity of the clivus to critical neurovascular structures, clival surgery is associated with a high rate of postoperative complications and recurrences (28).

In most cases, PA with clival invasion is located in only the epidural space and does not require a transcranial procedure. With the advanced EEA, the resection of clival lesions is relatively easy since this approach allows direct visualization and exposes the ventral side of the whole clivus without intracranial manipulation (29–31). The natural corridor of tumor invasion from the sellar to the clivus can be fully exposed with the EEA, which plays a significant role in total tumor resection. Therefore, the EEA should be considered the preferred approach for this type of tumor.

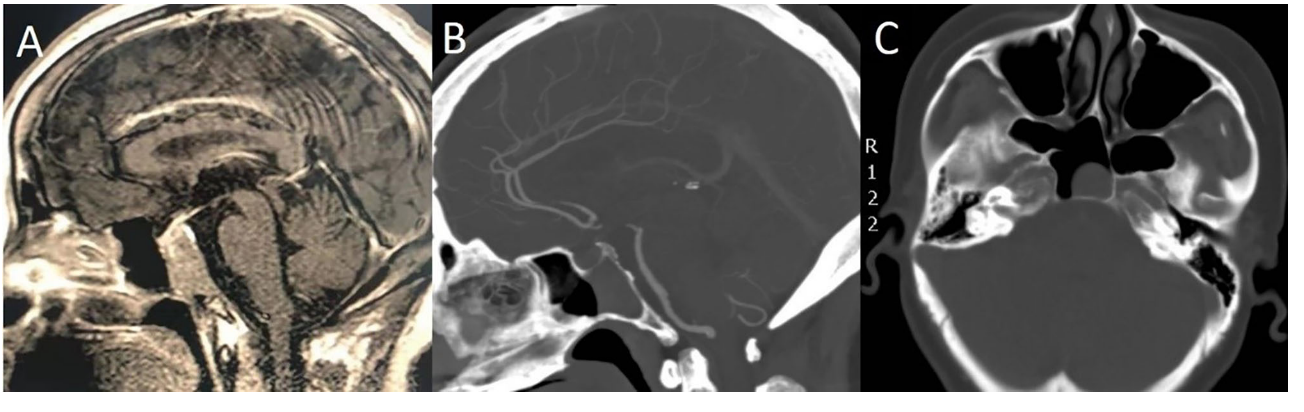

FIGURE 6 | A 55-year-old woman with headache for 4 months. **(A)** Preoperative sagittal T1-weighted MRI shows PA with clival invasion. **(B)** Sagittal CT bone window shows that the patient had sufficient SS pneumatization. The cortical bone of the SS floor was intact, and the tumors were all in the SS without clival bony erosion. **(C)** Axial CT bone window shows that the tumor was completely located in the SS.

Limitations

Most of the cases in our study had multidirectional invasion, and few tumors invaded only the clivus, which is more representative. Preoperative CT bone window imaging can be used to predict the locations of corridors, but this process is difficult in patients with a history of endoscopic surgery and giant PA with extensive bone destruction of the skull base.

CONCLUSION

We confirmed the intraoperative finding that PAs within the clivus was extend through the cancellous bone corridor by conducting microanatomic and plastination studies. PAs with petrous apex invasion are caused by the tumor invading the clivus and further crossing the petroclival fissure along the cancellous bone corridor. Moreover, we have also found that the degree of SS pneumatization has a large influence on clival invasion. These growth characteristics of clival invasion are different from those of tumors in other invasive regions, requiring different surgical techniques. On this basis, we will greatly improve the total resection rate of PA invading the clivus and reduce recurrence.

DATA AVAILABILITY STATEMENT

The original contributions presented in the study are included in the article/supplementary material. Further inquiries can be directed to the corresponding authors.

ETHICS STATEMENT

The studies involving human participants were reviewed and approved by the Institutional Review Board of Nanchang University. The patients/participants provided their written informed consent to participate in this study.

AUTHOR CONTRIBUTIONS

TH and LL: study concept and design. XW, HD, LY and XC: acquisition of data. SX, YB, and JW: analysis and interpretation of data. YY, LZ, ML, SL, BT, LX and CZ: critical revision of manuscript. All authors contributed to the article and approved the submitted version.

FUNDING

This work was supported by the National Natural Science Foundation of China (grant nos. 82060246 and 31500967), Natural Science Foundation of the Anhui Higher Education Institutions of China (No. KJ2020A0145).

ACKNOWLEDGMENTS

We express our sincere appreciation to Miss Jing Liu and Yi Su for the illustration.

REFERENCES

1. Meij BP, Lopes MB, Ellegala DB, Alden TD, Laws EJ. The Long-Term Significance of Microscopic Dural Invasion in 354 Patients With Pituitary Adenomas Treated With Transsphenoidal Surgery. *J Neurosurg* (2002) 96:195–208. doi: 10.3171/jns.2002.96.2.0195
2. Fernandez-Miranda JC, Zwagerman NT, Abhinav K, Lieber S, Wang EW, Snyderman CH, et al. Cavernous Sinus Compartments From the Endoscopic Endonasal Approach: Anatomical Considerations and Surgical Relevance to Adenoma Surgery. *J Neurosurg* (2018) 129:430–41. doi: 10.3171/2017.2.JNS162214
3. Cohen-Cohen S, Gardner PA, Alves-Belo JT, Truong HQ, Snyderman CH, Wang EW, et al. The Medial Wall of the Cavernous Sinus. Part 2: Selective Medial Wall Resection in 50 Pituitary Adenoma Patients. *J Neurosurg* (2018) 131:131–40. doi: 10.3171/2018.5.JNS18595
4. Micko A, Oberndorfer J, Weninger WJ, Vila G, Hoftberger R, Wolfsberger S, et al. Challenging Knosp High-Grade Pituitary Adenomas. *J Neurosurg* (2019) 132:1739–46. doi: 10.3171/2019.3.JNS19367
5. Niu J, Zhang S, Ma S, Diao J, Zhou W, Tian J, et al. Preoperative Prediction of Cavernous Sinus Invasion by Pituitary Adenomas Using a Radiomics Method Based on Magnetic Resonance Images. *Eur Radiol* (2019) 29:1625–34. doi: 10.1007/s00330-018-5725-3
6. Appel JG, Bergsneider M, Vinters H, Salamon N, Wang MB, Heaney AP. Acromegaly Due to an Ectopic Pituitary Adenoma in the Clivus: Case Report and Review of Literature. *Pituitary* (2012) 15(Suppl 1):S53–6. doi: 10.1007/s11102-011-0345-9
7. Mudd PA, Hohensee S, Lillehei KO, Kingdom TT, Kleinschmidt-Demasters BK. Ectopic Pituitary Adenoma of the Clivus Presenting With Apoplexy: Case Report and Review of the Literature. *Clin Neuropathol* (2012) 31:24–30. doi: 10.5414/np300421
8. Anand VK, Osborne CM, Harkey HR. Infiltrative Clival Pituitary Adenoma of Ectopic Origin. *Otolaryngol Head Neck Surg* (1993) 108:178–83. doi: 10.1177/019459989310800213
9. Tajudeen B, Kuan E, Adappa N, Han J, Chandra R, Palmer J, et al. Ectopic Pituitary Adenomas Presenting as Sphenoid or Clival Lesions: Case Series and Management Recommendations. *J Neurological Surg Part B: Skull Base* (2017) 78:120–4. doi: 10.1055/s-0036-1592081
10. Chen X, Dai J, Ai L, Ru X, Wang J, Li S, et al. Clival Invasion on Multi-Detector CT in 390 Pituitary Macroadenomas: Correlation With Sex, Subtype and Rates of Operative Complication and Recurrence. *AJNR Am J Neuroradiol* (2011) 32:785–9. doi: 10.3174/ajnr.A2364
11. Liang L, Qu L, Chu X, Liu Q, Lin G, Wang F, et al. Meningeal Architecture of the Jugular Foramen: An Anatomic Study Using Plastinated Histologic Sections. *World Neurosurg* (2019) 127:e809–17. doi: 10.1016/j.wneu.2019.03.272
12. Patel CR, Fernandez-Miranda JC, Wang WH, Wang EW. Skull Base Anatomy. *Otolaryngol Clin North Am* (2016) 49:9–20. doi: 10.1016/j.otc.2015.09.001
13. HAMMER G, RADBERG C. The Sphenoidal Sinus. An Anatomical and Roentgenologic Study With Reference to Transsphenoid Hypophysectomy. *Acta Radiol* (1961) 56:401–22. doi: 10.1177/028418516105600601
14. Wu X, Xie SH, Tang B, Yang YQ, Yang L, Ding H, et al. Pituitary Adenoma With Posterior Area Invasion of Cavernous Sinus: Surgical Anatomy, Approach, and Outcomes. *Neurosurg Rev* (2020). doi: 10.1007/s10143-020-01404-1
15. Barges-Coll J, Fernandez-Miranda JC, Prevedello DM, Gardner P, Morera V, Madhok R, et al. Avoiding Injury to the Abducens Nerve During Expanded Endonasal Endoscopic Surgery: Anatomic and Clinical Case Studies. *Neurosurgery* (2010) 67:144–54; discussion 154. doi: 10.1227/01.NEU.0000370892.11284.EA

16. Borghei-Razavi H, Truong HQ, Fernandes CD, Sun X, Celtikci E, Wang E, et al. Endoscopic Endonasal Petrosectomy: Anatomical Investigation, Limitations, and Surgical Relevance. *Oper Neurosurg (Hagerstown)* (2019) 16:557–70. doi: 10.1093/ons/opy195
17. Morera VA, Fernandez-Miranda JC, Prevedello DM, Madhok R, Barges-Coll J, Gardner P, et al. "Far-Medial" Expanded Endonasal Approach to the Inferior Third of the Clivus: The Transcondylar and Transjugular Tubercle Approaches. *Neurosurgery* (2010) 66:211–9; discussion 219-20. doi: 10.1227/01.NEU.0000369926.01891.5D
18. Micko AS, Wohrer A, Wolfsberger S, Knosp E. Invasion of the Cavernous Sinus Space in Pituitary Adenomas: Endoscopic Verification and its Correlation With an MRI-Based Classification. *J Neurosurg* (2015) 122:803–11. doi: 10.3171/2014.12.JNS141083
19. Jefferson G. Extrasellar Extensions of Pituitary Adenomas: (Section of Neurology). *Proc R Soc Med* (1940) 33:433–58. doi: 10.1177/003591574003300717
20. Rai R, Iwanaga J, Shokouhi G, Loukas M, Mortazavi MM, Oskouian RJ, et al. A Comprehensive Review of the Clivus: Anatomy, Embryology, Variants, Pathology, and Surgical Approaches. *Childs Nerv Syst* (2018) 34:1451–8. doi: 10.1007/s00381-018-3875-x
21. Sajisevi M, Hoang JK, Eapen R, Jang DW. Nasopharyngeal Masses Arising From Embryologic Remnants of the Clivus: A Case Series. *J Neurol Surg Rep* (2015) 76:e253–7. doi: 10.1055/s-0035-1564603
22. Goel A, Phalke U, Cacciola F, Muzumdar DP. Giant Pituitary Adenoma Invading the Clivus. *Neurol India* (2005) 53:105–7. doi: 10.4103/0028-3886.15073
23. Neelakantan A, Rana AK. Benign and Malignant Diseases of the Clivus. *Clin Radiol* (2014) 69:1295–303. doi: 10.1016/j.crad.2014.07.010
24. Xu Z, Tu L, Zheng Y, Ma X, Zhang H, Zhang M. Fine Architecture of the Fascial Planes Around the Lateral Femoral Cutaneous Nerve at Its Pelvic Exit: An Epoxy Sheet Plastination and Confocal Microscopy Study. *J Neurosurg* (2018) 131:1860–8. doi: 10.3171/2018.7.JNS181596
25. Xu T, Yan Y, Evins AI, Gong Z, Jiang L, Sun H, et al. Anterior Clinoidal Meningiomas: Meningeal Anatomical Considerations and Surgical Implications. *Front Oncol* (2020) 10:634. doi: 10.3389/fonc.2020.00634
26. Wang J, Bidari S, Inoue K, Yang H, Rhoton AJ. Extensions of the Sphenoid Sinus: A New Classification. *Neurosurgery* (2010) 66:797–816. doi: 10.1227/01.NEU.0000367619.24800.B1
27. Vaezi A, Cardenas E, Pinheiro-Neto C, Paluzzi A, Branstetter BT, Gardner PA, et al. Classification of Sphenoid Sinus Pneumatization: Relevance for Endoscopic Skull Base Surgery. *Laryngoscope* (2015) 125:577–81. doi: 10.1002/lary.24989
28. Kim YH, Jeon C, Se YB, Hong SD, Seol HJ, Lee JI, et al. Clinical Outcomes of an Endoscopic Transclival and Transpetrosal Approach for Primary Skull Base Malignancies Involving the Clivus. *J Neurosurg* (2018) 128:1454–62. doi: 10.3171/2016.12.JNS161920
29. Cheng Y, Zhang S, Chen Y, Zhao G. Safe Corridor to Access Clivus for Endoscopic Trans-Sphenoidal Surgery: A Radiological and Anatomical Study. *PloS One* (2015) 10:e0137962. doi: 10.1371/journal.pone.0137962
30. de Notaris M, Cavallo LM, Prats-Galino A, Esposito I, Benet A, Poblete J, et al. Endoscopic Endonasal Transclival Approach and Retrosigmoid Approach to the Clival and Petroclival Regions. *Neurosurgery* (2009) 65:42–50; discussion 50-2. doi: 10.1227/01.NEU.0000347001.62158.57
31. Kassam AB, Gardner P, Snyderman C, Mintz A, Carrau R. Expanded Endonasal Approach: Fully Endoscopic, Completely Transnasal Approach to the Middle Third of the Clivus, Petrous Bone, Middle Cranial Fossa, and Infratemporal Fossa. *Neurosurg Focus* (2005) 19:E6. doi: 10.3171/foc.2005.19.1.7

Conflict of Interest: The authors declare that the research was conducted in the absence of any commercial or financial relationships that could be construed as a potential conflict of interest.

frontiers in Oncology

ORIGINAL RESEARCH
published: 06 July 2021
doi: 10.3389/fonc.2021.674889

Balloon Test Occlusion of Internal Carotid Artery in Recurrent Nasopharyngeal Carcinoma Before Endoscopic Nasopharyngectomy: A Single Center Experience

Renhao Yang†, Hui Wu†, Binghong Chen†, Wenhua Sun, Xiang Hu, Tianwei Wang, Yubin Guo, Yongming Qiu* and Jiong Dai*

Department of Neurosurgery, Renji Hospital, School of Medicine, Shanghai Jiao Tong University, Shanghai, China

OPEN ACCESS

Edited by:
Xicai Sun,
Fudan University, China

Reviewed by:
Lin Kong,
Fudan University, China
Bian Liuguan,
Shanghai Jiao Tong University, China

***Correspondence:**
Jiong Dai
daijiong@renji.com
Yongming Qiu
qiuzhoub@126.com

†*These authors have contributed equally to this work and share first authorship*

Specialty section:
This article was submitted to Surgical Oncology, a section of the journal Frontiers in Oncology

Received: 02 March 2021
Accepted: 03 May 2021
Published: 06 July 2021

Citation:
Yang R, Wu H, Chen B, Sun W, Hu X, Wang T, Guo Y, Qiu Y and Dai J (2021) Balloon Test Occlusion of Internal Carotid Artery in Recurrent Nasopharyngeal Carcinoma Before Endoscopic Nasopharyngectomy: A Single Center Experience. Front. Oncol. 11:674889. doi: 10.3389/fonc.2021.674889

Objectives: Endoscopic nasopharyngectomy (ENPG) is a promising way in treating recurrent nasopharyngeal carcinoma (rNPC), but sometimes may require therapeutic internal carotid artery (ICA) occlusion beforehand. Balloon test occlusion (BTO) is performed to evaluate cerebral ischemic tolerance for ICA sacrifice. However, absence of neurological deficits during BTO does not preclude occur of delayed cerebral ischemia after permanent ICA occlusion. In this study, we evaluate the utility of near-infrared spectroscopy (NIRS) regional cerebral oxygen saturation (rSO_2) monitoring during ICA BTO to quantify cerebral ischemic tolerance and to identify the valid cut-off values for safe carotid artery occlusion. This study also aims to find out angiographic findings of cerebral collateral circulation to predict ICA BTO results simultaneously.

Material and Methods: 87 BTO of ICA were performed from November 2018 to November 2020 at authors' institution. 79 angiographies of collateral flow were performed in time during BTO and classified into several Subgroups and Types according to their anatomic and collateral flow configurations. 62 of 87 cases accepted monitoring of cerebral rSO_2. Categorical variables were compared by using Fisher exact tests and Mann–Whitney U tests. Receiver operating characteristic curve analysis was used to determine the most suitable cut-off value.

Results: The most suitable cut-off $\triangle rSO_2$ value for detecting BTO-positive group obtained through ROC curve analysis was 5% (sensitivity: 100%, specificity: 86%). NIRS rSO_2 monitoring wasn't able to detect BTO false-negative results ($p = 0.310$). The anterior Circle was functionally much more important than the posterior Circle among the primary collateral pathways. The presence of secondary collateral pathways was considered as a sign of deteriorated cerebral hemodynamic condition during ICA BTO. In Types 5 and 6, reverse blood flow to the ICA during BTO protected patients from delayed cerebral ischemia after therapeutic ICA occlusion ($p = 0.0357$). In Subgroup IV, absence of the posterior Circle was significantly associated with BTO-positive results ($p = 0.0426$).

Conclusion: Angiography of cerebral collateral circulation during ICA BTO is significantly correlated with ICA BTO results. Angiographic ICA BTO can be performed in conjunction with NIRS cerebral oximeter for its advantage of being noninvasive, real-time, cost-effective, simple for operation and most importantly for its correct prediction of most rSO_2 outcomes of ICA sacrifice. However, in order to ensure a safe carotid artery occlusion, more quantitative adjunctive blood flow measurements are recommended when angiography of cerebral collateral circulation doesn't fully support rSO_2 outcome among clinically ICA BTO-negative cases.

Keywords: balloon test occlusion, recurrent nasopharyngeal carcinoma, endoscopic nasopharyngectomy, near-infrared spectroscopy cerebral oximeter, regional cerebral oxygen saturation, cerebral collateral circulation

INTRODUCTION

Nasopharyngeal carcinoma (NPC) features itself by its distinct geographical distribution, particularly prevails in east and southeast Asia (1). Radiotherapy, combined with or without chemotherapy, is the primary treatment modality for initially untreated NPC (2). However, it is also noteworthy that about 10–20% of NPC patients have suffered from local recurrence on follow-up after primary treatment (3). The management of recurrent nasopharyngeal carcinoma (rNPC) is challenging, while re-irradiation and endoscopic nasopharyngectomy (ENPG) serve as the two mainstays of the treatment of rNPC (4, 5). Radiotherapy of recurrent locoregional tumor mass has reached the bottleneck among rNPC patients owing to its high rate of severe complications such as osteoradionecrosis, temporal lobe necrosis, multiple cranial nerve dysfunction and potentially fatal bleeding, which can greatly impair patients' quality of life and occasionally result in death (6). In comparison to re-irradiation, endoscopic surgical resection is a new, promising and better way in treating selected rNPC patients in terms of locoregional control rate and overall survival (OS) rate with lower incidence of long-term severe complications (2).

However, preoperative safety management of internal carotid artery (ICA) is of vital importance before surgery, because ICA bleeding can be catastrophic during the operation, especially for tumors invading the ICA. In fact, patients harboring head and neck tumors may require therapeutic occlusion of ICA before tumor resection as preoperative preparation (7). Permanent occlusion of ICA is a useful procedure, but carries the risk of severe and irreversible complications caused by immediate or delayed hemodynamic cerebral ischemia (8). Balloon test occlusion (BTO) of ICA is performed to evaluate cerebral ischemic tolerance for the purpose of reducing neurological ischemic complications after permanent occlusion of ICA among these patients (9). Awareness of the reliance of ICA among patients is quite essential, because covered stent implantation or vascular bypass might be needed for patients when ICA sacrifice is not tolerated (10–12). Scholars have demonstrated that ischemic complication rate for unselected ICA occlusion without BTO reached 26%, with 12% mortality rate related to the cerebral infraction, and was reduced to 13% when BTO was performed (13). However, several previous studies have also revealed that BTO alone still carried a false-negative risk of 3.3–10.0% (13, 14). That is why adjunctive techniques are used in combination with BTO to increase its sensitivity (15). However, most of the blood flow measurements proposed in addition to the basic method require specialized equipment, thus increasing the complexity and perioperative complications due to the extended inflation time of the balloon (16).

Meanwhile, blood flow obstructed during BTO of ICA can be recruited from other places, depending on the development of collateral pathways including the Circle of Willis (CoW) (17). Hence, we speculate that some of the ICA BTO results can be predicted by angiographic findings of cerebral collateral circulation.

The present study reviewed our institutional experience in a simple paradigm combining clinical tolerance with monitoring of regional cerebral oxygen saturation (rSO_2) and angiographic crossflow assessment. In this study, we evaluated the utility of near-infrared spectroscopy (NIRS) cerebral oximeter, which could calculate and monitor rSO_2 in real time during ICA BTO, to quantify ischemic tolerance and to identify the valid cut-off values for safe carotid artery occlusion. This study also tried to find out some angiographic findings of cerebral collateral circulation to predict ICA BTO results, which might help to choose a more suitable and individualized adjunctive measurement during BTO (18).

MATERIAL AND METHODS

Patients

From November 2018 to November 2020, 81 consecutive patients (59 males and 22 females, mean age: 52.5 years old, range from 28 to 70 years old) who underwent BTO for ICA on the lesion side were enrolled in the study. Apart from 81 patients, another six patients didn't manage to perform ICA BTO, because they were identified with chronic internal carotid artery occlusion (CICAO) on the lesion side after DSA confirmation before BTO (**Supplemental Table 4**). All patients had a clear diagnosis of rNPC and those with distant metastasis were excluded.

Balloon Test Occlusion Procedure

Informed consent was obtained from every patient. The probes of NIRS cerebral oximeter (MC-2030C cerebral oximeter, CAS MEDICAL SYSTEMS Inc., USA) were placed on the forehead of both sides, and rSO_2 was monitored continuously during all procedures. The whole procedure was performed under local anesthesia. The patients were wide awake and were aware that the operator would continuously communicate with them to evaluate his or her motor function, sensory system, speech, orientation and cognition during the procedure.

All procedures were performed with single plane DSA equipment, Innova 3100-IQ (GE Inc., USA) and Artis Q Zeego (Simens Inc., Germany). After local anesthesia induction, a 6-French femoral sheath was inserted into the right femoral artery. After that, control anteroposterior and lateral angiography of bilateral ICAs and unilateral vertebral artery (VA) were performed at six frames per second before BTO with a diagnostic catheter. Heparin was administered intravenously after a puncture to prevent procedure-related thromboembolic complications. A nondetachable balloon catheter was then introduced and placed in the distal cervical segment of ICA on the lesion side through the balloon guiding catheter. The balloon positioned in the lower segment of the ICA might lead to bradycardia and a transient drop of blood pressure (BP) caused by carotid sinus reflex, which might affect the result of BTO.

After performing the initial neurological evaluation, the balloon (Sterling Monorail, Boston Scientific Inc., USA) was then inflated under fluoroscopic visualization with angiographic confirmation of complete flow arrest of the vessel. The tested ICA was occluded for a total duration of 30 min and a neurological assessment was repeated immediately after the occlusion and every 5 min during the test. If the patient didn't show with sign of the symptoms caused by hemodynamic cerebral ischemia 15 min after the temporary occlusion of ICA, the operator would puncture the left femoral artery and performed angiography of the contralateral ICA and the unilateral VA to evaluate the collateral circulation with the balloon inflated. As soon as any neurological deficit with rSO_2 abnormality was detected during the procedure, the balloon was deflated immediately regardless of the collateral angiography. Under such circumstance, the BTO was considered positive. Once the patient clinically tolerated the 30-min occlusion, the BTO was judged to be negative. Patient developing delayed cerebral ischemia after therapeutic ICA occlusion was judged to be false-negative.

Post-Occlusion Protocol

Hemostasis at the femoral punctures were treated by electronic compressor. After permanent ICA occlusion by coiling, patients were transferred to the intensive care unit (ICU) where fluid balance, neurologic status, and blood pressure were carefully monitored. Subcutaneous heparin at therapeutic dosages was continued for 48 h. Routine head CT scanning was performed 24 h after carotid occlusion. Attention was focused on detecting symptoms of cerebral ischemia that might have been caused by the occlusion of a carotid artery. BP monitoring was another concern after the operation. BP should be kept pharmacologically elevated for 48 h to avoid possible episode of hypotension if necessary. Early stage of permanent blockage of the blood flow to the ICA might lead to an increased pressure within the carotid sinus, hence resulting in a temporary drop in BP and subsequent craniocerebral hypoperfusion. If no delayed cerebral hemodynamic ischemia was detected, the patients were discharged 5 days after the treatment and then transferred to EYE & ENT hospital of Fudan University for salvage ENPG.

Anatomic Configuration and Collateral Flow Configuration

It is widely acknowledged that the CoW exhibits considerable anatomical variations (19–21). A complete CoW only accounts for approximately 50% of the population (19, 20, 22). The anterior Circle of CoW is composed of the anterior communicating artery (AcomA) and the proximal anterior cerebral artery (ACA) segments (A1) (23). Asymmetry of anterior cerebral artery trunks (A1), with one side A1 (larger diameter) as the dominant supply to both pericallosal arteries (A2) is a common anatomic variation within the anterior part of the CoW and is regarded as an important factor in the formation of aneurysms of the AcomA by producing different hemodynamic stress (24). For another, blood flow through a vessel can be modeled mathematically by using the Pouseille equation relating flow (25). F; to vessel length, L; the pressure drops across the vessel, ΔP; the blood viscosity, η; and the vessel diameter, d:

$$F \propto \frac{\Delta P \cdot d^4}{\eta \cdot L}$$

Under this theory, for two vessels of similar length and pressure, a two times of difference in vessel diameter leads to a sixteen times of difference in blood flow. The Pouseille equation shows that vessel diameter influences the blood supply significantly.

Thus, we speculate that relative position of tested side ICA and dominant A1 will have a great impact on collateral blood flow recruitment and subsequently affect results of BTO. In the presence of AcomA, the A1 to A2 flow dominance was classified on a 3-point scale: symmetric, no clear dominance of the inflow contribution of one A1 segment over the other; dominant, one A1 segment clearly contributes more inflow to an A2 than the other; and complete, no detectable inflow contribution from the contralateral segment. As for the posterior Circle of CoW, it is composed of the posterior communicating arteries (PcomA) and the P1 segments of the posterior cerebral arteries (PCA) (23). Similarly, absence of PcomA and complete fetal PCA (cfPCA), who completely originates from the ICA with no connection with the basilar artery, are other common variants of cerebral circulation (26).

In our study, the CoW anatomical variations were categorized into several Subgroups (**Figure 1**) as follows based on the

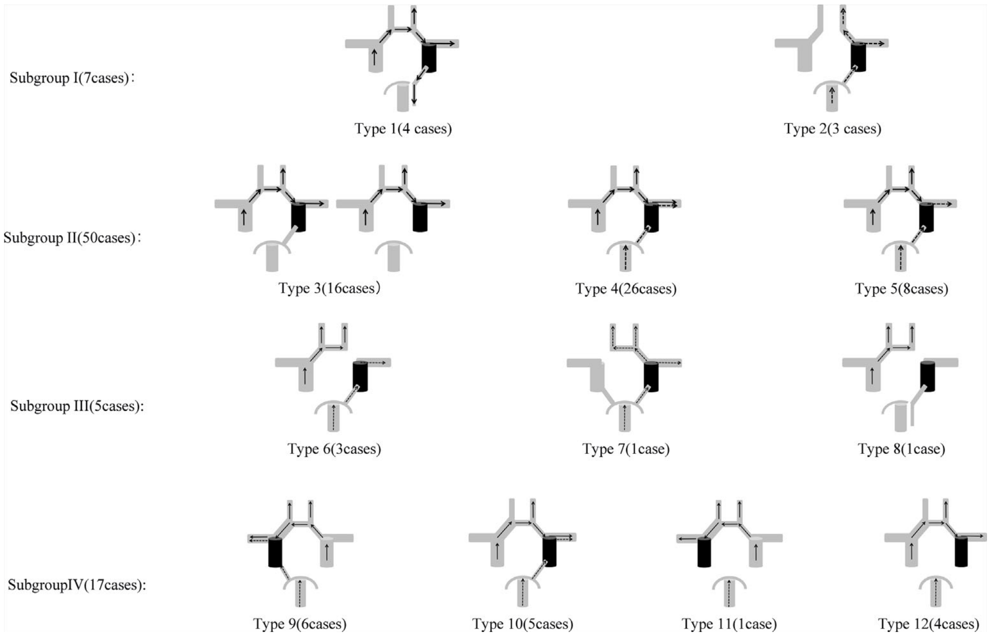

FIGURE 1 | Anatomic Configurations and Collateral Flow Configurations included in this study. Subgroup I: Type 1: A1 to A2 flow dominance: symmetric, cfPCA ipsilateral to tested side; Type 2: AcomA absence, complete posterior Circle ipsilateral to tested side. Subgroup II: A1 to A2 flow dominance: symmetric. Type 3: Tested side MCA area blood supply: the anterior Circle alone; Type 4: Tested side MCA area blood supply: both the anterior Circle and the posterior Circle; Type 5: Tested side MCA area blood supply: the posterior Circle alone. Subgroup III: A1 to A2 flow dominance: complete. Type 6: A1 absence ipsilateral to the tested side; Type 7: A1 absence contralateral to the tested side; Type 8: A1 absence ipsilateral to the tested side, cfPCA ipsilateral to tested side. Subgroup IV: A1 to A2 flow dominance: dominant. Type 9: A1 dominance ipsilateral to the tested side, complete posterior Circle on tested side; Type 10: A1 dominance contralateral to the tested side, complete posterior Circle on tested side; Type 11: A1 dominance ipsilateral to the tested side, PcomA absence on tested side; Type 12: A1 dominance contralateral to the tested side, PcomA absence on tested side.

presence/absence of AcomA, PcomA and cfPCA, as well as the asymmetry/symmetric of anterior cerebral artery trunks (A1). The Subgroups represented different anatomic configurations of CoW and the Types represented different collateral flow configurations during BTO. The Subgroups and Types only included those we found in this study.

Statistical Analysis

Continuous variables were reported as mean with standard deviations (SD) or median with interquartile ranges (IQR). Categorical variables were compared by using Fisher exact tests and Mann–Whitney U tests. Receiver operating characteristic (ROC) curve analysis was used to determine the most suitable cut-off value based on the shortest distance from the curve to the upper-left corner. The analysis was performed using SPSS Version 25.0 and Medcalc Version 19.0. The level of significance was established at a 0.05 level (two-sided).

RESULTS

87 BTO of ICA were performed, as six patients underwent BTO of bilateral ICAs (left: 48 cases; right: 39 cases). 17 cases were judged to be BTO-positive, three cases were judged to be BTO false-negative and the remaining 67 cases were judged to be BTO-negative. Clinical features of all 87 cases were given in **Supplemental Table 1**.

Cerebral rSO_2 Monitoring

62 of 87 cases accepted real-time monitoring of cerebral rSO_2, among which 12 cases were BTO-positive, 47 cases were BTO-negative and three cases were BTO false-negative. One BTO-positive case (Case No. 77) was excluded in ROC curve analysis because he was found significantly increase in rSO_2, as the patient complained of unbearable headache during the procedure. Decrease in muscle strength of the right limb (Grade 3/5) was also detected by our clinician. The increase in rSO_2 was considered to be attributed to increased blood pressure caused by the pain, and the subsequent angiography of the collateral circulation showed insufficient perfusion of the tested side MCA area. The remaining 11 BTO-positive demonstrated significant drop in tested side rSO_2. As for the decrease in rSO_2, there was no significant difference between BTO false-negative group (2; 3; 4%) and BTO negative group (median, 2%; IQR, 2%) ($p = 0.310$). In our study, the most suitable cut-off $\triangle rSO_2$ value for detecting the BTO-positive group obtained through ROC curve analysis was 5% (sensitivity: 100%, specificity: 86%) (**Figure 2**).

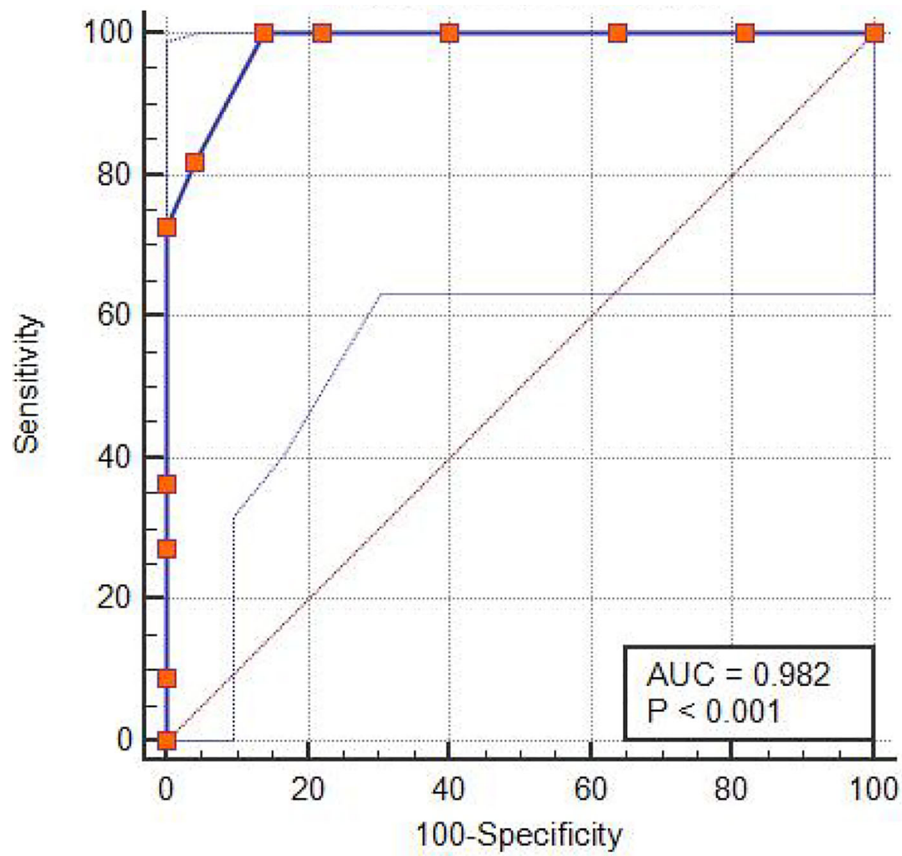

FIGURE 2 | ROC curve analysis for the BTO-positive group. The purple line with orange dots showing ROC curve analysis for the BTO-positive group detected by drop in rSO_2 value.

Angiographic Findings

79 of 87 cases performed complete collateral angiography of contralateral ICA and unilateral VA. Case No. 58 performed complete angiography of collateral circulation, but was excluded from all Types for his unique collateral flow configuration. 79 of 87 cases were included in Subgroups and Types based on their anatomic configurations and collateral flow configurations (**Figure 1**). Case No. 80 failed to perform complete angiography of collateral circulation, but was classified in Subgroup IV based on his anatomic configuration.

Subgroup I

A total of seven cases were classified in Subgroup I, among which four cases of tested side cerebral hemisphere blood supply were completely recruited *via* the anterior Circle alone (Type 1) and three cases of tested side cerebral hemisphere blood supply were completely recruited *via* the posterior Circle alone (Type 2). No immediate or delayed hemodynamic cerebral ischemia complications were found in cases in Type 1, while two cases among Type 2 were BTO-positive, but with no statistical difference of ischemic complication rates between two types ($p = 0.143$).

Subgroup II

All types had a complete anterior Circle in this subgroup and A1 to A2 blood flow showed no clear dominance of the inflow contribution of one A1 segment over the other. The classification in Subgroup II was based on the different blood supply to the tested side MCA area. Tested side ACA area of all cases in Subgroup II has already gained enough blood perfusion (ASITN/SIR Grade 4) (27) *via* the anterior Circle. Type 3 represented cross flow *via* the anterior Circle alone to the tested side MCA area, whereas Type 4 represented cross flow *via* both anterior Circle and posterior Circle to the tested side MCA area. Type 6 in Subgroup III and Type 5 had similar cerebral hemodynamic features during ICA BTO as they both represented cross flow *via* the posterior Circle alone to the tested side MCA area. The summary of tested side MCA area blood supply categorization and its BTO results for BTO alone group and therapeutic ICA occlusion group are given in **Tables 1** and **2**. All cases in Types 3 and 4 were BTO-negative and no patient suffered delayed ischemia after therapeutic ICA occlusion. When dividing the tested side MCA area blood supply into those with collateral flow *via* the posterior Circle alone (Type 5 +Type 6) and those with collateral flow *via* the anterior Circle alone (Type 3)/via both

TABLE 1 | The summary of tested side MCA area blood supply categorization in (Subgroup II + Type 6) and its BTO results for BTO alone group.

	BTO Alone		
Tested Side MCA Area Blood Supply	**BTO-negative (%) (n = 24)**	**BTO-positive (%) (n = 2)**	**Total (%) (n = 26)**
AC alone	6 (23)	0 (0)	6 (23)
PC alone	4 (15)	2 (8)	6 (23)
AC + PC	14 (54)	0 (0)	14 (54)
Total	24 (92)	2 (8)	26 (100)

AC, the anterior Circle; PC, the posterior Circle.

TABLE 3 | The summary of the sigh of reverse blood flow to ICA tested side MCA area blood supply in (Type 5 + Type 6) and its BTO results.

	Tested Side MCA Area Blood Supply: PC		
Reverse Blood Flow to ICA (+/–)	**BTO-negative (%) (n = 7)**	**BTO-positive + BTO false-positive (%)(n = 2 + 2)**	**Total (%) (n = 11)**
Presence (+)	6 (55)	0 (0)	6 (55)
Absence (–)	1 (9)	4 (36)	5 (45)
Total	7 (64)	4 (36)	11 (100)

PC, the posterior Circle.

anterior Circle and posterior Circle (Type 4), a higher BTO-positive rate (33% vs 0%; $p = 0.046$) and BTO false-negative rate (40% vs 0%, $p = 0.028$) in (Type 5 + Type 6) were observed, compared with (Type 3 + Type 4). Cross flow *via* the posterior Circle alone to the tested side MCA area was significantly associated with cerebral ischemic complications ($p = 0.0108$; OR:51; 95% CI: 2.4810 to 1,048.3629).

In cases among Types 5 and 6, we found that no patient experienced cerebral ischemia complications during and after BTO when the sign of reverse blood flow to the ICA was detected (**Table 3**). When we compared the groups with reverse blood flow to the ICA and the groups without reverse blood flow to the ICA during BTO, the odds of having a BTO-negative result given the presence of reverse blood flow to the ICA were 39.0 times greater, with the 95% CI, 1.2772 to 1,190.9128 ($p = 0.0357$).

Subgroup III

Subgroup III showed no evidence of A1 segment on one side, with total supply to both A2s from the single A1. In Subgroup III, Type 6 was classified into **Tables 1** and **2** and analysis. Only one case (Case No. 62), whose absent A1 was contralateral to the tested side ICA, was categorized in Type 7. This patient underwent BTO alone, with no rSO_2 abnormality detected during the BTO procedure simultaneously. So the case was considered to be BTO-negative, although angiographic findings showed cross flow not only *via* the posterior Circle to the affected hemisphere but also pial collaterals from contralateral MCA to contralateral ACA.

Subgroup IV

In Subgroup IV, all types had a complete anterior Circle and one A1 segment clearly contributed more inflow to an A2 than the contralateral segment. A total of 17 cases were classified in Subgroup IV, among which four cases were BTO-positive, 12 cases were BTO-negative and one case was BTO false-negative. Comparing BTO-negative group and BTO-positive group in Subgroup IV (1 BTO-positive case (Case No. 80) with severe and immediate neurological deficits was excluded, because angiography of collateral blood flow failed to complete in time), the absence of the posterior Circle was significantly associated with BTO-positive results ($p = 0.0426$; OR:29.4000; 95%CI:1.1190–772.4193) (**Table 4**). Statistical analysis showed that relative position of A1 (dominant side) and ICA (tested side) had nothing to do with the configurations of blood supply to tested side MCA area in BTO-negative group in Subgroup IV ($p = 0.470$) (**Supplemental Table 2**). The remaining BTO false-negative case (Case No. 69) was classified in Type 9 based on its hemodynamic change during BTO, but the stenosis of contralateral ICA was detected.

TABLE 2 | The summary of tested side MCA area blood supply categorization in (Subgroup II + Type 6) and its BTO results for Therapeutic ICA Occlusion group.

	Therapeutic ICA Occlusion		
Tested Side MCA Area Blood Supply	**BTO-negative (%)(n = 25)**	**BTO false-positive (%)(n = 2)**	**Total (%) (n = 27)**
AC alone	10 (37)	0 (0)	10 (37)
PC alone	3 (11)	2 (7)	5 (19)
AC + PC	12 (44)	0 (0)	12 (44)
Total	25 (93)	2 (7)	27 (100)

AC, the anterior Circle; PC, the posterior Circle.

Case Illustration

Case Nos. 76 and 80: A 63-year old male (Subgroup IV) was admitted to our neurosurgery department for bilateral ICA BTO and intended to have his left ICA occluded permanently. Control angiography of bilateral ICA and unilateral VA was shown in **Figures 3A–D**. Asymmetry of bilateral A1s was detected in this patient, with left A1 as the dominant side (**Figures 3A, B, F**). **Figure 3E** showed complete temporary blood flow blockage of right ICA (ipsilateral to dominant A1). When BTO of right ICA (contralateral to dominant A1) went on, the patient didn't show obvious neurological deficits at the beginning. However, rSO_2 did decrease by 8%, as soon as the balloon was inflated (**Figure 3H**). Subsequent angiography of left ICA showed that insufficient perfusion *via* the anterior Circle to right MCA area during right ICA BTO (ASITN/SIR Grade1) (**Figure 3F**). Angiography of VA showed absence of right PcomA and minor collateral flow *via* leptomengningeal branches from

TABLE 4 | The summary of the relationship between the absence of Posterior Circle and its BTO results in Subgroup IV.

Posterior Circle (+\–)	**BTO-positive (%) (n = 3)**	**BTO-negative (%) (n = 12)**	**Total (%) (n = 15)**
Presence (+)	0 (0)	10 (67)	10 (67)
Absence (–)	3 (20)	2 (13)	5 (33)
Total	3 (20)	12 (80)	15 (100)

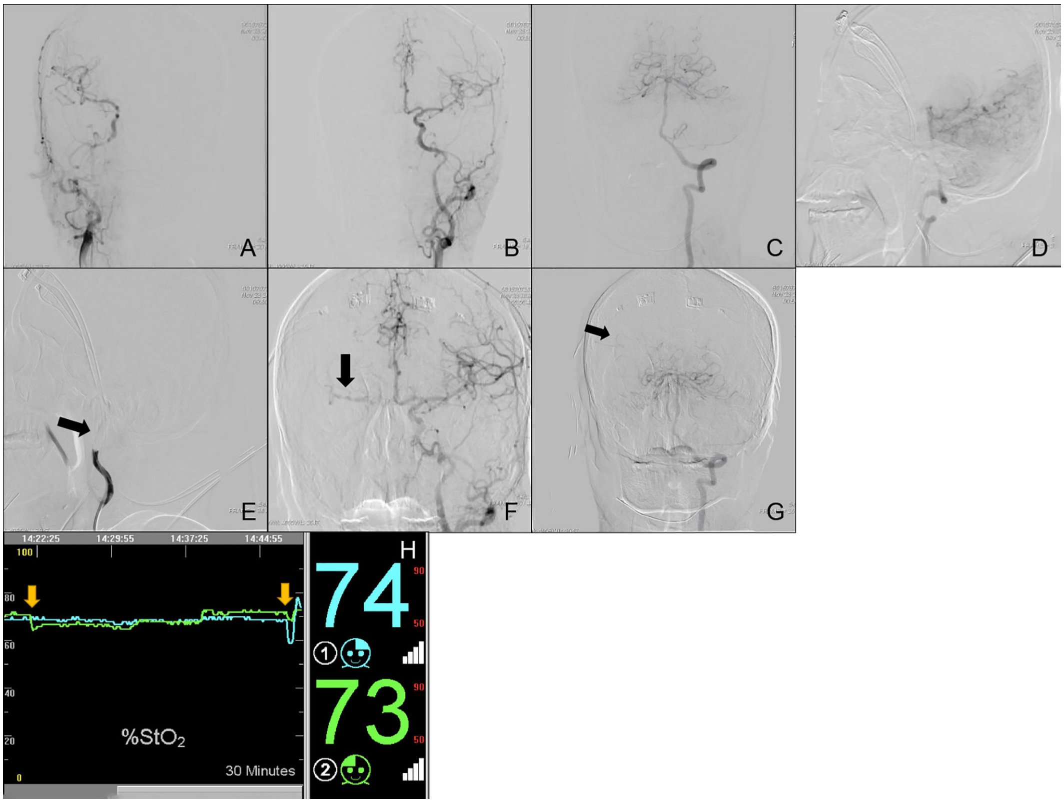

FIGURE 3 | Cerebral angiography and cerebral rSO_2 monitoring of Case Nos. 76 and 80. **(A–G)** Multi-side view of cerebral angiography. **(H)** Real-time rSO_2 monitoring. The blue line represented rSO_2 on the left cerebral hemisphere, the green line represented rSO_2 on the right cerebral hemisphere, the yellow arrow indicates a sudden drop in rSO_2.

posterior Circulation to the tested side MCA area (**Figure 3G**). The patient gradually became lethargic and demonstrated reduction in muscle strength of the right limb. Then we deflated the balloon in time and the patient recovered immediately. Right ICA BTO was classified into Type 12. When we performed BTO of left ICA, the patient demonstrated loss of consciousness instantly after the balloon was inflated and rSO_2 dropped more significantly by 11% (**Figure 3H**). Given the severe symptoms caused by cerebral ischemia, we were not able to perform angiography of collateral flow this time. The patient was considered as bilateral BTO-positive and finally underwent covered stent implantation of left ICA.

Case No. 50: A 42-year old male (Subgroup II, Type 5) was admitted to our neurosurgery department for left ICA BTO and intended to have his left ICA occluded permanently. Control angiography of bilateral ICA and unilateral VA was shown in **Figures 4A–D**, with bilateral A1s independently supplying their own A2s (**Figures 4A, B**). **Figure 4E** showed complete temporary blood flow blockage of left ICA. The blood flow from the right ICA only provided enough perfusion for left ACA area (ASITN/SIR Grade4) (**Figure 4F**). Angiography of VA demonstrated that left MCA area (ASITN/SIR Grade3) was supplied by the posterior Circulation *via* the posterior Circle and no reverse blood flow to the left ICA was found (**Figure 4G**). Not any acute cerebral ischemic symptom was detected during BTO. Meanwhile, rSO_2 monitoring was stable and the value of rSO_2 fluctuated subtly around the baseline (**Figure 4I**). The patient was considered as BTO-negative at that time and underwent therapeutic ICA occlusion after the test (**Figure 4H**). However, he unfortunately presented loss of muscle strength of right limb and aphasia hours later. Subsequent head CT scanning show cerebral fraction in the left basal ganglia (**Figure 4J**).

Case No. 58: A 61-year old male was admitted to our neurosurgery department for right ICA BTO. Since he was treated with percutaneous dilational tracheostomy (PDT) not long before and was wearing a tracheostomy tube, he wasn't able to communicate with us verbally. Control angiography of bilateral ICA and unilateral VA was similar to Case No. 50 (**Figures 5A–D**). **Figure 5E** showed complete temporary blood flow blockage of right ICA. The blood flow from the left ICA only provided enough perfusion for right ACA area (ASITN/SIR Grade4) and showed almost no perfusion to the right MCA area (ASITN/SIR Grade0) (**Figure 5F**). The patient developed moderate collateral flow *via* leptomengningeal branches from

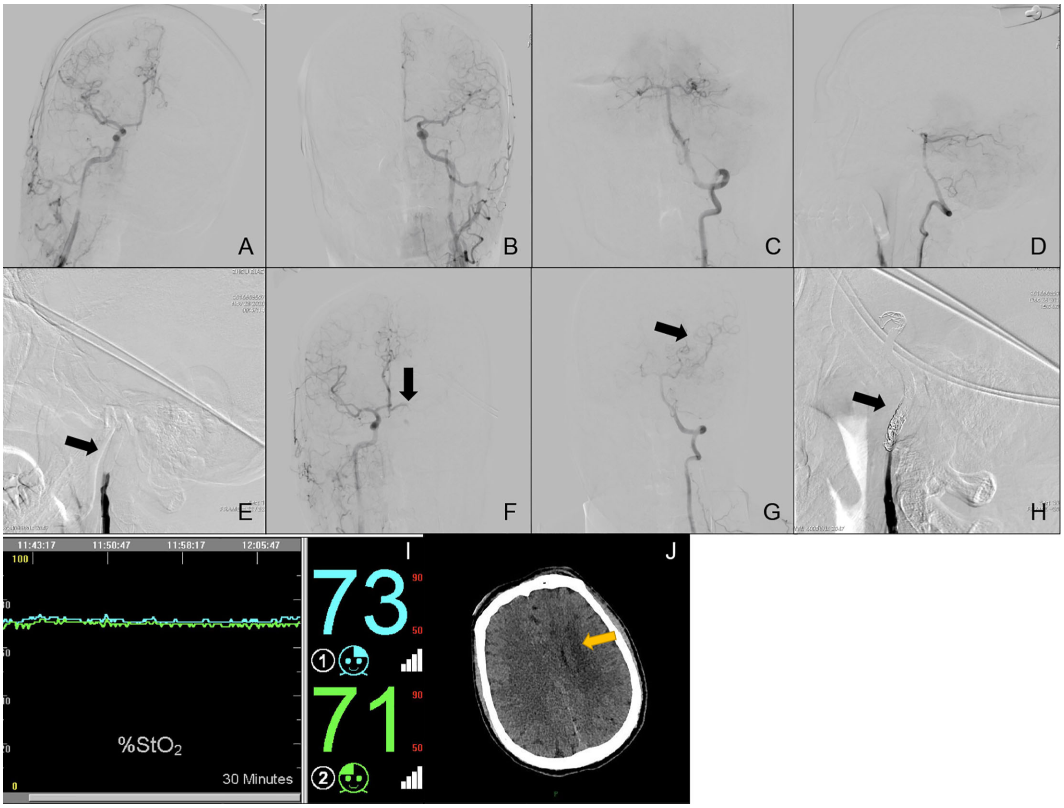

FIGURE 4 | Cerebral angiography and cerebral rSO_2 monitoring of Case No. 50. **(A–H)** Multi-side view of cerebral angiography. **(I)** Real-time rSO_2 monitoring. The blue line represented rSO_2 on the left cerebral hemisphere, the green line represented rSO_2 on the right cerebral hemisphere. **(J)** CT scan of Case No. 50 after BTO and ICA occlusion, the yellow arrow indicates delayed cerebral infraction after therapeutic ICA occlusion.

posterior Circulation to the MCA area without the presence of right PcomA (**Figures 5G, H**). rSO_2 on the right side decreased significantly by 7% and fluctuated far below the baseline (**Figure 5I**). The clinician didn't detect obvious symptoms of cerebral ischemia, but the patient seemed to be unresponsive during the test. Coupled with rSO_2 and angiography of collateral circulation, this patient was judged to be BTO-positive. This patient was not categorized in any Types.

DISCUSSION

ENPG for rNPC may involve therapeutic ICA sacrifice, which requires preoperative knowledge of the feasibility of permanent ICA occlusion (28). In comparison with abrupt ICA occlusion, the application of angiographic BTO with clinical surveillance is now a basic way to evaluate cerebral ischemic risks before permanent ICA blockage and greatly helps to reduce the incidence of postoperative cerebral infraction (13). However, BTO with clinical surveillance still has some deficiencies. For example, the clinical neurological testing is non-standardized (27) and sometimes it is difficult for clinicians to distinguish patients' reaction following the instructions and to make verbal communication with patients due to the differences in dialects and education levels. The test of muscle strength can also be cumbersome owing to patient draping constraints. Furthermore, although BTO with clinical surveillance is sufficient in prediction of acute cerebral ischemia in awaking patients, it doesn't work properly in evaluating delayed stroke after permanent occlusion (29). We believe that angiographic findings of collateral circulation and adjunctive blood flow measurements are quite imperative in ICA BTO.

Useful Angiography of Collateral Circulation in Prediction of ICA BTO

It has been widely accepted that the CoW is the major and most effective collateral pathway in the brain, which can respond quickly to low perfusion areas by recruiting blood from the contralateral hemisphere *via* the anterior Circle or by recruiting blood from the posterior circulation *via* the posterior Circle to the affected hemisphere (30). In the current study, according to **Tables 1** and **2**, patients whose tested side MCA area was supplied *via* both anterior Circle and posterior Circle (Type 4) or *via* the anterior Circle alone (Type 3) demonstrated a significant reduction in BTO-positive rate and BTO false-negative rate in comparison with patients whose tested side

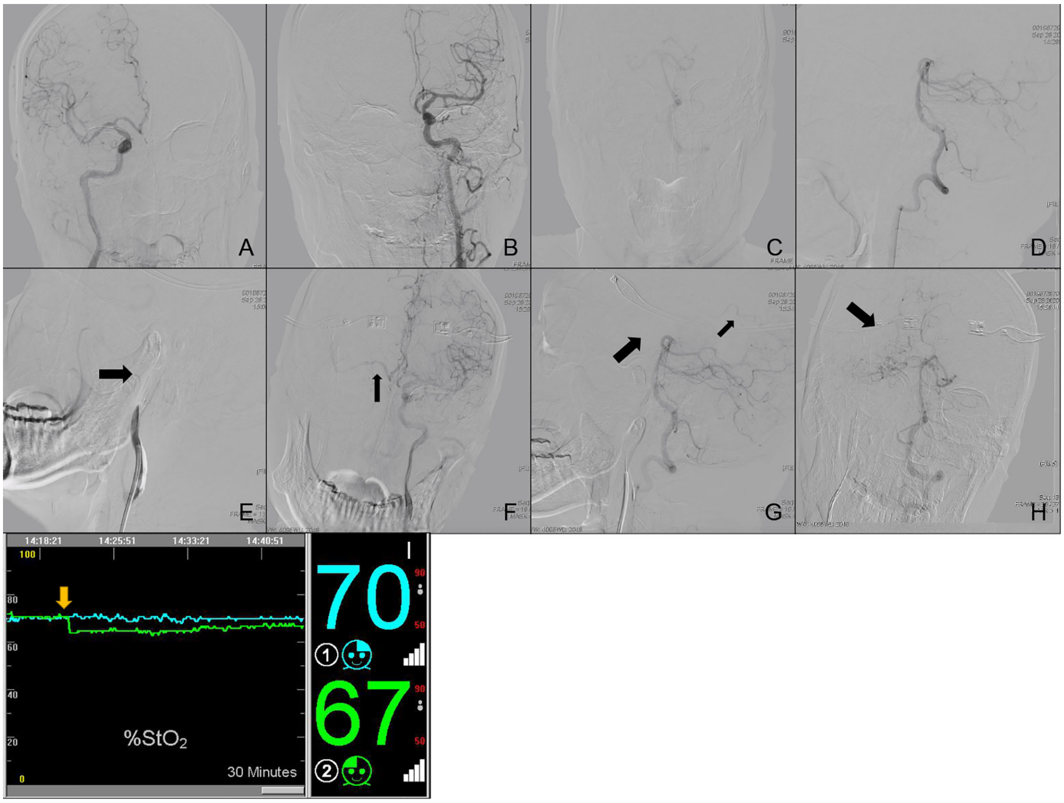

FIGURE 5 | Cerebral angiography and cerebral rSO_2 monitoring of Case No. 58. **(A–H)** Multi-side view of cerebral angiography. **(I)** Real-time rSO_2 monitoring. The blue line represented rSO_2 on the left cerebral hemisphere, the green line represented rSO_2 on the right cerebral hemisphere, the yellow arrow indicates a sudden drop in rSO_2.

MCA area was supplied *via* the posterior Circle alone (Type 5 + Type 6). In accordance with **Tables 1** and **2**, although we find no statistical difference of hemodynamic cerebral ischemia complication rates between Type 1 (0%) and Type 2 (67%) in Subgroup I, we speculate that the result might be caused by our limited sample size. Our findings are consistent with previous report that the anterior Circle might functionally be much more important than the posterior Circle among the primary collateral pathway (31, 32).

It is true that appearance on collateral flow can be evaluated by using the American Society of Interventional and Therapeutic Neuroradiology/Society of Interventional Radiology (ASITN/SIR) Collateral Flow Grading System for angiography (33). However, clinicians are not able to distinguish these differences clearly with their visual impression sometimes. To our experience, patients with no neurological deficits during BTO and similar hemodynamic changes like Types 5 and 6, all had collateral flow appearances of MCA areas that could be classified into ASITN/SIR Grade 3 or Grade 4, but some patients still developed delayed cerebral ischemia after therapeutic ICA occlusion.

However, reverse blood flow to tested side ICA from the posterior Circle during BTO can be easily detected in the DSA angiography. For cases among Types 5 and 6,cases without reverse blood flow to ICA suffered more from immediate or delayed cerebral ischemia by contrast with cases with reverse blood flow to ICA. So we suggest that more attention should be paid to clinical surveillance during BTO for patients with similar hemodynamic change like Types 5 and 6.We also recommend that should the sigh of reverse blood flow to tested side ICA from the posterior Circle, which indicated more than enough collateral blood perfusion, was detected among cases in Types 5 and 6, therapeutic ICA occlusion could be performed with no need to worry about delayed cerebral ischemic complications

Subgroup IV demonstrated an imbalanced anterior Circle, with one side A1 supplying more flow to an A2 than the other side A1. Relative position of A1 (dominant side) and ICA (tested side) was not associated with BTO-positive rate (p = 1) (**Supplemental Table 3**), while presence of the posterior Circle in Subgroup IV could reduce BTO-positive rate regardless of the relative position of A1 (dominant side) and ICA (tested side). The reason for such findings could be explained as follows: The fact that one side A1 supplying more blood flow to an A2 than the other side A1 is mainly caused by the differences in bilateral A1 diameters, with one A1 with larger diameter contributing more inflow than contralateral A1 with smaller diameter.

When the collateral flow goes from the dominant side to the weak side (ICA occluded) *via* the anterior Circle, originally relatively large collateral flow will be restricted by smaller A1 according to the Pouseille equation. Reversely, when the collateral flow goes from the weak side to the dominant side (ICA occluded) *via* the anterior Circle, originally collateral blood flow remains unchanged, but the cross flow has two more ACA areas to supply compared with the other situation. One situation shows smaller blood flow to a small low perfusion area, whereas the other situation shows normal blood flow to a larger low perfusion area. Cross flow *via* the anterior Circle might not be sufficient under these two circumstances, so that's the reason why collateral flow from the posterior Circle is indispensable for BTO-negative results in Subgroup IV. It is also crucial to point out not only BTO-positive cases but also BTO-negative cases presented themselves in Type 12. This situation could be explained by the fact that tested side MCA area could recruit enough blood perfusion *via* the anterior Circle, when there is rather little difference between A1 diameters on both sides, thus making subtle impact on cross flow *via* the anterior Circle. So, as a matter of fact, although statistical analysis shows that configurations of blood supply to tested side MCA area in BTO-negative group in Subgroup IV don't differ between group, whose tested side ICA is contralateral to dominant A1, and group, whose tested side ICA is ipsilateral to dominant A1, we speculate that difference will occur with the rise of sample size (**Supplemental Table 2**).

Another angiographic finding highlighted was ICA stenosis contralateral to tested side. All six cases in Type 9 showed no neurological deficiencies during ICA BTO, and four cases underwent therapeutic ICA occlusion after the procedure. One (Case No. 69) of four cases presented herself with symptoms of occasional limb weakness and dizziness to our division 7 days after permanent ICA occlusion. Head CT scanning showed newly-developed lacunar infraction in the left cerebral hemisphere in contrast to previous scanning. Contralateral ICA stenosis was detected last time during BTO and we once hesitated to perform the permanent ICA occlusion, but both rSO_2 monitoring and neurological surveillance supported the BTO-negative result. While dealing with her symptoms, we retrospectively studied the DSA angiography of the patient during BTO and considered contralateral ICA stenosis as the main reason for the newly-developed lacunar infraction. A previous study did reveal that the posterior circulation exerted a greater influence during ICA BTO in patients with high-grade contralateral ICA stenosis (31). Combining previous report with our case, we presume that ipsilateral posterior Circle plays a much more quantitatively significant role in protecting the hemisphere against hemodynamic ischemia. Contralateral ICA stenosis might still enable patients to narrowly tolerate temporary ICA sacrifice in resting state, but it does have an impact on the capacity to supply blood to the affected vascular area *via* the anterior Circle at times of stress.

For another, besides collateral flow through CoW, two of six rNPC patients with CICAO on the lesion side didn't have any cerebral ischemic symptoms and have gradually developed secondary collateral pathway, such as ophthalmic arteries and leptomengningeal arteries, to the low perfusion area (**Supplemental Table 4**). However, Case No. 58 in the Case Illustration, who developed collateral flow *via* leptomengningeal branches from PCA to the tested side MCA area without the presence of PcomA, was diagnosed with acute cerebral hemodynamic ischemia owing to drowsiness, decrease in muscle strength and simultaneous significant reduction in tested side rSO_2 during the procedure. Furthermore, Case No. 62 in Type 7 not only gained its collateral flow *via* the posterior Circle on the tested side, but also *via* leptomengningeal arteries contralateral to the tested side. The rSO_2 monitoring of this case also showed no abnormal fluctuation on tested side. Evidence above demonstrates the fact that secondary collateral pathways, which include but are not limited to extracranial-intracranial anastomoses *via* the meningeal or ophthalmic arteries and pial collaterals, need more time to function (34, 35). Based on our study, secondary collateral pathways usually present themselves as a substitution when the primary collateral pathways fall short or a supplement when the primary collateral pathways are insufficient. The presence of secondary collateral pathways alone is often linked with BTO-positive results, because it is considered to be a sign of deteriorated hemodynamic condition of the brain in acute ischemic phase.

Case No. 63 in Type 8 was found cfPCA and A1 absence ipsilateral to the tested side during ICA BTO and was regarded as BTO-positive 10 min after the balloon was inflated. Since the patient didn't have a complete anterior and posterior Circle, as a matter of fact, we could have predicted the intolerance of ICA sacrifice of this case earlier, should we had performed head CTA/MRA or Matas maneuver (angiography of the non-tested ICA during manual carotid compression on the tested side) and Allcock maneuver (angiography of the vertebral artery during manual carotid compression on the tested side) before ICA BTO. What also needed to mention was that another seven BTO-positive cases(Case Nos. 81–87) in our study were excluded from all the Subgroups,as they failed to perform angiography of collateral flow in time. For patients those who quickly fail the BTO, earlier awareness of their CoW development might spare them from unnecessary BTO. Anyway, though BTO is a simple procedure, it was reported to increase the rate of complications for neuroangiography from 1.3% (36) to 3 to 4% (16, 37). Unfortunately, we didn't perform head CTA/MRA or Matas maneuver and Allcock maneuver before the procedure in this study. However, these exams and operations might help to reduce overall cost and complication rate for each individual.

Suitable Adjunctive Techniques Chosen for Selected Cases During ICA BTO

When it came to the adjunctive techniques during BTO, we chose NIRS cerebral oximeter to monitor rSO_2 change during BTO. rSO_2 monitoring is a quantitative method that also carries the merits of being noninvasive and cost-effective. The baseline values of rSO_2 in our study ranged from 64 to 80% (mean 72.3 ± 5.1%) and was similar to previous reports (18, 38). Many scholars have applied rSO_2 monitoring during temporary ICA occlusion for the detection of cerebral ischemia. However, a critical ΔrSO_2 level to induce neurological deficit has not been well established yet. Our study revealed that the most suitable cut-off value detecting the BTO-positive group was 5%. All the cases regarded as BTO-positive by clinical surveillance showed an irreversible drop by at least 5% in rSO_2 on the tested side. However, comparison of change in rSO_2 between BTO false-negative group and BTO negative group showed no statistical difference. Furthermore, all BTO false-positive cases didn't showed obvious rSO_2 fluctuation during BTO in our study. These evidences supported our experience that rSO_2 monitoring didn't work well in detecting delayed cerebral ischemia after BTO. The fact that the sensors can only be put on the forehead of both sides and monitor limited to the frontal lobe may greatly affect the sensitivity and specificity in sorting out BTO false-negative cases.

That is why we consider that other more quantitative blood flow measurements, such as CTP, Technetium-99m hexamethyl propyleneamine oxime (^{99m}Tc-HMPAO), single-photon emission CT(SPECT) and xenon-enhanced CT(XeCT), might be essential for cases with certain kind of collateral flow configurations during BTO. According to our study, clinically BTO-negative cases, who recruit collateral flow *via* both primary and secondary pathways (e.g. Case No. 62), or who have similar hemodynamic changes like Types 5 and 6 (e.g. Case No. 50), or who have contralateral ICA stenosis (e.g. Case No. 69) are proper candidates for BTO in conjunction with these more quantitative blood flow measurements before permanent ICA occlusion. In fact, cases, whose angiography of collateral circulation doesn't fully support clinically BTO-negative results, are recommended to use more quantitative blood flow measurements to avoid delayed cerebral ischemia after permanent ICA occlusion. Tomoyoshi Kuribara et al. reported that patients whose MTT obtained through CT perfusion at less than 16.4% increase compared with that on the contralateral side might be treated with abrupt ICA occlusion (38). Quantitative CBF studies using XeCT pointed out that a flow of less than 30 ml/100 g/mg as the threshold for occurrence of neurological symptoms after ICA sacrifice (13, 39). However, BTO false-negative rate has also been reported in these method,with ^{99m}Tc-HMPAO studies up to 20% (13, 40, 41) and XeCT up to 3–10% (13, 39, 42). It has also been suggested that SPECT asymmetry analysis carries a high rate of BTO false-positive test results (43, 44). Despite the fact that room to room transfer, extended test time and complex operation are needed for these equipment, we believe more detailed information of cerebral hemodynamic changes during ICA BTO will decrease BTO false-negative rate to some extent.

Method chosen for distinguishing BTO results greatly influence the following treatment of patients with rNPC. For patients whom clinicians falsely think that will develop delayed cerebral stroke, patients will undergo covered stent implantation of ICA before ENPG. This might increase perioperative complication rate of a hurried ENPG caused by routine antiplatelet treatment after covered stent implantation, as rNPC patients want the surgery urgently and have little time to waste. That was also the reason why we didn't choose hypotensive challenge or neurophysiologic monitoring as adjunctive techniques, as such tests would possibly have withheld ICA sacrifice that actually was feasible (28, 45).

Overall, all adjunctive techniques coupled with ICA BTO have their own pearls and pitfalls, the results of ICA BTO need a comprehensive judgement.

Study Limitations

This study had several limitations. First, it was a retrospective study with limited samples in each subgroups and types. We didn't observe the long nature history of cases with therapeutic ICA occlusion, as patients were discharged from our neurosurgical division soon after the treatment and received ENPG. Secondly, all the BTO false-negative cases in our study only presented with symptomatic ischemic events. The following head CT scanning confirmed the diagnose of delayed stroke. However, there is cerebral ischemia identified radiographically that is asymptomatic, so it might be essential to perform diffusion-weighted or FLAIR MRI imaging before BTO and after therapeutic ICA occlusion. Thirdly, collateral angiography could not be performed in some patients owing to ischemic symptoms during temporal occlusion of the ICA. The data of these extremely poor collateral configurations were missing. In addition, some patients needed BTO alone for their low risk of ICA injury according to a new assessment of ICA invasion (46). This might also influence the detection of BTO false-negative cases and results. As a consequence of these limitations, it's necessary to confirm our results with prospective and large sample studies.

CONCLUSION

CTA/MRA scanning of the brain with Matas and Allcock maneuvers before ICA BTO is essential. Angiographic findings before ICA BTO and angiography of cerebral collateral circulation during ICA BTO are significantly correlated with ICA BTO results. Angiographic ICA BTO can be performed in conjunction with NIRS cerebral oximeter for its advantage of being noninvasive, real-time, cost-effective, simple for operation and most importantly for its correct prediction of rSO_2 outcome of ICA sacrifice. However, in order to ensure a safe carotid artery occlusion, more quantitative adjunctive blood flow measurements are recommended when angiography of cerebral collateral circulation doesn't fully support rSO_2 outcome among clinically ICA BTO-negative cases.

DATA AVAILABILITY STATEMENT

The original contributions presented in the study are included in the article/**Supplementary Material**. Further inquiries can be directed to the corresponding authors.

ETHICS STATEMENT

The studies involving human participants were reviewed and approved by the ethics committees of Renji Hospital, School of Medicine, Shanghai Jiao Tong University. This was a retrospective study, so informed patient consent was not required.

AUTHOR CONTRIBUTIONS

JD, YQ, RY, and BC conceived, designed and supervised the study. RY, HW, and BC wrote the manuscript. RY, WS, XH, TW, and YG collected and analyzed the data. RY and BC revised the manuscript All authors contributed to the article and approved the submitted version.

FUNDING

This work was supported by Shanghai 2020 'Science and Technology Innovation Action Plan' Medical Innovation Research Special Project (20Y11905900), National Natural Science Foundation of China (81874215), and Natural Science Research Project of Minhang District (Shanghai) (2019MHZ090).

SUPPLEMENTARY MATERIAL

The Supplementary Material for this article can be found online at: https://www.frontiersin.org/articles/10.3389/fonc.2021.674889/full#supplementary-material

REFERENCES

1. Chen YP, Chan ATC, Le QT, Blanchard P, Sun Y, Ma J. Nasopharyngeal Carcinoma. *Lancet (Lond Engl)* (2019) 394(10192):64–80. doi: 10.1016/s0140-6736(19)30956-0
2. Liu J, Yu H, Sun X, Wang D, Gu Y, Liu Q, et al. Salvage Endoscopic Nasopharyngectomy for Local Recurrent or Residual Nasopharyngeal Carcinoma: A 10-Year Experience. *Int J Clin Oncol* (2017) 22(5):834–42. doi: 10.1007/s10147-017-1143-9
3. Lee AWM, Ng WT, Chan JYW, Corry J, Mäkitie A, Mendenhall WM, et al. Management of Locally Recurrent Nasopharyngeal Carcinoma. *Cancer Treat Rev* (2019) 79:101890. doi: 10.1016/j.ctrv.2019.101890
4. Kong F, Zhou J, Du C, He X, Kong L, Hu C, et al. Long-Term Survival and Late Complications of Intensity-Modulated Radiotherapy for Recurrent Nasopharyngeal Carcinoma. *BMC Cancer* (2018) 18(1):1139. doi: 10.1186/s12885-018-5055-5
5. Yang J, Song X, Sun X, Liu Q, Hu L, Yu H, et al. Outcomes of Recurrent Nasopharyngeal Carcinoma Patients Treated With Endoscopic Nasopharyngectomy: A Meta-Analysis. *Int Forum Allergy Rhinology* (2020) 10(8):1001–11. doi: 10.1002/alr.22552
6. Ho AS, Kaplan MJ, Fee WE Jr., Yao M, Sunwoo JB, Hwang PH. Targeted Endoscopic Salvage Nasopharyngectomy for Recurrent Nasopharyngeal Carcinoma. *Int Forum Allergy Rhinology* (2012) 2(2):166–73. doi: 10.1002/alr.20111
7. Adams GL, Madison M, Remley K, Gapany M. Preoperative Permanent Balloon Occlusion of Internal Carotid Artery in Patients With Advanced Head and Neck Squamous Cell Carcinoma. *Laryngoscope* (1999) 109(3):460–6. doi: 10.1097/00005537-199903000-00022
8. Abud DG, Spelle L, Piotin M, Mounayer C, Vanzin JR, Moret J. Venous Phase Timing During Balloon Test Occlusion as a Criterion for Permanent Internal Carotid Artery Sacrifice. *AJNR Am J Neuroradiol* (2005) 26(10):2602–9.
9. Serbinenko FA. Balloon Catheterization and Occlusion of Major Cerebral Vessels. *J Neurosurg* (1974) 41(2):125–45. doi: 10.3171/jns.1974.41.2.0125
10. Maras D, Lioupis C, Magoufis G, Tsamopoulos N, Moulakakis K, Andrikopoulos V. Covered Stent-Graft Treatment of Traumatic Internal Carotid Artery Pseudoaneurysms: A Review. *Cardiovasc Intervent Radiol* (2006) 29(6):958–68. doi: 10.1007/s00270-005-0367-7
11. Matsukawa H, Tanikawa R, Kamiyama H, Tsuboi T, Noda K, Ota N, et al. Graft Occlusion and Graft Size Changes in Complex Internal Carotid Artery Aneurysm Treated by Extracranial to Intracranial Bypass Using High-Flow Grafts With Therapeutic Internal Carotid Artery Occlusion. *Neurosurgery* (2017) 81(4):672–9. doi: 10.1093/neuros/nyx075
12. Kalani MY, Kalb S, Martirosyan NL, Lettieri SC, Spetzler RF, Porter RW, et al. Cerebral Revascularization and Carotid Artery Resection At the Skull Base for Treatment of Advanced Head and Neck Malignancies. *J Neurosurg* (2013) 118(3):637–42. doi: 10.3171/2012.9.Jns12332
13. Linskey ME, Jungreis CA, Yonas H, Hirsch WL Jr., Sekhar LN, Horton JA, et al. Stroke Risk After Abrupt Internal Carotid Artery Sacrifice: Accuracy of Preoperative Assessment With Balloon Test Occlusion and Stable Xenon-Enhanced CT. *AJNR Am J Neuroradiol* (1994) 15(5):829–43.
14. Carotid Artery Balloon Test Occlusion. *AJNR Am J Neuroradiol* (2001) 22(8 Suppl):S8–9.
15. Elias AE, Chaudhary N, Pandey AS, Gemmete JJ. Intracranial Endovascular Balloon Test Occlusion: Indications, Methods, and Predictive Value. *Neuroimaging Clin North Am* (2013) 23(4):695–702. doi: 10.1016/j.nic.2013.03.015
16. Mathis JM, Barr JD, Jungreis CA, Yonas H, Sekhar LN, Vincent D, et al. Temporary Balloon Test Occlusion of the Internal Carotid Artery: Experience in 500 Cases. *AJNR Am J Neuroradiol* (1995) 16(4):749–54.
17. Kikuchi K, Yoshiura T, Hiwatashi A, Togao O, Yamashita K, Honda H. Balloon Test Occlusion of Internal Carotid Artery: Angiographic Findings Predictive of Results. *World J Radiol* (2014) 6(8):619–24. doi: 10.4329/wjr.v6.i8.619
18. Takeda N, Fujita K, Katayama S, Tamaki N. Cerebral Oximetry for the Detection of Cerebral Ischemia During Temporary Carotid Artery Occlusion. *Neurologia Medico Chirurgica* (2000) 40(11):557–62. doi: 10.2176/nmc.40.557
19. Alpers BJ, Berry RG, Paddison RM. Anatomical Studies of the Circle of Willis in Normal Brain. *AMA Arch Neurol Psychiatry* (1959) 81(4):409–18. doi: 10.1001/archneurpsyc.1959.02340160007002
20. Mount LA, Taveras JM. Arteriographic Demonstration of the Collateral Circulation of the Cerebral Hemispheres. *AMA Arch Neurol Psychiatry* (1957) 78(3):235–53. doi: 10.1001/archneurpsyc.1957.02330390017003
21. Pascalau R, Padurean VA, Bartos D, Bartos A, Szabo BA. The Geometry of the Circle of Willis Anatomical Variants as a Potential Cerebrovascular Risk Factor. *Turkish Neurosurg* (2019) 29(2):151–8. doi: 10.5137/1019-5149.Jtn.21835-17.3
22. Krabbe-Hartkamp MJ, van der Grond J, de Leeuw FE, de Groot JC, Algra A, Hillen B, et al. Circle of Willis: Morphologic Variation on Three-Dimensional Time-of-Flight MR Angiograms. *Radiology* (1998) 207(1):103–11. doi: 10.1148/radiology.207.1.9530305
23. Wang BH, Leung A, Lownie SP. Circle of Willis Collateral During Temporary Internal Carotid Artery Occlusion II: Observations From Computed Tomography Angiography. *Can J Neurological Sci Le J canadien Des Sci neurologiques* (2016) 43(4):538–42. doi: 10.1017/cjn.2016.10
24. Tarulli E, Fox AJ. Potent Risk Factor for Aneurysm Formation: Termination Aneurysms of the Anterior Communicating Artery and Detection of A1 Vessel Asymmetry by Flow Dilution. *AJNR Am J Neuroradiol* (2010) 31(7):1186–91. doi: 10.3174/ajnr.A2065
25. Badeer HS. Hemodynamics for Medical Students. *Adv Physiol Educ* (2001) 25(1-4):44–52. doi: 10.1152/advances.2001.25.1.44
26. Shaban A, Albright KC, Boehme AK, Martin-Schild S. Circle of Willis Variants: Fetal PCA. *Stroke Res Treat* (2013) 2013:105937. doi: 10.1155/2013/105937
27. Ma Y, Zhang Y, Jiang J, Li S, Ni T, Liu L, et al. Application and Reliability of the Superselective Balloon Occlusion Test in the Treatment of Complex Cerebral Artery Aneurysms: A Report of 12 Cases. *J Clin Neurosci Off J Neurosurg Soc Australasia* (2019) 64:57–63. doi: 10.1016/j.jocn.2019.04.016

28. Sorteberg A, Bakke SJ, Boysen M, Sorteberg W. Angiographic Balloon Test Occlusion and Therapeutic Sacrifice of Major Arteries to the Brain. *Neurosurgery* (2008) 63(4):651–60. doi: 10.1227/01.Neu.0000325727.51405.D5
29. Dare AO, Chaloupka JC, Putman CM, Fayad PB, Awad IA. Failure of the Hypotensive Provocative Test During Temporary Balloon Test Occlusion of the Internal Carotid Artery to Predict Delayed Hemodynamic Ischemia After Therapeutic Carotid Occlusion. *Surg Neurol* (1998) 50(2):147–55. doi: 10.1016/s0090-3019(97)00444-8
30. Bisschops RH, Klijn CJ, Kappelle LJ, van Huffelen AC, van der Grond J. Collateral Flow and Ischemic Brain Lesions in Patients With Unilateral Carotid Artery Occlusion. *Neurology* (2003) 60(9):1435–41. doi: 10.1212/01.wnl.0000061616.96745.90
31. Henderson RD, Eliasziw M, Fox AJ, Rothwell PM, Barnett HJ. Angiographically Defined Collateral Circulation and Risk of Stroke in Patients With Severe Carotid Artery Stenosis. North American Symptomatic Carotid Endarterectomy Trial (NASCET) Group. *Stroke* (2000) 31(1):128–32. doi: 10.1161/01.str.31.1.128
32. van Everdingen KJ, Visser GH, Klijn CJ, Kappelle LJ, van der Grond J. Role of Collateral Flow on Cerebral Hemodynamics in Patients With Unilateral Internal Carotid Artery Occlusion. *Ann Neurol* (1998) 44(2):167–76. doi: 10.1002/ana.410440206
33. Ben Hassen W, Malley C, Boulouis G, Clarençon F, Bartolini B, Bourcier R, et al. Inter- and Intraobserver Reliability for Angiographic Leptomeningeal Collateral Flow Assessment by the American Society of Interventional and Therapeutic Neuroradiology/Society of Interventional Radiology (ASITN/SIR) Scale. *J Neurointervent Surg* (2019) 11(4):338–41. doi: 10.1136/neurintsurg-2018-014185
34. Hofmeijer J, Klijn CJ, Kappelle LJ, Van Huffelen AC, Van Gijn J. Collateral Circulation Via the Ophthalmic Artery or Leptomeningeal Vessels is Associated With Impaired Cerebral Vasoreactivity in Patients With Symptomatic Carotid Artery Occlusion. *Cerebrovasc Dis (Basel Switzerland)* (2002) 14(1):22–6. doi: 10.1159/000063719
35. Powers WJ. Cerebral Hemodynamics in Ischemic Cerebrovascular Disease. *Ann Neurol* (1991) 29(3):231–40. doi: 10.1002/ana.410290302
36. Dion JE, Gates PC, Fox AJ, Barnett HJ, Blom RJ. Clinical Events Following Neuroangiography: A Prospective Study. *Stroke* (1987) 18(6):997–1004. doi: 10.1161/01.str.18.6.997
37. Tarr RW, Jungreis CA, Horton JA, Pentheny S, Sekhar LN, Sen C, et al. Complications of Preoperative Balloon Test Occlusion of the Internal Carotid Arteries: Experience in 300 Cases. *Skull Base Surg* (1991) 1(4):240–4. doi: 10.1055/s-2008-1057104
38. Fearn SJ, Mead GE, Picton AJ, Mortimer AJ, McCollum CN. Cerebral Oximetry: A Useful Monitor During Carotid Artery Surgery. *Anaesthesia* (1996) 51(6):610–1. doi: 10.1111/j.1365-2044.1996.tb12599.x
39. Witt JP, Yonas H, Jungreis C. Cerebral Blood Flow Response Pattern During Balloon Test Occlusion of the Internal Carotid Artery. *AJNR Am J Neuroradiol* (1994) 15(5):847–56.
40. Lorberboym M, Pandit N, Machac J, Holan V, Sacher M, Segal D, et al. Brain Perfusion Imaging During Preoperative Temporary Balloon Occlusion of the Internal Carotid Artery. *J Nucl Med Off Publication Soc Nucl Med* (1996) 37 (3):415–9.
41. Peterman SB, Taylor A Jr., Hoffman JC Jr. Improved Detection of Cerebral Hypoperfusion With Internal Carotid Balloon Test Occlusion and 99mTc-HMPAO Cerebral Perfusion SPECT Imaging. *AJNR Am J Neuroradiol* (1991) 12(6):1035–41.
42. de Vries EJ, Sekhar LN, Horton JA, Eibling DE, Janecka IP, Schramm VL Jr., et al. A New Method to Predict Safe Resection of the Internal Carotid Artery. *Laryngoscope* (1990) 100(1):85–8. doi: 10.1288/00005537-199001000-00017
43. Field M, Jungreis CA, Chengelis N, Kromer H, Kirby L, Yonas H. Symptomatic Cavernous Sinus Aneurysms: Management and Outcome After Carotid Occlusion and Selective Cerebral Revascularization. *AJNR Am J Neuroradiol* (2003) 24(6):1200–7.
44. Yonas H, Linskey M, Johnson DW, Horton JA, Janecka IP, Witt JP, et al. Internal Carotid Balloon Test Occlusion Does Require Quantitative CBF. *AJNR Am J Neuroradiol* (1992) 13(4):1147–52.
45. Liu AY, Lopez JR, Do HM, Steinberg GK, Cockroft K, Marks MP. Neurophysiological Monitoring in the Endovascular Therapy of Aneurysms. *AJNR Am J Neuroradiol* (2003) 24(8):1520–7.
46. Zhang H, Sun X, Yu H, Zhao W, Zhao K, Liu Q, et al. Assessment of Internal Carotid Artery Invasion With the Endoscopic Endonasal Approach: Implications of a New Grading System and Security Strategy. *J Craniofacial Surg* (2020). doi: 10.1097/scs.0000000000007045

Conflict of Interest: The authors declare that the research was conducted in the absence of any commercial or financial relationships that could be construed as a potential conflict of interest.

The reviewer BL declared a shared affiliation with the authors to the handling editor at time of review.

frontiers in Oncology

ORIGINAL RESEARCH
published: 26 July 2021
doi: 10.3389/fonc.2021.703954

Check for updates

Comparing the Effectiveness of Endoscopic Surgeries With Intensity-Modulated Radiotherapy for Recurrent rT3 and rT4 Nasopharyngeal Carcinoma: A Meta-Analysis

*Zhouying Peng, Yumin Wang, Yaxuan Wang, Ruohao Fan, Kelei Gao, Hua Zhang and Weihong Jiang**

Department of Otolaryngology Head and Neck Surgery, Xiangya Hospital, Central South University, Changsha, China

OPEN ACCESS

Edited by:
Xicai Sun,
Fudan University, China

Reviewed by:
Weitian Zhang,
Shanghai Jiao Tong University, China
Quan Liu,
Fudan University, China

****Correspondence:***
Weihong Jiang
weihongjiang@csu.edu.cn

Specialty section:
This article was submitted to Surgical Oncology, a section of the journal Frontiers in Oncology

Received: *01 May 2021*
Accepted: *06 July 2021*
Published: *26 July 2021*

Citation:
Peng Z, Wang Y, Wang Y, Fan R, Gao K, Zhang H and Jiang W (2021) Comparing the Effectiveness of Endoscopic Surgeries With Intensity-Modulated Radiotherapy for Recurrent rT3 and rT4 Nasopharyngeal Carcinoma: A Meta-Analysis. Front. Oncol. 11:703954. doi: 10.3389/fonc.2021.703954

Background: This meta-analysis aimed to compare the efficacy of intensity-modulated radiotherapy (IMRT) and endoscopic surgery (ES) for high T-stage recurrent nasopharyngeal carcinoma (NPC).

Methods: Relevant studies were retrieved in six databases from 02/28,2011 to 02/28,2021. The 2-year, 3-year, 5-year overall survival (OS) rates and 2-year disease-free survival (DFS) rates were calculated to compare the survival outcomes of the two treatments of IMRT and ES. Combined odds ratios (ORs) and 95% confidence interval (C Is) were measured as effect size on the association between high T-stage and 5-year OS rates.

Results: A total of 23 publications involving 2,578 patients with recurrent NPC were included in this study. Of these, 1611 patients with recurrent rT3-4 NPC were treated with ES and IMRT in 358 and 1,253 patients, respectively. The combined 2-year OS and 5-year OS rates for the two treatments were summarized separately, and the 2-year OS and 5-year OS rate for ES were 64% and 52%, respectively. The 2-year OS and 5-year OS rate for IMRT were 65% and 31%, respectively. The combined 2-year DFS rates of IMRT and ES were 60% and 50%, respectively. Combined ORs and 95% confidence intervals for 5-year survival suggest that ES may improve survival in recurrent NPC with rT3-4. In terms of complications, ES in the treatment of high T-stage recurrent NPC is potentially associated with fewer complications.

Conclusions: The results of our study suggest that ES for rT3-4 may be a better treatment than IMRT, but the conclusion still needs to be sought by designing more studies.

Keywords: recurrent nasopharyngeal carcinoma, endoscopic surgery, intensity-modulated radiotherapy, survival outcome, meta-analysis

INTRODUCTION

Nasopharyngeal carcinoma (NPC) is a type of squamous head and neck cancer with variable geographic distribution, with the highest incidence in Southeast Asia. Its main treatment modality is radiotherapy (1–4). With the development of diagnostic and treatment techniques, the 5-year OS rate of NPC reaches 50% to 64%, but 10% to 20% of patients still experience recurrence after the first treatment and improvement of their disease (5). According to National Comprehensive Cancer Network (NCCN) guidelines, surgical excision of the lesion or local radiotherapy is recommended for resectable head and neck squamous carcinoma after recurrence that has been treated with radiotherapy. Chemotherapy alone is usually reserved for palliative patients who are not candidates for radiotherapy or surgery (5, 6).

The 5-year survival rate for salvage nasopharyngectomy for resectable recurrent NPC is 40% to 60%, compared with 8% to 36% for patients with local recurrence treated with recourse radiotherapy and often with severe complications, such as multiple cranial nerve palsies, osteonecrosis, and internal carotid artery dissection (7). For patients with locally advanced rT3-4, endoscopic surgical resection of the lesion requires a high level of surgical skill on the lead surgeons, and the probability of subsequent complications is higher than that of early-stage patients if they are treated with re-radiotherapy (7, 8). The survival and prognosis studies of ES and IMRT for recurrent NPC have been reported in the literatures (5, 9, 10), but there is no literature comparing the efficacy of the two treatment modalities for locally advanced recurrent rT3-4 NPC.

For recurrent rT3-4 NPC, whether ES should be used or IMRT should be performed is unclear. There needs to be an evidence-based summary of which treatment is better for these patients to provide some basis for clinicians' treatment decisions. Therefore, we conducted a meta-analysis to synthesize the best currently available data to compare the efficacy and safety of ES and IMRT for the treatment of recurrent rT3-4 NPC.

MATERIALS AND METHODS

Search Strategy

We conducted a literature search on several medical databases, including Pubmed, Embase, Web of Science, Cochrane, and two Chinese databases (CNKI and Wanfang). The studies published from February 1, 2011, to February 1, 2021. The search strategy was predefined according to the following Medical Subject Headings (MeSH) and free terms: "recurrent" or "recurrence", "nasopharyngeal carcinoma", "endoscopy surgery", or "intensity modulated radiotherapy". Publications in a language other than Chinese and English were excluded. At the same time, the references of included papers were examined for potentially eligible studies.

Inclusion and Exclusion Criteria

The eligible studies in this meta-analysis meet the following criteria: (a) histologically confirmed residual and/or recurrent NPC patients with T-stage information; (b) initial treatment is at least one cycle of radiotherapy, with or without concurrent chemotherapy; (c) patients with recurrent NPC treated with endoscopic surgery or IMRT with or without chemotherapy; (d) the outcome of publication studies include randomized controlled studies with 2-year survival or 3-year survival or 5-year survival, 2-year DFS or 3-year LCR, retrospective studies, case series reports, and so on; (e) the number of patients with stage rT3 and rT4 is 5 or more than; (f) when multiple studies report the same sample, the one with the most complete data from the available studies will be selected.

The following criteria were used to exclude studies: (a) case reports, reviews, and meta-analyses; (b) studies without rT3 and rT4 stage cases; (c) various studies with incomplete survival rates.

Data Extraction and Assessment

All retrieved publications were read by two researchers simultaneously and independently. In case of disagreement between the two researchers, a detailed discussion by a third researcher was required. After the relevant publications were identified, each publication was screened based on its title and abstract, and inappropriate publications were eliminated. The retained publications were then reviewed in their entirety to determine their final inclusion in this study. The literature review workflow is shown in **Figure 1**. Finally, valid data were extracted from the publications that met the criteria for inclusion in this study. The extracted information included: sample characteristics, tumor T-stage, specific information on treatment, post-treatment follow-up time, and survival rate. If no survival rate information was required in the publications, they were reanalyzed as accurately as possible based on the data in the articles. **Tables 1** and **2** list the details of the studies included in this study.

All the included articles were assessed according to the Methodological Index for Non-Randomized Studies (MINORS). The MINORS instrument has eight dimensions assessing study objective, patients enrollment, data collection, endpoints definition, endpoints assessment, follow-up period, lost to follow-up, and sample size calculation. The high MINORS scores indicate good quality. The maximum ideal score is 16 for nonrandomized studies and 24 for controlled studies. Specific MINORS scores are detailed in **Tables 1** and **2**.

Statistical Analysis

We analyzed the obtained data for survival rate, OR, and other factors by using Review Manager 5.3. For survival rate, we merged the rate values and performed heterogeneity tests. I (2) > 50% was defined as significant heterogeneity. A random effect model was adopted and sub-analyses were made when heterogeneity existed among study results. Otherwise, a fixed-effect model was adopted to merge survival rate values and 95% CIs. Calculation results were presented as forest plots. OR is the ratio of the survival rates in the case of surgery group to the prognosis in the case of radiotherapy group. OR > 1 indicates that the patients with surgery have a better prognosis than the patients with radiotherapy. For the studies from which we could obtain survival data, we made a funnel plot to describe publication bias using S.E. of rate as the abscissa and mean rates as the ordinate.

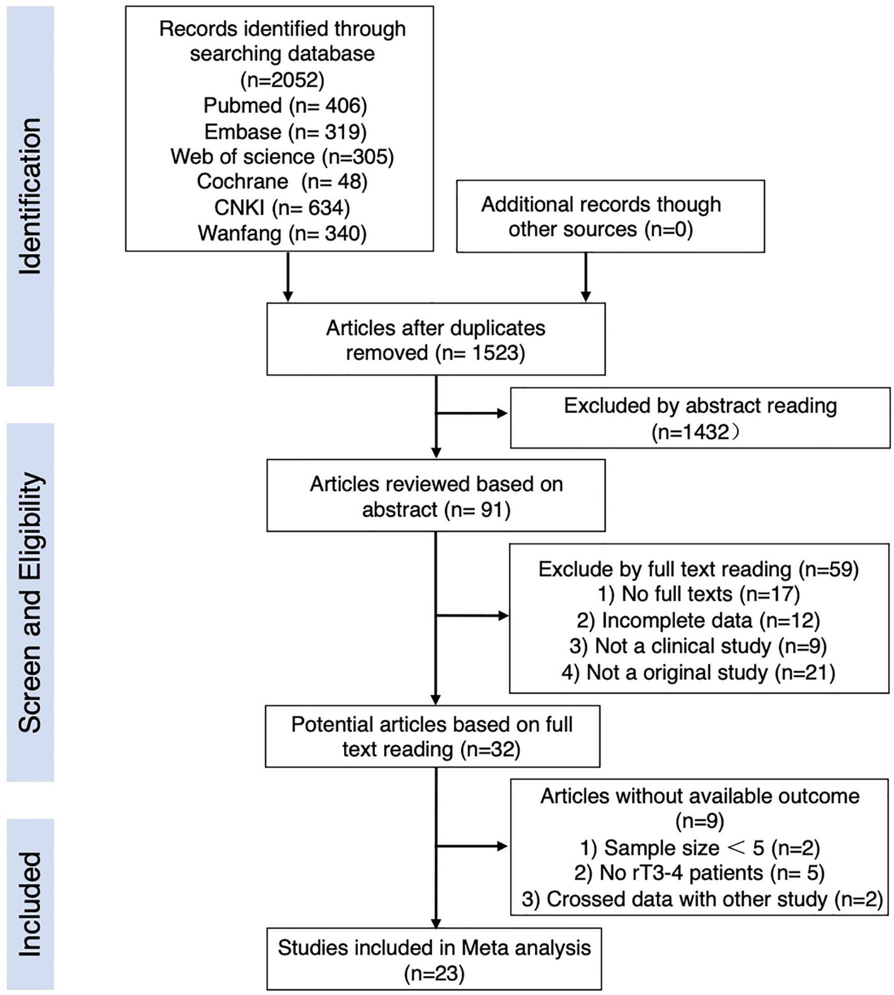

FIGURE 1 | Flowchart of the process of trial selection.

TABLE 1 | Main characteristics of included studies on endoscopic surgery.

Authors	Year	Publication language	No. of patients	M/F	rT classifications		Margins	2-year OS (%)		5-year OS (%)		2-year DFS (%)		MINORS
					rT1-2	rT3-4	+/-	Overall	rT3-4	overall	rT3-4	overall	rT3-4	
Castelnuovo et al. (11)	2013	English	27	—	13	14	3/27	—	78.6	72.5	—	—	57.1	9
You et al. (9)	2015	English	72	54/18	59	13	—	93.3	84.6	77.1	76.9	92.8	47.2	12
Wong et al. (7)	2017	English	15	9/6	0	15	6/9	66.7	66.7	—	50.0	40.0	40.0	9
Weng et al. (12)	2017	English	36	26/10	17	19	—	68.3	52.6	—	—	63.6	48.0	10
Liu et al. (13)	2017	English	91	71/20	43	48	—	64.8	53.7	38.3	—	57.5	57.5	11
Tang et al. (14)	2019	English	55	44/11	45	10	4/51	—	90.0	—	—	—	30.0	8
Zou et al. (10)	2015	English	92	70/22	79	13	—	91.3	—	78.1	48.5	—	—	10
Wong et al. (8)	2019	English	12	—	0	12	—	—	—	50.0	—	—	—	9
Li et al. (15)	2020	English	189	132/57	97	92	32/157	82.2	—	43.6	47.2	—	—	9
Sun et al. (16)	2015	Chinese	71	53/18	37	34	17/20	74.0	41.1	39.0	—	60.5	—	10
Chen and Qiu (17)	2015	Chinese	96	72/24	38	58	52/44	68.0	51.7	—	—	—	—	9
Liu et al. (5)	2021	English	96	—	66	30	6/90	89.9	—	73.8	—	81.8	—	21

CI, confidence interval; M, male; F, female; OS, overall survival; DFS, disease-free survival.

TABLE 2 | Main characteristics of included studies on IMRT.

Authors	Year	Publication language	No. of patients	M/F	rT classifications		ReRT mean GTV dose (Gy)	rT3-4 NPC' OS (%)			2-year DFS (%)	3-year LCR (%)	MINORS
					rT1-2	rT3-4		2-year	3-year	5-year			
Qiu et al. (18)	2012	English	70	56/14	30	40	70.0 (50–77.4)	64.7	–	–	62.0	–	8
Han et al. (19)	2012	English	239	182/57	59	180	69.9 (61.7–78.7)	–	–	35.1	–	–	10
Hua et al. (20)	2012	English	151	122/29	29	122	70.4 (62.1–77.6)	–	42.6	34.4	–	88.5	9
Chen et al. (21)	2013	English	54	44/10	11	43	70.0(49.8–76.6)	65.9	–	–	–	–	9
Tian et al. (22)	2013	English	251	195/56	53	198	70.7(61.1–79.7)	–	–	32.4	–	–	11
Karam et al. (23)	2016	English	27	20/7	21	6	54.0 (39.0–97.0)	–	23.0	–	–	8.0	10
Chan et al. (24)	2016	English	38	31/7	0	38		–	47.2	–	–	44.3	8
Ng et al. (25)	2017	English	33	–	0	33	–	–	63.8	–	–	49.2	8
Tian et al. (26)	2017	English	245	49/196	0	245	70.0 (60.1–78.7)	–	–	27.5	–	–	10
Kong et al. (27)	2018	English	184	133/51	64	120	66.7 (42.0–77.0)	–	42.9	–	–	–	9
Zhang et al. (28)	2018	Chinese	44	33/11	21	23	66.0 (54.0–70.0)	–	33.8	–	–	–	8
You et al. (9)	2015	English	72	18/54	59	13	–	–	46.1	46.1	53.8	–	12
Zou et al. (10)	2015	English	218	173/45	57	161	–	–	–	28.8	–	–	10
Liu et al. (5)	2021	English	100	72/28	69	31	–	–	–	–	–	–	21

CI, confidence interval; M, male; F, female; OS, overall survival; DFS, disease-free survival; LCR, local control rate.

Symmetry of the funnel plot was tested by linear regression models (Begg's method and Egger's method) in STATA 12.0 to evaluate publication bias. For the studies from which we could obtain survival of endoscopic surgery group and IMRT group, OR values were combined and heterogeneity tests was analyzed using Review Manager 5.3. The relationship between treatment methods and patients survival rate was shown by pooled OR. We calculated the OR values and performed to analyze P <0.05 was considered statistically significant. We use Engauge Digitizer 12.1 to calculate from Kaplan-Meier (K-M) Curve of published article (29).

RESULTS

Search Results and Study Characteristics

A total of 2,052 publications were captured though the initial systematic research of literature published between February 28, 2011, and February 28,2021, among which 1,078 were found in English databases, and 974 were found in Chinese databases. While reviewing the titles and abstracts, 91 of them were selected for full-text reading and 68 of them were excluded for the reasons shown in **Figure 1**. Twenty-three papers were finally left for our analysis.

The 23 publications meeting the inclusion criteria include a total of 2,578 patients diagnosed with recurrent NPC. Twelve articles investigated endoscopic surgery for recurrent NPC covered a total of 852 patients, including 494 patients with stage recurrent rT1-2 NPC and 358 patients with stage rT3-4. Fourteen studies investigated IMRT for recurrent NPC covered a total of 1,726 patients, including 473 patients with stage recurrent rT1-2 NPC and 1,253 patients with stage rT3-4, respectively. Three of the 23 studies were comparative studies of the efficacy of endoscopic surgery versus IMRT for recurrent NPC. The range of sample size was 12 to 251 with a mean of 112, sample size for endoscopic treatment, and IMRT ranging from 12 to 189 with a mean of 71 and 27 to 251 with a mean of 123, respectively. We used MINORS to assess the quality of the studies, and in all publications included in this paper, the average MINORS score was 10 (range,8-21) (**Tables 1** and **2**), so the quality of these studies is acceptable.

Comparison of OS in Patients Between Endoscopic Surgery and IMRT

First step meta-analysis, we performed on OS rate. We compared the 2-year and 5-year OS rates of endoscopic surgery and IMRT with or without chemotherapy for recurrent rT3-4 NPC, respectively (**Figures 2A, B**). For these patients, the 2-year OS rate was 64% (95% CI, 52%–77%, I^2 = 74%, P= 0.0003), the 5-year OS rate was 52% (95% CI, 43%–60%, I^2 = 45%, P= 0.14). Although the patients undertaking IMRT had better 2-year OS rate than those with endoscopic surgeries. However, there is just a little difference between them. In terms of 5-year OS rate, the patients undertaking ES had better survival experience than those with IMRT. In studies of IMRT for recurrent NPC, most investigators use the 3-year OS rate to express the effectiveness of

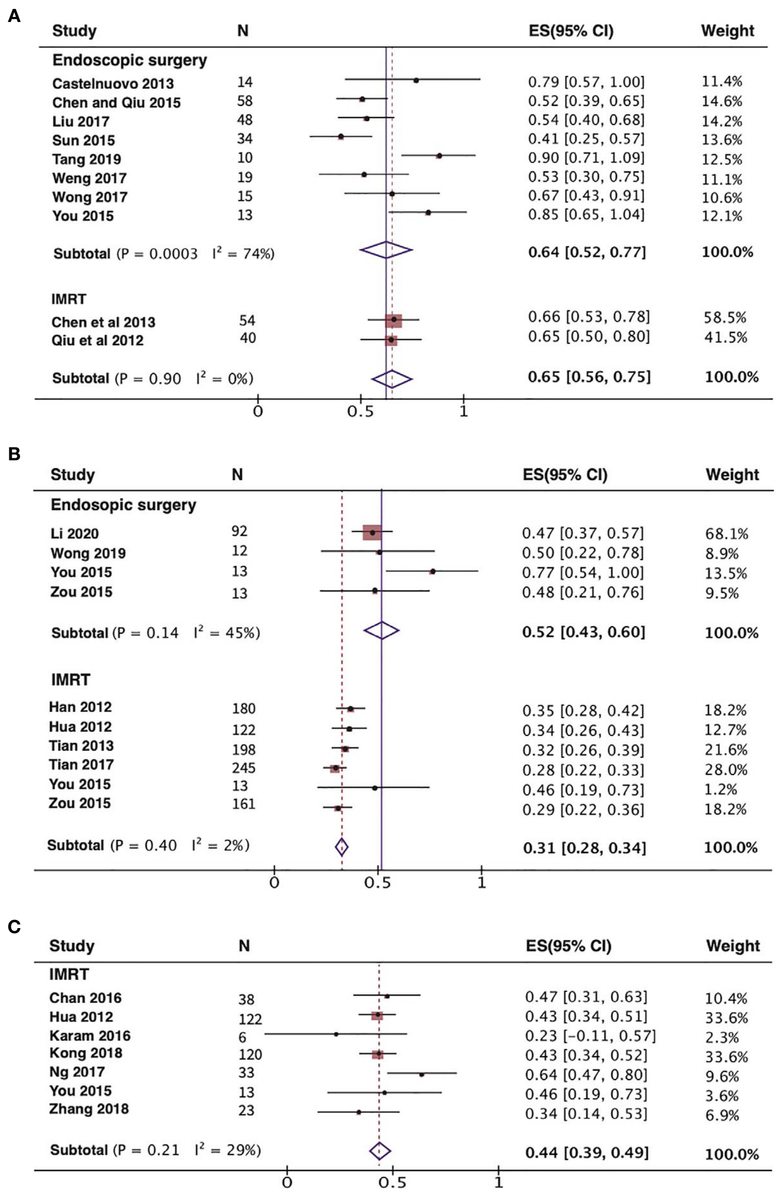

FIGURE 2 | Forest plot displaying the meta-analysis of OS in the endoscopic surgery and IMRT group with recurrent rT3-4 NPC. **(A)** Meta-analysis of 2-year OS rates. **(B)** Meta-analysis of 5-year OS rates. **(C)** Meta-analysis of 3-year OS rates for IMRT group. NPC, nasopharyngeal carcinoma; IMRT, intensity-modulated radiotherapy; OS, overall survival.

the treatment method, so we also analyzed the 3-year OS rate of the IMRT group as shown in **Figure 2C**. Then, we found that ES achieved better 5-year OS rate than IMRT's 3-year OS rate for recurrent rT3-4 NPC (52% *vs* 44%).

Association Between Treatment and OS, DFS, and LCR

The 2-year disease-free survival (DFS) rate are comparable between ES and IMRT for recurrent rT3-4 NPC. Although the 2-year DFS rate was higher in patients with recurrent NPC treated with IMRT than in those treated with ES, 60%(95% CI,47%–73%, I^2 = 0%, P= 0.6) and 50% (95% CI,41%–59%, I^2 = 0%, P= 0.55), respectively, the confidence interval was wider than for ES (**Figure 3A**). We also combined the 3-year local control rate (LCR) of recurrent rT3-4 NPC treated with IMRT as shown in **Figure 3B**, 48%(95% CI,13%-84%, I^2 = 96%, P<0.00001). However, this metric does not have enough data for comparison in ES. As shown in **Figure 4**, endoscopic surgery for recurrent NPC is more advantageous compared with IMRT, also in recurrent cases with high T-stage, but the confidence interval was wider, probably related to the relatively small number of included literatures.

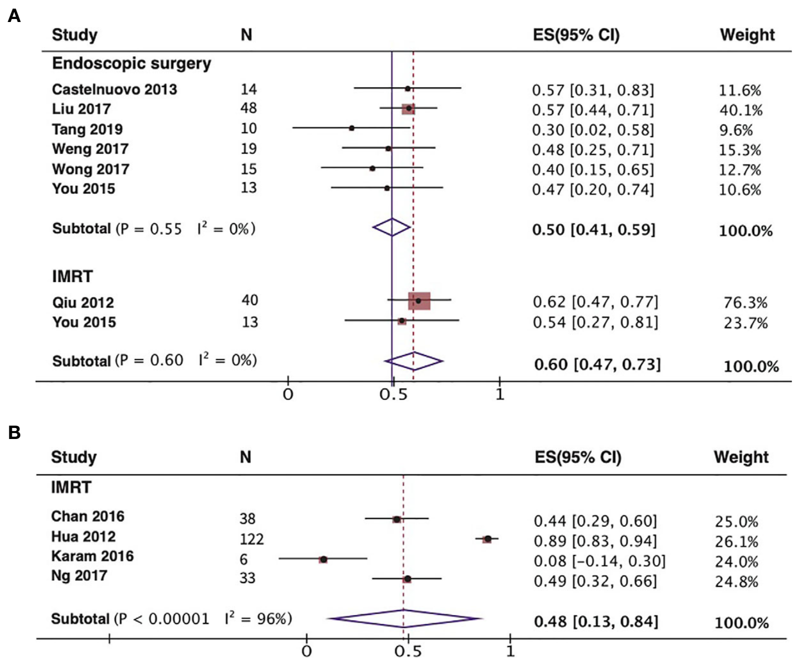

FIGURE 3 | Forest plot of DFS and LCR in the endoscopic surgery and/or IMRT group with recurrent rT3-4 NPC. **(A)** Meta-analysis of 2-year DFS rates. **(B)** Meta-analysis of 3-year LCR for IMRT group. NPC, nasopharyngeal carcinoma; IMRT, intensity-modulated radiotherapy; DFS, disease-free survival; LCR, local control rate.

I (2) > 50% indicates a high heterogeneity in the analytical results, so we further investigated possible causes of bias and heterogeneity. Meta-regression analysis showed that size of studies (≥15 cases or not) was a correlative factor of heterogeneity. Subgroup meta-analysis was then performed (**Supplementary Figure 1**). If we exclude the studies which size of study<15 cases, then combined the 2-year OS rate, N=5, the results obtained are shown in **Supplementary Figure 1A**. Similar results were also observed in meta-regression analyses for 3-year LCR for IMRT group. Combining the 3-year LCR rate of two studies with similar case numbers, we can obtain results as shown in **Supplementary Figure 1B**.

Comparison of Complications

We combined the occurrence of complications of the two treatments in 23 papers respectively; as shown in **Figure 5**, the incidence of most complications after IMRT for patients with recurrent NPC is higher than that of ES. Also, among the 13 publications on IMRT, three reported 23 cases of dysphagia in a total of 125 patients and 68 patients with radiation encephalopathy in another publications of 239 patients. Four publications reported tissue damage to the face and neck in 20 of a total of 288 patients treated with re-radiotherapy. Postoperative hemorrhage and wound infection have become complications specific to ES for recurrent NPC.

Publication Bias

Publication bias was evaluated using Begg's test. As shown in **Figure 6**, the funnel plot did not indicate any evidence of publication bias for endoscopic surgery's 2-year OS (p = 0.458) and 5-year OS (p = 0.497); IMRT 2-year OS (p = 0.317) and 5-year OS (p = 0.188); endoscopic surgery's 2- year DFS (p = 0.091).

DISCUSSION

Nasopharyngeal carcinoma is sensitive to radiotherapy but more prone to recurrence. Tumor size, pathological staging, tumor necrosis, tumor stage, the presence of lymph node metastasis, or distant metastasis have important effects on patient survival and recurrence, and the prognosis of high T-stage NPC is relatively poor. There is no accepted unified standard treatment for the recurrent NPC (7, 8, 26). IMRT with or without chemotherapy is a more widely used treatment modality at present. With the development of endoscopic surgical techniques and the deepening of nasocranial base surgeons' understanding of the anatomy of the nasopharynx in recent years, endoscopic surgery for recurrent NPC has been well developed and has good efficacy (5, 9, 10). Our study synthesized the publications in the last 10 years for patients with high T-stage recurrent NPC and compared the survival rates of ES and IMRT as well as some other indicators to determine the prognosis. This article is the first meta-analysis comparing the efficacy of ES with IMRT for recurrent rT3-4 NPC only, and it is also the article with the largest number of cases of recurrent rT3-4 NPC combined. In conclusion, endoscopic surgery for recurrent rT3-4 NPC was superior to IMRT, in terms of both 2-year and 5-year OS rates, and had a lower complication rate.

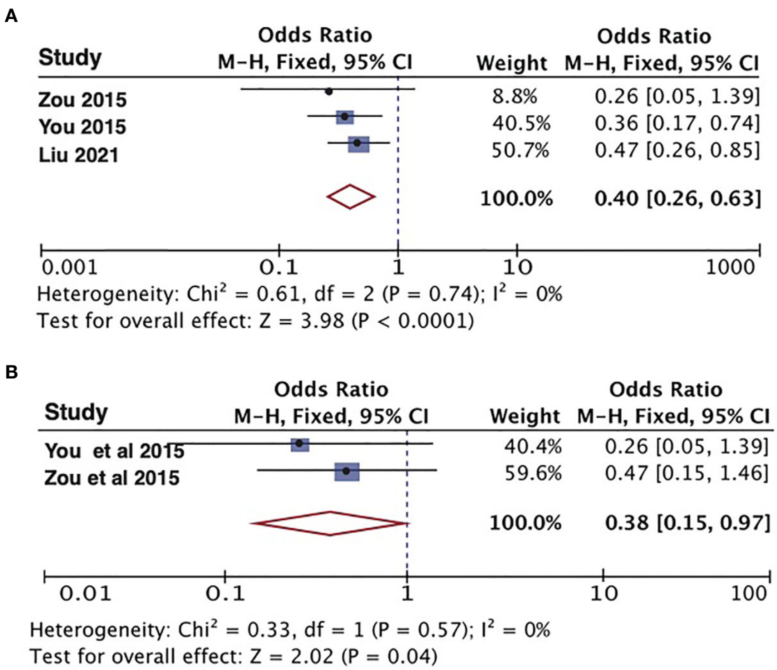

FIGURE 4 | Meta-analysis the impact on 5-year OS rate with endoscopic surgery and IMRT. **(A)** Results of the overall cases. **(B)** Results of the recurrent rT3-4 NPC. NPC, nasopharyngeal carcinoma; OS, overall survival.

Radiotherapy is the traditional treatment modality for NPC. For the first occurrence of NPC, especially if the tumor is relatively limited in growth and has not yet involved the skull base structures and important blood vessels or nerves, radiotherapy with or without synchronous or neoadjuvant chemotherapy can achieve good results (30). In recurrent NPC, reirradiation with conventional external beam techniques have yielded largely unsatisfactory results with high rates of late complications even with transition from 2-D to 3-D conformal techniques. IMRT allows for conformation of multiple small beamlets to irregularly shaped tumors, such as NPC (31). Compared with conventional radiotherapy techniques, IMRT is better at reducing complications, but the toxic effects of radiotherapy are still present, and the efficacy is not conclusive. A meta-analysis by Leong et al, which investigated 12 studies including 1768 patients, concluded that the 5-year local failure-free survival of IMRT for recurrent NPC was 72%, 5-year distant failure-free survival was 85%, and 5-year OS was 41% (31). From the above survival data, the long-term survival rate of recurrent NPC treated with IMRT still needs to be improved. With the development of endoscopic surgical techniques and anatomical studies, endoscopic surgery for recurrent NPC is increasingly performed. In 2005, Yoshizaki et al. introduced ES to treat patients with recurrent NPC by selecting four different approaches according to the T-stage of the tumor and the site of growth (32). Yang et al. summarized 23 papers; they combined survival outcomes for recurrent NPC treated with ES and reported that 1-year, 2-year, and 5-year OS rates were 97%, 92%, and 73%, respectively (33). These data are more favorable compared with the same type of data for IMRT.

In the treatment of recurrent NPC, surgery not only leads to similar survival and prognosis as IMRT but also has better

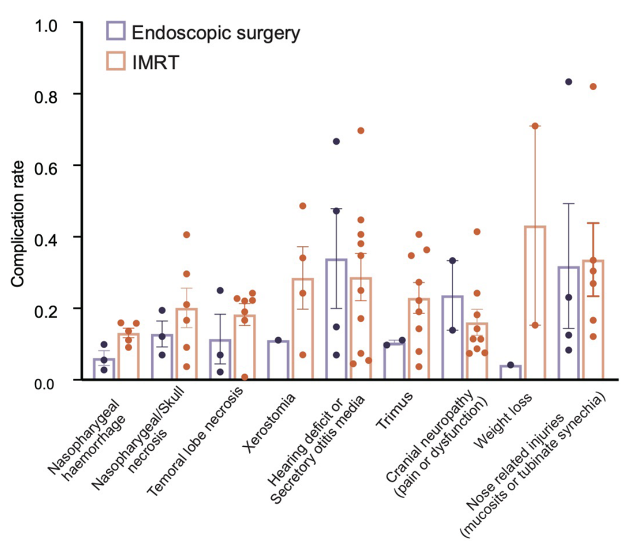

FIGURE 5 | Comparison of the combined incidence of major complications of endoscopic surgery and IMRT.

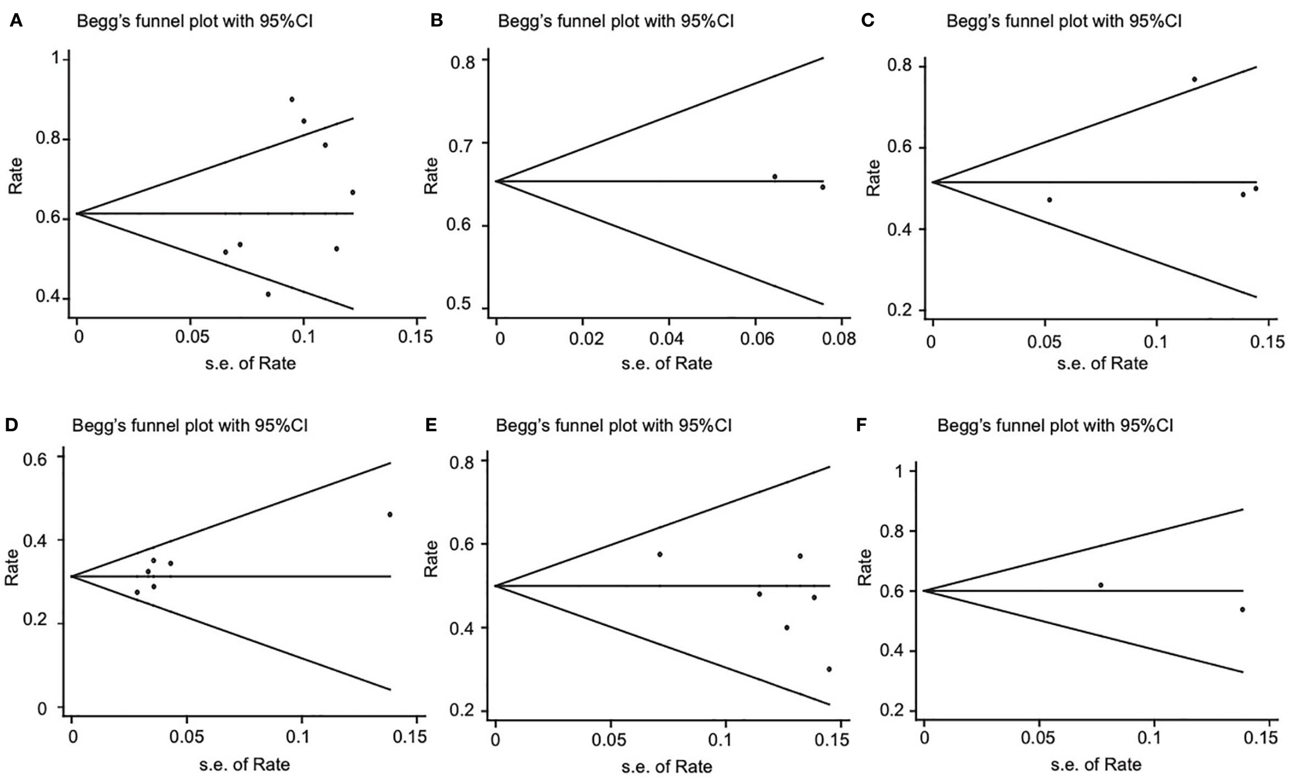

FIGURE 6 | Funnel plots for publication bias of 2-year OS, 5-year OS, 2-year DFS. **(A)** 2-year OS of endoscopic surgery. **(B)** 2-year OS of IMRT. **(C)** 5-year OS of endoscopic surgery. **(D)** 5-year OS of IMRT. **(E)** 2-year DFS of endoscopic surgery. **(F)** 2- year DFS of IMRT. OS, overall survival; DFS, disease-free survival.

outcomes in terms of complications and severity compared with those who undergo IMRT. A review of previous publications shows that the T-stage of NPC has a significant impact on survival outcomes, with patients with T1-2 tumors, who had almost all better OS, DFS, and LCR than patients with T3-4. Combining the 2-year OS rate according to rT1 to rT4 stage were 100%, 87%, 78%, and 38%, respectively, indicating a trend toward diminishing OS rate correlated with staging of tumors (33). You et al. reported improved survival in ES cases compared to IMRT in rT1 to rT3 patients in a subgroup analysis (9). For patients with recurrent rT3-4 NPC, surgery provides better targeted protection of important nerves and blood vessels than conventional IMRT. Of course, the abovementioned results presuppose that the surgeon should be very familiar with the structures of the nasopharynx and related skull base anatomical regions and proficient in endoscopic surgical techniques, at the same time, because many patients will have different degrees of radiation injury after their first radiation treatment, such as secretory otitis media, head and facial pain, difficulty in opening the mouth, slurred speech, and so on, and even more serious post-radiation complications, such as carotid artery hemorrhage and cranial nerve injury can occur in some patients. Patients in this category cannot receive re-radiation if they relapse, regardless of their T-stage. Although chemotherapy has a certain effect on controlling metastatic tumors, it cannot completely replace radiotherapy and can only be used to assist in killing the residual tumor cells. Therefore, for such patients, endoscopic surgery may be offered as a new hope.

In recent years, some surgeons believe that open surgery provides better clarity for late recurrent NPC, and a better safety margin can be obtained with an open view. In contrast, endoscopic surgery seems to be more suitable for the treatment of early recurrent NPC. In fact, a meta-analysis study of endoscopic and open surgery for recurrent NPC by investigators showed that for patients with rT3 stage, the 2-year OS rate was 67% for endoscopic surgery compared with 53% for open surgery. For patients with rT4, there was no difference in the 2-year OS rate between the two treatments, which were both 35% (34). Although there are no comparative results for 5-year OS rates, it is at least clear that modern high-definition endoscopic surgery is not inferior in the management of tumor safety margins. Also compared with the occurrence of postoperative complications, such as infection and bleeding, endoscopic surgery is more advantageous than open surgery.

There are some limitations worth noting of this study that should be acknowledged. First, all but one of the publications included in this study were retrospective studies and lacked randomized controlled trials, increasing the risk of bias. Second, although three papers on endoscopic treatment and IMRT for recurrent NPC at the same institution were included in this study, the literature was mostly from different medical centers. IMRT was acceptable, although the prognosis and survival of ES were actually related to the surgical technique and even surgical equipment of the physicians in the medical institutions and the presence of these objective factors may affect the results of this meta-analysis. Furthermore, some results in this study were analyzed with less literature included, which can introduce bias to the analysis results. Finally, because some of the original clinical data were not available, some of the data obtained by statistical methods may not be accurate enough, which ultimately affects the results of the analysis.

CONCLUSIONS

Our study showed that, compared with IMRT, endoscopic surgery was a more effective treatment modality in managing patients with recurrent rT3-4 NPC. However, there is still insufficient evidence to suggest that ES can replace IMRT, but only to provide some support for the choice of perhaps more appropriate treatment. Ultimately, RCT will need to be designed to corroborate the current view.

DATA AVAILABILITY STATEMENT

The raw data supporting the conclusions of this article will be made available by the authors, without undue reservation.

AUTHOR CONTRIBUTIONS

WJ, HZ, ZP, and YMW conceived and designed the study. ZP, YXW, RF, and KG performed the analysis, prepared the figures and tables, and wrote the main manuscript. All authors contributed to the article and approved the submitted version.

FUNDING

This Research was funded by the National Natural Science Foundation of China (81770985); the Hunan Province Graduate Education Innovation Project (CX20200386); and the Independent Exploration and Innovation Project for Graduate Students of Central South University (506021703). The funders had no role in study design, data collection and analysis, decision to publish, or preparation of the manuscript.

SUPPLEMENTARY MATERIAL

The Supplementary Material for this article can be found online at: https://www.frontiersin.org/articles/10.3389/fonc.2021.703954/full#supplementary-material

REFERENCES

1. Chen YP, Chan ATC, Le QT, Blanchard P, Sun Y, Ma J. Nasopharyngeal Carcinoma. *Lancet* (2019) 394(10192):64–80. doi: 10.1016/S0140-6736(19)30956-0
2. Xu T, Tang J, Gu M, Liu L, Wei W, Yang H. Recurrent Nasopharyngeal Carcinoma: A Clinical Dilemma and Challenge. *Curr Oncol* (2013) 20(5):e406–19. doi: 10.3747/co.20.1456
3. Wang Y, Mo Y, Gong Z, Yang X, Yang M, Zhang S, et al. Circular RNAs in Human Cancer. *Mol Cancer* (2017) 16(1):25. doi: 10.1186/s12943-017-0598-7
4. Peng Z, Wang Y, Wang Y, Jiang S, Fan R, Zhang H, et al. Application of Radiomics and Machine Learning in Head and Neck Cancers. *Int J Biol Sci* (2021) 17(2):475–86. doi: 10.7150/ijbs.55716
5. Liu YP, Wen YH, Tang J, Wei Y, You R, Zhu XL. Endoscopic Surgery Compared With Intensity-Modulated Radiotherapy in Resectable Locally Recurrent Nasopharyngeal Carcinoma: A Multicentre, Open-Label, Randomised, Controlled, Phase 3 Trial. *Lancet Oncol* (2021) 22(3):381–90. doi: 10.1016/S1470-2045(20)30673-2
6. Hao CY, Hao SP. The Management of Rnpc: Salvage Surgery Vs. Re-irradiation. *Curr Oncol Rep* (2020) 22(9):86. doi: 10.1007/s11912-020-00949-0
7. Wong EHC, Liew YT, Abu Bakar MZ, Lim EYL, Prepageran N. A Preliminary Report on the Role of Endoscopic Endonasal Nasopharyngectomy in Recurrent rT3 and rT4 Nasopharyngeal Carcinoma. *Eur Arch Otorhinolaryngol* (2017) 274(1):275–81. doi: 10.1007/s00405-016-4248-2
8. Wong EHC, Liew YT, Loong SP, Prepageran N. Five-Year Survival Data on the Role of Endoscopic Endonasal Nasopharyngectomy in Advanced Recurrent rT3 and Rt4 Nasopharyngeal Carcinoma. *Ann Otol Rhinol Laryngol* (2020) 129(3):287–93. doi: 10.1177/0003489419887410
9. You R, Zou X, Hua YJ, Han F, Li L, Zhao C, et al. Salvage Endoscopic Nasopharyngectomy Is Superior to Intensity-Modulated Radiation Therapy for Local Recurrence of Selected T1-T3 Nasopharyngeal Carcinoma – A Case-Matched Comparison. *Radiother Oncol* (2015) 115(3):399–406. doi: 10.1016/j.radonc.2015.04.024
10. Zou X, Han F, Ma WJ, Deng MQ, Jiang R, Guo L, et al. Salvage Endoscopic Nasopharyngectomy and Intensity-Modulated Radiotherapy Versus Conventional Radiotherapy in Treating Locally Recurrent Nasopharyngeal Carcinoma. *Head Neck* (2015) 37(8):1108–15. doi: 10.1002/hed.23719
11. Castelnuovo P, Nicolai P, Turri-Zanoni M, Battaglia P, Bolzoni Villaret A, Gallo S, et al. Endoscopic Endonasal Nasopharyngectomy in Selected Cancers. *Otolaryngol Head Neck Surg* (2013) 149(3):424–30. doi: 10.1177/0194599813493073
12. Weng J, Wei J, Si J, Qin Y, Li M, Liu F, et al. Clinical Outcomes of Residual Or Recurrent Nasopharyngeal Carcinoma Treated With Endoscopic Nasopharyngectomy Plus Chemoradiotherapy or With Chemoradiotherapy Alone: A Retrospective Study. *PeerJ* (2017) 5:e3912. doi: 10.7717/peerj.3912
13. Liu J, Yu H, Sun X, Wang D, Gu Y, Liu Q, et al. Salvage Endoscopic Nasopharyngectomy for Local Recurrent or Residual Nasopharyngeal Carcinoma: A 10-Year Experience. *Int J Clin Oncol* (2017) 22(5):834–42. doi: 10.1007/s10147-017-1143-9
14. Tang IP, Ngui LX, Ramachandran K, Lim LY, Voon PJ, Yu KL, et al. A 4-Year Review of Surgical and Oncological Outcomes of Endoscopic Endonasal Transpterygoid Nasopharyngectomy in Salvaging Locally Recurrent Nasopharyngeal Carcinoma. *Eur Arch Otorhinolaryngol* (2019) 276(9):2475–82. doi: 10.1007/s00405-019-05522-5
15. Li W, Lu H, Wang H, Zhang H, Sun X, Hu L, et al. Salvage Endoscopic Nasopharyngectomy in Recurrent Nasopharyngeal Carcinoma: Prognostic Factorsand Treatment Outcomes. *Am J Rhinol Allergy* (2021) 35(4):458–66. doi: 10.1177/1945892420964054
16. Sun X, Liu J, Wang H, Yu H, Wang J, Li H, et al. Endoscopic Nasopharyngectomy for Recurrent Nasopharyngeal Carcinoma: A Review of 71 Patients and Analysis of Theprognostic Factors. *Zhonghua Er Bi Yan Hou Tou Jing Wai Ke Za Zhi* (2015). 50(11):890–95.
17. Chen Z, Qiu Q. Analysis of Clinical Eifcacy and the Quality of Life After Endoscopic Nasopharyngectomy for Residual or Recurrent Nasopharyngela Carcinoma. *Zhonghua Er Bi Yan Hou Tou Jing Wai Ke Za Zhi* (2015) 50(11):896–903.
18. Qiu S, Lin S, Tham IW, Pan J, Lu J, Lu JJ. Intensity-Modulated Radiation Therapy in the Salvage of Locally Recurrent Nasopharyngeal Carcinoma. *Int J Radiat Oncol Biol Phys* (2012) 83(2):676–83. doi: 10.1016/j.ijrobp.2011.07.006
19. Han F, Zhao C, Huang SM, Lu LX, Huang Y, Deng XW, et al. Long-Term Outcomes and Prognostic Factors of Re-Irradiation for Locally Recurrent

Nasopharyngeal Carcinoma Using Intensity-Modulated Radiotherapy. *Clin Oncol (R Coll Radiol)* (2012) 24(8):569–76. doi: 10.1016/j.clon.2011.11.010
20. Hua YJ, Han F, Lu LX, Mai HQ, Guo X, Hong MH, et al. Long-Term Treatment Outcome of Recurrent Nasopharyngeal Carcinoma Treated With Salvage Intensity Modulated Radiotherapy. *Eur J Cancer.* (2012) 48(18):3422–8. doi: 10.1016/j.ejca.2012.06.016
21. Chen HY, Ma XM, Ye M, Hou YL, Xie HY, Bai YR. Effectiveness and Toxicities of Intensity-Modulated Radiotherapy for Patients With Locally Recurrent Nasopharyngeal Carcinoma. *PLoS One* (2013) 8(9):e73918. doi: 10.1371/journal.pone.0073918
22. Tian YM, Tian YH, Zeng L, Liu S, Guan Y, Lu TX, et al. Prognostic Model for Survival of Local Recurrent Nasopharyngeal Carcinoma With Intensity-Modulated Radiotherapy. *Br J Cancer* (2014) 110(2):297–303. doi: 10.1038/bjc.2013.715
23. Karam I, Huang SH, McNiven A, Su J, Xu W, Waldron J, et al. Outcomes After Reirradiation for Recurrent Nasopharyngeal Carcinoma: North American Experience. *Head Neck* (2016) 38(Suppl 1):E1102–9. doi: 10.1002/hed.24166
24. Chan OS, Sze HC, Lee MC, Chan LL, Chang AT, Lee SW, et al. Reirradiation With Intensity-Modulated Radiotherapy for Locally Recurrent T3 to T4 Nasopharyngeal Carcinoma. *Head Neck* (2017) 39(3):533–40. doi: 10.1002/hed.24645
25. Ng WT, Ngan RKC, Kwong DLW, Tung SY, Yuen KT, Kam MKM, et al. Prospective, Multicenter, Phase 2 Trial of Induction Chemotherapy Followed by Bio-Chemoradiotherapy for Locally Advanced Recurrent Nasopharyngeal Carcinoma. *Int J Radiat Oncol Biol Phys* (2018) 100(3):630–8. doi: 10.1016/j.ijrobp.2017.11.038
26. Tian YM, Huang WZ, Yuan X, Bai L, Zhao C, Han F. The Challenge in Treating Locally Recurrent T3-4 Nasopharyngeal Carcinoma: The Survival Benefit and Severe Late Toxicities of Re-Irradiation With Intensity-Modulated Radiotherapy. *Oncotarget* (2017) 8(26):43450–7. doi: 10.18632/oncotarget.15896
27. Kong F, Zhou J, Du C, He X, Kong L, Hu C. Long-Term Survival and Late Complications of Intensity-Modulated Radiotherapy for Recurrent Nasopharyngeal Carcinoma. *BMC Cancer* (2018) 18(1):1139. doi: 10.1186/s12885-018-5055-5
28. Zhang HH, Zhang XW, Jiang H. Clinical Efficacy and Prognostic Factors of Locally Recurrent Nasopharyngeal Carcinoma With Intensity- Modulated Radiotherapy. *J Shanghai Jiao Tong Uni* (2018) 38(6):662–9.
29. Shi X, Chen Q, Wang F. Mesenchymal Stem Cells for the Treatment of Ulcerative Colitis: A Systematic Review and Meta-Analysis of Experimental and Clinical Studies. *Stem Cell Res Ther* (2019) 10(1):266. doi: 10.1186/s13287-019-1336-4
30. Kong L, Lu JJ. Reirradiation of Locally Recurrent Nasopharyngeal Cancer: History, Advances, and Promises for the Future. *Chin Clin Oncol* (2016) 5(2):26. doi: 10.21037/cco.2016.03.19
31. Leong YH, Soon YY, Lee KM, Wong LC, Tham IWK, Ho FCH. Long-Term Outcomes After Reirradiation in Nasopharyngeal Carcinoma With Intensity-Modulated Radiotherapy: A Meta-Analysis. *Head Neck* (2018) 40(3):622–31. doi: 10.1002/hed.24993
32. Yoshizaki T, Wakisaka N, Murono S, Shimizu Y, Furukawa M. Endoscopic Nasopharyngectomy for Patients With Recurrent Nasopharyngeal Carcinoma at the Primary Site. *Laryngoscope* (2005) 115(8):1517–9. doi: 10.1097/01.MLG.0000165383.35100.17
33. Yang J, Song X, Sun X, Liu Q, Hu L, Yu H, et al. Outcomes of Recurrent Nasopharyngeal Carcinoma Patients Treated With Endoscopic Nasopharyngectomy: A Meta-Analysis. *Int Forum Allergy Rhinol* (2020) 10(8):1001–11. doi: 10.1002/alr.22552
34. Li G, Wang J, Tang H, Han R, Zhao Y, Wang X, et al. Comparing Endoscopic Surgeries With Open Surgeries in Terms of Effectiveness and Safety in Salvaging Residual or Recurrent Nasopharyngeal Cancer: Systematic Review and Meta-Analysis. *Head Neck* (2020) 42(11):3415–26. doi: 10.1002/hed.26397

Conflict of Interest: The authors declare that the research was conducted in the absence of any commercial or financial relationships that could be construed as a potential conflict of interest.

Publisher's Note: All claims expressed in this article are solely those of the authors and do not necessarily represent those of their affiliated organizations, or those of the publisher, the editors and the reviewers. Any product that may be evaluated in this article, or claim that may be made by its manufacturer, is not guaranteed or endorsed by the publisher.

frontiers in Oncology

METHODS
published: 13 August 2021
doi: 10.3389/fonc.2021.714342

The Use of Micro Retractor in Endoscopic Endonasal Posterior Pseudocapsule Resection of Pituitary Macroadenoma. Technical Note

Tao Xie[1], *Xiaobiao Zhang*[1,2,3*], *Chenghui Qu*[1] *and Chen Li*[1]

[1] *Department of Neurosurgery, Zhongshan Hospital, Fudan University, Shanghai, China,* [2] *Digital Medical Research Center, Fudan University, Shanghai, China,* [3] *Shanghai Key Laboratory of Medical Image Computing and Computer-Assisted Intervention, Shanghai, China*

Background: The endoscopic endonasal approach and extra-pseudocapsule resection may be the main progress in modern pituitary surgery. However, for pituitary macroadenomas, discerning the pseudocapsule in the posterior plane of the tumor may be difficult. When the anterior-inferior debulking is performed, the early subsidence of the thinning normal pituitary gland and enlarged diaphragm may obstruct the surgical dissection view.

Method: We describe the technique of using a micro retractor for the endoscopic endonasal posterior pseudocapsule resection of pituitary macroadenomas. This micro retractor that was 2 mm in width was placed at the 12 o'clock position on the nostrils, and the end was fixed in the flexible arms of the self-retaining retractor system. The head of the micro retractor elevated the herniated diaphragm sellae in order to continue the posterior pseudocapsule resection of the pituitary macroadenoma.

Result: The technique was performed very easily and no complication was observed.

Conclusion: The use of this micro retractor can increase the view of the posterior margin of the adenomas to facilitate the pseudocapsule dissection.

Keywords: endoscopic endonasal approach, pituitary adenoma, pseudocapsule, retractor, neurosurgery

Edited by:
Xicai Sun,
Fudan University, China

Reviewed by:
Qing Wang,
Nanjing Medical University, China
Peizhi Zhou,
Sichuan University, China

****Correspondence:***
Xiaobiao Zhang
xiaobiao_zhang@163.com

Specialty section:
This article was submitted to Surgical Oncology, a section of the journal Frontiers in Oncology

Received: *25 May 2021*
Accepted: *23 July 2021*
Published: *13 August 2021*

Citation:
Xie T, Zhang X, Qu C and Li C (2021) The Use of Micro Retractor in Endoscopic Endonasal Posterior Pseudocapsule Resection of Pituitary Macroadenoma. Technical Note. Front. Oncol. 11:714342. doi: 10.3389/fonc.2021.714342

INTRODUCTION

The advent of endoscopy has begun a new era for pituitary (1). The endoscope and the updated high-definition endoscopes provide a panoramic, close-up surgical view, and allow the eyes of a neurosurgeon to focus not only on the tumor structures but also on the subtle surrounding normal architecture, which has been ignored in the past. The pseudocapsule is one of these structures. The pseudocapsule is not a new concept, as an extraordinarily detailed description was provided by Costello 80 years ago (2). That autopsy research described that many of the adenomas had a thin layer of compressed reticulin, which could easily be distinguished from the pituitary adenoma. Obviously, many neurosurgeons have neglected this small and delicate structure. However, using this pseudocapsule, as the surgical plane for the dissection of an adenoma, is currently gaining increasing attention. This technique improves the gross total resection (3). However, with the increased use of this technique, we found that pseudocapsule dissection might be difficult in the posterior and superior directions for the resection of macroadenomas because of the early subsidence of the thinning normal pituitary gland, and an enlarged diaphragm may obstruct the surgical dissection view after anterior debulking (4, 5). In this report, we describe the use of a micro-retractor to elevate the redundant gland and diaphragm to facilitate the dissection of the posterior pseudocapsule (**Figures 1**, **2**).

Surgical Technique

We used the standard endoscopic endonasal transsphenoidal approach which has been widely described in our and other studies (6). A widely anterior sphenoidotomy was performed, and part of the posterior ethmoid sinus was also removed. Then, the anatomic landmarks around the sella were ascertained. After the entire sella floor was removed, the exposure of the 4-Blue criterion (upper and lower intercavernous sinuses and bilateral cavernous sinus) was required. A No.15 scalpel was used to incise the dura matter (two membranes) with the type, while leaving the underlying pituitary capsule intact. The next incision was made very superficially to incise the pituitary capsule, which is as thin as the wings of a cicada (for macroadenomas, the anterior pituitary gland usually disappears). Blunt microdissection was patiently attempted to develop a surgical plane around the pseudocapsule from the lateral compressed pituitary gland or the medial wall of the cavernous sinus. At this time, a large ring curette was used as a handy tool to peel, rather than scrape, the pseudocapsule. This action informed us that the pseudocapsule dissection was workable. However, in many cases, it was particularly difficult to perform *en bloc* pseudocapsule resection on the macroadenomas. Under these circumstances, suitable debulking was used to create a befitting peripheral margin that was thick enough to provide adequate integrity to the dissection plane. In the real practice, the dissection plane may be ruptured especially in the posterior margin of the pseudocapsule, piecemeal pseudocapsule resection was also typically employed. When the adenoma was gross-totally removed, the thinning normal pituitary gland and enlarged diaphragm would have

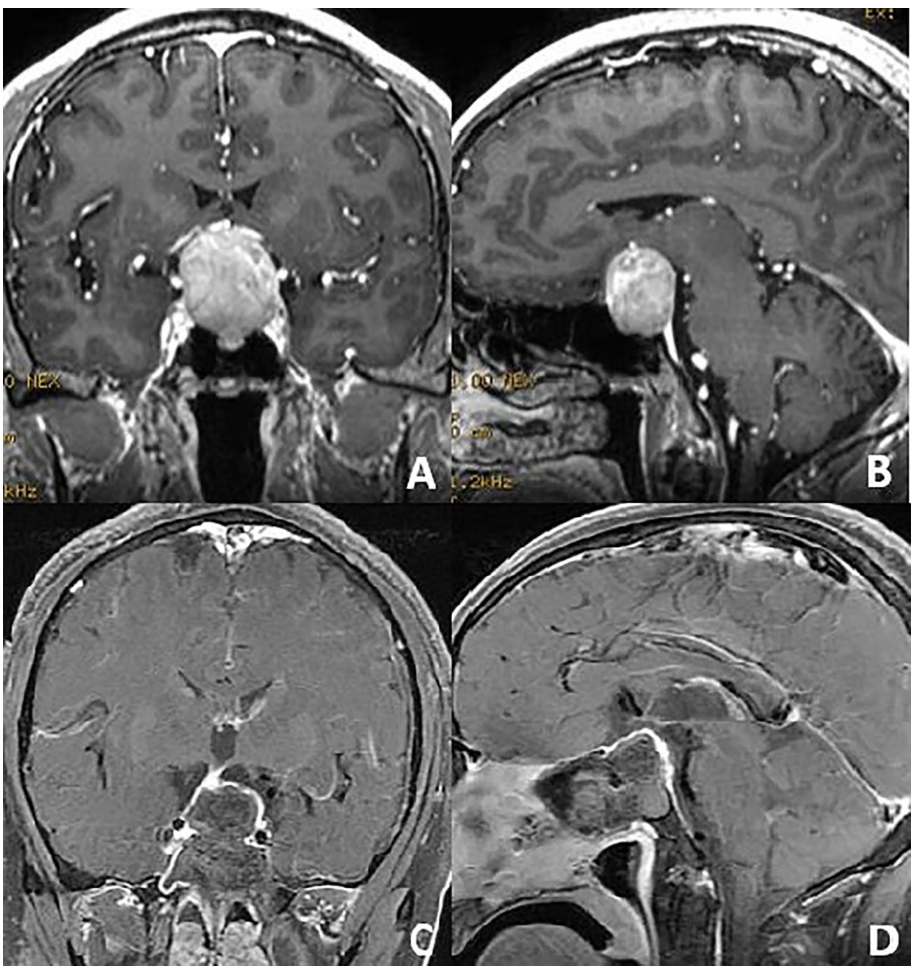

FIGURE 1 | Preoperative coronal and sagittal **(A, B)** contrast-enhanced magnetic resonance T1-weighted images of a non-functional pituitary macroadenoma. After the endoscopic anterior and posterior pseudocapsule dissection, the adenoma was achieved total resection **(C, D)**.

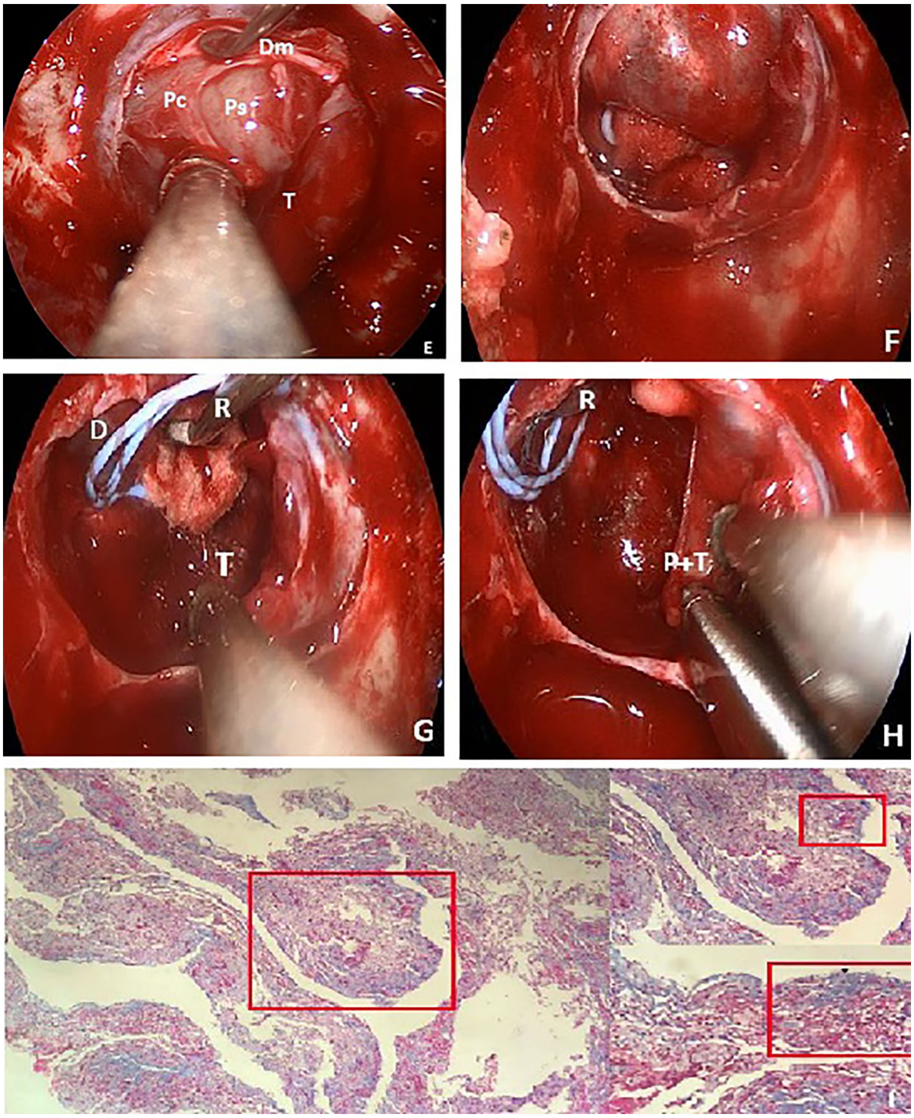

FIGURE 2 | Endoscopic intraoperative views **(E)** showing the anterior layers of the membranes. First is the incised two layers of dura matter (Dm), followed by the pituitary capsule (Pc) and the normal compressed pituitary gland (on the right side). The inner layer is the pseudocapsule (Ps) and the debulking adenoma (T). After the resection, the ballooned diaphragm sellae descended into the sella **(F)**, and it was obstructed to find the posterior fractured pseudocapsule and the remnant adenoma. The micro retractor was used to elevate the descending diaphragm **(G)**. When the vision-blocking diaphragm was pushed up, the posterior fractured pseudocapsule and the remnant adenoma were removed bimanually **(H)**. Pathologic Masson staining **(I)** of this finally removed pseudocapsule and the adenoma. Partial enlarged drawing showed that the pseudocapsule (black arrow) was surrounded around by the adenoma (white arrow).

descended into the surgical view and obstructed the posterior and lateral views. We used a micro retractor (Budde Halo self retaning retractor system, Integra Inc.) which was used to retract the artery during the skull base craniotomy operation to elevate the redundant diaphragm and the gland. The width of the retractor was 2 mm, length was 12 cm, and the end was attached to an automatic retractor (Leyla brain retractor system, Aesculap). This micro retractor was placed at the 12 o'clock position on the nostril to reduce the instrument conflict in the sphenoid sinus (**Figure 3**). When the retractor was in place, a distinct surgical plane between the adenoma and the compressed gland or the redundant diaphragm was visible, and a bimanual microdissection surgical technique was used for a posterior piecemeal pseudocapsule resection could be used for the operator. Multilayer skull base reconstruction was used for the closure.

DISCUSSION

The use of the histological pseudocapsule to act as a surgical plane to complete the *en bloc* extracapsular resection is the ideal model in

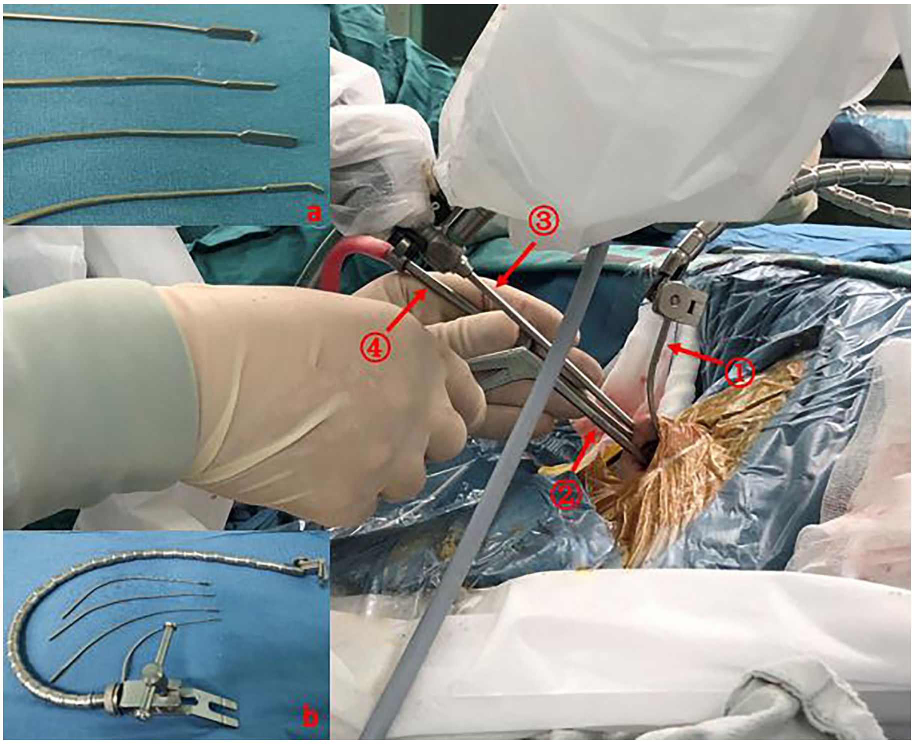

FIGURE 3 | The location of the micro retractor and the other instruments during the endoscopic endonasal approach. The micro retractor (with a self-retaining arm) and the endoscope (with a pneumatic holder) were fixed at the 12 o'clock position on the nostrils. The other instruments could be manipulated bimanually free under the corridor. **(A)** Different lengths and widths of the micro retractor with or without serrated blades. **(B)** The blades were connected with a Leyla flexible self-retaining arm. ①: Micro retractor; ②: Bayonet forceps; ③: Endoscope; ④: Suction.

pituitary surgery (6). For some pituitary adenomas, this method is feasible. The pseudocapsule consists of several compressed layers of acini and reticulin, which is a type of connective tissue that provides sufficient strength for dissection. As shown in a previous report, the thickness of this membrane can be 0.5–1 mm (7). However, for the majority of adenomas, the *en bloc* resection is difficult. In our opinion, the concept is more important than the surgical skills. The use of the pseudocapsule dissection concept during macroadenoma resection can aid in the performance of pseudocapsule dissection even though the tumor can only be resected in a piecemeal fashion. In terms of macroadenomas, it is easy to perform a pseudocapsule dissection of the anterior and anterior-lateral sides of the tumor when the anatomical layering of the membranes is mastered: the two layers of dura mater, the pituitary capsule, and the pseudocapsule. However, when debulking is performed, further posterior and superior extrapseudocapsular dissection may be difficult because of the early descent of the redundant diaphragm and the compressed gland.

Although the endoscopic approach provides an excellent illumination, high magnification, and a panoramic view of the surgical area, it only provides the possibility of discerning the pseudocapsule; when the redundant diaphragm descends, this possibility disappears. Another "hand" is expected to hold the herniation of the diaphragm. A common approach is to use an aspirator and a small cottonoid to elevate the diaphragm. Additionally, Q-tips (8) or self-retaining retractors (5) have also been reported to solve the herniation problem. However, these techniques are still associated with the problems of a non-bimanual dissection or a limited working space.

The abovementioned micro retractor blade system has been used to move cerebral blood vessels or delicate neurological structures during cranial procedures (9). The micro retractor is part of the Budde Halo self-retaining retractor system (Integra Inc., USA). The optimum use for this retractor is to avail the surgeon of both hands for a bimanual procedure in the supraclinoid or cerebellopontine angle regions. In our opinion, this self-retaining retractor can also free the hands of the surgeon during the endoscopic endonasal approach. The flexible articulate arm can be placed in any direction to facilitate the procedures in the narrow sella region. Micro- and vimineous blades can hold the diaphragm to facilitate a bimanual posterior pseudocapsule margin dissection. When the retractor blade is fixed in the 12 o'clock position on the nostril, the lower working space and surgical freedom are never affected. This retractor blade can be recombined with the Leyla brain retractor, which can be attached to the operating bed. This recombination reduces the obstruction of the arch of the Budde Halo system and avoids the connection of the head clamp (10).

The reason why the posterior pseudocapsule surgical plane is hard to expose is partly because of the obstruction of the macrovolume of the adenoma and is partly due to the early descent of the redundant diaphragm and the compressed gland. The debulking procedure and the micro retractor system can solve this difficulty. After anterior and lateral pseudocapsule dissection, even when the pseudocapsule is fractured, the remnant posterior and superior planes of the pseudocapsule can be clearly exposed to avoid blind curettage and remnant tumors.

CONCLUSION

This micro retractor can increase the view of the posterior margin of the adenomas to facilitate the pseudocapsule dissection. Increasing the clinical use of this micro retractor is expected during the endoscopic endonasal surgery when a "third hand" is needed.

DATA AVAILABILITY STATEMENT

The original contributions presented in the study are included in the article/supplementary material. Further inquiries can be directed to the corresponding author.

AUTHOR CONTRIBUTIONS

All authors contributed to the article and approved the submitted version.

FUNDING

Foundation of Science and Technology Commission of Shanghai Municipality (21ZR1413100).

REFERENCES

1. Paluzzi A, Fernandez-Miranda JC, Tonya Stefko S, Challinor S, Snyderman CH, Gardner PA. Endoscopic Endonasal Approach for Pituitary Adenomas: A Series of 555 Patients. *Pituitary* (2014) 17(4):307–19. doi: 10.1007/s11102-013-0502-4
2. Costello RT. Subclinical Adenoma of the Pituitary Gland. *Am J Pathol* (1936) 12:205–16.
3. Xie T, Liu T, Zhang X, Chen LL, Luo RK, Sun W, et al. Time to Revive the Value of the Pseudocapsule in Endoscopic Endonasal Transsphenoidal Surgery for Growth Hormone Adenomas. *World Neurosurg* (2016) 89:65–71. doi: 10.1016/j.wneu.2016.01.036
4. Taylor DG, Jane JA, Oldfield EH. Resection of Pituitary Macroadenomas *via* the Pseudocapsule Along the Posterior Tumor Margin: A Cohort Study and Technical Note. *J Neurosurg* (2018) 128(2):422–8. doi: 10.3171/2017.7.JNS171658
5. Kutlay M, Gönül E, Düz B, Yusuf I, Ozkan T, Cağlar T, et al. The Use of a Simple Self-Retaining Retractor in the Endoscopic Endonasal Transsphenoidal Approach to the Pituitary Macroadenomas: Technical Note. *Neurosurgery* (2013) 73(2 Suppl Operative):206–9. doi: 10.1227/01.neu.0000430292.39046.10
6. Oldfield EH, Vortmeyer AO. Development of a Histological Pseudocapsule and Its Use as a Surgical Capsule in the Excision of Pituitary Tumors. *J Neurosurg* (2006) 104(1):7–19. doi: 10.3171/jns.2006.104.1.7
7. Lee EJ, Ahn JY, Noh T, Se Hun K, Tai Seung K, Sun Ho K, et al. Tumor Tissue Identification in the Pseudocapsule of Pituitary Adenoma: Should the Pseudocapsule be Removed for Total Resection of Pituitary Adenoma? *J Neurosurg* (2009) 64(3 Suppl):62–9. doi: 10.1227/01.NEU.0000330406.73157.49
8. Prevedello DM, Kassam AB, Gardner P, Zanation A, Snyderman CH, Carrau RL. "Q-Tip" Retractor in Endoscopic Cranial Base Surgery. *Neurosurgery* (2010) 66(2):363–6. doi: 10.1227/01.NEU.0000363703.05995.B8
9. Youssef AS, van Loveren HR. Microvascular Retractor: A New Concept of Retracting and Repositioning Cerebral Blood Vessels. *Neurosurgery* (2005) 57 (1):199–202. doi: 10.1227/01.NEU.0000164457.86335.A3
10. Assina R, Rubino S, Sarris CE, Gandhi CD, Prestigiacomo CJ. The History of Brain Retractors Throughout the Development of Neurological Surgery. *Neurosurg Focus* (2014) 36(4):E8.1–12. doi: 10.3171/2014.2.FOCUS13564

Conflict of Interest: The authors declare that the research was conducted in the absence of any commercial or financial relationships that could be construed as a potential conflict of interest.

The handling editor declared a shared affiliation with the authors at time of review.

frontiers in Oncology

ORIGINAL RESEARCH
published: 22 September 2021
doi: 10.3389/fonc.2021.724972

Endoscopic Endonasal Surgical Strategy for Skull Base Chordomas Based on Tumor Growth Directions: Surgical Outcomes of 167 Patients During 3 Years

Jiwei Bai[1,2†], Mingxuan Li[2†], Yujia Xiong[2], Yutao Shen[2], Chunhui Liu[1], Peng Zhao[1], Lei Cao[1], Songbai Gui[1], Chuzhong Li[2] and Yazhuo Zhang[1,2,3,4,5*]*

[1] Department of Neurosurgery, Beijing Tiantan Hospital, Capital Medical University, Beijing, China, [2] Beijing Neurosurgical Institute, Capital Medical University, Beijing, China, [3] Beijing Institute for Brain Disorders Brain Tumor Center, Beijing, China, [4] China National Clinical Research Center for Neurological Diseases, Beijing, China, [5] Key Laboratory of Central Nervous System Injury Research, Capital Medical University, Beijing, China

OPEN ACCESS

Edited by:
Xicai Sun,
Fudan University, China

Reviewed by:
Peizhi Zhou,
Sichuan University, China
Tomasz Dziedzic,
Medical University of Warsaw, Poland
Emrah Celtikci,
Gazi University, Turkey

***Correspondence:**
Yazhuo Zhang
zyz2004520@yeah.net
Chuzhong Li
lichuzhong@163.com

†These authors have contributed equally to this work

Specialty section:
This article was submitted to Surgical Oncology, a section of the journal Frontiers in Oncology

Received: *14 June 2021*
Accepted: *02 September 2021*
Published: *22 September 2021*

Citation:
Bai J, Li M, Xiong Y, Shen Y, Liu C, Zhao P, Cao L, Gui S, Li C and Zhang Y (2021) Endoscopic Endonasal Surgical Strategy for Skull Base Chordomas Based on Tumor Growth Directions: Surgical Outcomes of 167 Patients During 3 Years. Front. Oncol. 11:724972. doi: 10.3389/fonc.2021.724972

Background: Skull base chordomas (SBCs) are rare malignant bone tumors with dismal long-term local control. Endoscopic endonasal surgeries (EESs) are increasingly adopted to resect SBCs recently. Gross total resection (GTR) favors good outcomes. However, the SBCs often invade the skull base extensively and hide behind vital neurovascular structures; the tumors were challenging to remove entirely. To improve the GTR, we established a surgical strategy for EES according to the tumor growth directions.

Methods: A total of 112 patients with SBCs from 2018 to 2019 were classified into the derivation group. We retrospectively analyzed their radiologic images and operation videos to find the accurate tumor locations. By doing so, we confirmed the tumor growth directions and established a surgical strategy. Fifty-five patients who were operated on in 2020 were regarded as the validation group, and we performed their operations following the surgical strategy to verify its value.

Results: In the derivation group, 78.6% of SBCs invade the dorsum sellae and posterior clinoid process region. 62.5% and 69.6% of tumors extend to the left and right posterior spaces of cavernous ICA, respectively. 59.8% and 61.6% of tumors extend to the left and right posterior spaces of paraclival and lacerum ICA (pc-la ICA), respectively. 30.4% and 28.6% of tumors extended along the left and right petroclival fissures that extend toward the jugular foramen, respectively. 30.4% of tumors involved the foramen magnum and craniocervical junction region. The GTR was achieved in 60.8% of patients with primary SBCs in the derivation group. Based on the tumors' growth pattern, pituitary transposition and posterior clinoidectomy techniques were adopted to resect tumors that hid behind cavernous ICA. Paraclival ICA transposition was used when the tumor invaded the posterior spaces of pc-la ICA. Lacerum fibrocartilage resection and eustachian tube transposition may be warranted to resect the tumors that extended to the jugular foramen. GTR was achieved in 75.0% of patients with primary SBCs in the validation group.

Conclusion: Besides the midline clival region, the SBCs frequently grow into the eight spaces mentioned above. The surgical strategy based on the growth pattern contributes to increasing the GTR rate.

Keywords: endoscopic, endonasal, skull base, chordoma, treatment

INTRODUCTION

Skull base chordomas (SBCs) are traditionally considered to be histologically low-grade bony neoplasms. Although proliferation index ki-67 is low in most chordoma tissues except for poorly differentiated chordomas and dedifferentiated chordomas (1–3), SBCs show robust proliferation and invasive local growth capabilities. Furthermore, it was believed to be chemoresistant and resistant to traditional low-dose radiotherapy. The recurrence rate was high because of the unsatisfied resection rate and no effective adjuvant therapy available. Many advances have been achieved in medical treatment in recent years, and some drugs have shown effectiveness, but the overall response rate is still low in SBCs. Long-term survival and favorable neurological outcome continue to be challenging. The best available evidence supports a more aggressive surgical resection with negative microscopic margins; this radical resection correlates with improved local control and improved survival (4, 5). Although the resection rate seems improved with new equipment and endoscopic endonasal surgery (EES), the radical resection rate was still challenging for SBCs. Chordomas arising from the clivus are among the most challenging neoplasms for skull base surgeons (6). By summing up our recent surgical results and referring to previous literature, we established the surgical strategy that improved our resection rate lately.

MATERIALS AND METHODS

Patients

This study includes all consecutive patients with SBCs between January 2018 and December 2020. They were treated by our single neuro-endoscopic group (which is directed by senior surgeons Y Zhang and S Gui). Pathologists confirmed the final diagnosis. All these patients underwent at least one EES in our ward. These patients were divided into two groups: the derivation group that includes the patients treated between January 2018 and December 2019 and the validation group that consists of the other patients treated in 2020. Our institutional review board approved this study. All patients signed informed consents before surgeries. We performed the final follow-up on May 2021 through WeChat or phone.

Tumor Locations and Surgical Strategy

J Bai, M Li, C Li, and Y Zhang retrospectively analyzed the pre- and postoperative images of patients in the derivation group. For patients in the validation group, all neurosurgeons examined the locations of the tumors during preoperative discussions, formulated surgical strategies, and judged the degree of resection during postoperative meetings. All patients were checked with CT on the same evening after surgery; unless the patient has serious complications or cannot safely perform MRI, the patients were usually scanned with MRI within 48 h. The degree of tumor resection is judged according to postoperative MR and CT images combined with surgical video, which includes gross-total resection (GTR), near-total resection (NTR), and partial resection (PR). GTR was defined as no residual soft tumor tissue during the operative inspection, and the surrounding bone was drilled to the normal-appearing bony structure, and no residual tumor was observed on postoperative images. No suspicious tumor was found during operation, and >90% tumoral resection on images was defined as NTR; <90% tumoral resection on images was defined as PR. Combined with literature reports on the location of chordoma (2, 6, 7), endoscopic anatomy (8), and our group's experience in the EES treatment of chordoma (9), we found that chordoma has the characteristics of extending along the skull base sutures (**Figure 1**). Besides the central part of chordoma often located in the midline region of the clivus, the most commonly involved areas include the following eight spaces: dorsum sellae and posterior clinoid process (DS-PCP), bilateral posterior spaces of cavernous ICA (cICA), bilateral posterior spaces of paraclival and lacerum ICA (pc-la ICA), bilateral petroclival fissure spaces that extend toward the medial part of the jugular foramen, and foramen magnum and craniocervical junction (FM-CCJ). When retrospectively reviewing the images of the derivation group, we analyzed the distribution of chordomas in these eight spaces and confirmed the characteristics of chordoma extension along the sutures. A surgical strategy was formed; that is, the tumors in these eight areas were sequentially explored and removed during the operation. By analysis of surgical video and postoperative images, we evaluated our surgical strategy in the validation group.

Most SBCs can be resected through EES, and a few SBCs that extend beyond the inferior limit of EES need to be exposed by the combined endoscopic endonasal and transoral surgery. A vascularized nasal septal flap was prepared if possible, and then a standard sphenoidotomy was performed. We emphasize sufficient and safe tumor exposure, followed by exploring the eight aforementioned spaces according to the tumor growth directions. See below for the detailed descriptions. We mainly perform EES using the binostril four-hand technique, and three surgeons' five-hand technique may be used when necessary. The

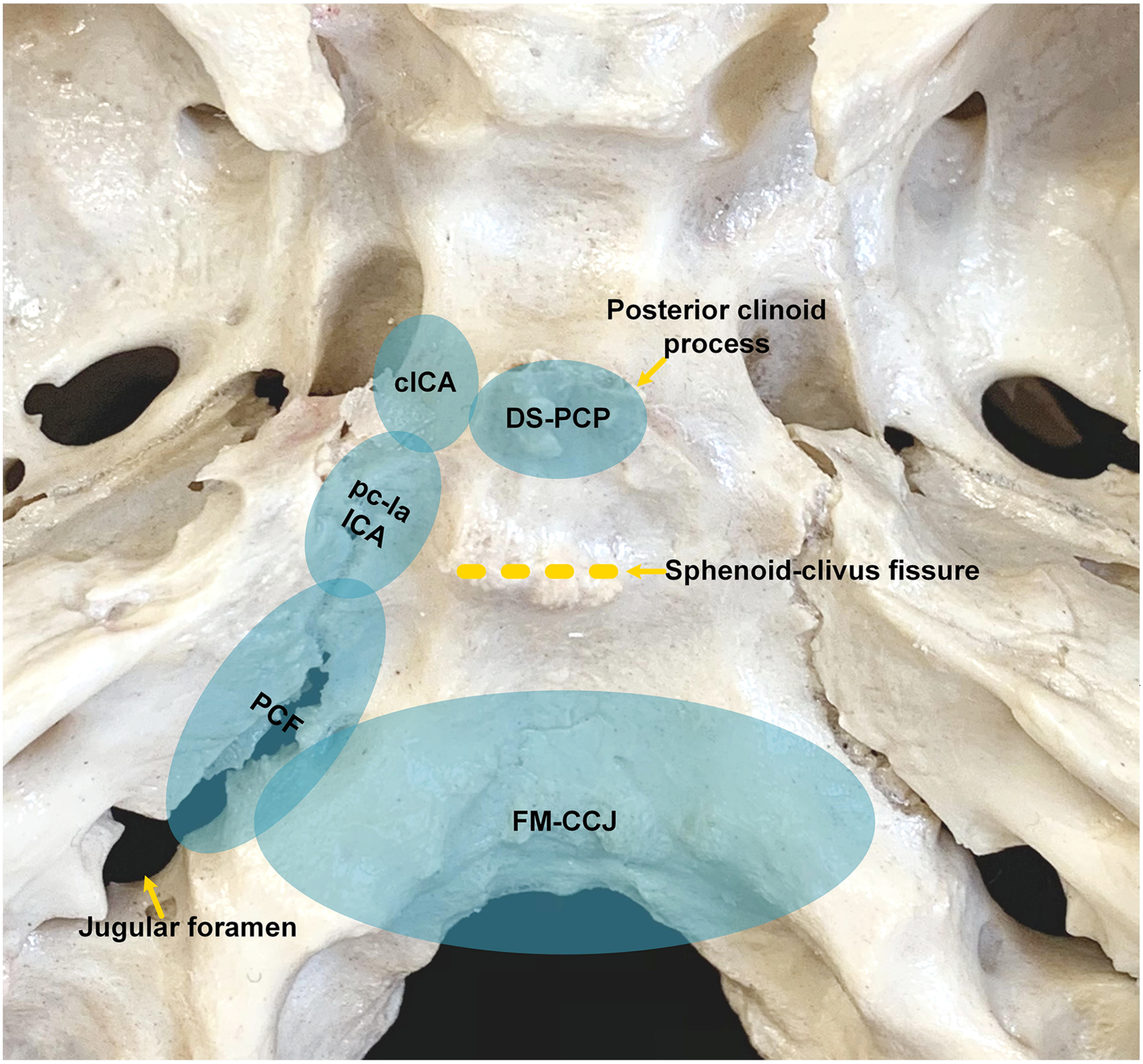

FIGURE 1 | Anatomic spaces that skull base chordomas frequently invade. cICA, cavernous internal carotid artery; DS-PCP, dorsum sellae and posterior clinoid process; FM-CCJ, foramen magnum and craniocervical junction; PCF, petroclival fissure; pc-la ICA, paraclival and lacerum ICA.

surrounding bony structure, which was suspected to be eroded by the tumor, should be drilled to a healthy margin in a maximal safe manner.

Chordomas in Dorsum Sellae and Posterior Clinoid Process

The bone of the sellar floor, middle clivus, and cavernous sinus were drilled. For small DS-PCP, the pituitary gland was elevated extradurally; then, dorsum sellae was split into two pieces in its middle part. After that, DS-PCPs were removed (**Figure 2**). When DS-PCP is large or adheres tightly with the dura mater, or the tumor invades into the intradural space and grows into the retro-infundibular region or inter-peduncular cistern, the interdural approach (10) is beneficial to resect DS-PCP and expose chordoma extensively.

Chordomas in Posterior Spaces of Cavernous ICA

For certain chordoma, the extradural maneuver is sufficient to remove the small part hiding behind the cICA. When the chordoma extends even more laterally, and the extradural procedure is not adequate to visualize the tumor, we use the interdural pituitary transposition technique to access the posterior space of cICA (10). An angled endoscope (30° and 45°) and angled instruments are helpful for better visualization

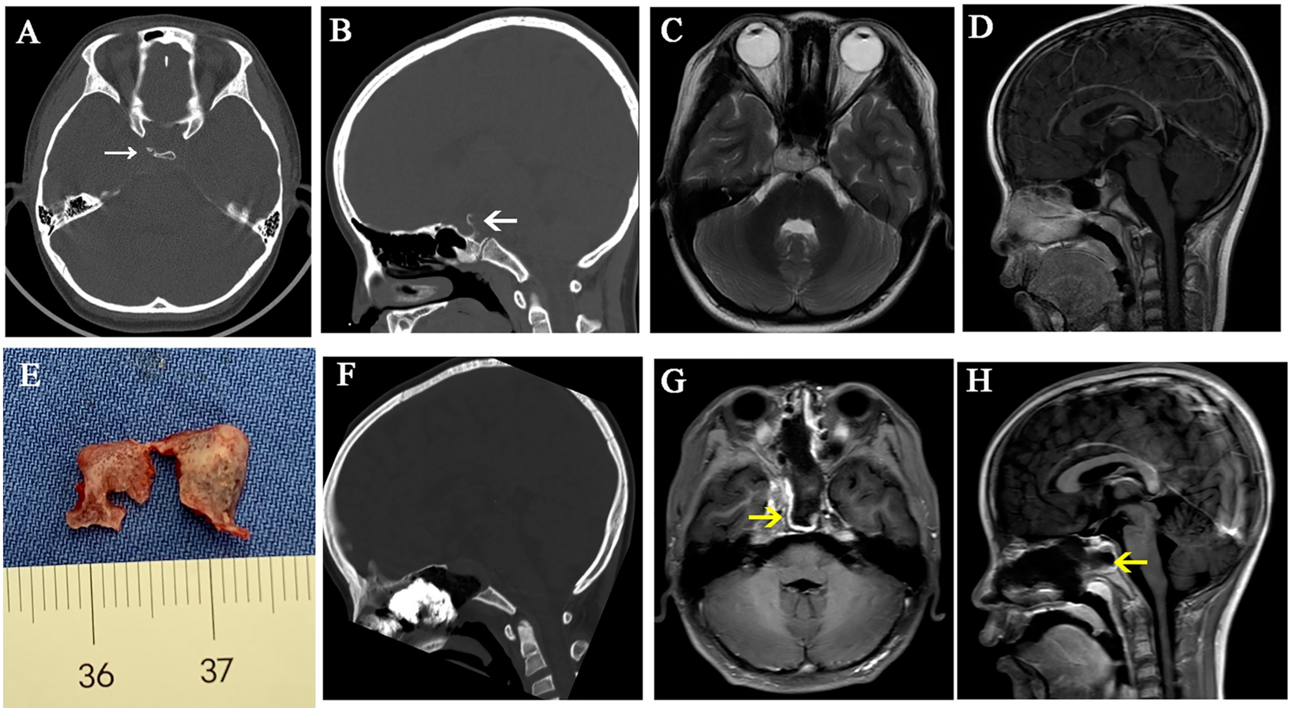

FIGURE 2 | A case illustrates dorsum sellae and posterior clinoid process resection. **(A–D)** Preoperative CT and MR images show that the tumor is located in the upper and mid-clivus and erodes the dorsum sellae and posterior clinoid processes. **(E)** The dorsum sellae was split into two pieces and taken out with posterior clinoid processes. **(F–H)** Postoperative CT and MR images show that the dorsum sellae and posterior clinoid processes were removed. The white arrows represent the eroded dorsum sellae and posterior clinoid processes. The yellow arrows represent the vascularized nasal septal flap.

and maneuver. After tumor resection, the posterior wall of the cavernous sinus and superior-medial part of the petrous apex is visualized (**Figure 3**).

Chordomas in Posterior Spaces of Paraclival and Lacerum ICA

Suppose the tumor is soft and the lateral extension is not much. In that case, it can be resected with the angled endoscope and the angled instruments without drilling the bone covering the paraclival ICA. When the tumors extend more laterally, lateralization of the paraclival ICA is necessary to expose chordomas in posterior spaces of paraclival ICA. The medial and front bone covering paraclival ICA is drilled. Next, paraclival ICA transposition is made, and the bone posterior to ICA is drilled (**Figure 3**) (11). To mobilize the paraclival ICA more laterally, we can thoroughly drill the bone surrounding the lacerum ICA, including the lingual process.

Chordomas in Foramen Magnum and Craniocervical Junction Space and Petroclival Fissure

The FM-CCJ space belongs to the lower clivus. We use a similar strategy to deal with tumors in petroclival fissure spaces, which often extend toward the medial part of the jugular foramen. When the chordoma locates in the midline area of the lower clivus, and the tumor volume is small, the tumor can be accessed by the inverted U-shaped rhinopharyngeal mucosal flap. The rhinopharyngeal mucosa and the basipharyngeal fascia, as well as longus capitis muscle and rectus capitis muscle, are inferiorly mobilized. Thus, the entire inferior clivus can be accessed, including the pharyngeal tubercle, anterior border of the foramen magnum, the anterior ring of C1, and the craniocervical junction (12). If the hard palate is high and hampers the caudal surgical corridor, the rear of the hard palate may be drilled to increase the nasopalatine angle and the caudal exposure. Generally, EES can reach the cervical spine of the C2 level. When the chordomas extend more inferiorly, a combined transoral approach or pure transoral approach may be performed. When the chordomas grow along the petroclival fissure significantly and extend toward jugular foramen, inferior turbinate, pterygoid process, eustachian tube, and parapharyngeal muscles may limit the tumor exposure laterally. In this circumstance, a prelacrimal recess approach is performed firstly (13), then lateral nasal wall flap is elevated and displaced into maxillary sinus; sequentially, pterygoid base and pterygoid plates are drilled, and the fibrocartilage around lacerum ICA and the eustachian tube are cut. By doing so, petrous ICA can be well exposed, and a more lateral view to the jugular foramen is achieved (**Figure 4**) (11).

Skull Base Reconstruction

A vascularized nasoseptal flap is extremely useful for skull base reconstruction in patients with primary chordoma. The nasoseptal flap is big enough to reconstruct the defect in the upper and middle clivus. However, it is too small to cover the

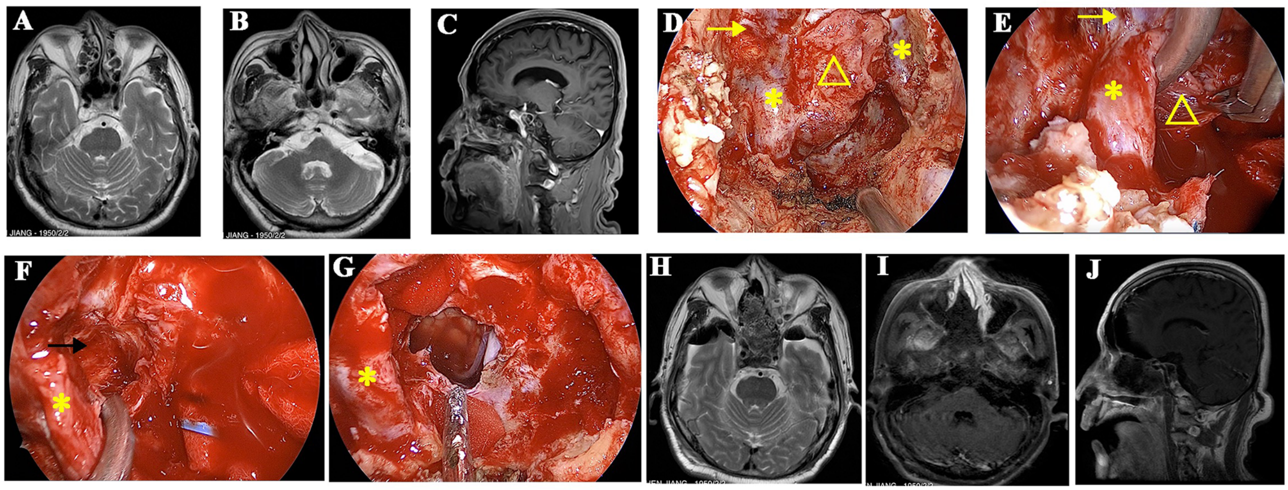

FIGURE 3 | A recurrent chordoma locates in the upper and mid-clivus. **(A, B)** The axial MR images show that the tumor locates in the right posterior space of cavernous ICA and the right posterior space of paraclival ICA, respectively. **(C)** The sagittal view shows that the tumor locates in the upper and mid-clivus and invades into the posterior space of paraclival ICA. **(D)** Intraoperative image shows that the bone covering the paraclival and lacerum ICA was drilled. **(E)** The paraclival ICA is gently retracted, and the tumor behind ICA was resected with the angled instruments under the view of 45° endoscopy. **(F)** The posterior space of cavernous ICA is seen after tumor resection, and the margin is clear. **(G)** The tumor is totally removed, and brain stem is visible. **(H–J)** Postoperative MR images showed that the tumor was totally removed. The yellow arrows represent cavernous ICA. The yellow triangles represent the recurrent chordoma. The yellow asterisks represent paraclival ICA. The black arrow represents the posterior space of the cavernous ICA.

more extensive defects in the lower clivus and the craniocervical junction. In this circumstance, an extended vascularized flap was harvested. Nasal floor mucoperiosteum was included in the vascularized flap. Intradural collagen was used as an inlay graft; then, autologous fat tissue was used as the second layer to eliminate dead space and avoid the ventral herniation of the brainstem through the dural defect (14). Then, autologous fascia lata covered onlay, followed by the extended vascularized nasoseptal flap and the inverted-U flap. For recurrent chordomas after EES, harvesting vascularized nasoseptal flap is difficult. Therefore, we will suture fat pad to dura mater using 6-0 prolene sutures with interrupted suture technique, which is an essential step for reconstruction. For the patient with radiotherapy history and refractory CSF leakage, the CSF leakage was successfully resolved with a vascularized temporalis muscle–fascia–periosteum flap. The temporalis muscle–fascia–periosteum flap was harvested through an open frontotemporal incision with its pedicle locating on the coronal process of the mandible. The flap includes the temporalis muscle, the temporalis fascia, and the periosteum between the supratemporal line and the skin incision. Then, the temporalis muscle–fascia–periosteum flap was displaced through the maxillary sinus to cover the defect (**Figure 5**).

Statistics

SPSS software (version 19.0, IBM Inc.) was used for the statistical analysis. Student's *t*-test was used for continuous variables (shown as mean ± SD); chi-square test or Mann–Whitney *U* test was applied for categorical variables (presented as number, %). All tests were two-sided, and $p < 0.05$ was regarded as statistically significant.

RESULTS

Patient Characteristics

During the study period, 170 patients received 197 operations, namely, 100 males and 70 females. Two patients underwent staged surgery; among them, one patient had EEA first, followed by far lateral approach craniotomy, and the other had two EEAs. This study only included their first operation information in our institute for further analysis. Three patients who received craniotomy were excluded from the current study. Since some chordomas in the craniocervical junction and upper cervical segment require a combination of transoral approach (three patients), which have similar treatment strategies to the transnasal approach, these patients were also included in this study. Therefore, 167 patients with chordoma were eventually included in the study, with 112 patients in the derivation and 55 patients in the validation group (**Figure 6**).

The age of the entire cohort was 43.12 ± 17.53 years (mean ± SD), and there was no difference in age distribution between the derivation group and the validation group (43.03 ± 17.20 *versus* 43.31 ± 18.34 years, $p = 0.922$). Ninety-nine (59.3%) males and 68 (40.7%) males were included, and no difference in gender was observed between the two groups (male/female, 68/44 *versus* 31/24, $p = 0.591$). The derivation group included 51 (45.5%) primary patients and 61 (54.5%) recurrent patients, and the validation group included 24 (43.6%) primary patients and 31 (56.4%) recurrent patients ($p = 0.817$) (**Table 1**).

Diplopia caused by VI cranial nerve palsy [76 (45.5%) patients], which exhibits double vision increasing when looking lateral, was the most common clinical symptom, followed by headache/neck

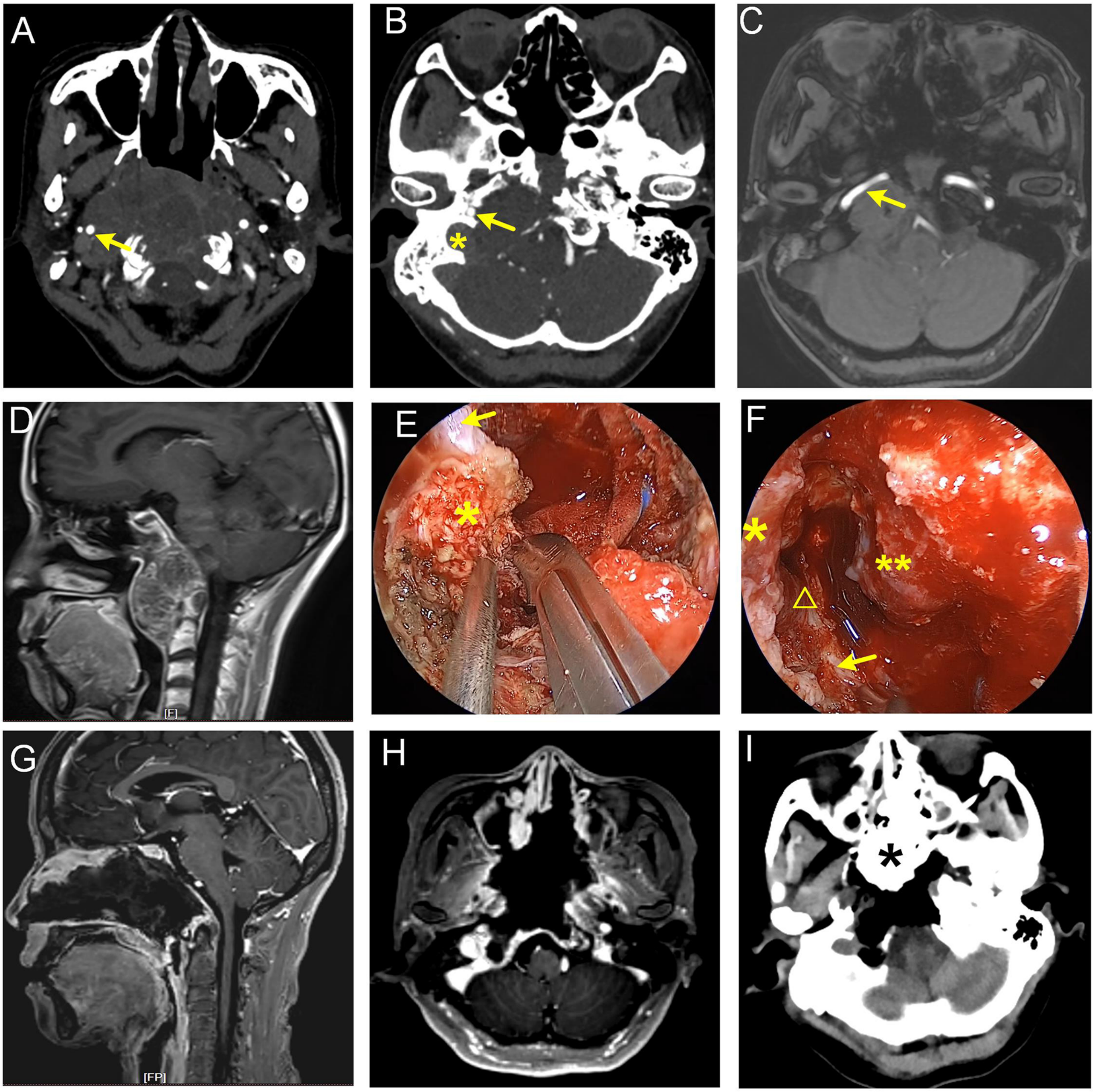

FIGURE 4 | Giant recurrent chordoma involving petroclival fissure, jugular foramen, and craniocervical junction. **(A–D)** Preoperative images show that the tumor grew along the right petroclival fissure and destroyed petrous and clival bone. Parapharyngeal, petrous, lacerum, and paraclival ICA were involved. The arrow in **(A)** represents parapharyngeal ICA. Arrows in **(B, C)** represent petrous ICA, and the asterisk in **(B)** represents jugular foramen. **(E, F)** Intraoperative view. **(E)** Cut the hard scar and fibrocartilage following the course of the ICA with a sharp knife. The arrow denotes paraclival ICA. The asterisk indicates fibrocartilage tissue at lacerum. **(F)** Lacerum, petrous, and parapharyngeal ICA were exposed. Asterisk represents lacerum ICA, the triangle represents petrous ICA, the arrow represents parapharyngeal ICA, and the double-asterisk represents clival dura matter. **(G–I)** Postoperative images show that the tumor was near-totally removed. The asterisk in the panel I represents iodoform gauze.

pain [45 (26.9%) patients], visual impairment [38 (22.8%) patients], blepharoptosis [16 (9.6%) patients], and dysphagia [15 (9.0%) patients]. The symptom distribution of the derivation group and the validation group was similar (**Table 1**).

There were 37 (22.2%) patients with a history of preoperative radiotherapy, and no significant difference was identified between the two groups [23 (20.5%) patients *versus* 14 (25.5%) patients, $p = 0.472$]. As the availability of different types of

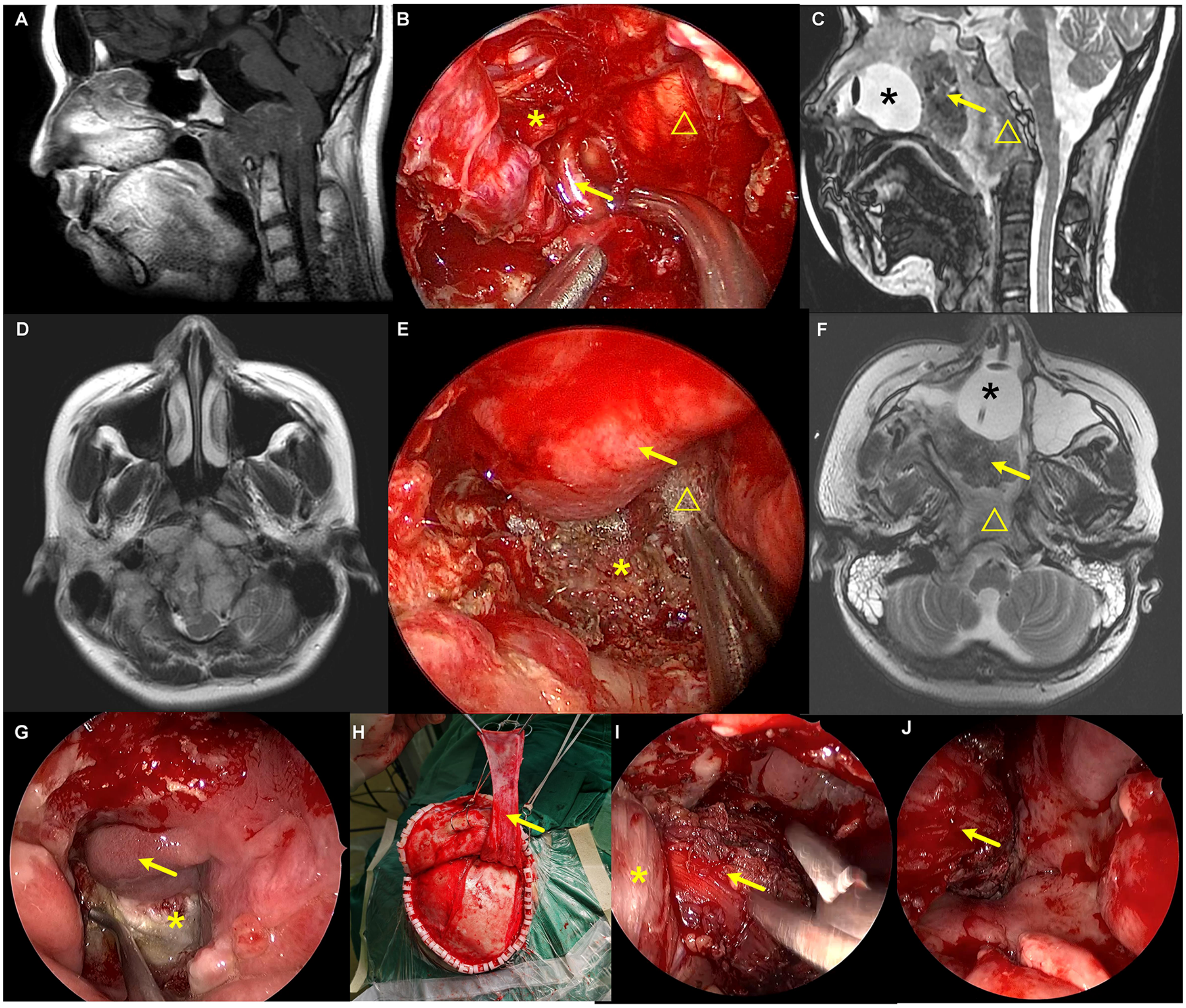

FIGURE 5 | The repair of a refractory CSF leakage in the lower clivus and craniocervical junction with temporalis muscle–fascia–periosteum flap. **(A, D)** Preoperative images showed that the tumor was located in the lower clivus and extended into the cervical spinal canal. The medulla oblongata was pushed by the tumor and severely deformed. **(B, E)** Intraoperative view of the tumor resection. **(B)** Arrow represents the right vertebral artery. Asterisk represents the vagus nerve. Triangle represents the medulla oblongata. **(E)** Skull base reconstruction with artificial dura mater, autologous fat tissue, fascia lata, and pedicled nasoseptal flap. Arrow represents the nasoseptal flap. Asterisk represents the tip of the odontoid. Triangle represents the fascia lata. **(C, F)** Postoperative images after the tumor resection and three CSF leakage repairing surgeries. Asterisk represents the balloon of the urethral catheter. Arrow represents the iodoform gauze. Triangle represents the temporalis muscle flap. **(G–J)** Repairing CSF leakage with pedicled vascularized temporalis muscle–fascia–periosteum flap after two failed repairing surgeries. **(G)** Arrow represents the pedicled nasoseptal flap. Asterisk represents the fascia lata used for skull base reconstruction in the tumor resection surgery, which was found to be necrosis. **(H–J)** Arrow represents the pedicled temporalis muscle–fascia–periosteum flap. Asterisk represents the lateral pterygoid muscle.

radiotherapy in different institutions and the high cost of particle radiation therapy, the patients received no uniform postoperative radiotherapy. Forty-nine (29.3%) patients received postoperative radiotherapy, including 11 cases with radiosurgery, 10 cases with intensity-modulated radiation therapy, and 25 cases with particle radiation therapy (proton beam therapy/carbon ion therapy). The rate of receiving postoperative radiotherapy was higher in the validation group (41.8%) compared to the derivation group (23.2%) (p = 0.013). In addition, proton beam therapy/carbon ion therapy accounted for the majority (16/23 patients) of the validation group (**Table 1**).

Tumor Locations and Involved Anatomical Spaces

According to the classification of upper, middle, and lower clival, the most common locations are the upper-middle clival region [77 (46.1%) patients; derivation group, 54 (48.2%) patients; validation group, 23 (41.8%) patients] and the whole clival

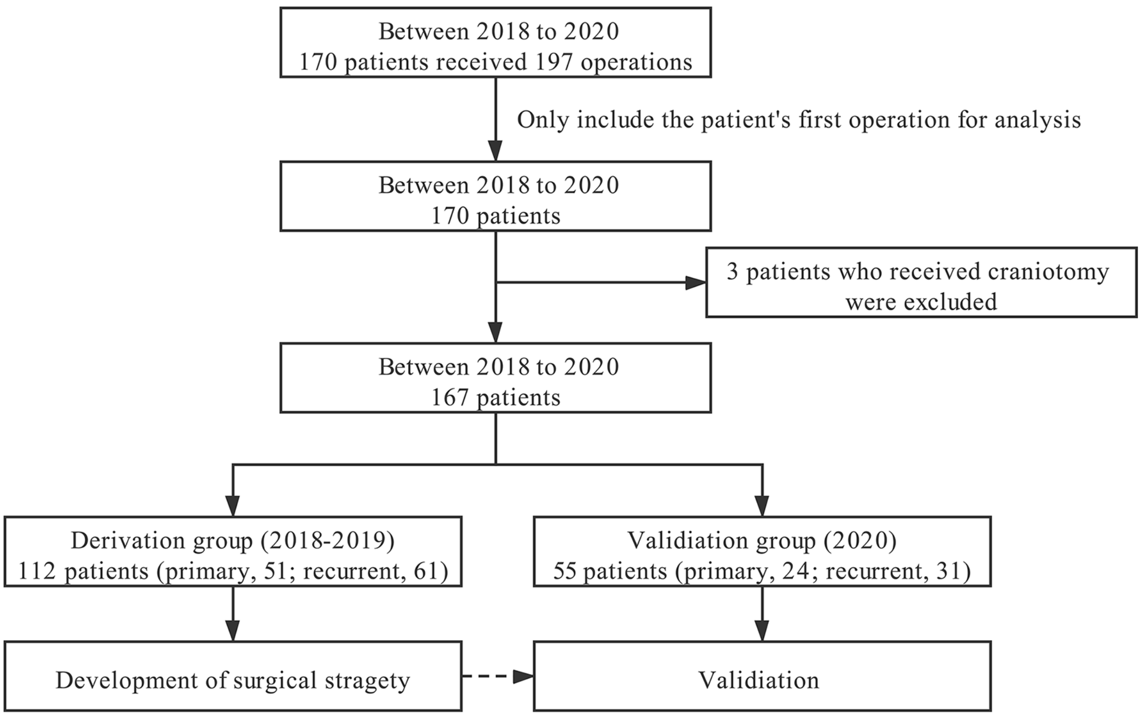

FIGURE 6 | Flowchart for patient selection.

TABLE 1 | Demographic and clinical characteristics of skull base chordoma patients.

Variables	**Number of patients (%)**			***p*-value**
	Total	**Derivation group**	**Validation group**	
Age (mean ± SD)	43.12 ± 17.53	43.03 ± 17.20	43.31 ± 18.34	0.922
Sex				0.591
Male	99 (59.3%)	68 (60.7%)	31 (56.4%)	
Female	68 (40.7%)	44 (39.3%)	24 (43.6%)	
Primary or recurrent tumor				0.817
Primary	75 (44.9%)	51 (45.5%)	24 (43.6%)	
Recurrent	92 (55.1%)	61 (54.5%)	31 (56.4%)	
Symptoms				
Diplopia	76 (45.5%)	57 (50.9%)	19 (34.5%)	
Headache/neck pain	45 (26.9%)	32 (28.6%)	13 (23.6%)	
Visual impairment	38 (22.8%)	29 (25.9%)	9 (16.4%)	
Blepharoptosis	16 (9.6%)	12 (10.7%)	4 (7.3%)	
Dysphagia	15 (9.0%)	9 (8.0%)	6 (10.9%)	
Nasal obstruction	13 (7.8%)	9 (8.0%)	4 (7.3%)	
Hearing loss	9 (5.4%)	5 (4.5%)	4 (7.3%)	
Limb weakness	8 (4.8%)	5 (4.5%)	3 (5.5%)	
Dizziness	7 (4.2%)	4 (3.6%)	3 (5.5%)	
Facial numbness	5 (3.0%)	2 (1.8%)	3 (5.5%)	
Accident	16 (9.6%)	9 (8.0%)	7 (12.7%)	
Preoperative radiotherapy	37 (22.2%)	23 (20.5%)	14 (25.5%)	0.472
Postoperative radiotherapy	49 (29.3%)	26 (23.2%)	23 (41.8%)	**0.013**
Radiosurgery	11	8	3	
IMRT	10	6	4	
Proton beam therapy/Carbon ion therapy	25	9	16	
Unclear	3	3	0	

IMRT, Intensity-modulated radiation therapy.
Bold values indicate p < 0.05.

region [52 (31.1%) patients; derivation group, 36 (32.1%) patients; validation group, 16 (29.1%) patients]. Twenty-five (15.0%) patients showed a tumor location of both cranio-vertebral joint and clival [derivation group, 15 (13.4%) patients; validation group, 10 (18.2%) patients]. There was no significant difference in the different segments of clivus between the two groups (p = 0.409) (**Table 2**).

DS-PCP [126 (75.4%) patients; derivation group, 88 (78.6%) patients; validation group, 38 (69.1%) patients; p = 0.181] was the most common involved anatomical area, followed by right cICA [117 (70.1%) patients; derivation group, 78 (69.6%) patients; validation group, 39 (70.9%) patients; p = 0.591] and left cICA [102 (61.1%) patients; derivation group, 70 (62.5%) patients; validation group, 32 (58.2%) patients; p = 0.867]. Left pc-la ICA and right pc-la ICA involvement were observed in 98 (58.7%) and 100 (59.9%) patients, respectively, and no distribution difference was identified between two groups (59.8% *versus* 56.4%, p = 0.670 and 61.6% *versus* 56.4%, p = 0.516). As for the petroclival fissure region, 50 (29.9%) patients had left petroclival fissure involvement [derivation group, 34 (30.4%) patients; validation group, 16 (29.1%) patients; p = 0.867], 51 (30.5%) patients had right petroclival fissure involvement [derivation group, 32 (28.6%) patients; validation group, 19 (34.5%) patients; p = 0.431], and 55 (32.9%) patients with tumors involved FM-CCJ, of which 34 (30.4%) patients were in the derivation group and 21 (38.2%) patients were in the validation group (p = 0.312) (**Table 2**). In summary, the involved anatomical area showed no difference between the two groups (all p > 0.05).

Extent of Resection

The most intriguing result of the current study was the extent of resection. As shown in **Table 3**, patients with GTR, NTR, and PR were 73 (43.7%), 66 (39.5%), and 28 (16.8%), respectively. Interestingly, we observed a higher degree of resection in the validation group than in the derivation group (p = 0.003). Specifically, the GTR rate was 58.2% in the validation group, while it was 36.6% in the derivation group.

Next, we stratified patients into the primary and recurrent cohorts for analysis. In the primary cohort, 18 (75.0%) patients received GTR in the validation group, which is higher than that in the derivation group (31, 60.8% patients), though the difference was not significant (p = 0.227). In the recurrent cohort, a significant difference was observed between the two groups (p = 0.001). The validation group showed a higher GTR rate and a lower PR rate than the derivation group (GTR rate, 45.2% *versus* 16.4%; PR rate, 9.7% *versus* 32.8%) (**Table 3**).

We also analyzed the extent of resection in patients with different tumor locations. Interestingly, we found a trend of higher resection rates in the validation group compared to those in the derivation group regardless of the tumor locations (**Table 4**). Of note, for the whole clival chordomas, a significant difference was observed; the GTR, NTR, and PR rates were 57.4%, 35.2%, and 7.4% in the derivation group, and 65.2%, 34.8%, and 0.0% in the validation group, respectively (p = 0.001). In addition, for chordomas in the craniovertebral joint and clivus, a higher resection rate was identified in the validation group than the derivation group (GTR rate, 30% *versus* 6.7%). However, the p-value (0.140) was not significant. It may arise due to the limited patients in each group (15 patients and 10 patients).

Complications

Twenty-two (13.2%) patients suffered from surgical complications in the current study (derivation group, 15 patients; validation group, 7 patients). The most common complications were cerebrospinal fluid leakage (9, 5.4% patients; among them, 4 patients with primary SBC and 5 patients with recurrent tumor), intracranial infection (5, 3.0% patients), and cranial nerve defect (5, 3.0% patients). In

TABLE 2 | The detailed tumor locations and involved anatomical spaces.

Variables	Number of patients (%)			p-value
	Total	Derivation group	Validation group	
Tumor locations				0.409
Upper clivus	0 (0.0%)	0 (0.0%)	0 (0.0%)	
Upper-middle clivus	77 (46.1%)	54 (48.2%)	23 (41.8%)	
Middle clivus	2 (1.2%)	0 (0.0%)	2 (3.6%)	
Middle-lower clivus	5 (3.0%)	3 (2.7%)	2 (3.6%)	
Whole clivus	52 (31.1%)	36 (32.1%)	16 (29.1%)	
Cranio-vertebral joint	5 (3.0%)	3 (2.7%)	2 (3.6%)	
Cranio-vertebral joint and clivus	25 (15.0%)	15 (13.4%)	10 (18.2%)	
Other location	1 (0.6%)	1 (0.9%)	0 (0.0%)	
Involved anatomical spaces				
DS-PCP	126 (75.4%)	88 (78.6%)	38 (69.1%)	0.181
Left cICA	102 (61.1%)	70 (62.5%)	32 (58.2%)	0.591
Right cICA	117 (70.1%)	78 (69.6%)	39 (70.9%)	0.867
Left pc-la ICA	98 (58.7%)	67 (59.8%)	31 (56.4%)	0.670
Right pc-la ICA	100 (59.9%)	69 (61.6%)	31 (56.4%)	0.516
Left PCF	50 (29.9%)	34 (30.4%)	16 (29.1%)	0.867
Right PCF	51 (30.5%)	32 (28.6%)	19 (34.5%)	0.431
FM-CCJ	55 (32.9%)	34 (30.4%)	21 (38.2%)	0.312

DS-PCP, dorsum sellae and posterior clinoid process; cICA, cavernous internal carotid artery; pc-la ICA, paraclival and lacerum internal carotid artery; PCF, petroclival fissure; FM-CCJ, foramen magnum and craniocervical junction.

TABLE 3 | Extent of resection in the derivation group and the validation group.

Extent of resection	Number of patients (%)			*p*-value
	Total	Derivation group	Validation group	
Whole cohort				**0.003**
GTR	73 (43.7%)	41 (36.6%)	32 (58.2%)	
NTR	66 (39.5%)	47 (42.0%)	19 (34.5%)	
PR	28 (16.8%)	24 (21.4%)	4 (7.3%)	
Primary cohort				0.227
GTR	49 (65.3%)	31 (60.8%)	18 (75.0%)	
NTR	21 (28.0%)	16 (31.4%)	5 (20.8%)	
PR	5 (6.7%)	4 (7.8%)	1 (4.2%)	
Recurrent cohort				**0.001**
GTR	24 (26.1%)	10 (16.4%)	14 (45.2%)	
NTR	45 (48.9%)	31 (50.8%)	14 (45.2%)	
PR	23 (25.0%)	20 (32.8%)	3 (9.7%)	

GTR, Gross total resection; NTR, Near-total resection; PR, Partial resection.
Bold values indicate p < 0.05.

TABLE 4 | Extent of resection of skull base chordoma in different locations between the two groups.

Extent of resection	Whole cohort (%)			Derivation group (%)			Validation group (%)			*p*-value
	GTR	NTR	PR	GTR	NTR	PR	GTR	NTR	PR	
Tumor locations										
Upper clivus	0	0	0	0	0	0	0	0	0	NA
Upper-middle clivus	46 (59.7%)	27 (35.1%)	4 (5.2%)	31 (57.4%)	19 (35.2%)	4 (7.4%)	15 (65.2%)	8 (34.8%)	0 (0.0%)	0.405
Middle clivus	2 (100.0%)	0 (0.0%)	0 (0.0%)	0	0	0	2 (100.0%)	0 (0.0%)	0 (0.0%)	NA
Middle-lower clivus	2 (40.0%)	3 (60.0%)	5 (0.0%)	1 (33.3%)	2 (66.7%)	0(0.0%)	1 (50.0%)	1 (50.0%)	0 (0.0%)	NA
Whole clivus	17 (32.7%)	26 (50.0%)	9 (17.3%)	7 (19.4%)	20 (55.6%)	9 (25.0%)	10 (62.5%)	6 (37.5%)	0 (0.0%)	**0.001**
Craniovertebral joint	2 (40.0%)	3 (60.0%)	0 (0.0%)	1 (33.3%)	2 (66.7%)	0(0.0%)	1 (50.0%)	1 (50.0%)	0 (0.0%)	NA
Craniovertebral joint and clivus	4 (16.0%)	7 (28.0%)	14 (56.0%)	1 (6.7%)	4 (26.7%)	10 (66.7%)	3 (30.0%)	3 (30.0%)	4 (40.0%)	0.140
Other location	0 (0.0%)	0 (0.0%)	1 (100.0%)	0 (0.0%)	0 (0.0%)	1(100.0%)	0	0	0	NA

GTR, Gross total resection; NTR, Near-total resection; PR, Partial resection; NA, not applicable.
Bold values indicate p < 0.05.

addition, respiratory dysfunction was observed in four (2.4%) patients, and two (1.2%) patients suffered from carotid artery injury. Of note, no significant difference in complication rate was observed between the discovery and validation groups (13.4% *versus* 12.7%, p = 0.905) (**Table 5**).

Follow-Up

One patient died due to surgical complications, and three patients were lost to follow-up. The dead patient has undergone three operations previously and RT and chemotherapy history. He underwent the fourth operation for debulking and died of brain extensive cerebral ischemia due to continuing low blood pressure during operation, related to the patient's poor base performance status. The remaining 163 patients (derivation group, 109 patients; validation group, 54 patients) were regularly followed up with a mean time of 18.7 months (derivation group, 23.7 months; validation group, 8.4 months) (range, 2–39 months). Seventy-five (46.0%) patients [derivation group, 65 (59.6%) patients; validation

TABLE 5 | Surgical complications in skull base chordoma patients.

Variables	Number of patients			*p*-value
	Total	Derivation group	Validation group	
Complications (%)	22 (13.2%)	15 (13.4%)	7 (12.7%)	0.905
Cerebrospinal fluid leakage	9 (5.4%)	5 (4.5%)	4 (7.3%)	
Intracranial infection	5 (3.0%)	4 (3.6%)	1 (1.8%)	
Cranial nerve defect	5 (3.0%)	3 (2.7%)	2 (3.6%)	
Respiratory dysfunction	4 (2.4%)	4 (3.6%)	0 (0.0%)	
Carotid artery injury	2 (1.2%)	2 (1.8%)	0 (0.0%)	
Hypopituitarism	2 (1.2%)	1 (0.9%)	1 (1.8%)	
Paralysis	1 (0.6%)	0 (0.0%)	1 (1.8%)	

group, 10 (18.5%) patients] suffered from tumor progression or recurrence and 25 (15.3%) patients [derivation group, 24 (22.0%) patients; validation group, 1 (1.9%) patients] died during the follow-up.

DISCUSSION

The incidence of SBCs is extremely low, and its mortality and recurrence rate remain high. Surgical treatment is the initial and indispensable treatment for SBCs. The resection quality is associated with the patients' long-term outcomes (15). However, to our knowledge, only limited studies with a relatively large patient number reported the surgical experience and outcomes (3, 7, 16–19). Given their ideal midline location and ventral to the skull base dura mater (2), SBCs are increasingly treated through EES with the development of neuroendoscopic instruments, surgical experience acquisition, and surgical technique advancement (20–23). During the present study, three patients underwent open surgeries in 2018 and 2019, and one patient experienced a staged craniotomy after EES in 2020. The EES contributes to a high tumor removal and symptom control rate, with low morbidity and high quality of life (2). In our opinion, further improvement of the surgical resection extent and safety is the focus of EES. However, the learning curve is remarkable in EES (2, 19). Previous studies (2, 7, 9) included the patients during a relatively long period; therefore, the learning curve significantly impacted tumor resection (20). Our group started EES in 1998 and has extensive SBC surgical experience (9). Only the SBC patients treated from 2018 to 2020 were included in the present study; hence, the impact of the learning curve was minimized. Furthermore, the adjuvant equipment (such as intraoperative Doppler, neuronavigation, and neuromonitoring) and materials for skull base reconstruction (such as collagen graft and iodoform gauze) did not change in the last 3 years and had no impact on the surgery. Therefore, the present study is suitable for exploring the relationship between surgical strategy and resection rate.

Several classifications of SBCs have been proposed to guide the operation or judge the prognosis. Based on open surgery experience and SBCs' extension patterns, Amelfty et al. proposed a surgical classification to clarify the best microsurgical approach (5). At the same time, EES was beginning to be used to resect SBC (24). However, EES has rapidly increased in SBC surgeries in recent years, and EES can access cervical 2 as the most inferior limit of dissection; the microsurgical classification cannot direct EES anymore. In 2014, Fernandez-Miranda et al. described the EES treating SBCs according to dividing clivus into three parts (i.e., upper clivus, mid-clivus, and lower clivus) (6).

Similarly, our group proposed a clinical classification for EES in SBCs in 2016 (9). The results suggested that EES may improve the resection degree and surgical efficacy of SBCs. The limitation of our previous classification is that it ignores the tumor-extending direction. In 2018, Sekhar et al. proposed a preoperative grading system that is helpful in predicting resection and outcome (18). The tumor site has the highest weight in the score. The more sites were involved, the score was higher, and the progression-free survival was shorter. Sekhar's grading system indicated that the growth pattern of chordoma plays a vital role in guiding surgery and judging prognosis. Most recently, Wang et al. proposed that the SBCs were classified into four types based on the analysis of 55 patients (25). This classification introduced a new line that connects the anterior part of the sellar floor with the intersection of the sphenoid floor plane and the dorsal margin of the clivus. Although Wang's classification was based on the tumor origin and growth pattern, the category does not use the anatomical sites that surgeons are familiar with, so it is impossible to direct surgical strategy accurately, which is its main disadvantage. Furthermore, it is difficult to classify tumors in patients with multiple recurrent tumors because their skull base structures are complex, and the affected scope is too broad (25). In the present study, we found that the tumors extend along the bone sutures after analyzing the images and surgeries of SBC patients in the derivation group. This feature was also hypothesized in the study of another craniotomy team (7). We further confirmed that the hypothesis is reasonable by analyzing the images and surgeries of SBC patients in the validation group. In addition, we designed and validated our surgical strategies based on the spaces of the SBCs' eight most common extending areas. These eight spaces have little anatomic variations, even in patients with multiple recurrent chordomas or extensive invasion chordomas.

Traditionally, EES is best used for midline lesions that lack significant lateral extension. We found that almost all SBCs are involved in at least one of the eight spaces mentioned above besides the main body of the tumors located in the midline region of the skull base. These eight spaces are difficult to access directly and are the most common spaces for residual tumors (25). Previously, we performed surgeries following the "tumor-based" resection strategy. Small residual tumors were sometimes found in the spaces mentioned above on the postoperative MRI, although all the tumors seemed to be removed during the operation. Benefiting from recognizing the potential extending directions of SBCs, we perform "tumor-based" and "anatomy-based" resection now, i.e., to explore the possible hidden tumors in the eight spaces after resection of the main tumor. Although we found no statistical difference between the derivation and validation groups in the GTR of primary SBCs, it showed an increasing trend. It may be limited by the small sample size of primary SBCs. Furthermore, it may correlate with the relatively apparent anatomy in primary SBCs, and the endoscopic surgical technique for primary SBCs resection in our group is mature. The operations of recurrent SBCs were challenging. The recurrent SBC's anatomy is complex, and the texture is more rigid. The tumor may be divided into multi-cavities by smooth fiber tissue membrane, resulting in the surgeon mistakenly regarding the membrane as the tumor margin. However, it is exciting that our new surgical strategy increased the GTR significantly in recurrent SBCs. In summary, our strategy is suitable for both primary SBCs and recurrent SBCs.

This strategy emphasizes using the corresponding EES technique according to the different spaces. The standard transnasal sphenoid approach was performed to expose the sphenoid sinus and middle clivus and explore the tumor according to the eight possible extending areas. SBCs are osteo-destructive tumors that erode the surrounding bony structures; therefore, bone margin removal is critical for radical resection (5, 7). It is necessary to visualize the bone margin directly with a 0° endoscope to drill the lateral bony tumors. However, the soft tumors may be removed with angled instruments in the view field of angled endoscopy. Every blind spot should be carefully reviewed after tumor resection to confirm no residue tumors.

EES provides adequate exposure to the clivus' upper, middle, and lower parts (22). The upper clivus is formed by the dorsum sellae and the posterior clinoid processes (6, 9). Wang's study showed that residual tumors were mainly in the cavernous sinus or the rear upper part of the dorsum sellae (25). In our experience, SBCs often erode the dorsum sellae and the posterior clinoid processes, and the resection rate can be improved by posterior clinoidectomy. When the dorsum sellae is small, the dorsum sellae and posterior clinoid processes can be removed extradurally by splitting the dorsum sellae into two pieces and separating them from the dura mater. The extradural approach is relatively safe because this technique does not maneuver the cavernous sinus; the pituitary gland can be superior elevated without a significant bleeding risk (26). When the dorsum sellae is large, or the adhesion between the dura mater and posterior clinoid processes is tight, the intradural pituitary transposition is an alternative for posterior clinoidectomy (21). However, this technique has the potential risk of damaging the pituitary gland. Therefore, we favor the interdural transcavernous approach to perform posterior clinoidectomies (10). Even for the SBCs that invade the retro-infundibular region and interpeduncular cistern, EES can safely remove it following the corridor after the dorsum sellar resection and posterior clinoidectomy.

The middle clivus extends vertically from the sellar floor to the floor of the sphenoid body, which is at the level of paraclival ICA and lacerum ICA (6, 9). In most cases, manipulation with angled instruments combined with angled endoscopy allows for the resection of the soft SBCs located behind the paraclival ICA. If the tumors extend more laterally, the pterygoid tubercle and lingual process should be drilled extensively, and then the paraclival can be moved laterally (27). With the eustachian tube resection, more lateralization of ICA can be achieved (28). The most medial aspect of the petrous apex also locates behind the ICA (6). SBCs often extend laterally and inferiorly toward the petrous apex and foramen lacerum, and a sublacerum approach is helpful for complete resection of the petrous apex tumor component (27). To expose more laterally, EES combined with the transmaxillary operation (Denker procedure or Caldwell-Luc procedure) is helpful to access the petrous apex (12). Recently, Patel et al. suggested that a contralateral transmaxillary corridor offers a more lateral trajectory with improved access to the petrous apex with decreased need for manipulation of the ICA (29). Therefore, it is possible to increase the GTR safely.

The lower clivus extends from the floor of the sphenoid body to the foramen magnum and is shorter but difficult to access (6, 9). The lower part of the petroclival fissure, the jugular foramen, and the foramen magnum were at the level of the lower clivus. The SBCs located in these spaces have the lowest GTR rate, whether with open surgery or EES (2, 19, 23). We can resect the SBCs located above the body of C2 by EES (30). While for the tumors extending to lower than C2, which is regarded as below the inferior limitation of EES, we will use EES combined with transoral approach or purely use the transoral method. At our initial EES stage, we performed the midline linear incision on the nasopharyngeal and pulled the mucous membranes and muscles laterally. However, the exposed field is small. It resulted in the meager GTR rate previously. After that stage, we excised the nasopharyngeal muscle-mucosal tissue, which improved the resection. However, the local infection and CSF leakage limited the GTR of SBCs. Recently, we use the inverted U-shaped rhinopharyngeal flap (31). We once hypothesized that the rhinopharyngeal flap would help improve the skull base reconstruction, just like the initial hypothesis of Champagne et al.; however, their recent retrospective analysis suggests that the rhinopharyngeal flap may not help to reduce CSF leakage (31). This result needs further prospective studies with a larger sample size, and we still use the rhinopharyngeal flap combined with pedicled nasal septal flap for skull base reconstruction. The larger inferior turbinate, eustachian tube, and pterygoid plates limit access to the tumors and the vital structure located lateral region (28). Drilling these bone structures and resecting the eustachian tube supply a more sideways view. However, the resection of the eustachian tube may cause hearing damage and otitis media with effusion, which may need to be dealt with by surgery. Recently, Labib et al. introduced that the surgical skill with the anterolateral mobilization of the eustachian tube provides excellent access to the ventral jugular foramen and infra-petrous region (32). This technique may minimize the complication caused by eustachian tube injury.

CSF leakage was one of the most common complications in EES surgery. In the present series, the tumors in the nine patients with CSF leakage invaded the subdural space, and the tumor volume was large, and five of them were recurrent tumors. Furthermore, two patients have RT history and underwent delayed CSF leakage. Hence, the reconstruction of the skull base is crucial for improving the quality of SBCs surgery, especially in patients with recurrent SBCs and RT history. ICA injury is the most urgent and dangerous complication in EES treatment of SBCs, related to the close relationship between tumors and ICA. Two patients in this series suffered from ICA injuries. These two patients both experienced surgical and RT history previously, and the tumor texture was hard. DSA and balloon occlusion test in patients with a high risk of ICA injury are helpful for preoperative evaluation, and endovascular treatment provides a pivotal safeguard for ICA injuries during EES (2, 33). Simply put, the complications are low in the current series, which may represent the safety of the surgical strategy and be associated with the fact that our group had experienced a long learning curve in EES. Furthermore, navigation, intraoperative Doppler, and intraoperative electrophysiology monitor have considerably improved surgical safety (12, 21).

The limitation of our study is that the follow-up is short and that we cannot deduce the correlation between the surgical resection and prognosis. However, previous studies have suggested that the quality of surgery is crucial for post-surgical outcomes (15, 23). To our knowledge, this study included the largest number of patients in a short period. However, the number of primary SBC patients was still not big enough to get a statistical difference between the derivation group and the validation group. We continue to use the strategy to resect SBC now, and it may lead to the finding of statistical difference with the increasing number of the primary SBCs. Another limitation is that we did not analyze the pathological and genomic features, and these characteristics are correlated with the recurrence (3, 16, 34). These characteristics may indicate the origin and growth direction of SBCs and may be associated with the degree of resection.

CONCLUSION

Our results support the concept that SBCs extend along the bone suture and often invade the eight spaces mentioned above (i.e., DS-PCP, bilateral posterior spaces of cICA, bilateral posterior spaces of pc-la ICA, bilateral petroclival fissure spaces that extend toward the medial part of the jugular foramen, and FM-CCJ). Based on this extending character, the surgical strategy introduced in the present study is to explore the hidden spaces sequentially using the EES techniques. This strategy potentially improves surgical resection and decreases residue. This strategy is applicable in both primary SBCs and recurrent SBCs.

DATA AVAILABILITY STATEMENT

The original contributions presented in the study are included in the article/supplementary material. Further inquiries can be directed to the corresponding authors.

ETHICS STATEMENT

The studies involving human participants were reviewed and approved by the Ethics Review board of Beijing Tiantan Hospital. Written informed consent to participate in this study was provided by the participants' legal guardian/next of kin.

AUTHOR CONTRIBUTIONS

JB, ML, CZL, and YZ designed the study. JB and ML wrote the manuscript and performed the analysis. YX, YS, CHL, PZ, LC, and SG contributed to data collection, manuscript discussion, figures, and tables. All authors contributed to the article and approved the submitted version.

FUNDING

This study was supported by the National Natural Science Foundation of China (81771489, 82071559, and 82072804).

ACKNOWLEDGMENTS

We are grateful for the support of all patients.

REFERENCES

1. Zhang S, Bai J, Li M, Zhai Y, Wang S, Liu Q, et al. Predictive Value of Transforming Growth Factor-Alpha and Ki-67 for the Prognosis of Skull Base Chordoma. *World Neurosurg* (2019) 129:e199–206. doi: 10.1016/j.wneu.2019.05.110
2. Zoli M, Milanese L, Bonfatti R, Faustini-Fustini M, Marucci G, Tallini G, et al. Clival Chordomas: Considerations After 16 Years of Endoscopic Endonasal Surgery. *J Neurosurg* (2018) 128(2):329–38. doi: 10.3171/2016.11.JNS162082
3. Zenonos GA, Fernandez-Miranda JC, Mukherjee D, Chang YF, Panayidou K, Snyderman CH, et al. Prospective Validation of a Molecular Prognostication Panel for Clival Chordoma. *J Neurosurg* (2018) 130(5):1528–37. doi: 10.3171/2018.3.JNS172321
4. Bongers MER, Dea N, Ames CP, Schwab JH. Surgical Strategies for Chordoma. *Neurosurg Clinics North Am* (2020) 31(2):251–61. doi: 10.1016/j.nec.2019.11.007
5. O a-M, LA B. Skull Base Chordomas: A Management Challenge. *J Neurosurg* (1997) 86(2):182–9. doi: 10.3171/jns.1997.86.2.0182
6. Fernandez-Miranda JC, Gardner PA, Snyderman CH, Devaney KO, Mendenhall WM, Suarez C, et al. Clival Chordomas: A Pathological, Surgical, and Radiotherapeutic Review. *Head Neck* (2014) 36(6):892–906. doi: 10.1002/hed.23415
7. Wang L, Wu Z, Tian K, Wang K, Li D, Ma J, et al. Clinical Features and Surgical Outcomes of Patients With Skull Base Chordoma: A Retrospective Analysis of 238 Patients. *J Neurosurg* (2017) 127(6):1257–67. doi: 10.3171/2016.9.JNS16559
8. Fernandez-Miranda JC, Zwagerman NT, Abhinav K, Lieber S, Wang EW, Snyderman CH, et al. Cavernous Sinus Compartments From the Endoscopic Endonasal Approach: Anatomical Considerations and Surgical Relevance to Adenoma Surgery. *J Neurosurg* (2018) 129(2):430–41. doi: 10.3171/2017.2.JNS162214
9. Gui S, Zong X, Wang X, Li C, Zhao P, Cao L, et al. Classification and Surgical Approaches for Transnasal Endoscopic Skull Base Chordoma Resection: A 6-Year Experience With 161 Cases. *Neurosurg Rev* (2016) 39(2):321–32; discussion 32-3. doi: 10.1007/s10143-015-0696-1
10. Fernandez-Miranda JC, Gardner PA, Rastelli MMJr., Peris-Celda M, Koutourousiou M, Peace D, et al. Endoscopic Endonasal Transcavernous Posterior Clinoidectomy With Interdural Pituitary Transposition. *J Neurosurg* (2014) 121(1):91–9. doi: 10.3171/2014.3.JNS131865
11. Scopel TF, Fernandez-Miranda JC, Pinheiro-Neto CD, Peris-Celda M, Paluzzi A, Gardner PA, et al. Petrous Apex Cholesterol Granulomas: Endonasal *Versus* Infracochlear Approach. *Laryngoscope* (2012) 122(4):751–61. doi: 10.1002/lary.22448
12. Vaz-Guimaraes F, Nakassa ACI, Gardner PA, Wang EW, Snyderman CH, Fernandez-Miranda JC. Endoscopic Endonasal Approach to the Ventral Jugular Foramen: Anatomical Basis, Technical Considerations, and Clinical Series. *Oper Neurosurg (Hagerstown)* (2017) 13(4):482–91. doi: 10.1093/ons/opx014
13. Bing ZH HD, Cui SJ, Huang Q, Wang CS. Intranasal Endoscopic Prelacrimal Recess Approach to Maxillary Sinus. *Chin Med J* (2013) 126(7):1276–80. doi: 10.3760/cma.j.issn.0366-6999.20121754
14. Koutourousiou M, Filho FV, Costacou T, Fernandez-Miranda JC, Wang EW, Snyderman CH, et al. Pontine Encephalocele and Abnormalities of the Posterior Fossa Following Transclival Endoscopic Endonasal Surgery. *J Neurosurg* (2014) 121(2):359–66. doi: 10.3171/2013.12.JNS13756
15. Stacchiotti S, Sommer J. Chordoma Global Consensus G. Building a Global Consensus Approach to Chordoma: A Position Paper From the Medical and Patient Community. *Lancet Oncol* (2015) 16(2):e71–83. doi: 10.1016/S1470-2045(14)71190-8

16. Zhai Y, Bai J, Li M, Wang S, Li C, Wei X, et al. A Nomogram to Predict the Progression-Free Survival of Clival Chordoma. *J Neurosurg* (2019) 1(aop):1–9. doi: 10.3171/2019.10.JNS192414
17. Cavallo LM, Mazzatenta D, d'Avella E, Catapano D, Fontanella MM, Locatelli D, et al. The Management of Clival Chordomas: An Italian Multicentric Study. *J Neurosurg* (2020) 135(1):93–102. doi: 10.3171/2020.5.JNS20925
18. Brito da Silva H, Straus D, Barber JK, Rostomily RC, Ferreira MJr., Sekhar LN. Cranial Chordoma: A New Preoperative Grading System. *Neurosurgery* (2018) 83(3):403–15. doi: 10.1093/neuros/nyx423
19. Koutourousiou M, Gardner PA, Tormenti MJ, Henry SL, Stefko ST, Kassam AB, et al. Endoscopic Endonasal Approach for Resection of Cranial Base Chordomas: Outcomes and Learning Curve. *Neurosurgery* (2012) 71(3):614–24. doi: 10.1227/NEU.0b013e31825ea3e0
20. Champagne PO, Passeri T, Jabre R, Bernat AL, Voormolen EH, Froelich S. Vertebrobasilar Artery Encasement by Skull Base Chordomas: Surgical Outcome and Management Strategies. *Oper Neurosurg (Hagerstown)* (2020) 19(4):375–83. doi: 10.1093/ons/opaa091
21. Kassam A, Snyderman CH, Mintz A, Gardner P, Carrau RL. Expanded Endonasal Approach: The Rostrocaudal Axis. Part II. Posterior Clinoids to the Foramen Magnum. *Neurosurg Focus* (2005) 19(1):E4. doi: 10.3171/foc.2005.19.1.5
22. Yumiko O, Tamura R, Takahashi S, Morimoto Y, Sato M, Horikoshi T, et al. A Comparative Study Between Traditional Microscopic Surgeries and Endoscopic Endonasal Surgery for Skull Base Chordomas. *World Neurosurg* (2020) 134:e1099–107. doi: 10.1016/j.wneu.2019.11.113
23. Sen C, Triana AI, Berglind N, Godbold J, Shrivastava RK. Clival Chordomas: Clinical Management, Results, and Complications in 71 Patients. *J Neurosurg* (2010) 113(5):1059–71. doi: 10.3171/2009.9.JNS08596
24. Jho HD, Carrau RL, McLaughlin MR, Somaza SC. Endoscopic Transsphenoidal Resection of a Large Chordoma in the Posterior Fossa. *Acta Neurochir* (1997) 139 (4):343–7; discussion 7-8. doi: 10.1007/BF01808831
25. Wang Q, Wang Y, Wang J, Wang Y. Clinical Classification of Clival Chordomas for Transnasal Approaches. *Neurosurg Rev* (2020) 43(4):1201–10. doi: 10.1007/s10143-019-01153-w
26. Kong DS, Hong SD, Kang H, Seo Y, Kim MS, Seol HJ, et al. Safety and Efficacy of Endoscopic Dorsum Sellar Resection for Access to Retroinfundibular or Upper Clival Tumors (Korean Society of Endoscopic Neurosurgery-008). *World Neurosurg* (2021) 150:e675–80. doi: 10.1016/j.wneu.2021.03.085
27. Wang WH, Lieber S, Mathias RN, Sun X, Gardner PA, Snyderman CH, et al. The Foramen Lacerum: Surgical Anatomy and Relevance for Endoscopic Endonasal Approaches. *J Neurosurg* (2018) 131(5):1571–82. doi: 10.3171/2018.6.JNS181117
28. Simal-Julian JA, Miranda-Lloret P, Beltran-Giner A, Plaza-Ramirez E, Botella-Asuncion C. Full Endoscopic Endonasal Extreme Far-Medial Approach: Eustachian Tube Transposition. *J Neurosurg Pediatr* (2013) 11(5):584–90. doi: 10.3171/2013.1.PEDS12462
29. Patel CR, Wang EW, Fernandez-Miranda JC, Gardner PA, Snyderman CH. Contralateral Transmaxillary Corridor: An Augmented Endoscopic Approach to the Petrous Apex. *J Neurosurg* (2018) 129(1):211–9. doi: 10.3171/2017.4.JNS162483
30. Pacca P, Tardivo V, Pecorari G, Garbossa D, Ducati A, Zenga F. The Endoscopic Endonasal Approach to Craniovertebral Junction Pathologies: Surgical Skills and Anatomical Study. *Acta Neurochir Suppl* (2019) 125:25–36. doi: 10.1007/978-3-319-62515-7_5
31. Champagne PO, Zenonos GA, Wang EW, Snyderman CH, Gardner PA. The Rhinopharyngeal Flap for Reconstruction of Lower Clival and Craniovertebral Junction Defects. *J Neurosurg* (2021), 1–9. doi: 10.3171/2020.8.JNS202193
32. Labib MA, Belykh E, Cavallo C, Zhao X, Prevedello DM, Carrau RL, et al. The Endoscopic Endonasal Eustachian Tube Anterolateral Mobilization Strategy: Minimizing the Cost of the Extreme-Medial Approach. *J Neurosurg* (2020) 134(3):831–42. doi: 10.3171/2019.12.JNS192285
33. Zhang Y, Tian Z, Li C, Liu J, Zhang Y, Yang X, et al. A Modified Endovascular Treatment Protocol for Iatrogenic Internal Carotid Artery Injuries Following Endoscopic Endonasal Surgery. *J Neurosurg* (2019) 1(aop):1–8. doi: 10.3171/2018.8.JNS181048
34. Bai J, Shi J, Li C, Wang S, Zhang T, Hua X, et al. Whole Genome Sequencing of Skull-Base Chordoma Reveals Genomic Alterations Associated With Recurrence and Chordoma-Specific Survival. *Nat Commun* (2021) 12 (1):757. doi: 10.1038/s41467-021-21026-5

Conflict of Interest: The authors declare that the research was conducted in the absence of any commercial or financial relationships that could be construed as a potential conflict of interest.

frontiers in Oncology

ORIGINAL RESEARCH
published: 01 October 2021
doi: 10.3389/fonc.2021.733838

Do We Need Intraoperative Magnetic Resonance Imaging in All Endoscopic Endonasal Pituitary Adenoma Surgery Cases? A Retrospective Study

Emrah Celtikci[1], Muammer Melih Sahin[2], Mustafa Caglar Sahin[1], Emetullah Cindil[3], Zuhal Demirtaş[1] and Hakan Emmez[1]*

[1] Department of Neurosurgery, Gazi University Medical School, Ankara, Turkey, [2] Department of Otorhinolaryngology, Gazi University Medical School, Ankara, Turkey, [3] Department of Radiology, Gazi University Medical School, Ankara, Turkey

OPEN ACCESS

Edited by:
Xicai Sun,
Fudan University, China

Reviewed by:
Ye Gu,
Fudan University, China
Abuzer Gungor,
Yeditepe University, Turkey

***Correspondence:**
Emrah Celtikci
emrahceltikci@gazi.edu.tr

Specialty section:
This article was submitted to Surgical Oncology, a section of the journal Frontiers in Oncology

Received: *30 June 2021*
Accepted: *07 September 2021*
Published: *01 October 2021*

Citation:
Celtikci E, Sahin M M, Sahin M C, Cindil E, Demirtaş Z and Emmez H (2021) Do We Need Intraoperative Magnetic Resonance Imaging in All Endoscopic Endonasal Pituitary Adenoma Surgery Cases? A Retrospective Study. Front. Oncol. 11:733838. doi: 10.3389/fonc.2021.733838

There are previous reports investigating effectiveness of intraoperative magnetic resonance imaging (IO-MRI) in pituitary adenoma surgery but there is no clear data in the literature recommending when there is no need of intraoperative scan. This retrospective analysis was based on determining which patients does not need any IO-MRI scan following endoscopic endonasal pituitary adenoma surgery. Patients with functional or non-functional pituitary adenomas that were operated *via* endoscopic endonasal approach (EEA) between June 2017 and May 2019 were enrolled. Patients younger than 18 years old, patients who did not underwent IO-MRI procedure or not operated *via* EEA were excluded from the study. Hence, this study is designed to clarify if IO-MRI is useful in both functional and non-functional pituitary adenomas, functional adenomas did not split into subgroups. A total of 200 patients treated with pituitary adenoma were included. In Knosp Grade 0 – 2 group, primary surgeon's opinion and IO-MRI findings were compatible in 150 patients (98.6%). In Knosp Grade 3 – 4 correct prediction were performed in 32 (66.6%) patients. When incorrectly predicted Knosp Grade 3 – 4 patients (n = 16) was analyzed, in 13 patients there were still residual tumor in cavernous sinus and in 3 patients there were no residual tumor. Fisher's exact test showed there is a statistically significant difference of correct prediction between two different Knosp Grade groups (two-tailed $P < 0.0001$). Eighteen patients had a residual tumor extending to the suprasellar and parasellar regions which second most common site for residual tumor. Our findings demonstrate that there is no need of IO-MRI scan while operating adenomas limited in the sellae and not invading the cavernous sinus. However, we strongly recommend IO-MRI if there is any suprasellar and parasellar extension and/or cavernous sinus invasion.

Keywords: adenoma, endoscopy, intraoperative, magnetic resonance, pituitary

INTRODUCTION

Endoscopic endonasal approach (EEA) to the sellar region provides wide panoramic view during pituitary adenoma surgery allowing visualization of far lateral parts of the surgical field which is not possible with microscopic transsphenoidal surgery. Recent studies demonstrated superiority of EEA in resection of pituitary adenomas (1). Even to the advances in the endoscopy technology, gross total resection rates are not more than 80% in large series (2–9).

Following the first report by Jolesz and Blumenfeld, intraoperative magnetic resonance imaging (IO-MRI) became popular all over the world (10). Expected benefit of this MRI system in pituitary adenoma surgery is achieving higher rates of gross total resection (GTR) however, there are also controversies over higher costs and increased surgical time (11–21).

Here we present a study comprising 200 patients who underwent EEA pituitary adenoma resection by using IO-MRI. This retrospective analysis was based on the hypothesis, IO-MRI scan is not necessary during EEA in a particular group of patients. We aimed to clarify when we need IO-MRI scan and when we do not.

MATERIALS AND METHODS

Patients

Patients with functional or non-functional pituitary tumors that were operated *via* EEA between June 2017 and May 2019 in Gazi University Faculty of Medicine Department of Neurosurgery were enrolled. The Institutional Review Board and Ethics Committee approved this retrospective study; oral and written consents of the patients were obtained prior to the study. Also, all patients were informed about the technique and gave their signed consent to IO-MRI during surgery and to the data being used for research purpose. Patients younger than 18 years old, patients who did not underwent IO-MRI procedure or not operated *via* EEA were excluded from the study. Hence, this study is designed to clarify if IO-MRI is useful in both functional and non-functional pituitary adenomas, functional adenomas did not split into subgroups.

Technique

All patients were screened to exclude any contraindication to magnetic resonance imaging (MRI). All data were acquired using a 3-Tesla Magnetom Verio® (Siemens, Erlangen, Germany). Intraoperative scans were performed with 8–channel 2–part coils and compatible head holders (NORAS MRI products GmbH, Hochberg, Germany). EEA was performed using skull base neurosurgical endoscopic instruments, including 4-mm rod-lens endoscopes (0°, 30° and 45°) that were coupled to a high-definition camera and an AIDA HD system (Karl Storz GmbH and Co.). Four-hand technique was used, both surgeons were neurosurgeons. Medial or lateral cavernous approaches were performed when needed. Prior performing IO-MRI scan, primary surgeon declared and noted his decision if he thinks there is residual tumor or not. Following IO-MRI scan, if there is a residual tumor primary surgeon decided for further removal of tumor or not. All patients underwent a final post-operative MRI scan when the senior surgeon decided not to continue the surgery. Cavernous sinus invasion was classified according to Knosp Grading (22).

Complications

Postoperative meningitis was defined when antibiotic treatment was required because of clinical signs of meningeal inflammation even if no pathogen was isolated. Cerebrospinal fluid (CSF) fistula was considered as a complication if a lumbar drain or revision surgery was necessary. Furthermore, intraoperative and postoperative bleeding and new transient or permanent neurologic deficits were included.

Data Analysis

Analysis of the retrospective data was performed using SPSS 21.0 (IBM Corp., Armonk, New York, USA). In order to compare predictions and to compare residual mass ratios between two Knosp Grade groups, Fisher's exact test were used. Variables were; preoperative largest diameter of tumor (< 4 cm or ≥ 4 cm), Knosp grade, age, gender, and recurrent surgery.

RESULTS

Patient and Tumor Characteristics

A total of 200 patients treated with pituitary adenoma were included. A mean age of 57.4 years (range, 19 – 75 years) was noted. 105 patients were male (52.5%). Eleven patients who had a history of previous adenoma surgery were operated for recurrent or residual adenoma. Patient and tumor characteristics are summarized in **Table 1**.

Knosp Grade and Hormonal Activity

Twenty-two patients had a Knosp Grade 3 – 4 functional pituitary adenoma. Following IO-MRI residual adenoma was

TABLE 1 | Demographic and tumor characteristics of 200 patients underwent endoscopic endonasal resection of pituitary adenoma with intraoperative magnetic resonance imaging.

Characteristic	Value
Age (years)	
Median	57.4
Range	19 – 75
Gender	
Male	105
Female/Male ratio	1/1.05
Tumor Volume and Cavernous Extension	
Knosp Grade 3 – 4	48
Knosp Grade 0 – 2	152
Giant adenoma (≥ 4 cm in largest diameter)	31
Hormonal Activity	
Non-functional	94
History of Pituitary Adenoma Surgery	
Recurrent Surgery	28

Values other than ratios or patient age are number of patients.

detected in 9 (40.9%) patients and further resection is performed in all of them (100%). In 4 patients, in order to avoid complications, primary surgeon decided not to perform anymore residual tumor removal from cavernous sinus after the second IO-MRI scan. Twenty-six patients had a Knosp Grade 3 – 4 non-functional pituitary adenoma. Following IO-MRI residual adenoma was detected in 16 (61.5%) patients and further resection is performed in 3 (18.7%) of them. In all Knosp Grade 3 – 4 patients.

Following IO-MRI scan, 9 of 84 (10.7%) and 13 of 68 (19.1%) functional and non-functional residual adenoma was detected in Knosp Grade 0 – 2 group respectively. All Knosp Grade 0 – 2 patients who has a residual adenoma in both functional and non-functional groups underwent further removal of tumor. Tumor characteristics according to Knosp Grade is summarized in **Table 2**.

Primary Surgeon Opinion and IO-MRI

In Knosp Grade 0 – 2 group, primary surgeon's opinion and IO-MRI findings were compatible in 150 patients (98.6%). Both two patients which were incorrectly predicted by primary surgeon had giant adenomas and had residual tumor on IO-MRI scan. In Knosp Grade 3 – 4 correct prediction were performed in 32 (66.6%) patients. When incorrectly predicted Knosp Grade 3 – 4 patients (n = 16) was analyzed, in 13 patients there were still residual tumor in cavernous sinus and in 3 patients there were no residual tumor. Fisher's exact test showed there is a statistically significant difference of correct prediction between two different Knosp Grade groups (two-tailed P < 0.0001) (**Table 3**).

Complications

One patient (0.5%) had post-operative meningitis signs without any isolated pathogen. Two patients who had Knosp Grade 3 – 4 adenomas had ICA injury (1%), both on cavernous segment of the right ICA. Two patients had post-operative unilateral oculomotor nerve paralysis. In both patients IO-MRI showed residual tumor in the cavernous sinus and further resection was performed following scan. After 3-months follow up oculomotor function recovered completely in both patients. Eighteen patients had CSF fistula (9%) 15 of them treated with lumbar drain and 3 of them underwent revision surgery.

TABLE 2 | Percentage and distribution of residual adenoma finding in first intraoperative magnetic resonance imaging according to tumor characteristic and Knosp Grade.

Tumor Characteristic	Knosp Grade		two-tailed P value
	0 – 2 (n = 152)	3 – 4 (n = 48)	
Functional	10.7% (9)	40.9% (9)	
Non-functional	19.1% (13)	61.5% (16)	
Total	14.4% (22)	52% (25)	< 0.001

Values are percentages of patients and number of patients are in parenthesis.

TABLE 3 | Comparison of primary surgeon opinion before intraoperative magnetic resonance imaging and findings after scan.

Opinion before IO-MRI	Knosp Grade				two-tailed P value
	0 – 2		3 – 4		
	No residual mass	Residual mass	No residual mass	Residual mass	
Correct	143	7	19	13	
Incorrect	0	2	13	3	< 0.0001

Values are number of patients.

Additional Findings

Retrospective analysis of the patients' scans revealed second most common site for residual tumor following cavernous sinus was suprasellar and parasellar extension. Eighteen patients (9%) had a residual tumor extending to the suprasellar and parasellar regions (**Figure 1**).

DISCUSSION

In this study we demonstrate that IO-MRI scan during EEA for resection of pituitary adenomas is not necessary for all tumor types. Our findings are showing that IO-MRI is beneficial in adenomas with suprasellar and parasellar extension and/or invading cavernous sinus (Knosp Grade 3 & 4). We found no additional benefit of IO-MRI in microadenomas, adenomas with no cavernous sinus invasion or adenomas limited in the sellae without any suprasellar and parasellar extension.

Endoscopic surgery of the pituitary adenomas became preferred treatment method in time by providing a viable median corridor and improved visualization of the anatomical landmarks (2, 23). Even to the technological advances, recurrence rates are up to 20% in the literature and first surgery is the most important intervention (24, 25). As a result, all efforts should be made to achieve total resection in the first surgery. One of the important factors preventing total resection of pituitary adenomas is cavernous sinus invasion. Following reevaluation of their MRI-based classification, Knosp et al. demonstrated that resection rates at the superior compartment of the cavernous sinus were higher than those at the inferior one (22, 26). Hence, cavernous sinus is on the agenda of neurosurgeons performing EEA, there are recent reports defining anatomical relationships and approaches to the cavernous sinus (3, 27–29). For this reason, we designed our retrospective study to clarify if IO-MRI scans were necessary when there is no significant cavernous sinus invasion or is there any pre-operative indicator to determine which patients will benefit from IO-MRI scans.

Other than our findings defining benefit of IO-MRI in resection of invasive adenomas, parasellar or suprasellar extension took our attention. Ramm-Pettersen et al. emphasized importance of IO-MRI when there is a parasellar or suprasellar extension of the adenoma (19). We agree that utilization of IO-MRI in endoscopic endonasal pituitary adenoma surgery improves resection rates when there is parasellar or suprasellar extension.

There are previous reports investigating effectiveness of IO-MRI in pituitary adenoma surgery but there is no clear data in

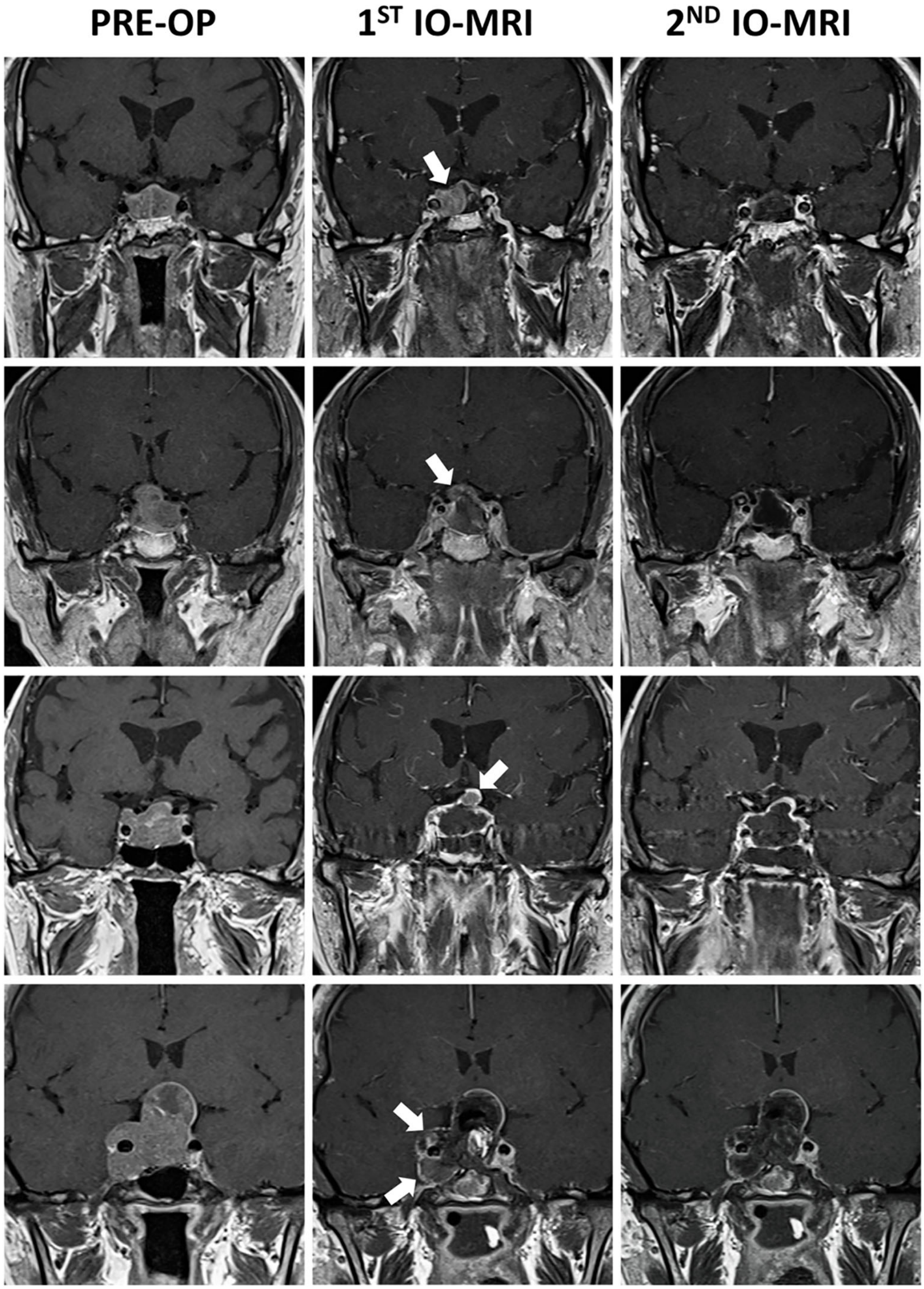

FIGURE 1 | Figure demonstrating pre-operative and intraoperative contrast enhanced coronal T1-weighted pituitary MRIs of 4 different patients. First patient (first row) had a prolactin secreting macroadenoma which had two different signal intensity on pre-operative MRI scan without any cavernous invasion. Right side of the tumor was showing high signal intensity. First IO-MRI scan demonstrating residual mass on the right side. Second IO-MRI scan demonstrating that total removal was achieved. Second patient (second row) had a non-functioning macroadenoma causing visual disturbance. First IO-MRI scan demonstrating residual mass where tumor was penetrating the sellar diaphragm. Surgeon decided further excision and total removal was achieved. Third patient (third row) had a Knosp Grade 3A growth hormone secreting macroadenoma. Following excision, surgeon's decision was in favor of total removal. However, first IO-MRI scan showed residual tumor was not in the cavernous sinus but in the region where tumor was penetrating the sellar diaphragm. Total removal was achieved following further excision. Last patient (fourth row) had a Knosp Grade 4 non-functioning pituitary adenoma causing severe visual disturbances. Following excision first IO-MRI demonstrated residual mass in the cavernous sinus. Further excision was performed which resulted in total removal of the tumor. Patient had a 3rd nerve palsy following the surgery which totally improved after 3 months post-operatively. White arrows demonstrating residual tumor tissues on IO-MRIs.

the literature recommending when there is no need of intraoperative scan (14, 16, 17, 19–21). Previous studies are focusing effects of IO-MRI on surgical time, cost effectiveness, GTR and recurrence rates. On the other hand, we focused on to determine which patients does not need any IO-MRI scan. We believe our findings will guide neurosurgeons especially in the countries where MRI scans are costly.

There are limitations of this study. First, this is a retrospective study and tries to correlate results with only using MRI data. Study does not include and correlate any long-term follow up data including progression free survival rates. However, one of the aims of this study was to determine if there is any correlation between prediction of the surgeon and MRI findings. Additionally, we did not perform any cost-effectiveness analysis because study was performed in a country which has a universal health care plan for all the citizens and costs of MRI scans are relatively cheap (about 15 U.S. dollars per scan). This is one of the reasons why authors performed IO-MRI scans for all the patients in the study cohort.

Even though our findings are demonstrating IO-MRI does not have additional benefit in microadenomas, adenomas with no cavernous sinus invasion or adenomas limited in the sellae, we will continue to collect and analyze data *via* performing intraoperative scans in every patient undergoing EEA for pituitary adenomas. We are planning to determine effects of IO-MRI in endoscopic surgery of pituitary adenoma subtypes.

Utilization of IO-MRI in endoscopic endonasal pituitary adenoma surgery is increasing but current literature is focusing on surgical time, cost effectiveness, GTR and recurrence rates. Our findings demonstrate that there is no need of IO-MRI scan while operating adenomas limited in the sellae and not invading the cavernous sinus. However, we strongly recommend IO-MRI if there is any suprasellar and parasellar extension and/or cavernous sinus invasion.

DATA AVAILABILITY STATEMENT

The original contributions presented in the study are included in the article/supplementary material. Further inquiries can be directed to the corresponding author.

ETHICS STATEMENT

The studies involving human participants were reviewed and approved by The Institutional Review Board and Ethics Committee. The patients/participants provided their written informed consent to participate in this study.

AUTHOR CONTRIBUTIONS

ECe and ZD wrote the paper. HE, MMS, and MCS edited the paper. ECi analyzed the IO-MRI. All authors contributed to the article and approved the submitted version.

REFERENCES

1. Almutairi RD, Muskens IS, Cote DJ, Dijkman MD, Kavouridis VK, Crocker E, et al. Gross Total Resection of Pituitary Adenomas After Endoscopic *vs.* Microscopic Transsphenoidal Surgery: A Meta-Analysis. *Acta Neurochir (Wien)* (2018) 160:1005–21. doi: 10.1007/s00701-017-3438-z
2. Cappabianca P, Cavallo LM, Colao A, de Divitiis E. Surgical Complications Associated With the Endoscopic Endonasal Transsphenoidal Approach for Pituitary Adenomas. *J Neurosurg* (2002) 97:293–8. doi: 10.3171/jns.2002.97.2.0293
3. Fernandez-Miranda JC, Zwagerman NT, Abhinav K, Lieber S, Wang EW, Snyderman CH, et al. Cavernous Sinus Compartments From the Endoscopic Endonasal Approach: Anatomical Considerations and Surgical Relevance to Adenoma Surgery. *J Neurosurg* (2017) 129:430–41. doi: 10.3171/2017.2.JNS162214
4. Frank G, Pasquini E, Farneti G, Mazzatenta D, Sciarretta V, Grasso V, et al. The Endoscopic *Versus* the Traditional Approach in Pituitary Surgery. *Neuroendocrinology* (2006) 83:240–8. doi: 10.1159/000095534
5. Gondim JA, Almeida JPC, Albuquerque LAF, Schops M, Gomes E, Ferraz T, et al. Endoscopic Endonasal Approach for Pituitary Adenoma: Surgical Complications in 301 Patients. *Pituitary* (2011) 14:174–83. doi: 10.1007/s11102-010-0280-1
6. Jang JH, Kim KH, Lee YM, Kim JS, Kim YZ. Surgical Results of Pure Endoscopic Endonasal Transsphenoidal Surgery for 331 Pituitary Adenomas: A 15-Year Experience From a Single Institution. *World Neurosurg* (2016) 96:545–55. doi: 10.1016/j.wneu.2016.09.051
7. Lampropoulos KI, Samonis G, Nomikos P. Factors Influencing the Outcome of Microsurgical Transsphenoidal Surgery for Pituitary Adenomas: A Study on 184 Patients. *Hormones (Athens)* (2013) 12:254–64. doi: 10.14310/horm.2002.1409
8. Liu J, Li C, Xiao Q, Gan C, Chen X, Sun W, et al. Comparison of Pituitary Adenomas in Elderly and Younger Adults: Clinical Characteristics, Surgical Outcomes, and Prognosis. *J Am Geriatr Soc* (2015) 63:1924–30. doi: 10.1111/jgs.13590
9. Zhan R, Ma Z, Wang D, Li X. Pure Endoscopic Endonasal Transsphenoidal Approach for Nonfunctioning Pituitary Adenomas in the Elderly: Surgical Outcomes and Complications in 158 Patients. *World Neurosurg* (2015) 84:1572–8. doi: 10.1016/j.wneu.2015.08.035
10. Jolesz FA, Blumenfeld SM. Interventional Use of Magnetic Resonance Imaging. *Magn Reson Q* (1994) 10:85–96.
11. Bohinski RJ, Warnick RE, Gaskill-Shipley MF, Zuccarello M, van Loveren HR, Kormos DW, et al. Intraoperative Magnetic Resonance Imaging to Determine the Extent of Resection of Pituitary Macroadenomas During Transsphenoidal Microsurgery. *Neurosurgery* (2001) 49:1133–43; discussion 1143–4. doi: 10.1097/00006123-200111000-00023
12. Chittiboina P. iMRI During Transsphenoidal Surgery. *Neurosurg Clin N Am* (2017) 28:499–512. doi: 10.1016/j.nec.2017.05.005
13. Fahlbusch R, Ganslandt O, Buchfelder M, Schott W, Nimsky C. Intraoperative Magnetic Resonance Imaging During Transsphenoidal Surgery. *J Neurosurg* (2001) 95:381–90. doi: 10.3171/jns.2001.95.3.0381
14. Fomekong E, Duprez T, Docquier M-A, Ntsambi G, Maiter D, Raftopoulos C. Intraoperative 3t MRI for Pituitary Macroadenoma Resection: Initial Experience in 73 Consecutive Patients. *Clin Neurol Neurosurg* (2014) 126:143–9. doi: 10.1016/j.clineuro.2014.09.001
15. Gerlach R, du Mesnil de Rochemont R, Gasser T, Marquardt G, Reusch J, Imoehl L, et al. Feasibility of Polestar N20, an Ultra-Low-Field Intraoperative Magnetic Resonance Imaging System in Resection Control of Pituitary Macroadenomas: Lessons Learned From the First 40 Cases. *Neurosurgery* (2008) 63:272–84; discussion 284–5. doi: 10.1227/01.NEU.0000312362.63693.78

16. Li J, Cong Z, Ji X, Wang X, Hu Z, Jia Y, et al. Application of Intraoperative Magnetic Resonance Imaging in Large Invasive Pituitary Adenoma Surgery. *Asian J Surg* (2015) 38:168–73. doi: 10.1016/j.asjsur.2015.03.001
17. Makary M, Chiocca EA, Erminy N, Antor M, Bergese SD, Abdel-Rasoul M, et al. Clinical and Economic Outcomes of Low-Field Intraoperative MRI-Guided Tumor Resection Neurosurgery. *J Magn Reson Imaging* (2011) 34:1022–30. doi: 10.1002/jmri.22739
18. Martin CH, Schwartz R, Jolesz F, Black PM. Transsphenoidal Resection of Pituitary Adenomas in an Intraoperative MRI Unit. *Pituitary* (1999) 2:155–62. doi: 10.1023/a:1009943700810
19. Ramm-Pettersen J, Berg-Johnsen J, Hol PK, Roy S, Bollerslev J, Schreiner T, et al. Intra-Operative MRI Facilitates Tumour Resection During Trans-Sphenoidal Surgery for Pituitary Adenomas. *Acta Neurochir (Wien)* (2011) 153:1367–73. doi: 10.1007/s00701-011-1004-7
20. Sylvester PT, Evans JA, Zipfel GJ, Chole RA, Uppaluri R, Haughey BH, et al. Combined High-Field Intraoperative Magnetic Resonance Imaging and Endoscopy Increase Extent of Resection and Progression-Free Survival for Pituitary Adenomas. *Pituitary* (2015) 18:72–85. doi: 10.1007/s11102-014-0560-2
21. Szerlip NJ, Zhang Y-C, Placantonakis DG, Goldman M, Colevas KB, Rubin DG, et al. Transsphenoidal Resection of Sellar Tumors Using High-Field Intraoperative Magnetic Resonance Imaging. *Skull Base* (2011) 21:223–32. doi: 10.1055/s-0031-1277262
22. Micko ASG, Wöhrer A, Wolfsberger S, Knosp E. Invasion of the Cavernous Sinus Space in Pituitary Adenomas: Endoscopic Verification and Its Correlation With an MRI-Based Classification. *J Neurosurg* (2015) 122:803–11. doi: 10.3171/2014.12.JNS141083
23. Kassam A, Snyderman CH, Mintz A, Gardner P, Carrau RL. Expanded Endonasal Approach: The Rostrocaudal Axis. Part I. Crista Galli to the Sella Turcica. *Neurosurg Focus* (2005) 19:E3. doi: 10.3171/foc.2005.19.1.4
24. Dallapiazza RF, Grober Y, Starke RM, Laws ER, Jane JA. Long-Term Results of Endonasal Endoscopic Transsphenoidal Resection of Nonfunctioning Pituitary Macroadenomas. *Neurosurgery* (2015) 76:42–52; discussion 52–3. doi: 10.1227/NEU.0000000000000563
25. Przybylowski CJ, Dallapiazza RF, Williams BJ, Pomeraniec IJ, Xu Z, Payne SC, et al. Primary *Versus* Revision Transsphenoidal Resection for Nonfunctioning Pituitary Macroadenomas: Matched Cohort Study. *J Neurosurg* (2017) 126:889–96. doi: 10.3171/2016.3.JNS152735
26. Knosp E, Steiner E, Kitz K, Matula C. Pituitary Adenomas With Invasion of the Cavernous Sinus Space: A Magnetic Resonance Imaging Classification Compared With Surgical Findings. *Neurosurgery* (1993) 33:610–7; discussion 617–8. doi: 10.1227/00006123-199310000-00008
27. Ceylan S, Anik I, Cabuk B, Caklili M, Anik Y. Extension Pathways of Pituitary Adenomas With Cavernous Sinus Involvement and Its Surgical Approaches. *World Neurosurg* (2019) 127:e986–95. doi: 10.1016/j.wneu.2019.04.013
28. Cohen-Cohen S, Gardner PA, Alves-Belo JT, Truong HQ, Snyderman CH, Wang EW, et al. The Medial Wall of the Cavernous Sinus. Part 2: Selective Medial Wall Resection in 50 Pituitary Adenoma Patients. *J Neurosurg* (2018) 131:1–10. doi: 10.3171/2018.5.JNS18595
29. Truong HQ, Lieber S, Najera E, Alves-Belo JT, Gardner PA, Fernandez-Miranda JC. The Medial Wall of the Cavernous Sinus. Part 1: Surgical Anatomy, Ligaments, and Surgical Technique for its Mobilization and/or Resection. *J Neurosurg* (2018) 131:1–9. doi: 10.3171/2018.3.JNS18596

Conflict of Interest: The authors declare that the research was conducted in the absence of any commercial or financial relationships that could be construed as a potential conflict of interest.

frontiers in Oncology

ORIGINAL RESEARCH
published: 08 October 2021
doi: 10.3389/fonc.2021.702574

Blood Supply of Cranial Nerves Passing Through the Cavernous Sinus: An Anatomical Study and Its Implications for Microsurgical and Endoscopic Cavernous Sinus Surgery

*Edinson Najera, Bilal Ibrahim, Baha'eddin A. Muhsen, Assad Ali, Clariza Sanchez, Michal Obrzut, Hamid Borghei-Razavi and Badih Adada**

Cleveland Clinic Florida, Weston, United States

OPEN ACCESS

Edited by:
Xicai Sun,
Fudan University, China

Reviewed by:
Marco Artico,
Sapienza University of Rome, Italy
Ziv Radisavljevic,
Brigham and Women's Hospital and Harvard Medical School, United States

***Correspondence:**
Badih Adada
ADADAB@ccf.org

Specialty section:
This article was submitted to Surgical Oncology, a section of the journal Frontiers in Oncology

Received: *13 May 2021*
Accepted: *21 September 2021*
Published: *08 October 2021*

Citation:
Najera E, Ibrahim B, Muhsen B'eA, Ali A, Sanchez C, Obrzut M, Borghei-Razavi H and Adada B (2021) Blood Supply of Cranial Nerves Passing Through the Cavernous Sinus: An Anatomical Study and Its Implications for Microsurgical and Endoscopic Cavernous Sinus Surgery. Front. Oncol. 11:702574. doi: 10.3389/fonc.2021.702574

Background: Despite improvements in surgical techniques, cranial nerve (CN) deficits remain the most frequent cause of disability following cavernous sinus (CS) surgery. The most common tumor affecting the CS is meningioma. They originate from lateral wall and have their blood supply from meningohypophyseal trunk (MHT) and inferolateral trunk (ILT). Pituitary adenomas commonly invade the CS through its medial wall and receive blood supply form medial branches of the internal carotid artery (ICA) (superior and inferior hypophyseal arteries). Some tumors may grow within the CS (e.g. trigeminal schwannomas, hemangiomas). These tumors are fed by all the intracavernous ICA branches. Tumors involving the CS may also displace the neurovascular structures, therefore, a better understanding of intracavernous neurovascular anatomy may reduce the postoperative morbidity associated with approaching CS tumors. In this anatomical study, the anatomic variations and their clinical implications of the intracavernous CNs' blood supply were evaluated through transcranial and endonasal routes.

Methods: Twenty sides of ten adult cadaveric formalin-fixed, latex-injected specimens were dissected in stepwise fashion under microscopic and endoscopic magnification. The origin and course of the intracavernous ICA branches supplying the intracavernous CNs are studied.

Results: The proximal segment of the oculomotor nerve receives blood supply from the ILT in 85%, and the tentorial artery of the MHT in 15% of specimens. The distal segment is exclusively supplied by the ILT. The proximal trochlear nerve receives blood supply from the ILT (75%) and the tentorial artery (25%); the distal segment is exclusively supplied by the superior orbital branch. The proximal third of the abducens nerve receives its vascularity exclusively from the dorsal meningeal artery, and its middle and distal thirds from the ILT. The ophthalmic and proximal maxillary segments of the trigeminal nerve also receive blood supply from the ILT. The distal maxillary segment is supplied by the artery of the foramen rotundum. All ILT branches terminate on the inferomedial aspects of the intra-cavernous CNs. Extensive anastomoses are found between ILT branches and the branches arising from external carotid artery.

Conclusion: Understanding the anatomy of the intracavernous ICA's branches is important to improving surgical outcomes with tumors involving the CS.

Keywords: intracavernous cranial nerves, inferolateral trunk, meningohypophyseal trunk, oculomotor nerve, trochlear nerve, abducens nerve, trigeminal nerve

INTRODUCTION

Tumors with cavernous sinus (CS) invasion present a neurosurgical challenge. The most common tumor seen in cavernous sinus is meningioma (1). However, many tumors can arise in or invade the CS, these include trigeminal schwannomas, pituitary adenomas, chordomas and chondrosarcomas. Advances in cranial base surgery over the last two decades including better anatomical understanding, improvement in microsurgical technics and incorporation of the endonasal endoscopic approach (EEA) into the skull base armamentarium, now allow for 360° access to the CS. Despite the improvements in microscopic and endoscopic surgical techniques, cranial nerve (CN) deficits remain the most frequent cause of disability following CS surgery (1–3). Nerve dysfunction can occur due to direct trauma caused by the manipulation of the nerve during surgery or from ischemic injury caused by damage to the nerve's blood supply. Permanent CN deficits may occur even if the nerves are anatomically preserved (1, 2, 4). Thorough knowledge in the anatomy of blood vessels supplying CNs inside the CS is necessary for approaching tumors with expansion in to the CS. This understanding is particularly important to minimize inadvertent occlusion of supplying blood vessels from excessive coagulation or manipulation during tumor resection. The branches of the intracavernous internal carotid artery (ICA) have been described by several authors, mostly from the microsurgical transcranial perspective (1, 5–11). There are only a few descriptions providing a detailed anatomy of the blood supply to the intracavernous CNs from both a transcranial and an EEA perspective (12–14).

In this anatomical study, we evaluate the anatomic variations and clinical implications of the intracavernous CNs' blood supply when approaching the CS region from transcranial and endonasal routes. A detailed understanding of the intracavernous CNs' blood supply is essential for improving outcomes when operating on lesions involving the CS.

METHODS

Ten adult head specimens (20 sides) were lightly fixed in a formalin solution and prepared for dissection after injecting them with intravascular colored silicone. This research was approved by the Research Ethics Board. A microsurgical transcranial approach and an EEA to the sellar and parasellar regions were performed simultaneously on all heads. A pterional craniotomy was performed, followed by extradural drilling of the anterior clinoid process. Then, a 5-cm temporal lobectomy was performed, and the lateral, posterior wall of the CS was exposed. Under microscopic magnification, the dura covering the lateral wall of the CS was removed, exposing the CNs in the lateral wall of the sinus. From the EEA perspective, wide bilateral sphenoidotomies were performed to expose the posterior wall of the sphenoid sinus. The bone overlying the sellar and parasellar regions was removed to allow access to the medial and anterior walls of the CS. The origin, course, and different anatomic patterns of the intracavernous ICA branches vascularizing the intracavernous CNs were documented from both the transcranial and the EEA perspectives. CNs are then followed proximal and distal to CS segments and vascularizing branches to these segments were studied and documented. A tumor with CS invasion was selected to illustrate the surgical application of these findings.

RESULTS

The Intracavernous ICA and Its Branches

The arterial branches arising from the intracavernous segment of the ICA vary in origin and number. The intracavernous ICA from proximal to distal can be divided into four segments: 1) the short vertical segment (a continuation of the paraclival ICA); 2) the posterior genu; 3) the horizontal segment; and 4) the anterior genu, which continues with the paraclinoidal ICA as it emerges from the CS. The most common branches of the intracavernous ICA observed in this study are the meningohypophyseal trunk (MHT) (present in 100% of specimens), the inferolateral trunk (ILT) (85%) and McConnell's capsular artery (20%). Less frequent branches of the intracavernous ICA are the superolateral trunk (10%) and a persistent trigeminal artery (5%).

The MHT, the largest and most constant branch of the cavernous ICA, arises from the short vertical segment of the intracavernous ICA, close to the posterior genu, in 20% of the specimens studied. In the other 80% of specimens, the MHT arises from the middle third of the posterior genu. It typically gives rise to three branches: 1) the inferior hypophyseal, which travels medially to supply the posterior lobe of the pituitary gland; 2) the tentorial artery (known as the artery of Bernasconi-Cassinari), which courses lateraly towards the tentorium to contribute to the blood supply of the interdural segment of the oculomotor and trochlear nerves; and 3) the dorsal meningeal artery (also called the lateral clival artery), which passes posteriorly through the CS to supply the clival dura and abducens nerve within Dorello's canal. This artery usually divides into medial and lateral branches. The medial branch accompanies the abducens nerve into Dorello's canal and sometimes anastomoses with the clival ramus of the jugular branch of the ascending pharyngeal artery (**Figures 1A–C**).

The ILT is present in 85% of the specimens. It arises from the lateral side of the midportion of the horizontal segment of the intracavernous ICA, and courses inferiorly. The ILT arises directly from the carotid artery in 80% of the specimens and from the MHT in 5%. The ILT typically divides into three to four branches: 1) the superior orbital branch (also called the antero-medial branch), which runs to the superior orbital fissure; 2) the foramen rotundum artery (known as the antero-Iateral branch), typically accompanies the maxillary nerve (V2) through the foramen rotundum, supplies the V2 segment of the trigeminal nerve, and anastomoses with the internal maxillary artery (IMAX); 3) the foramen ovale branch, which travels with the mandibular (V3) segment of the trigeminal nerve through the foramen ovale and has anastomoses with the IMAX and/or petrosal branch of the middle meningeal artery; 4) the superior branch of the ILT, which follows the III and IV nerve along the lateral wall of the CS (**Figures 2A–C**).

In 10% of the specimens a superolateral trunk is found to arise from the supero-lateral aspect of the horizontal segment of the intracavernous ICA, it directs superiorly, and then runs adjacent to the oculomotor and trochlear cranial nerves and provides them with blood supply at their dural entrance. McConnell's capsular artery is present in 20% of the cases and arises from the medial aspect of the horizontal segment of the intracavernous ICA and courses toward the capsule of the pituitary gland, where it anastomoses with the opposite artery. The capsular artery does not provide any blood supply to the CNs.

In one specimen (5%) a persistent trigeminal artery is identified. It arises from the middle third of the posterior genu of the intracavernous ICA, courses backward through the posterior wall of the CS lateral to Dorello's canal and medial to Meckel's cave to join the basilar artery between the origin of the superior cerebellar artery and the anterior inferior cerebellar artery (**Figure 3A**). In this particular case, the MHT and its three branches originate from the persistent trigeminal artery.

Blood Supply of the Intracavernous Nerves

The Oculomotor Nerve

The oculomotor nerve is supplied by the ILT branches in all studied specimens. The proximal cavernous segment of the oculomotor CN receives its blood supply through the superior branch of the ILT in 85% of the specimens and the tentorial artery of the MHT in 15%. In addition, the proximal segment of the III CN receives blood supply from the superolateral trunk in 10% of the cases; the distal segment of the III CN is supplied exclusively by the superior orbital branch of the ILT (**Figure 1** and **Table 1**). The superior orbital branch of the ILT supplies the distal segments of all CNs passing through the superior orbital fissure. The cisternal segment of the oculomotor nerve receives blood supply from the thalamoperforating arteries that originate from the P1 and the proximal P2 segments of the posterior cerebral artery (**Figures 3B–D**).

The Trochlear Nerve

The proximal trochlear nerve (IV) receives its vascularity from the superior branch of the ILT and from the tentorial artery in

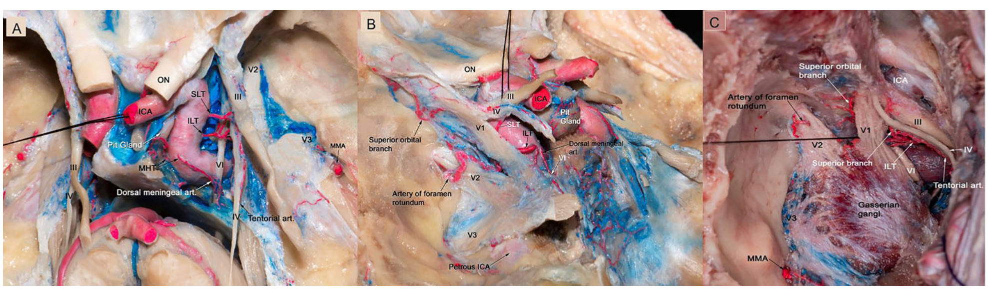

FIGURE 1 | **(A)** Microscopic view of the roof and lateral wall of the CS in a colored silicone-injected human cadaveric specimen showing the branches of the intracavernous ICA supplying the intracavernous CN. The dural covering of the right cavernous sinus has been removed to expose the cavernous sinus contents. The MHT originating from the proximal cavernous segment of the ICA, in this specimen a double trunk is present, the main trunk is giving off the dorsal meningeal artery, which passed posteriorly through the CS to supply the clival dura and abducens nerve within Dorello's canal. The ILT arose from the lateral side of the midportion of the horizontal segment of the intracavernous ICA, and is directed inferiorly. It provides blood supply to CN III, CN IV, middle and distal segments of CN VI. The SLT arises from the supero-lateral aspect of the horizontal segment of the intracavernous ICA, courses superiorly, and then runs adjacent to CN III and IV as they run through the dura and provide them with blood supply. In this specimen, the tentorial artery is originating from the ILT, which courses lateral to the tentorium to contribute to the blood supply of the interdural segment of the trochlear nerve. **(B)** The dura of the lateral wall of the left CS has been removed to show the intracavernous CNs and terminal branches of the ILT. The ILT giving off the superior orbital branch, which goes through the superior orbital fissure and supplies blood to the distal segments of all CNs passing through the superior orbital fissure. The ILT then courses laterally over V1 and gives off the artery of the foramen rotundum, which supplies the distal segment of V2. **(C)** Microscopic view of the lateral wall of left cavernous sinus showing terminal branches of the ILT. The ILT giving off the superior orbital branch, and the superior branch. It then courses laterally under V2 segment and gives off the artery of foramen rotundum. The ILT also gives rise to tentorial branch which is supplying CN IV. CN, cranial nerve; CS, cavernous sinus; ICA, internal carotid artery; ILT, inferolateral trunk; MHT, meningohypophyseal trunk; SLT, superolateral trunk.

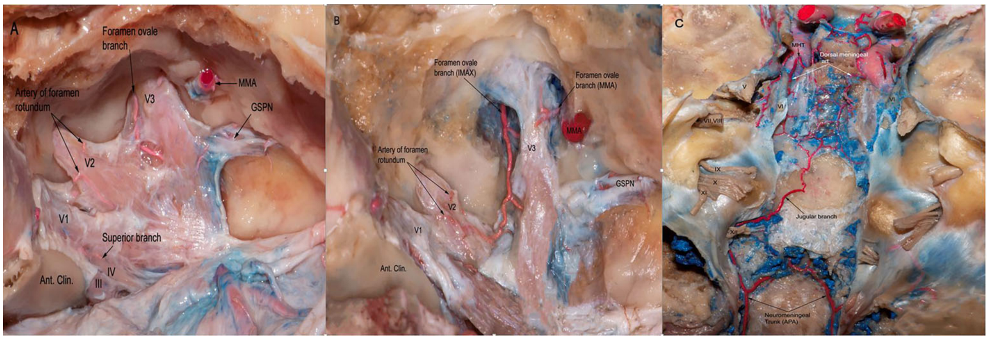

FIGURE 2 | **(A)** The dura of the lateral wall of the right CS has been removed to show the terminal branches of the ILT providing blood supply to CN III,IV as well asV1,V2,V3 branches of the trigeminal nerve. ILT giving off the superior branch, the artery of foramen rotundum, and the foramen ovale branch. **(B)** Another view from the same specimen after careful drilling of the foramen ovale showing the anastomotic network between the terminal branches of ILT and branches from the internal maxillary artery. Note the branches arising from MMA supplying the V3 segment of the trigeminal nerve. **(C)** Posterior view of the clivus in a colored silicone-injected human cadaveric specimen showing a rich anastomotic network between the dorsal meningeal branches arising from MHT and the jugular branches arising from neuromeningeal trunk, which is a branch of the ascending pharyngeal artery. APA, ascending pharyngeal artery; MMA, medial meningeal artery.

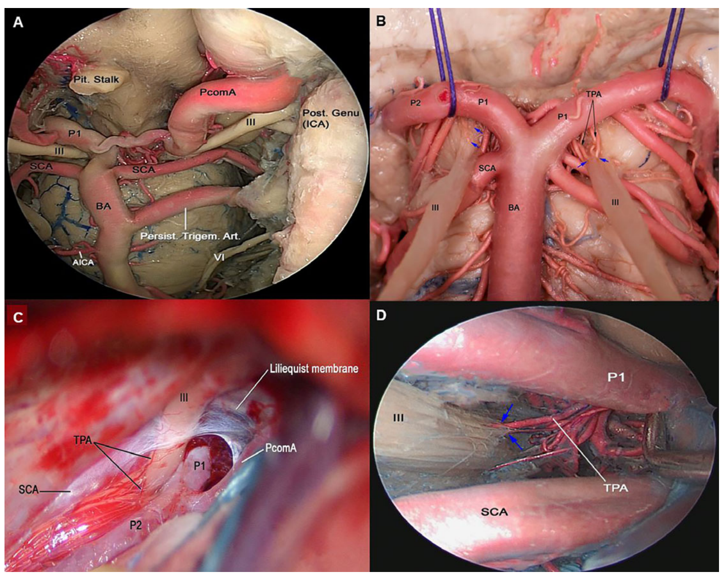

FIGURE 3 | **(A)** Endoscopic view in a colored silicone-injected human cadaveric specimen showing a persistent trigeminal artery anastomosing with the left intracavernous ICA with the basilar artery between SCA and AICA origins. **(B)** Cross-section of midbrain at the level of the superior colliculus demonstrating the course of cisternal segment of the III nerve, which passes between PCA and SCA. Note the thalamoperforating branches arising from P1 supplying the cisternal segment (blue arrow). BA, basilar artery; PCA, posterior cerebral artery; SCA, superior cerebellar artery **(C)** Left trans-sylvian exposure of the ambient cistern, revealing: the PCA and SCA perforating branches supplying the cisternal segment of the III nerve. **(D)** Endoscopic view of the interpeduncular region, showing the cisternal segment of right CN III. TPA arising from pre-communicating segment of PCA (P1) supplying the cisternal segment of CN III are shown (blue arrow). AICA, anterior inferior cerebellar artery; CN, Cranial Nerve; PCA, posterior cerebral artery; PcomA, posterior communicating artery; SCA, Superior Cerebellar Artery; TPA, Thalamoperforating Arteries.

75% and 25% of the specimens, respectively (**Figures 1A–C**); when the superior branch is present, it usually curves superiorly and posteriorly and follows the trochlear nerve along the lateral wall of the CS. The distal segment of the trochlear nerve is exclusively supplied by the superior orbital branch of the ILT.

The Abducens Nerve

In all of the specimens studied the proximal third of the abducens nerve (VI), at the level of Dorello's canal, receives blood supply exclusively from the dorsal meningeal artery arising from the MHT. The middle and distal thirds of the

TABLE 1 | The Blood Supply of Intracavernous Cranial Nerves: Microscopic and Endoscopic perspective.

Cranial nerve	Blood supply		Frequency	Transcranial perspective	Endoscopic endonasal perspective
Oculomotor nerve	Proximal segment	Proximal superior branch (ILT)	85%	Lateral wall of the CS	No visible
		Tentorial artery (MHT)	15%	No visible	Posterior compartment of the CS
		Superior lateral trunk	10%	Lateral wall of the CS	No visible
	Distal segment	Superior orbital branch (ILT)	85%	Lateral wall of the CS	No visible
Trochlear nerve	Proximal segment	Proximal superior branch (ILT)	75%	Lateral wall of the CS	No visible
		Tentorial artery (MHT)	25%	Lateral wall of the CS	Superior compartment of the CS
	Distal segment	Superior orbital branch (ILT)	85%	Lateral wall of the CS	No visible
Abducens nerve	Proximal third	Dorsal meningeal artery (MHT)	100%	Posterior wall of the CS	Posterior compartment of the CS
	Middle third	ILT branches	85%	Lateral wall of the CS	Inferior and lateral compartment of the CS
	Distal third	Superior orbital branch (ILT)	85%	Lateral wall of the CS	No visible
Ophthalmic branch	Proximal segment	ILT branches	85%	Lateral wall of the CS	No visible
	Distal segment	Superior orbital branch. (ILT)	85%	Lateral wall of the CS	
Maxillary branch	Proximal segment	ILT branches	85%	Lateral wall of the CS	Lateral compartment of the CS
	Distal segment	Foramen rotundum artery (ILT)	80%	Lateral wall of the CS	
Gasserian ganglion	Medial half	ILT and/or Tentorial artery (MHT)	100%		
	Lateral half	ILT and/or Dorsal branches (MMA)	100%		

CS, cavernous sinus; MHT, meningohypophyseal trunk; MMA, medial meningeal artery; ILT, inferolateral trunk.

abducens nerve are vascularized by branches of the ILT. When the ILT is present, it crosses over the middle third segment of the abducens nerve. This constant relationship between the ILT and the 6^{th} CN is a reliable surgical landmark for the identification of the abducens nerve when performing surgery in this region.

The Trigeminal Nerve

The proximal ophthalmic (V1) and proximal maxillary (V2) segments of the trigeminal nerve are also vascularized by small branches of the ILT or its equivalent in 100% of the specimens. The distal ophthalmic segment of the trigeminal nerve is also supplied by the superior orbital branch of the ILT, while the distal maxillary segment is supplied by the artery of the foramen rotundum, arising from the ILT.

The medial side of the Gasserian ganglion receives its vascularity from the small branches of the ILT and the tentorial artery; the lateral side is supplied by branches from the artery of the foramen rotundum and the dorsal branches of the middle meningeal artery.

All ILT branches end on the inferomedial aspects of the intracavernous CNs. The MHT branches are located in the posterior compartment of the CS. From a transcranial perspective, all intracavernous ICA branches supplying the intracavernous CNs are found in the lateral wall of the CS, except the dorsal meningeal artery, which is located in the posterior wall. From an endoscopic endonasal perspective, the tentorial artery and dorsal meningeal artery are found in the superior compartment and posterior compartment of the CS, respectively. The ILT is found in the lateral and inferior compartments of the CS (**Figures 4A–C**).

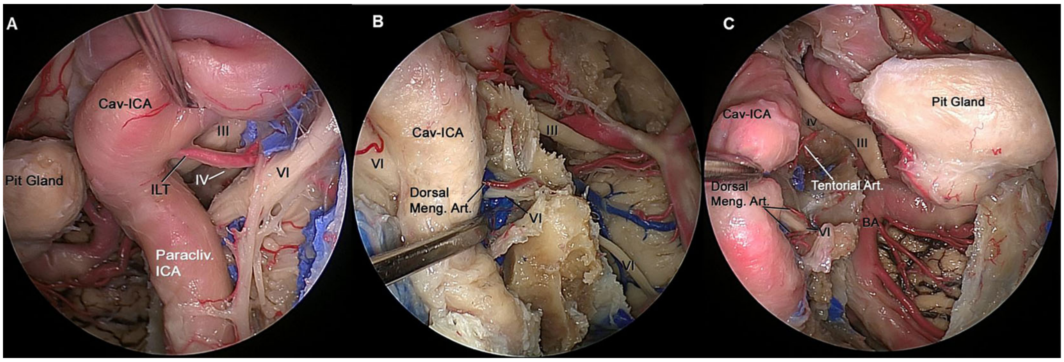

FIGURE 4 | **(A)** Endoscopic view of left CS showing the neurovascular relationships in the lateral compartment. The ILT arising from the midportion of the horizontal segment of the intracavernous ICA, and its branches can be identified running from medial to lateral where they distribute along the lateral wall of the CS and supplies to the of CN III, CN IV and distal CN VI. **(B)** The paraclival ICA is retracted laterally to expose CN VI inside Dorelo's canal. Dorsal meningeal artery (Dorsal Meng. Art.), a branch from MHT, which is located in the posterior compartment of cavernous sinus and supply proximal segment of CN VI at the level of Dorelo's canal. **(C)** Endoscopic view of right CS showing the neurovascular relationships in the superior and posterior compartment of the CS. The Cav-ICA is retracted laterally. The tentorial artery and dorsal meningeal artery can be identified running in the superior and posterior compartment of the CS, respectively. The dorsal meningeal artery supplying proximal segment of CN VI at the level of Dorelo's canal and the tentorial artery supplying the CN IV are shown. BA, Basilar Artery; Cav, Cavernous; CAV-ICA, Cavernous Internal Carotid Artery; CN, Cranial Nerve; Dorsal Meng. Art, Dorsal Meningeal Artery; ICA, Internal Carotid Artery; ILT, inferolateral trunk.

Case Illustrations

A tumor with CS invasion is selected to illustrate the surgical application of these findings.

CS Meningioma

A 43-year-old right-handed male had an initial presentation of right facial numbness. An MRI scan of his brain showed a right CS tumor consistent with a meningioma. The patient underwent stereotactic radiosurgery at an outside hospital. His facial numbness gradually improved. Four years later, he had recurrence of the right facial numbness in the V3 distribution with associated right eyelid ptosis and diplopia. On neurological examination he had decreased sensation to light touch in the three branches of the trigeminal nerve. He had a right eyelid ptosis and a six-nerve palsy. A new MRI scan of the brain showed radiological progression of the tumor (**Figures 5A, B**). An orbitozygomatic craniotomy was performed and gross total tumor resection was achieved. The facial numbness he had preoperatively gradually improved, and his extraocular movements and eyelid ptosis recovered completely. An MRI revealed a gross total resection of the tumor. The histopathology showed a clear cell grade 2 meningioma. Postoperatively He received fractionated radiation therapy to the surgical bed. He remained tumor free at his last follow-up four years after his surgery (**Figures 5C, D**).

DISCUSSION

Lesions involving the CS and lateral sellar region, including tumors, vascular lesions, infections, and inflammatory pathologies have an intimate relationship with the intracavernous CNs and their blood supply originating from the intracavernous ICA. Despite a decrease in the morbidity and mortality rates associated with CS surgery, CN deficits remain the most frequent cause of disability following CS surgery (1–4, 9). In this study we investigate the anatomic variations of the intracavernous CNs blood supply when exposed from a microsurgical transcranial as well as endoscopic endonasal perspectives. This relevant information can be applied or endoscopic and microsurgical approaches of the cavernous sinus.

The underlying mechanisms of intraoperative nerve injury is thought to be multimodal. Although ischemic insults secondary to devascularization of the cavernous segment of the cranial nerves might cause cranial nerve deficits, usually those deficits are transient as the ensuing ischemic insult mainly affects the myelin sheet of the nerve which tends to regenerate within weeks. This is a process similar to what is seen in peripheral nerves that can be extensively dissected and mobilized with minimal or transient nerve dysfunction. In contrast a more proximal, cisternal ischemic injury to the same cranial nerves might also affect their nuclei causing a more permanent deficit. Direct injury to the intracavernous cranial nerves is usually a cause of permanent deficit. Such injuries can be from a direct mechanical trauma or from thermal insults secondary to bipolar coagulation (10, 12, 15). This is where a thorough understanding of the cranial nerves blood supply becomes important as precise control of those vessels during cavernous sinus surgery will preserve a bloodless field and avoid cranial nerve injuries. In order to avoid permanent injury to the CNs, a dissection of the CNs has to be tangential to the nerves along a longitudinal axis. When the CNs are released in this way, they can tolerate a certain amount of manipulation without permanent deficits.

Our findings are in concordance with the study conducted by Krisht et al. (1) and Harris et al. (6) We describe the details of the

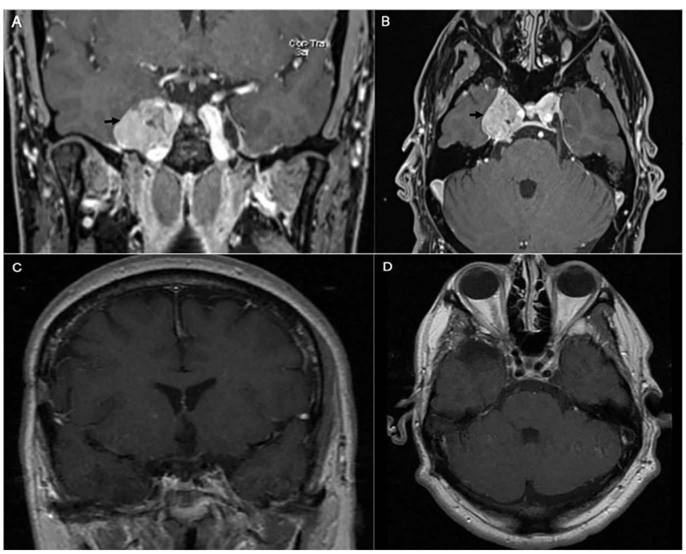

FIGURE 5 | Preoperative coronal **(A)** and axial **(B)** brain MRI with contrast showing heterogeneous enhancing tumor involving the right cavernous sinus (arrow). The patient is known to have right cavernous sinus meningioma for which he had stereotactic radiosurgery 4 years prior to presentation. Postoperative coronal **(C)** and axial **(D)** brain MRI with contrast showing gross total excision of the meningioma.

most common anatomic patterns of blood supply to the intracavernous CNs and observed that the ILT branches play an important role in vascularizing the III, IV, V, and VI CNs as they pass into the CS and the superior orbital fissure, and through the foramen rotundum. Furthermore, we observed that the dorsal meningeal artery branch of the MHT provides blood supply to the proximal third of the abducens nerve at the level of Dorello's canal. The ILT also provides vascularity to the mesial surface of the Gasserian ganglion as it anastomoses with the artery of the foramen ovale, originating from the internal maxillary artery, which in turn provides blood supply to V3 and the lateral aspect of the Gasserian ganglion.

The ILT typically arises from the lateral aspect of the intracavernous ICA and usually supplies the intracavernous CNs, with extensive anastomoses with the extracranial circulation, particularly branches of the IMAX, the middle meningeal artery, and the ophthalmic artery (**Figures 2A, B**). These anastomoses, mainly the superior orbital fissure branch anastomoses with the deep recurrent meningeal branch of the ophthalmic artery, are an important consideration during embolization (16–18).

We also observed that the dorsal meningeal artery (medial branch) arising from the MHT anastomoses with the clival ramus of the jugular branch of the ascending pharyngeal artery (**Figure 2C**).

All ILT trunk branches were located on the inferomedial aspects of the intracavernous CNs; the MHT branches were located on the posterior compartment of the CS. From a transcranial perspective, all intracavernous ICA branches that supplied blood to the intracavernous CNs were found in the lateral wall of the CS, except the dorsal meningeal artery, which was located in the posterior wall. From an endoscopic endonasal perspective, the tentorial artery and the dorsal meningeal artery were found in the superior and posterior compartments of the CS, respectively. The ILT was found in the lateral and inferior compartments of the CS.

Of surgical interest, we observed that each foramen had an artery, which are summarized as follows: the superior orbital branch, which passed through the superior orbital fissure and supplied blood to the distal segments of all of the CNs passing through to it; the artery to the foramen rotundum, another very important vessel, which supplies the V2 segment of the trigeminal nerve; the foramen ovale branch supplies the V3 segment of the trigeminal nerve (**Figure 2A**); and the dorsal meningeal artery, which ran into Dorello's canal and provided blood supply to the abducens nerve within Dorello's canal (**Figure 1**).

Beyond studying the blood supply of CNs in the CS from both transcranial and endoscopic endonasal perspectives the study presented here describes the blood supply to the cisternal III nerve and the anastomoses of the intracavernous ICA's branches with the external carotid artery. In addition, we report for the first time that the superolateral trunk can provide blood supply to the III and IV CNs, as found in 10% of our specimens (**Figures 1A, B**).

Based on the above findings we were able to identify 3 vascular zones to the cranial nerves passing through the cavernous sinus: Zone 1 being the cisternal segment of the

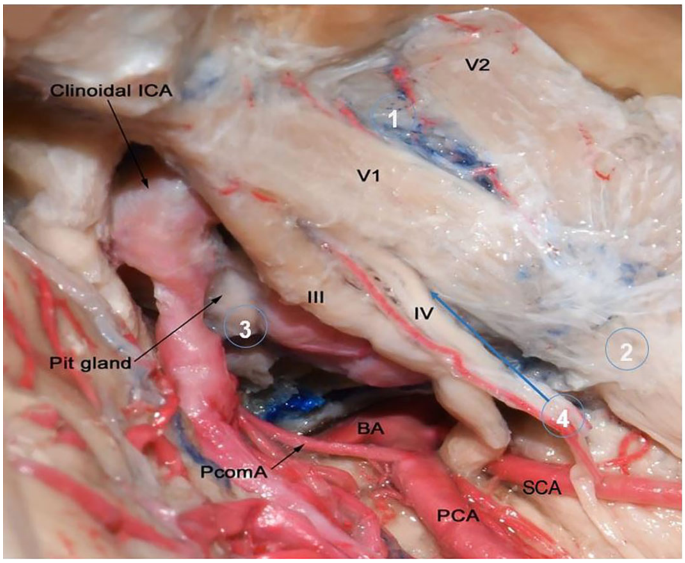

FIGURE 6 | Microscopic lateral view of right cavernous sinus to show the origin of most common tumors that involve the cavernous sinus. Circle number 1 is over the lateral wall of cavernous sinus which is the most common origin of CS meningiomas and they get their blood supply from MHT and ILT (not shown in this image). They account around 41% of all cavernous sinus tumors. Circle 2 is over trigeminal nerve which is the origin of schwannomas. Trigeminal schwannomas are the second most common cavernous sinus tumors and 49% originate in middle cranial fossa (19). They receive their blood supply from MHT and branches from external carotid artery. Circle 3 is over pituitary gland. Pituitary adenomas are the most common tumors that may extend into the cavernous sinus with an incidence of 10%. Their blood supply obtained from superior and inferior hypophyseal arteries. Circle 4 points to intracavernous sinus compartment. Cavernous hemangiomas are benign vascular tumors which are the most common primary intracavernous lesion. Metastasis is also may be seen in intracavernous compartment. Tumors originating from intracavernous compartment may get their blood supply from all intracavernous ICA branches. BA, Basilar Artery; ICA, Internal Cerebral Artery; PCA, Posterior Cerebral Artery; PcomA, Posterior Communicating Artery; Pit, Pituitary; SCA, Superior Cerebellar Artery.

cranial nerves, receiving blood supply from the vertebrobasilar system. Zone 2 being the intracavernous segment of the cranial nerves receiving their blood supply from the internal carotid artery and Zone 3, the extracranial portion of those cranial nerves and receiving blood supply from branches of the external carotid artery. As such Zone 1 of those cranial nerves is most sensitive to ischemic insults and Zones 2 and 3 are more resilient. For these reasons experts recommend avoiding the manipulation of the proximal cisternal segment of the III nerve as it arises from the midbrain of the brainstem as manipulation at this level can cause a permanent deficit.

Certainly, several other anatomic variations may exist in the intracavernous ICA's branch anatomy and the CNs' blood supply, even among patients without CS disease. In addition, tumors involving the CS, once a certain size, may cause significant distortion of the region's microanatomy, posing an additional surgical challenge. Therefore, a detailed understanding of the blood supply of the intracavernous CNs is essential for improving outcomes when operating on lesions involving the CS.

The most common tumor affecting the cavernous sinus is meningioma and accounts for 41% of cavernous sinus tumors (**Figure 6**) (20). It originates from arachnoid cap cells of CNs in the lateral wall of cavernous sinus (21). Blood supply of CS meningiomas are from external carotid artery branches (the same of middle cranial fossa dura blood supply) and branches from MHT and ILT (22, 23). However, meningiomas originating from nearby regions (e.g. petroclival region, medial sphenoid wing) may extend into CS and may have a different blood supply. Other common tumor affecting cavernous sinus is trigeminal schwannomas. They are the second most common intracranial schwannomas after vestibular schwannoma with an incidence of 1-8% of all intracranial schwannomas (19). Trigeminal nerve schwannomas receive their blood supply through MHT or branches from external carotid artery (24). Also, pituitary adenomas are common to invade the CS by extending through its medial wall and 6%-10% of all pituitary adenomas invade the CS (25). They supplied by the medial branches of ICA, namely the superior and inferior hypophyseal trunks.

CONCLUSION

ILT branches provide blood supply to all intracavernous CNs except the proximal segment of the abducens nerve at the level of Dorello's canal. MHT branches supply the proximal segment of the abducens nerve and the medial aspect of the Gasserian ganglion. Middle meningeal artery branches supply the lateral aspect of the Gasserian ganglion. This study demonstrated extensive anastomoses between ILT branches and branches arising from the external carotid artery. Understanding the anatomy of the intracavernous ICA's branches is important to improving surgical outcomes with tumors involving the CS.

DATA AVAILABILITY STATEMENT

The raw data supporting the conclusions of this article will be made available by the authors, without undue reservation.

ETHICS STATEMENT

This study was reviewed and approved by the Ethical Committee at Cleveland Clinic Florida.

AUTHOR CONTRIBUTIONS

EN: data collection, data analysis, writing the manuscript. BI: data collection, data analysis, writing the manuscript. BM: data collection, writing and review the manuscript. AA: writing and review the manuscript. CS: revising the manuscript. MO: contributed to study design, critically revised the manuscript. HB-R: contributed to study design, critically revised the manuscript. BA: study design, supervised the whole study and critically revised the manuscript. All authors contributed to the article and approved the submitted version.

SUPPLEMENTARY MATERIAL

The Supplementary Material for this article can be found online at: https://www.frontiersin.org/articles/10.3389/fonc.2021.702574/full#supplementary-material

REFERENCES

1. Al-Mefty O, Smith RR. Surgery of Tumors Invading the Cavernous Sinus. *Surg Neurol* (1988) 30(5):370–81. doi: 10.1016/0090-3019(88)90200-5
2. Dolenc V. Direct Microsurgical Repair of Intracavernous Vascular Lesions. *J Neurosurg* (1983) 58(6):824–31. doi: 10.3171/jns.1983.58.6.0824
3. Krisht A, Barnett DW, Barrow DL, Bonner G. The Blood Supply of the Intracavernous Cranial Nerves: An Anatomic Study. *Neurosurgery* (1994) 34 (2):275–9. doi: 10.1227/00006123-199402000-00011
4. Fernandez-Miranda JC, Zwagerman NT, Abhinav K, Lieber S, Wangm EW, Snyderman CH, et al. Cavernous Sinus Compartments From the Endoscopic Endonasal Approach: Anatomical Considerations and Surgical Relevance to Adenoma Surgery. *J Neurosurg* (2017) 129(2):430–41. doi: 10.3171/2017.2.JNS162214
5. Dolenc VV, Kregar T, Ferluga M, Fettich M, Mozrina A. Treatment of Tumors Invading the Cavernous Sinus. In: Dolenc VV, editor. *The Cavernous Sinus*. Wien New York: Springer (1987). p. 377–91.
6. Lasjaunias P, Moret J, Manelfe C, Theron J, Hasso T, Seeger J. Arterial Anomalies at the Base of the Skull. *Neuroradiology* (1977) 13(5):267–72. doi: 10.1007/BF00347072
7. Parkinson D, Shields CB. Persistent Trigeminal Artery: Its Relationship to the Normal Branches of the Cavernous Carotid. *J Neurosurg* (1974) 40(2):244–8. doi: 10.3171/jns.1974.40.2.0244

8. Harris FS, Rhoton AL. Anatomy of the Cavernous Sinus. A Microsurgical Study. *J Neurosurg* (1976) 45(2):169–80. doi: 10.3171/jns.1976.45.2.0169
9. Knosp E, Müller G, Perneczky A. The Blood Supply of the Cranial Nerves in the Lateral Wall of the Cavernous Sinus. In: *The Cavernous Sinus*. Vienna: Springer (1987). p. 67–80.
10. Tekdemir I, Tüccar E, Çubuk HE, Ersoy M, Elhan A, Deda H. Branches of the Intracavernous Internal Carotid Artery and the Blood Supply of the Intracavernous Cranial Nerves. *Ann Anat* (1998) 180(4):343–8. doi: 10.1016/S0940-9602(98)80040-X
11. Tran-Dinh H. Cavernous Branches of the Internal Carotid Artery: Anatomy and Nomenclature. *Neurosurgery* (1987) 20(2):205–10. doi: 10.1227/00006123-198702000-00001
12. Willinsky R, Lasjaunias P. Intracavernous Branches of the Internal Carotid Artery. *Surg Radiol Anat* (2005) 9(3):201–15. doi: 10.1007/BF02109631
13. d'Avella E, Tschabitscher M, Santoro A, Delfini R. Blood Supply to the Intracavernous Cranial Nerves: Comparison of the Endoscopic and Microsurgical Perspectives. *Oper Neurosurg* (2008) 62(suppl_5):ONS305–11. doi: 10.1227/01.neu.0000326011.53821.ea
14. Alfieri A, Jho HD. Endoscopic Endonasal Cavernous Sinus Surgery: An Anatomic Study. *Neurosurgery* (2001) 48(4):827–36; discussion 836–7.
15. Aydin S, Cavallo LM, Messina A, Dal Fabbro M, Cappabianca P, Barlas O, et al. The Endoscopic Endonasal Trans-Sphenoidal Approach to the Sellar and Suprasellar Area. Anatomic Study. *J Neurosurg Sci* (2007) 51:129–38.
16. Conti M, Prevedello DM, Madhok R, Faure A, Ricci UM, Schwarz A, et al. The Antero-Medial Triangle: The Risk for Cranial Nerves Ischemia at the Cavernous Sinus Lateral Wall: Anatomic Cadaveric Study. *Clin Neurol Neurosurg* (2008) 110(7):682–6. doi: 10.1016/j.clineuro.2008.04.007
17. Toma N. Anatomy of the Ophthalmic Artery: Embryological Consideration. *Neurol Med Chirurg* (2016) 56(10):585–91. doi: 10.2176/nmc.ra.2015-0324
18. Bertelli E, Regoli M, Bracco S. An Update on the Variations of the Orbital Blood Supply and Hemodynamic. *Surg Radiol Anat* (2017) 39(5):485–96. doi: 10.1007/s00276-016-1776-9
19. Samii M, Migliori MM, Tatagiba M, Babu R. Surgical Treatment of Trigeminal Schwannomas. *J Neurosurg* (1995) 82(5):711–8. doi: 10.3171/jns.1995.82.5.0711
20. Amelot A, van Effenterre R, Kalamarides M, Cornu P, Boch AL. Natural History of Cavernous Sinus Meningiomas. *J Neurosurg* (2018) 1:1–8. doi: 10.3171/2017.7.JNS17662
21. Kehrli P, Maillot C, Wolff Quenot MJ. Sheaths of Cranial Nerves in the Lateral Wall of the Cavernous Sinus. An Embryological and Anatomical Study. *Neurochirurgie* (1995) 41:403–12.
22. Robinson DH, Song JK, Eskridge JM. Embolization of Meningohypophyseal and Inferolateral Branches of the Cavernous Internal Carotid Artery. *AJNR Am J Neuroradiol* (1999) 20(6):1061–7.
23. Barr JD, Mathis JM, Horton JA. Iatrogenic Carotid-Cavernous Fistula Occurring After Embolization of a Cavernous Sinus Meningioma. *AJNR Am J Neuroradiol* (1995) 16(3):483–5.
24. Abramowitz J, Dion JE, Jensen ME, Lones M, Duckwiler GR, Viñuela F, et al. Angiographic Diagnosis and Management of Head and Neck Schwannomas. *AJNR Am J Neuroradiol* (1991) 12(5):977–84.
25. Cottier JP, Destrieux C, Brunereau L, Bertrand P, Moreau L, Jan M, et al. Cavernous Sinus Invasion by Pituitary Adenoma: MR Imaging. *Radiology* (2000) 215(2):463–9. doi: 10.1148/radiology.215.2.r00ap18463

Conflict of Interest: The authors declare that the research was conducted in the absence of any commercial or financial relationships that could be construed as a potential conflict of interest.

ORIGINAL RESEARCH
published: 03 December 2021
doi: 10.3389/fonc.2021.740410

Reinvestigating Tumor–Ventricle Relationship of Craniopharyngiomas With Predominantly Ventricular Involvement: An Endoscopic Endonasal Series Based on Histopathological Assessment

Jun Fan[†], *Yi Liu*[†], *Chaohu Wang*[†], *Zhanpeng Feng*, *Jun Pan*, *Yuping Peng*, *Junxiang Peng*, *Yun Bao*, *Jing Nie*, *Binghui Qiu* and *Songtao Qi*[*]

Department of Neurosurgery, Nanfang Hospital, Southern Medical University, Guangzhou, China

Objective: Craniopharyngiomas (CPs) predominantly involving the third ventricle were commonly termed "intraventricular" lesions. The aim of this study was to clarify the anatomical relationship between the tumor and the third ventricle by both surgical and histological investigation.

Methods: A retrospective review of primarily resected CPs by endoscopic endonasal surgery was performed. CPs with predominantly ventricular involvement were selected for study inclusion by preoperative imaging. The surgical procedure of each case was reviewed. The wholly removed tumor specimens were histologically analyzed, in all cases, to investigate the tumor–third ventricle relationship using hematoxylin and eosin, immunochemical, and immunofluorescence staining.

Results: Twenty-six primary CPs predominantly involving the third ventricle were selected from our series of 223 CPs treated by endoscopic endonasal surgery between January 2017 and March 2021. Gross-total resection was achieved in 24 (92.3%) of 26 patients, with achievement of near-total resection in the remaining patients. A circumferential layer of stretched third ventricle floor was identified surrounding the tumor capsule, which could be peeled off easily from the ventricle floor remnants at most areas of the plane of tumor attachment. Some portions of the tumor capsule tightly adhered to the third ventricle floor were removed together with the floor. A breach of various size was observed at the third ventricle floor after tumor removal in most cases, the floor remaining intact in only two cases (7.7%). Histological examination on marked portions of tumor capsule showed that the pia mater was frequently detected at most of the tumor–brain interface, except at the antero-frontal border of tumor contacting with the third ventricle floor. At this point, a layer of gliosis with various thickness was observed between the tumor and the neural tissue of the third ventricle floor.

Edited by:
*Xicai Sun,
Fudan University, China*

Reviewed by:
*Hermann Lothar Mueller,
Klinikum Oldenburg, Germany
Jose Maria Pascual,
Hospital Universitario La Princesa, Spain
Xiaobiao Zhang,
Fudan University, China*

***Correspondence:**
*Songtao Qi
nfsjwk@gmail.com*

[†]*These authors have contributed equally to this work*

Specialty section:
This article was submitted to Surgical Oncology, a section of the journal Frontiers in Oncology

Received: *13 July 2021*
Accepted: *29 October 2021*
Published: *03 December 2021*

Citation:
Fan J, Liu Y, Wang C, Feng Z, Pan J, Peng Y, Peng J, Bao Y, Nie J, Qiu B and Qi S (2021) Reinvestigating Tumor–Ventricle Relationship of Craniopharyngiomas With Predominantly Ventricular Involvement: An Endoscopic Endonasal Series Based on Histopathological Assessment. Front. Oncol. 11:740410. doi: 10.3389/fonc.2021.740410

Conclusion: CPs with predominantly ventricular involvement should be considered as lesions with an extraventricular, epi-pia topography rather than “intraventricular” or “subpial” topography. Accurate understanding of the relationship between the third ventricle and such tumors would predict the circumferential cleavage plane of dissection, and remind neurosurgeons of performing dissection along the safe surgical plane to achieve total tumoral resection with minimizing hypothalamic damage.

Keywords: craniopharyngioma, endonasal, endoscopic, histology, intraventricular, pituitary surgery, third ventricle

INTRODUCTION

Craniopharyngiomas (CPs) are benign tumors believed to originate from ectodermal remnants of the craniopharygeal duct, accounting for 2% to 5% of all intracranial tumors (1). These tumors may arise at any point along the hypothalamus–pituitary axis, intrasellar or suprasellar (2, 3). CPs predominantly involving the third ventricle remain among the most challenging to form a surgical perspective due to their upward extension against the third ventricle and their close relationship with the hypothalamus. An accurate understanding of the topographical relationships between the CPs and the third ventricle floor/hypothalamus is essential for proper, safe surgical planning or manipulation.

CPs predominantly involving the third ventricular compartment were commonly described as “intraventricular” or “third ventricle” lesions in most publications, and these tumors were thereby classified into “intraventricular” subset by many authors in their classification system (4–14). Since the term “intraventricular” specifically denote lesions that arise from the brain parenchyma and grow exophytically into the ventricular system, “intraventricular” CPs were thought to originally develop within the neural tissue of the third ventricle floor and progressively grow into the third ventricle leaving an intact third ventricle floor below (15, 16). However, the theory is in conflict with the universally accepted hypothesis that CPs arise from ectodermal remnants of the craniopharygeal duct. On the other hand, previous classification systems including the “intraventricular” subset of CPs were established based on tumor–third ventricle relationships observed on autopsies, surgical procedures, and/or neuroradiological studies (7, 11, 17, 18). Accurate histological evidence of the CP boundaries contacting the third ventricle floor and the third ventricle walls is lacking in most reports on intraventricular CPs to unequivocally define the strict “intraventricular” category.

Endoscopic endonasal surgery use a corridor along the hypothalamic–pituitary axis and allows direct visualization of retrochiasmatic compartment, especially for the ventral area of the third ventricle (17, 19, 20). Accordingly, this approach provides more precise information for illuminating the tumor–third ventricle relationships than traditional microscopic transcranial approach. In this series, we retrospectively reviewed surgical procedures of CPs with predominantly ventricular involvement by endoscopic endonasal approach, and made comprehensive histological evaluation of tumor–third ventricle interface on these tumors. The aim of this study is to reveal the real relationships between the tumor and the third ventricle with more convincing evidence, and to provide useful information for neurosurgeons when managing such tumors with appropriate surgical planning and minimizing the risk of damage to the hypothalamus.

MATERIALS AND METHODS

Patient Selection and Perioperative Assessment

All patients with CPs treated by endoscopic endonasal surgery at our institution between January 2017 and March 2021 were retrospectively reviewed. Patients with recurrent tumors and/or who underwent radiotherapy were excluded to avoid incorrect identification of the tumor–ventricular relationship. Preoperative imaging was reviewed in each case to evaluate the location and growth pattern of the tumor in determining the potential for study inclusion. According to our QST classification based on tumor origin as reported previously (21, 22), all tumors were classified into three types: infrasellar/subdiaphragmatic CPs (Q-CPs), subarachnoidal CPs (S-CPs), and pars tuberalis CPs (T-CPs). Confirmation of a CP with predominantly ventricular involvement was then performed by concordant assessment of three senior neurosurgeons. According to the criteria described in previous publications (2, 4, 8, 9, 14), the tumor was characterized as a CP with predominantly ventricular involvement if its main body occupy the compartment of the third ventricle on preoperative imaging, above an identifiable, almost or partially intact pituitary stalk, with or without the lower pole of the tumor slightly extending into the suprasellar area (**Figures 1A**, **2A**, **3A**, **4H**).

All data were collected from a prospectively maintained database. Each enrolled patient’s clinical chart was studied to categorize age, gender, presenting symptoms, imaging data, and surgical outcomes (**Table 1**). The tumor size was determined by the maximum diameter on preoperative sagittal or coronal MRI. Tumor consistency (solid, cystic, or mixed) was also identified on preoperative MRI. Extent of resection was determined by immediate MRI review within 48 h after surgery by an independent neuroradiologist. Accordingly, gross total resection (GTR) was defined as 100% macroscopic tumor resection, near-total resection (NTR) was defined as ≥95% but <100% resection, subtotal resection (STR) was defined as ≥80% but <95% resection, and partial resection was defined as <80% resection.

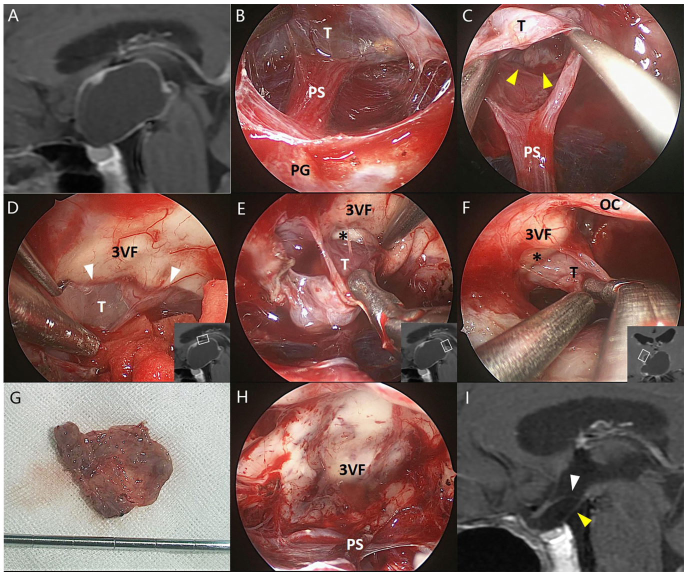

FIGURE 1 | Illustrative endonasal case 1 clarifying the tumor–ventricle relationship. In **(A)**, preoperative MRI shows that the CP mainly occupies the third ventricle chamber. In **(B)**, intraoperative photograph indicates the intact pituitary stalk beneath the tumor. In **(C)**, a clear plane of dissection (yellow arrowhead) was identified at the tumor–infundibulum interface. In **(D)**, the top portion of the tumor was easily stripped away from the third ventricle floor through a cleavage pial plane (white arrowhead). In **(E, F)**, the pia mater was absent at some areas of the tumor–ventricle interface (asterisk) while a safe plane of surgical dissection could still be identified to perform the total tumoral resection without trespassing the third ventricle floor. In **(G)**, the tumor was removed en bloc after circumferential dissection. In **(H)**, the third ventricle floor as well as the pituitary stalk remained intact without any defect after total tumoral removal, suggesting the extraventricular rather than the "intraventricular" topography of such tumors. In **(I)**, postoperative MRI confirms the total removal of the tumor and the integrity of the third ventricle floor (white arrowhead) and the pituitary gland (yellow arrowhead). 3VF, the third ventricle floor; OC, optic chiasm; PG, pituitary gland; PS, pituitary stalk; T, tumor.

Surgical Procedure

The surgical procedure of each individual CP case was recorded by HD video and carefully reviewed after dura opening, focusing on the dissection of the tumor–brain interface. A standard endoscopic endonasal transtuberculum approach was used for tumor resection in all cases as described elsewhere. A thin translucent membrane formed by the stretched par tuberalis can be found overlying the tumor. Careful dissection and preservation of the membrane is essential to maintain the continuity of the hypothalamus–pituitary axis to maximize the possibility of recovery of postoperative hormonal function. Therefore, a longitudinal incision along the infundibulum was made in the membrane, and gentle dissection was then performed between the tumor and the membrane.

Tumors with cystic component were emptied before resection to gain better exposure and sufficient manipulating space. For large purely solid lesions, the decompressive intratumor debulking was necessary while the intact tumor capsule should be preserved. A combination of blunt and sharp extracapsular dissection was then performed to dissect the tumor away from the third ventricle floor/hypothalamus. During the dissection, the interface between the tumor and the third ventricle was carefully identified under the close-up endoscopic visualization, in an effort to maximally preserve the integrity of the third ventricular floor/hypothalamus and minimize the risk of leaving unnoticed tumor remnants behind. Finally, the surgical cavity was examined using angled endoscope after tumor removal to evaluate the integrity of the third ventricular floor/hypothalamus, and further validate tumor–third ventricle relationships.

Histopathologic Assessment

The wholly removed tumor specimens of each case were sent for histological evaluation to identify the pathological type and investigate the tumor–third ventricle relationships. For the tumor area with dense adhesions to the third ventricular floor and unlikely to be separated from each other, the involved tissue of the third ventricle floor was removed with the tumor to ensure complete resection. As described in our previous studies, the different portions of tumor capsule in contact with the third ventricle were marked during surgery, and each marked specimen was histologically examined separately to provide a comprehensive synthesis of overall information regarding the relationships between the tumor and third ventricle.

H&E, immunochemical, and immunofluorescence staining were performed as described previously (22, 23). The antibodies used were Neurofilament (NF) (1:400, Abcam, ab7794), Glial Fibrillary Acidic Protein (GFAP) (1:200, Abcam, ab7260); pan Cytokeratin (Pan-CK) (1:300, Abcam, ab215838), Laminin β1 (1:400, Sigma, MAB1921P), CK5/6 (1:400, Sigma, SAB5600242), and Oxytocin (OXT) (1:400, Abcam, ab212193). NF was selected to mark the axon of neuron; GFAP was used to mark the gliosis; Pan-CK and CK 5/6 were used to mark the tumor; Laminin β1 was used to mark the pia mater; OXT was used to mark the secretion and transport of oxytocin in the hypothalamus.

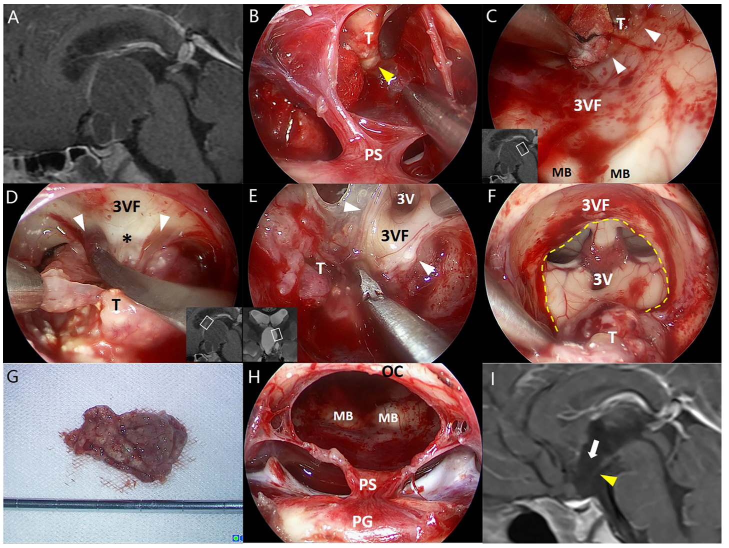

FIGURE 2 | Illustrative endonasal case 2 clarifying the tumor–ventricle relationship. In **(A)**, a CP with predominantly ventricular involvement was identified on preoperative MRI. In **(B)**, the thin layer of pars tuberalis was incised longitudinally and careful dissection was performed along the tumor–infundibulum interface (yellow arrowhead) to preserve the continuity of the stretched pituitary stalk. In **(C)**, a cleavage pial plane (white arrowhead) ensured the successful dissection of the tumor and the integrity of adjacent third ventricle floor remained. In **(D)**, the pia mater was absent at some areas of the tumor–ventricle interface, while a layer of reactive gliosis (asterisk) could provide a safe cleavage plane for surgical dissection instead. In **(E)**, a clear boundary between the tumor and the third ventricle floor was observed at the lateral folder of the third ventricle, although partial remnants of the third ventricle floor was removed with the tumor due to the dense adhesion. In **(F)**, most portions of the tumor capsule were dissected with an opening left at the third ventricle floor (dashed line). In **(G)**, the tumor was removed en bloc after dissection. In **(H)**, the stretched thin layer of the pituitary stalk was mostly preserved after tumor removal. In **(I)**, postoperative MRI reveals the defect of anterior third ventricle floor (white arrow) and the stretched thin pituitary stalk (yellow arrowhead). 3V, the third ventricle; 3VF, the third ventricle floor; MB, mamillary body; OS, optic chiasm; PG, pituitary gland; PS, pituitary stalk; T, tumor.

RESULTS

Patient and Tumor Characteristics

During the period from January 2017 to March 2021, a total of 223 patients with CPs underwent resection by endoscopic endonasal surgery. Of these, 78 patients with recurrent tumor and/or radiotherapy were excluded from the analysis. Accordingly, 145 patients with primary CPs were classified into three subtypes according to QST classification: 46 patients were identified with Q-CPs, 23 with S-CPs, and 76 with T-CPs. Among the 76 patients with T-CPs, 26 (34.2%) identified to have CPs with predominantly ventricular involvement were enrolled in this study. A mostly intact pituitary stalk above the tumor could be identified in 15 cases (57.7%) on preoperative sagittal or coronal MRI. The average age of the patients was 46.3 ± 14.2 years (range 2–73 years), and 11 (42.3%) of the patients were female. The maximal tumor diameter on preoperative MR images averaged 37 mm (range 15–57 mm). In regard to consistency, mixed (solid-cystic) tumors were noted in 17 cases (65.4%), purely cystic in 6 cases (23.1%), and purely solid in 3 cases (11.5%), respectively.

Surgical Findings

GTR was achieved in 24 of 26 patients (92.3%), and NTR was noted in the remaining 2 patients. During the dissection of the tumor capsule, a circumferential, easily recognizable layer of stretched third ventricle floor was always detected surrounding the tumor. In most areas of the tumor–brain interface, the tumor capsule was usually easy to strip away from the third ventricle floor/hypothalamus upon a clear plane of the pia mater or gliosis. By contrast, in some areas (mostly at the central area) of the tumor–brain interface, it is difficult to remove the tumor capsule without trespassing the ventricle floor due to extremely thin floor and/or dense adhesion. Therefore, the tightly adhered portions of the tumor were removed together with adjacent third ventricle floor, leaving an opening with various size at the floor in most cases (**Figures 1–3**). Only two patients (7.7%) with moderate tumor size had the intact third ventricle floor after tumor removal. The infundibulum was mostly preserved with pituitary–hypothalamus continuity in 12 patients (46.1%), partially preserved in 8 patients (30.8%), and sacrificed in 6 patients (23.1%) due to extremely thin fiber remnants.

Histopathological Results

According to pathological reports, adamantinomatous CPs were the predominant type, noting in 21 cases (80.8%). H&E and immunofluorescence staining on marked portions of tumor capsule involving third ventricle showed that the pia matter was frequently detected at most of the tumor–brain interface, except at the antero-basal border of tumor contacting with the third ventricle floor, which is often near the presumed site of tumor origin. In this situation, a layer of gliosis with various thickness was instead observed between the tumor and the neural tissue of the third ventricle floor (**Figures 4–6**).

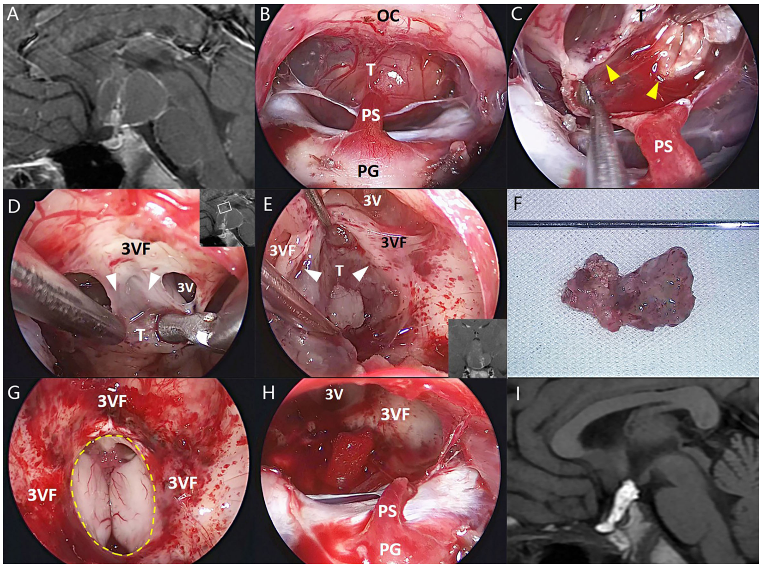

FIGURE 3 | Illustrative endonasal case 3 clarifying the tumor–ventricle relationship. In **(A)**, preoperative MRI shows a tumor with predominantly ventricular development above the pituitary stalk. In **(B)**, intraoperative photograph indicates the mostly intact pituitary stalk beneath the tumor. In **(C)**, the surgical dissection was performed along a clear tumor–infundibulum interface (yellow arrowhead). In **(D, E)**, a non-functional layer of reactive gliosis between the tumor and the third ventricle floor without leptomeningeal tissue (white arrowhead) was used in this case as a safe plane of dissection, although it is difficult to remain the integrity of the third ventricle floor at some areas associated with extremely stretched thin ventricular floor or tight attachment. In **(F)**, the tumor was removed en bloc after dissection. In **(G, H)**, a moderate defect of the third ventricle floor (dashed line) and the remnants of the stretched pituitary stalk were preserved after tumor removal. In **(I)**, postoperative MRI demonstrates the total tumor removal, and the hyperintense T1 signal represents the fat used for skull base reconstruction. 3V, the third ventricle; 3VF, the third ventricle floor; OS, optic chiasm; PG, pituitary gland; PS, pituitary stalk; T, tumor.

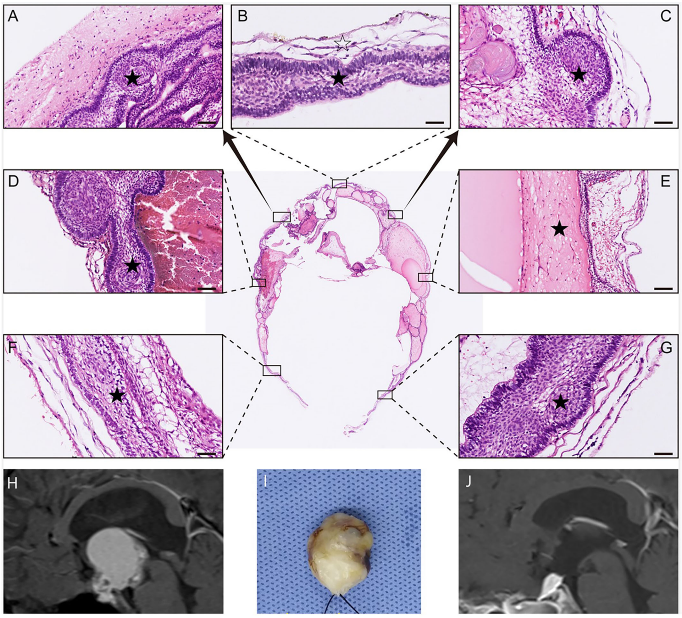

FIGURE 4 | Histological examination of a remodeling tumor with mainly ventricular involvement. In **(A–G)**, multiple portions of the tumor sample were stained with HE for histopathological examination. The result of HE staining shows that the whole tumor (black pentagram) was resected along either a dense band of gliosis or some membranous structures (white pentagram). In **(H)**, preoperative MRI indicates the tumor primarily involves the third ventricle. In **(I)**, the photograph showed the gross appearance of the remodeling tumor by packing with cotton after an en bloc tumor removal. In **(J)**, postoperative MRI demonstrates the total tumoral resection, and the hyperintense T1 signal represents the fat used for skull base reconstruction.

TABLE 1 | Clinical chart of each enrolled patients.

Case No.	Age (years), Sex	Preoperative Presentation				Surgical Outcomes			Postoperative Outcomes		
		Symptoms	Hypothalamic Disturbance	Tumor Size* (mm)	Tumor Consistency	Histological Type	EOR	Defect of 3VF	Follow-up (months)	Hypothalamic Status	Recurrence
1	41, F	HA, HP	No	23	Mixed	AD	GTR	Yes	27	Unchanged	No
2	38, F	VD	No	37	Cystic	AD	GTR	Yes	24	Worsened	No
3	41, F	HA, HP	Yes	42	Mixed	AD	GTR	Yes	17	Unchanged	No
4	16, M	HP	No	25	Mixed	AD	GTR	Yes	3	Unchanged	No
5	63, F	HA	No	15	Mixed	AD	GTR	Yes	15	Unchanged	No
6	48, M	VD	No	38	Cystic	PAP	GTR	No	54	Unchanged	No
7	33, M	HA, DI	Yes	47	Mixed	AD	GTR	Yes	9	Worsened	No
8	2, F	HA	Yes	28	Mixed	AD	GTR	Yes	36	Worsened	No
9	53, M	VD	Yes	43	Mixed	AD	GTR	Yes	47	Unchanged	No
10	50, M	HP	No	28	Mixed	AD	GTR	Yes	24	Unchanged	No
11	55, M	HA	No	19	Cystic	PAP	GTR	Yes	35	Unchanged	No
12	61, F	VD	No	51	Mixed	AD	GTR	Yes	7	Unchanged	No
13	47, F	HA, VD	Yes	57	Mixed	AD	NTR	Yes	11	Unchanged	Yes
14	52, M	HA, VD, HP	No	46	Cystic	AD	GTR	Yes	5	Worsened	No
15	57, M	HA	Yes	48	Solid	PCP	GTR	Yes	28	Improved	No
16	48, F	HA	No	35	Mixed	AD	GTR	Yes	45	Unchanged	No
17	73, M	HA	No	36	Mixed	AD	GTR	Yes	22	Worsened	No
18	45, M	VD	Yes	42	Solid	PAP	GTR	Yes	27	Improved	No
19	45, F	VD	No	45	Mixed	AD	GTR	Yes	32	Unchanged	No
20	29, F	HA	No	33	Mixed	AD	GTR	Yes	28	Worsened	No
21	55, M	HA	Yes	37	Cystic	AD	GTR	Yes	36	Improved	No
22	54, M	VD, HP	No	39	Mixed	AD	NTR	Yes	24	Worsened	No
23	47, M	HA	No	28	Mixed	AD	GTR	Yes	21	Unchanged	No
24	44, F	HA	No	35	Solid	PAP	GTR	No	33	Unchanged	No
25	49, M	VD	Yes	48	Cystic	AD	GTR	Yes	9	Worsened	No
26	58, M	VD, HP	No	39	Mixed	AD	GTR	Yes	10	Worsened	No

3VF, the third ventricle floor; AD, adamantinomatous; DI, diabetes insipidus; EOR, extent of resection; GTR, gross total resection; HA, headache; HP, hypopituitarism; NTR, near-total resection; PAP, papillary; VD, visual deterioration.
**The tumor size was determined by the maximum diameter on preoperative sagittal or coronal MRI.*

Collectively, three morphological patterns between the tumor and the third ventricle floor were noted in this series: (1) the moat-like pattern, in which the pia matter was intact at the tumor–brain interface and a gap was found between the tumor and the pia mater; (2) the beach-like pattern, in which there existed a continuous smooth plane between the tumor and the ventricle floor without any gap, and the intact pia mater was still detected at the tumor–ventricle interface; and (3) the finger-like pattern, in which the tumor formed finger-like structures that invaded the third ventricle floor, with the absence of the pia mater and the development of reactive gliosis between the tumor and the neural tissue of the third ventricle floor (**Figure 7**).

DISCUSSION

Study Inclusion

CPs predominantly involving the third ventricle are not common while posing the greatest surgical challenge of all CPs due to their intimate anatomical and functional relationships with the hypothalamus. In the late 1920s, Cushing first realized that some CPs had an "intraventricular" position (24). In 1985, Steno (25) demonstrated an "intraventricular" subset among suprasellar CPs by stereoscopic and microscopic investigation in 30 autopsies. Since then, the term "intraventricular" was widely used by many authors as a subset of CPs in their classification schemes. Yasargil et al. (13) classified CPs into five subtypes in their surgical series of 144 cases and type f was assigned to define "purely intraventricular" CPs, which was described as "lying within the third ventricle". Kassam et al. (7) described tumors isolated to the third ventricle as "intraventricular" (type IV) CPs in their surgical series using an endoscopic endonasal approach. Pascual et al. (26) analyzed 130 CPs previously described as "intraventricular" in various publications, and further recategorized four subtypes: (1) "strictly intraventricular", (2) "not strictly intraventricular", (3) "secondarily intraventricular", and (4) "pseudointraventricular". In categorizing the tumors in this paper, tumors predominantly occupying the compartment of the third ventricle that satisfied the Pascual criteria of "strictly intraventricular" and "not strictly intraventricular" were selected for study inclusion, which is consistent with Forbes et al.'s study (6). According to our QST classification, the enrolled 26 cases belonged to the subset of T-CPs, which were presumed to arise in the top of the par tuberalis. The specific originating site should be primarily responsible for the predominantly upper extension of such tumors, and the purpose of this study is to reveal the real relationship between the tumor and the third ventricle floor.

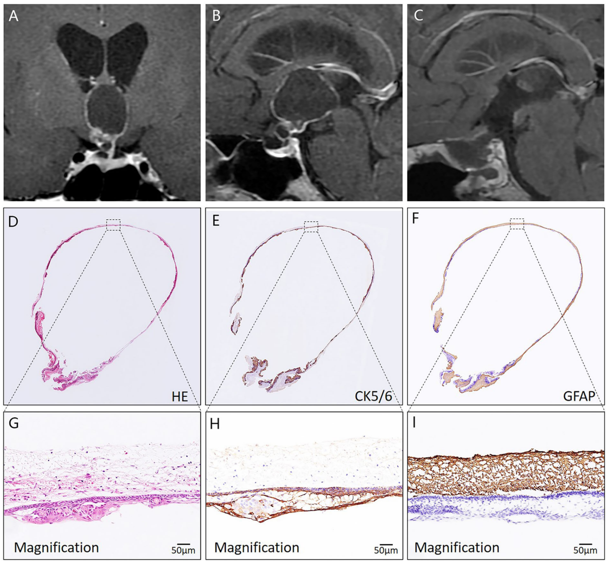

FIGURE 5 | Histological assessment of a CP with predominantly ventricular involvement using HE and immunohistochemical staining. In **(A, B)**, preoperative coronal and sagittal MRI reveals that a cystic-solid mass mainly develops into the compartment of the third ventricle. In **(C)**, postoperative MRI demonstrates complete tumor removal. In **(D–I)**, the pathological image of the tumor specimen indicates that the whole tumor (CK5/6 positive) was resected along a dense band of gliosis (GFAP positive).

Endoscopic Endonasal Surgery for Intraoperative Investigation

In the era of micro-neurosurgery, the basic knowledge regarding the tumor–brain relationship of CPs was mainly established based on microscopic findings. The investigation of the delicate anatomy of the hypothalamic–pituitary axis was limited by poor visualization. During the last two decades, the refinement of the endoscopic endonasal surgery has significantly changed the management of CPs. This approach can provide direct visualization of the retrochiasmatic space and is especially suitable for the exposure of the third ventricle undersurface (17, 19, 20). Additionally, close-up observation provided by endoscope and great advance of visualization technologies allows for gaining more anatomical and detailed information of this intricate area. The CP classification proposed by Kassam et al. (7) in 2008 was established based on the relevant relationship between the tumor and the pituitary stalk observed through the endoscopic transsphenoidal approach, although the visual resolution of endoscopy seemed not satisfactory according to current standard. Despite the controversy regarding the approach selection of "intraventricular" CPs between the transcranial and the endonasal approach, it is undoubted that the latter may provide optimal visualization of the third ventricle floor. Therefore, we intentionally reviewed the surgical procedure of such CPs treated by endoscopic endonasal approach in this series, in an attempt to present more anatomical evidence illuminating the tumor–ventricle relationships compared with traditional microsurgery.

Surgical Findings at the Tumor–Ventricle Interface

Although the tumors appeared to be "intraventricular" on preoperative MRI, a circumferential, well-defined layer of stretched third ventricle floor was always observed surrounding the tumors involving the third ventricle during the surgical dissection. Most portions of the tumor capsule could be easily stripped away from the third ventricle floor along a cleavage plane of the pia mater or the gliosis, except at some points with tight adherence or extremely thin remnants of the stretched third ventricle floor. These points were probably associated with the origin of the tumor. The findings strongly suggest that the

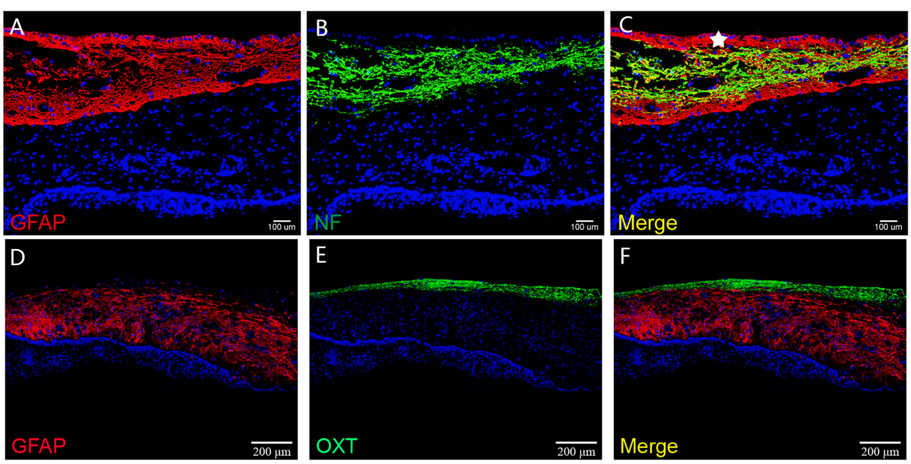

FIGURE 6 | The histological architecture between the tumor and the third ventricular floor. In **(A–F)**, immunofluorescent staining shows a layer of gliosis (GFAP positive) with various thickness between the tumor and the neural tissue of the third ventricle floor. The neural tissue of the third ventricle floor/hypothalamus (NF and OXT positive) can be observed on the outer border of the gliosis. The ependymal cells of the third ventricle (white pentagram) could be found in some samples, which indicated the extraventricular topography of CP.

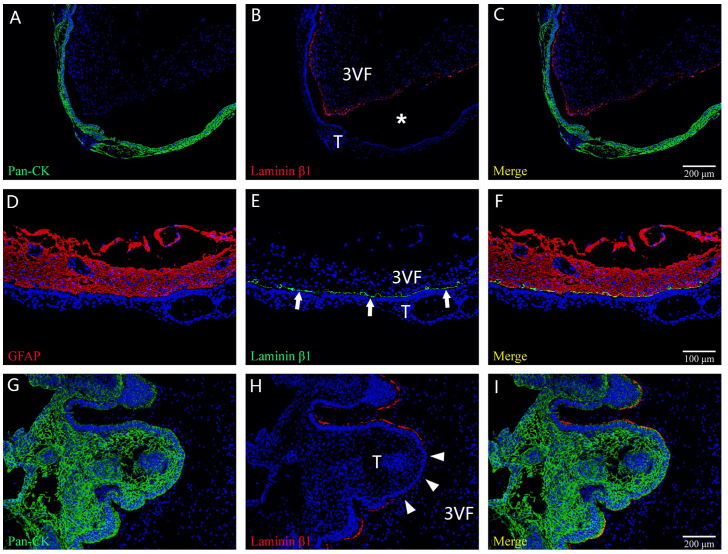

FIGURE 7 | The main histological patterns found for the tumor–ventricle floor interface among tumors with a predominant ventricular involvement. In **(A–C)**, immunofluorescent staining shows a moat-like structure in which a gap (white asterisk) is detected between the tumor and third ventricle floor with the presence of the intact pia mater. In **(D–F)**, immunofluorescent staining indicates a beach-like structure (white arrow) characterized by a smooth boundary at the tumor–ventricle interface without interposed gap, and the pia mater of the third ventricle floor is intact. In **(G–I)**, immunofluorescent staining demonstrates a finger-like structure in which the tumor forms a finger-like bulge in the third ventricle floor, with the absence of the pia mater at some areas (white arrowhead) and the development of gliosis between the tumor and the neural tissue of the third ventricle floor. 3VF, third ventricle floor; T, tumor.

progressive upward growth of the tumor originally developing outside the floor of the third ventricle would cause a circumferential layer of the stretched floor surrounding the tumor and finally occupy the compartment of the third ventricle. Therefore, such tumors should be regarded as having an extraventricular origin instead of a primary intraventricular development. The proposal can be strengthened by the fact that two patients in this series had the intact third ventricle floor after tumor removal (**Figure 1**).

We found that a wide defect of the third ventricle floor after tumor resection occurred more commonly in those cases with large tumor, and an intact or small deficient third ventricle floor was usually observed in the cases with papillary CPs, suggesting that the extent of ventricular floor preservation may be related to tumor size and pathological type. Adamantinomatous CPs seemed more likely to cause tight adhesion between the tumor and the third ventricle floor/hypothalamus. Some authors observed that the defect left in the floor of the third ventricle after tumor removal did not necessarily correlate to iatrogenic hypothalamic injury (27). The possible explanation is that the functional hypothalamic nucleus was displaced bilaterally with the progressive growth of the tumor, leaving a nonfunctional tissue layer of the third ventricle floor overlying the dome of the tumor.

Histological Relationships Between the Tumor and the Third Ventricle

Among the ill-defined category of "intraventricular" CPs, a group of infundibulo-tuberal lesions were previously characterized as those replacing the third ventricular floor, above an identifiable, almost intact pituitary stalk, and whole mass is occupying partial or the entire third ventricle chamber (11, 18). CPs with such a topography were thought to originate within the neural tissue of the third ventricle floor and then progressively grow into the ventricle cavity (15, 16). The above conclusive demonstration on the topographical relationships of tumors with the third ventricle were established on basis of numerous previously reported necropsy or pathohistological studies (11). In these studies, most of intraoperative tumor specimens were obtained *via* piecemeal resection, and more importantly, the accurate investigation regarding the components of multiple layers of tissue in contact with tumors was absent. Therefore, previous evidence was inadequate to support the address of "intraventricular" or "subpial" topography of such CPs. In this series, we used H&E and immunochemical/immunofluorescent staining to precisely identify different layers of tissue in contact with tumors in histological samples taken from wholly removed lesions. We believed that it may provide a more explicit and powerful evidence for investigating the real tumor–ventricle relationships of CPs with predominantly ventricular involvement.

Our histological results revealed that the pia mater was detected overlying most of the tumor–brain interface in the tumors predominantly involving the third ventricle, regardless of tumor size or tomography. The pia mater may be absent at some areas of the interface, while a layer of reactive gliosis with various thickness was instead observed between the tumor and the neural tissue of the third ventricle floor, which is consistent with previous descriptions (18, 28–30). Moreover, a thin layer of neural tissue and ependyma was also identified on the outer border of the gliosis. Early in 1904, Erdheim also observed a thin layer of stretched neural tissue corresponding to the remnant of the third ventricle floor enveloping circumferentially the tumor in his cadaveric study of a patient with CPs apparently strictly confined within the third ventricle (31, 32). Our findings further confirmed that several layers of tissue constituting the floor of third ventricle covers the dorsal aspect of the CPs with ventricular involvement, and such tumors should not be defined as "intraventricular" lesions.

According to the literature (3, 31, 33), CPs involving third ventricle are presumably originated from nests of epithelial cells incorporated or derived from metaplastic transformation of glandular cells of the pars tuberalis of the pituitary gland. The reason for predominantly ventricular development of these tumors remains unknown. Ciric and Cozzens (34) attributed it to the tumor origin within the neural tissue of the third ventricle floor before the formation of the leptomeningeal layer of arachnoid–pia mater. However, the theory cannot explain the fact observed in our histological investigation that the main body of the tumors was located outside the pia mater of the third ventricle floor. Interestingly, in our previous surgical cases of CP involving the third ventricle, bundles of dense arachnoid trabeculae were frequently observed surrounding the infundibulo-tuberal area, which tends to form a firm barrier preventing the tumor from extending ventrally. Aguado et al. (35) also described in their study that the pars tuberalis is perforated by subarachnoid channels. Therefore, we postulate that the predominantly intraventricular development of such tumor may be associated with its originating site at the uppermost area of the pars tuberalis combining dense trabecular barrier at the point of infundibulo-tuberal area. Nevertheless, further evidence regarding the relationship between the characteristics of arachnoid trabeculae and the tumor genesis is required to validate the hypothesis.

Three morphological relationships of the tumor to the third ventricular floor based on histological assessment were summarized in this series: moat-like, beach-like, or finger-like. The moat-like and beach-like patterns had intact pia mater and could provide a clear cleavage plane of dissection, in which the integrity of the third ventricle floor/hypothalamus was expected to be achieved after tumor resection. For the finger-like pattern, a band of reactive gliosis with various thickness instead of the pia mater separated tumor from the neural layer of the third ventricle floor. The tight tumoral adherence at some areas was thought to be related to the lack of a leptomeningeal layer separating the neural tissue from the tumor wall, and a reactive gliosis layer will develop between the lesion and the hypothalamic nuclei during the progressive tumor development (10, 30).

The functionality of the layer overlying the dome of CPs with predominantly ventricular involvement remains controversial. Some authors warned about the risk of trespassing this still viable layer through a transventricular or a translaminar terminalis approach, while others affirmed the nonfunctional gliotic nature of such tissue, which provides a safe cleavage plane for surgical dissection of the lesion (11, 27). According to our histological assessment, the pia mater or gliosis layer separated the tumor from neural tissue of the third ventricle floor and may provide a safe dissection plane for most tumors. However, at some areas with thin gliosis layer, it is difficult to remove the tumor without trespassing the adjacent neural tissue due to the extreme thinness of the third ventricle floor and the dense adhesion in between.

Multiple factors, including the heterogeneity of the reactive gliosis, the thickness of the stretched ventricular floor, the adhesiveness of tumor interface, and possible displaced hypothalamic nuclei, were associated with the difficulty of tumor dissection and high risk of damaging the adjacent functional neural tissue. Landolt (36) found in his electron microscopic study on the boundaries of CPs that the basal membranes of epithelial and reactive glia were separated by a few collagen fibers, providing a safe cleavage plan of dissection for neurosurgeon. However, the gliosis boundary had a heterogeneous, variable thickness even in the same tumor, and the existence of a gliosis layer separating the tumor from hypothalamus could not guarantee the safety of surgical dissection. Taken together, three possibilities may occur during surgical dissection, the presence of an easily dissectible plane separated by the pia mater, an identifiable functionless interface composed of thick reactive gliosis, or the lack of a safe manipulable cleavage plane associated with the extremely thin gliosis layer and dense adhesion.

Prevention of hypothalamic injury remains as the neurosurgeon's principal concern during removal of CPs with predominantly ventricular involvement. Awareness of not real "intraventricular" nature histologically for these lesions would predict that the cleavage plane of dissection will be circumferential surrounding the tumor, and remind neurosurgeons of carefully identifying the plane and performing delicate dissection along the safe surgical plane of the tumor–ventricle interface, instead of the "blind" pulling of the tightly adhered portions of the tumor. In other words, the surgical and histological findings in this study regarding the tumor–third ventricle floor relationship in CPs with predominantly ventricular involvement could provide theoretical evidence for the attempt of total tumor resection while minimizing the risk of hypothalamic injury.

CONCLUSION

CPs with predominantly ventricular involvement were separated from the third ventricle floor by the intact pia mater at most of the tumor–brain interface. Histologically, these tumors should not be considered as "intraventricular" or "subpial" lesions. The pia mater could be absent at some areas where a layer of reactive gliosis with various thickness developed instead between the tumor and the neural tissue of the third ventricle floor. On the basis of surgical and histological results, we postulated that these tumors originate from the top of par tuberalis, then develop a progressive growing dorsally, which would cause a circumferential layer of the stretched third ventricle floor surrounding the tumor, and finally occupy the third ventricle chamber. Awareness of not real "intraventricular" nature histologically for these lesions would predict the circumferential cleavage plane of dissection surrounding the tumor, and remind neurosurgeons of performing delicate dissection along the safe surgical plane of the tumor–ventricle interface to achieve total tumoral resection with minimized risk of hypothalamic damage.

DATA AVAILABILITY STATEMENT

The original contributions presented in the study are included in the article/supplementary material. Further inquiries can be directed to the corresponding author.

AUTHOR CONTRIBUTIONS

Conception and design: JF and YL. Acquisition of data: YL, YB, ZF, JN, BQ, and JPe. Analysis and interpretation of data: YL and CW. Histopathological assessment: YL and CW. Drafting the article: JF. Critically revising the article: JF. Reviewed submitted version of manuscript: SQ. Approved the final version of the manuscript on behalf of all authors: SQ. Administrative/technical/material support: JPa and YP. Study supervision: SQ. All authors contributed to the article and approved the submitted version.

FUNDING

This study was supported by grants from the Science and Technology Program of Guangdong (2016A020213006, 2017A020215048, and 2017A020215191), the Natural Science Foundation of Guangdong (2016A030310377), the Science and Technology Program of Guangzhou (201707010149), and the President Foundation of Nanfang Hospital, Southern Medical University (2015C018, 2016L002, 2016B006, and 2017Z009). The authors have no other personal financial or institutional interest in any of the drugs, materials, or devices described in this article.

REFERENCES

1. Karavitaki N, Cudlip S, Adams CB, Wass JA. Craniopharyngiomas. *Endocr Rev* (2006) 27(4):371–97. doi: 10.1210/er.2006-0002
2. Wang KC, Kim SK, Choe G, Chi JG, Cho BK. Growth Patterns of Craniopharyngioma in Children: Role of the Diaphragm Sellae and Its Surgical Implication. *Surg Neurol* (2002) 57(1):25–33. doi: 10.1016/s0090-3019(01)00657-7
3. Zada G, Lin N, Ojerholm E, Ramkissoon S, Laws ER. Craniopharyngioma and Other Cystic Epithelial Lesions of the Sellar Region: A Review of Clinical, Imaging, and Histopathological Relationships. *Neurosurg Focus* (2010) 28(4):E4. doi: 10.3171/2010.2.Focus09318
4. Almeida JP, Workewych A, Takami H, Velasquez C, Oswari S, Asha M, et al. Surgical Anatomy Applied to the Resection of Craniopharyngiomas: Anatomic Compartments and Surgical Classifications. *World Neurosurg* (2020) 142:611–25. doi: 10.1016/j.wneu.2020.05.171
5. de Lara D, Ditzel Filho LF, Muto J, Otto BA, Carrau RL, Prevedello DM. Surgical Management of Craniopharyngioma With Third Ventricle Involvement. *Neurosurg Focus* (2013) 34(1 Suppl):Video 5. doi: 10.3171/2013.V1.Focus12330
6. Forbes JA, Ordóñez-Rubiano EG, Tomasiewicz HC, Banu MA, Younus I, Dobri GA, et al. Endonasal Endoscopic Transsphenoidal Resection of Intrinsic Third Ventricular Craniopharyngioma: Surgical Results. *J Neurosurg* (2018) 131:1152–62. doi: 10.3171/2018.5.Jns18198
7. Kassam AB, Gardner PA, Snyderman CH, Carrau RL, Mintz AH, Prevedello DM. Expanded Endonasal Approach, a Fully Endoscopic Transnasal Approach for the Resection of Midline Suprasellar Craniopharyngiomas: A New Classification Based on the Infundibulum. *J Neurosurg* (2008) 108 (4):715–28. doi: 10.3171/jns/2008/108/4/0715
8. Lubuulwa J, Lei T. Pathological and Topographical Classification of Craniopharyngiomas: A Literature Review. *J Neurol Surg Rep* (2016) 77(3):e121–7. doi: 10.1055/s-0036-1588060
9. Morisako H, Goto T, Goto H, Bohoun CA, Tamrakar S, Ohata K. Aggressive Surgery Based on an Anatomical Subclassification of Craniopharyngiomas. *Neurosurg Focus* (2016) 41(6):E10. doi: 10.3171/2016.9.Focus16211
10. Pascual JM, González-Llanos F, Barrios L, Roda JM. Intraventricular Craniopharyngiomas: Topographical Classification and Surgical Approach Selection Based on an Extensive Overview. *Acta Neurochir* (2004) 146(8):785–802. doi: 10.1007/s00701-004-0295-3
11. Pascual JM, Prieto R, Carrasco R. Infundibulo-Tuberal or Not Strictly Intraventricular Craniopharyngioma: Evidence for a Major Topographical Category. *Acta Neurochir* (2011) 153(12):2403–25; discussion 26. doi: 10.1007/s00701-011-1149-4
12. Prieto R, Pascual JM, Hofecker V, Winter E, Castro-Dufourny I, Carrasco R, et al. Craniopharyngioma Adherence: A Reappraisal of the Evidence. *Neurosurg Rev* (2020) 43(2):453–72. doi: 10.1007/s10143-018-1010-9
13. Yaşargil MG, Curcic M, Kis M, Siegenthaler G, Teddy PJ, Roth P. Total Removal of Craniopharyngiomas. Approaches and Long-Term Results in 144 Patients. *J Neurosurg* (1990) 73(1):3–11. doi: 10.3171/jns.1990.73.1.0003
14. Yu T, Sun X, Ren X, Cui X, Wang J, Lin S. Intraventricular Craniopharyngiomas: Surgical Management and Outcome Analyses in 24 Cases. *World Neurosurg* (2014) 82(6):1209–15. doi: 10.1016/j.wneu.2014.06.015
15. Pascual JM, Carrasco R, Prieto R, Gonzalez-Llanos F, Alvarez F, Roda JM. Craniopharyngioma Classification. *J Neurosurg* (2008) 109(6):1180–2; author reply 2-3. doi: 10.3171/jns.2008.109.12.1180
16. Pascual JM, Prieto R, Navas M, Carrasco R. Conquest of Third Ventricle Craniopharyngiomas. *J Neurosurg* (2010) 112(5):1156–61; author reply 61. doi: 10.3171/2009.8.Jns091094
17. de Divitiis E, Cappabianca P, Cavallo LM, Esposito F, de Divitiis O, Messina A. Extended Endoscopic Transsphenoidal Approach for Extrasellar Craniopharyngiomas. *Neurosurgery* (2007) 61(5 Suppl 2):219–27. doi: 10.1227/01.neu.0000303220.55393.73
18. Kubota T, Yamamoto S, Kohno H, Ito H, Hayashi M. Operative Procedures of Craniopharyngioma Estimated by Autopsy Findings (Author's Transl). *Neurol Med Chir* (1980) 20(4):341–54. doi: 10.2176/nmc.20.341
19. Gardner PA, Prevedello DM, Kassam AB, Snyderman CH, Carrau RL, Mintz AH. The Evolution of the Endonasal Approach for Craniopharyngiomas. *J Neurosurg* (2008) 108(5):1043–7. doi: 10.3171/jns/2008/108/5/1043
20. Laufer I, Anand VK, Schwartz TH. Endoscopic, Endonasal Extended Transsphenoidal, Transplanum Transtuberculum Approach for Resection of Suprasellar Lesions. *J Neurosurg* (2007) 106(3):400–6. doi: 10.3171/jns.2007.106.3.400
21. Fan J, Liu Y, Pan J, Peng Y, Peng J, Bao Y, et al. Endoscopic Endonasal *Versus* Transcranial Surgery for Primary Resection of Craniopharyngiomas Based on a New QST Classification System: A Comparative Series of 315 Patients. *J Neurosurg* (2021) 135:1298–309. doi: 10.3171/2020.7.Jns20257
22. Liu Y, Qi ST, Wang CH, Pan J, Fan J, Peng JX, et al. Pathological Relationship Between Adamantinomatous Craniopharyngioma and Adjacent Structures

Based on QST Classification. *J Neuropathol Exp Neurol* (2018) 77(11):1017–23. doi: 10.1093/jnen/nly083
23. Qi S, Liu Y, Wang C, Fan J, Pan J, Zhang X, et al. Membrane Structures Between Craniopharyngioma and the Third Ventricle Floor Based on the QST Classification and Its Significance: A Pathological Study. *J Neuropathol Exp Neurol* (2020) 79(9):966–74. doi: 10.1093/jnen/nlaa087
24. Prieto R, Pascual JM, Barrios L. Harvey Cushing's Craniopharyngioma Treatment: Part 2. Surgical Strategies and Results of His Pioneering Series. *J Neurosurg* (2018) 131(3):964–78. doi: 10.3171/2018.5.Jns18154
25. Steno J. Microsurgical Topography of Craniopharyngiomas. *Acta Neurochir Supplementum* (1985) 35:94–100. doi: 10.1007/978-3-7091-8813-2_16
26. Pascual JM, Prieto R, Carrasco R, Barrios L. Displacement of Mammillary Bodies by Craniopharyngiomas Involving the Third Ventricle: Surgical-MRI Correlation and Use in Topographical Diagnosis. *J Neurosurg* (2013) 119 (2):381–405. doi: 10.3171/2013.1.Jns111722
27. Sweet WH. Radical Surgical Treatment of Craniopharyngioma. *Clin Neurosurg* (1976) 23:52–79. doi: 10.1093/neurosurgery/23.cn_suppl_1.52
28. Kobayashi T, Kageyama N, Yoshida J, Shibuya N, Yonezawa T. Pathological and Clinical Basis of the Indications for Treatment of Craniopharyngiomas. *Neurol Med Chir* (1981) 21(1):39–47. doi: 10.2176/nmc.21.39
29. Northfield DW. Rathke-Pouch Tumours. *Brain: J Neurol* (1957) 80(3):293–312. doi: 10.1093/brain/80.3.293
30. Qi S, Lu Y, Pan J, Zhang X, Long H, Fan J. Anatomic Relations of the Arachnoidea Around the Pituitary Stalk: Relevance for Surgical Removal of Craniopharyngiomas. *Acta Neurochir* (2011) 153(4):785–96. doi: 10.1007/s00701-010-0940-y
31. Erdheim J. Über Hypophysengangsgeschwulste Und Hirmcholesteatome. *Sitzungsb Kais Akad Wissen Math Naturw Klin* (1904) 113:537–726.
32. Pascual JM, Prieto R, Rosdolsky M, Strauss S, Castro-Dufourny I, Hofecker V, et al. Cystic Tumors of the Pituitary Infundibulum: Seminal Autopsy Specimens (1899 to 1904) That Allowed Clinical-Pathological Craniopharyngioma Characterization. *Pituitary* (2018) 21(4):393–405. doi: 10.1007/s11102-018-0889-z
33. Attwell W. The Development of the Hypophysis Cerebri in Man, With Special Reference to the Pars Tuberalis. *Am J Anat* (1926) 37:159–93. doi: 10.1002/aja.1000370107
34. Ciric IS, Cozzens JW. Craniopharyngiomas: Transsphenoidal Method of Approach–for the Virtuoso Only? *Clin Neurosurg* (1980) 27:169–87. doi: 10.1093/neurosurgery/27.CN_suppl_1.169
35. Aguado LI, Schoebitz K, Rodríguez EM. Intercellular Channels in the Pars Tuberalis of the Rat Hypophysis and Their Relationship to the Subarachnoid Space. *Cell Tissue Res* (1981) 218(2):345–54. doi: 10.1007/bf00210349
36. Landolt AM. The Ultrastructure of Craniopharyngioma. *Schweiz Archiv Neurol Neurochir Psychiatr Arch Suisse Neurol Neurochir Psychiatr* (1972) 111(2):313–29.

Conflict of Interest: The authors declare that the research was conducted in the absence of any commercial or financial relationships that could be construed as a potential conflict of interest.

Publisher's Note: All claims expressed in this article are solely those of the authors and do not necessarily represent those of their affiliated organizations, or those of the publisher, the editors and the reviewers. Any product that may be evaluated in this article, or claim that may be made by its manufacturer, is not guaranteed or endorsed by the publisher.

frontiers in Oncology

ORIGINAL RESEARCH
published: 10 January 2022
doi: 10.3389/fonc.2021.733088

Intraoperative Magnetic Resonance Imaging Assisted Endoscopic Endonasal Resection of Clival Chordomas

Beste Gulsuna[1], Burak Karaaslan[1], Memduh Kaymaz[1], Hakan Emmez[1], Emetullah Cindil[2], Muammer Melih Sahin[3] and Emrah Celtikci[1]*

[1] Department of Neurosurgery, Gazi University Faculty of Medicine, Ankara, Turkey, [2] Department of Radiology, Gazi University Faculty of Medicine, Ankara, Turkey, [3] Department of Otorhinolaryngology, Gazi University Faculty of Medicine, Ankara, Turkey

OPEN ACCESS

Edited by:
Lin Kong,
Fudan University, China

Reviewed by:
Tomasz Dziedzic,
Medical University of Warsaw, Poland
Ye Gu,
Fudan University, China

***Correspondence:**
Emrah Celtikci
emrahceltikci@gazi.edu.tr
orcid.org/0000-0001-5733-7542

Specialty section:
This article was submitted to Surgical Oncology, a section of the journal Frontiers in Oncology

Received: 29 June 2021
Accepted: 13 December 2021
Published: 10 January 2022

Citation:
Gulsuna B, Karaaslan B, Kaymaz M, Emmez H, Cindil E, Sahin MM and Celtikci E (2022) Intraoperative Magnetic Resonance Imaging Assisted Endoscopic Endonasal Resection of Clival Chordomas. Front. Oncol. 11:733088. doi: 10.3389/fonc.2021.733088

Background: Cranial base chordomas are typically indolent and usually appear as encapsulated tumors. They slowly grow by infiltrating the bone, along with the lines of least resistance. Due to its relationship with important neurovascular structures, skull base chordoma surgery is challenging.

Objective: The usefulness of intraoperative magnetic resonance imaging (IO-MRI) in achieving the goal of surgery, is evaluated in this study.

Methods: Between March 2018 and March 2020, 42 patients were operated on for resection of skull base chordomas in our institution. All of them were operated on under IO-MRI. Patients were analyzed retrospectively for identifying common residue locations, complications and early post-operative outcomes.

Results: In 22 patients (52,4%) gross total resection was achieved according to the final IO-MRI. In 20 patients (47,6%) complete tumor removal was not possible because of extension to the petrous bone (8 patients), pontocerebellar angle (6 patients), prepontine cistern (4 patients), temporobasal (1 patient), cervical axis (1 patient). In 13 patients, the surgery was continued after the first IO-MRI control was performed, which showed a resectable residual tumor. 7 of these patients achieved total resection according to the second IO-MRI, in the other 6 patients all efforts were made to ensure maximal resection of the tumor as much as possible without morbidity. Repeated IO-MRI helped achieve gross total resection in 7 patients (53.8%).

Conclusions: Our study proves that the use of IO-MRI is a safe method that provides the opportunity to show the degree of resection in skull base chordomas and to evaluate the volume and location of the residual tumor intraoperatively. Hence IO-MRI can improve the life expectancy of patients because it provides an opportunity for both gross total resection and maximal safe resection in cases where total resection is not possible.

Keywords: chordoma, intraoperative magnetic resonance imaging, skull base, IO-MRI, endoscopic

INTRODUCTION

Chordoma is an uncommon, locally aggressive tumor originating from remnants of the primitive notochordal tissue along the cranial-spinal axis, which accounts 1% to 4% of all bone malignancies and constitutes 0.1% to 0.2% of all primary intracranial neoplasms (1–4). Approximately 35% of chordomas occur in the skull base predominantly in the clivus, cavernous sinus, and petrous apex (1, 3, 4). Cranial base chordomas are often indolent lesions because of their typically slow growth pattern (1–3, 5). They progress by infiltrating the low-resistance areas of the bone so cause the local destruction of the anatomic markers (1–3, 5). They may also envelop or compress the dura and other neurovascular structures adjacent to the tumor site, thereby causing brain stem or cranial nerve symptoms (1, 4).

There are various arguments regarding the optimal therapy for skull base chordomas (5–7). In most cases, maximal resection followed by adjuvant radiation therapy for the residual or recurrent tumor is recommended (5, 6, 8). However, due to the rarity of the disease, a standard treatment guideline has not been established yet (4, 5, 7, 9). Also, some studies showed that some tumor biological features, such as histological factors, Ki 67 labeling index, chromosomal abnormalities may affect survival (10, 11). Chordomas show varying degrees of radioresistance and a tendency to recurrence, so total tumor resection prolongs progression-free survival (1, 4–8, 10).

The development of intraoperative imaging and physiological monitoring methods in the last two decades has both supported the understanding of surgical anatomy and contributed to the safe removal of even the most complicated skull base lesions by surgeons (12). Surgical navigation systems based on preoperative imaging methods have been developed and are used in current practice, but the accuracy rate of these systems decreases significantly with surgical intervention, tumor resection, and CSF drainage (12, 13).

Intraoperative imaging methods are very useful and effective in the surgery of skull base lesions, due to the complex anatomical structure of this region, the destruction of some landmarks by the lesion, and the loss of three-dimensional relationship with important neurovascular structures (12, 14). There are a few analyses involving small patient groups for the value of IO-MRI in resection of skull base chordoma (4, 15). In this article, the usefulness of IO-MRI in achieving the goal of surgery is discussed. We present our experience with 42 patients with skull base chordomas, which is the first case series of skull base chordomas operated with a fully endonasal endoscopic approach combined with neuronavigation system and under IO-MRI reported in the literature.

MATERIALS AND METHODS

The study and usage of IO-MRI was approved by the Gazi University Clinical Research Ethics Committee with the approval number 2020-596. All patients were informed about the technique and gave their signed consent to IO-MRI during tumor resection and to the data being used for research purposes.

We performed a retrospective analysis of patients operated on for resection of skull base chordomas from March 2018 to March 2020. Admission and discharge notes, hospital records, surgery notes, preoperative radiological imaging, IO-MRI and follow-up control imaging were used as data sources. The patient population, preoperative clinical features, radiologic images, tumor extension, intraoperative images, location of the residual tumor, and postoperative complications were analyzed.

Before surgery, all patients were evaluated radiographically, MRI with and without contrast, tumor relation with the critical neurovascular structures is defined. High-resolution computed tomography (CT) with bone window was performed in all patients to evaluate the bony structures and extent of bone invasion.

All surgeries were performed under general anesthesia with orotracheal intubation. After the intubation, the patient was placed in the lateral decubitus position, the iliac crest was palpated to estimate the position of the L4-5 interspace. After a 14-gauge Tuohy needle was inserted at the midline through the interspinous space to the thecal sac, a drainage catheter was placed. Following the catheterization, the patient has placed supine position and the neuronavigation system (StealthStation® Medtronic® Inc, Minneapolis, USA) was set up. Rigid endoscopes (Karl Storz Endoskope®, Tuttlingen, Germany) 4 mm diameter, 18 cm length, and equipped with 0°, 30°, 45°, and 70° lenses, according to the different steps of the surgery, were used.

For use at closure, the Hadad-Bassagasteguy flap which is a pedicled nasoseptal flap that is vascularized by the sphenopalatine artery was prepared. This flap is temporarily stored by placing it anteriorly towards the nasopharynx or maxillary sinus depending on the surgical area in order not to obscure the surgical field and to protect its vascular supply during surgery. Each step was performed for all of the patients and all surgeries were performed fully endonasal endoscopic.

During each surgical procedure, we used a micro doppler to identify the internal carotid artery. CSF drainage *via* lumbar drainage catheter was applied when dural damage and CSF leakage were detected. We kept the lumbar drainage catheter for 48 hours in order to provide postoperative csf drainage in patients with intraoperative csf leakage. Finally, we went to the IO-MRI unit (3T, MagnetomVida®, Siemens Healthineers, Erlangen, Germany) to evaluate the surgical resection rate and the presence of the residual tumor.

3-Tesla IO-MRI System

Our 3T MRI site is built next to the operating theatre and end of the operating room corridor that is dedicated to neurosurgical operations. The magnet room interconnects with the operating room corridor by a door RF-shielded. Our system differs from the twin room concept but the contribution of this system to us is that patients in each operating room can go to the IO-MRI unit when the neurosurgeon needs, rather than only accessing the one patient in a single operating room. Also, our 3T IO-MRI unit was designed both to be used intraoperatively and in outpatient

Abbreviations: IO-MRI, intraoperative magnetic resonance imaging; MRI, magnetic resonance imaging; CT, computed tomography; CSF, cerebrospinal fluid.

clinics. The design of our MR unit gives us the possibility to decrease the cost of the system, as it allows us to use standard surgical equipment.

When the surgeon needs it, the IO-MRI room is properly disinfected and the door of the magnet room and operating room is opened, and the patient is transported to the IO-MRI unit with an MRI compatible stretcher in less than 3 minutes. When the patient is taken to the IO-MRI unit, the anesthesia team monitors the patient and provides the connection with the fixed MRI compatible anesthesia unit in this room. The transport of the patient, the analysis of the images, and the decision-making process take approximately 15 minutes in total. If we decide to continue surgery, the examination procedure is repeated.

Statistical Methods

For statistical analysis, odds ratio and significance level were calculated with Medcalc software (version 7; Medcalc Software, Mariakerke, Belgium) to evaluate and compare clinical outcome and disease recurrence between groups.

RESULTS

Between March 2018 and March 2020, 42 patients were operated on for resection of skull base chordomas in our institution and all of them were operated on under IO-MRI. Patients were analyzed retrospectively for the disease recurrence and complications.

Four patients have previous surgery, and none of the patients had received radiation previously. 22 patients were male, and 20 were female (male/female ratio of 1.1:1). The age ranged from 23 to 79 years (mean, 45,6 years). The average follow-up was 22.5 ± 2.4 months (range, 10-36 months). 27 patients presented with headache; 11 with cranial nerve deficit; 2 with hemiparesis; 2 with visual field narrowing. When we examined the reason why most of the patients applied with headache complaints, we found that most of them developed these complaints secondary to underlying causes such as dizziness, drowsiness, blurred vision, nasal obstruction, and nasopharyngeal fullness.

The aim of chordoma surgery is that maximum safe resection of the tumor. Radical surgical resection, defined as no residual tumor with evaluating the final IO-MRI. In 22 patients (52,4%) gross total resection was achieved according to the final IO-MRI. The presence of any residual tumor was defined as subtotal resection and it was achieved in 20 patients (47,6%). In these patients, complete tumor removal was not possible because of extension in the petrous bone (8 patients), pontocerebellar angle (6 patients), prepontine cistern (4 patients), temporobasal (1 patient), cervical axis (1 patient) (**Figure 1**).

In this case series, the first intraoperative exam demonstrated gross total removal in 15 patients. Other 27 patients demonstrate residual tumor but 14 of these patients' operations terminated due to achieving the targeted resection rate and proximity of residual lesion with vital neurovascular structures. Residual tumor localizations were prepontine cistern (4 patients), petrous bone (4 patients), pontocerebellar angle (4 patients), temporo basal (1 patient), and cervical axis (1 patient). C1 body and odontoid process invasion were seen in this patient and it was evaluated as cervical axis invasion (**Figure 2**).

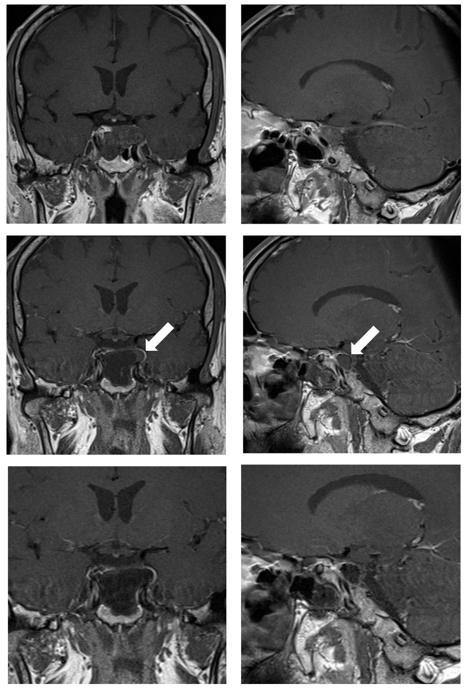

FIGURE 1 | Case sample 1, a mass is detected after the 6th cranial nerve paralysis on the left. Upper row: Preoperative coronal and sagittal contrast-enhanced T1 weighted MRI demonstrates a chordoma that invades the left cavernous sinus and passes lateral to the internal carotid artery. Middle row: Contrast-enhanced T1 weighted IO-MRI slices, the white arrow indicating residual tumor superior to the cavernous sinus. Bottom row: Final contrast-enhanced T1 weighted IO-MRI slices demonstrate gross total surgical resection.

In 13 patients surgical intervention was continued due to the demonstration of resectable remnants which were located in petrous bone (6 patients), cavernous sinus (5 patients), and pontocerebellar angle (2 patients). A second intraoperative exam in 7 of these patients revealed total tumor excision (**Figure 3**). The remnants of these patients were located in cavernous sinus (5 patients) and petrous bone (2 patients). In the remaining 6 patients, the surgery was terminated despite the presence of residual tumor to avoid additional morbidity. These patients' remnant localization was petrous bone (4 patients) and pontocerebellar angle (2 patients).

Tumor progression was determined in 2 of the patients who achieved radical surgical resection and 17 of the patients who couldn't achieve radical surgical resection (**Table 1**). In the postoperative period, 2 patients have developed rhinorrhea and one of them has evolved morbidity after meningitis seconder to the rhinorrhea. Both of the patients who developed rhinorrhea were operated on. And 2 patients underwent ventriculoperitoneal shunt surgery. Communicating hydrocephalus developed in 1 patient in the postoperative period. In other patient, the tumor that filled the prepontine cistern was totally resected, and in the postoperative

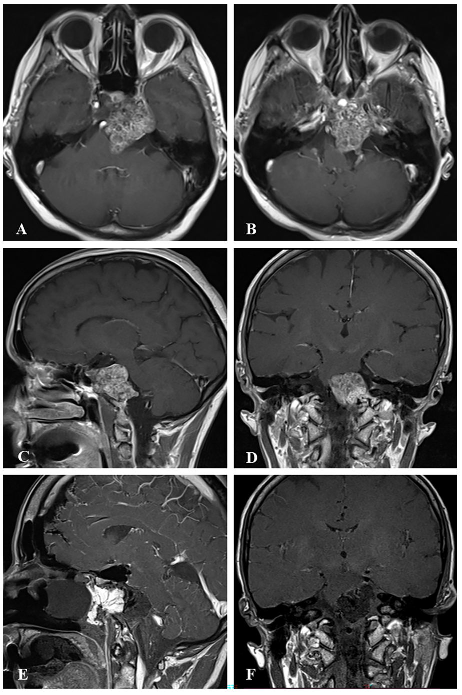

FIGURE 2 | Case sample 2, the patient presenting with headache, diplopia, and reduced sensation of the left side of the face. **(A, B)** Preoperative axial contrast-enhanced T1 weighted MRI shows a tumor invading the left cavernous sinus and compressing the brainstem. **(C)** Preoperative sagittal contrast-enhanced T1 weighted MRI shows a tumor invading the lower clivus and upper cervical spine. **(D)** Preoperative coronal contrast-enhanced T1 weighted MRI shows the tumor relation to the internal acoustic canal and brainstem. **(E)** Final contrast-enhanced T1 weighted IO-MRI demonstrates residual tumor located at the lower clivus and upper cervical spine. This IO-MRI slice also demonstrates the fat graft and nasal package closure. **(F)** Final contrast-enhanced T1 weighted IO-MRI demonstrates tumor resection.

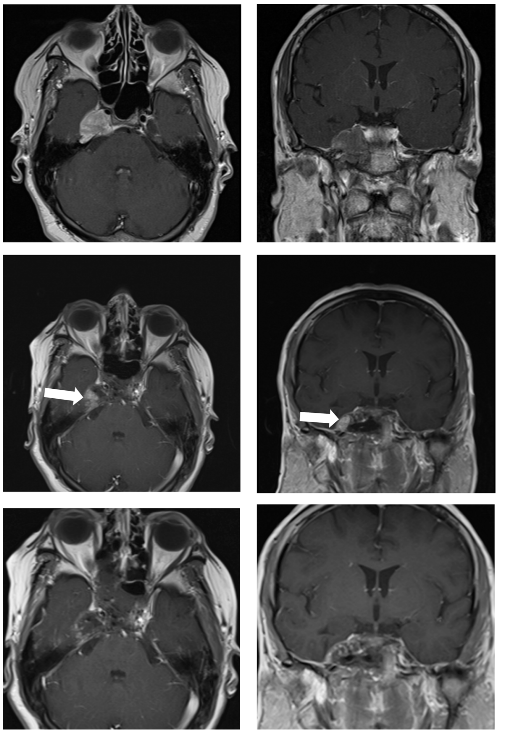

FIGURE 3 | Case sample 3, the patient presenting cranial nerve deficit because of the tumor which invades the right cavernous sinus. Upper row: Preoperative axial and coronal contrast-enhanced T1 weighted MRI shows a tumor invading the right cavernous sinus. Middle row: First contrast-enhanced T1 weighted IO-MRI demonstrates residual tumor located at the inferolateral cavernous sinus. Bottom row: Final contrast-enhanced T1 weighted IO-MRI slices demonstrate gross total surgical resection.

period, the patient has been developed hydrocephalus, and shunt surgery was applied (**Figure 4**).

Our findings support today's knowledge about chordoma; the most important factor for preventing recurrence is total surgical resection. However, what we want to emphasize in this article is the contribution of IO-MRI at this point.

DISCUSSION

In this study, 42 chordoma patients underwent IO-MRI, 27 patients were found to have residual tumors, and 13 of these patients were evaluated as resectable which was located mostly petrous bone (6 patients), cavernous sinus (5 patients), and pontocerebellar angle (2 patients). Repeated IO-MRI helped achieve gross total resection in 7 of these patients (53.8%) whose tumor was located in the cavernous sinus (5 patients) and petrous bone (2 patients) (**Table 2**).

Total tumor resection has been shown to be the most important factor in progression-free survival and overall survival in skull base chordomas (4–8, 16). Controversy over aggressive tumor resection in skull base chordomas arises from the tumor's relationship to critical neurovascular structures and that total resection often results in significant morbidity (2, 7, 8). Tumor diameter and aggressive growth pattern, previous surgery and radiation therapy have been found to be associated with postoperative morbidity rates (7, 8, 17, 18). Although modern skull base techniques implemented in experienced centers have reduced the mortality and morbidity associated with chordoma resection, chordomas are considered to be tumors that cannot be curable surgically (2, 4–6, 17).

The aim of surgery in tumors that are not suitable for total resection is to decompress critical neurovascular structures, reduce the tumor burden, and establish a pathological diagnosis (4, 6, 11, 16). Thus, adjuvant radiotherapy can be made safer by creating a suitable space between the tumor and radiosensitive structures such as the brain stem and optic nerve (7, 8, 18). In cases of residual tumors or recurrence after surgical treatment, radiation therapy modalities are used in the treatment management, and the radiotherapy response depends on the tumor volume, the radiation dose administered, as well as the biomolecular characteristics of the tumor (2, 7, 8, 10, 11).

Fixed anatomic landmarks play an important role for skull base chordoma surgery because surgeons ensure anatomic

TABLE 1 | Number of relapses in patients with and without total resection.

	Total resection	Subtotal resection	Total number of patient
Recurrence	2	17	19
Progression free	18	5	23
Total number of patient	20	22	42

Odds ratio 30,6000/z statistic 3,791/Significance level P = 0,0002.

orientation and estimation of the degree of resection and the adequacy of neural decompression based on these landmarks (3, 16). However, chordomas tend to destroy surgical landmarks, especially by infiltrating bone structures due to their nature (8, 19). Despite various technical advances, tumor spread and destruction of anatomical landmarks making skull base chordoma surgery are challenging (19–21). In these complex and destructive lesions, direct visual assessment with an operative endoscope may not be sufficient to estimate the residual tumor volume and confirm the completeness of the resection (20, 21). In addition, when large-volume resections are made, it becomes difficult for the surgeon to judge due to the large cavity that occurs (21, 22). At the same time, since the tumor is debulked starting from the center, the reliability of navigation is impaired when the cavity collapses or CSF leakage occurs (4, 9, 14, 22).

IO-MRI is an important tool that can provide real-time feedback on resection grade, residual tumor volume, localization and adequacy of neural decompression (4, 7, 14, 15). The decompression mentioned here is the elimination of tumoral compression, as compression-related changes in neural structures are not expected to disappear immediately in early imaging. Also, IO-MRI can be transferred to the neuronavigation system, making it a useful tool when continuing surgery for residual tumor (15). The main purpose of using IO-MRI in skull base chordoma surgery is to provide a reliable anatomic directive for maximum safe tumor resection with minimum surgical morbidity and mortality (14, 15). Even if IO-MRI does not lead to total resection, it is an important tool to assist the surgeon in preventing neurological comorbidity and making the decision to leave residual tumor (13, 14, 22).

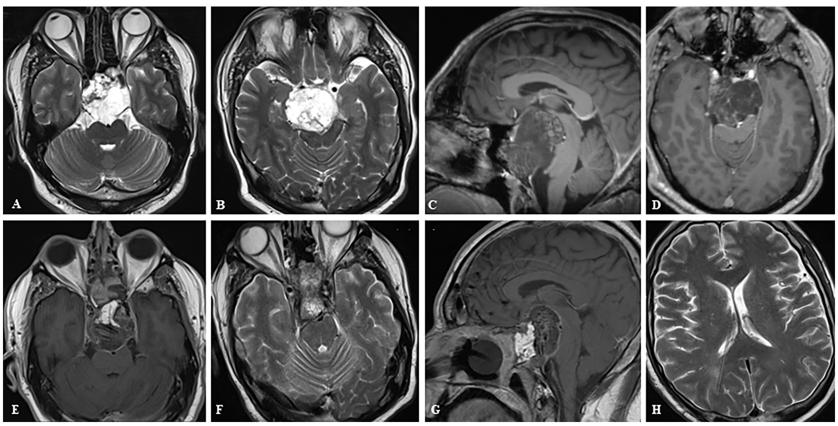

FIGURE 4 | Case sample 4, the patient presenting with headache and impaired cognitive functions. **(A, B)** Preoperative axial T2 weighted MRI shows a huge tumor that extremely compresses the brainstem. **(C, D)** Preoperative sagittal and axial contrast-enhanced T1 weighted MRI shows tumor relation to neurovascular structures. **(E–G)** Final contrast-enhanced T1 weighted IO-MRI shows the gross total tumor resection and also our nasal closure procedure. **(F, G)** The patient developed hydrocephalus in the postoperative period and a ventriculoperitoneal shunt was placed, and these axial T2 weighted MRI images were taken before the patient was discharged after an intensive care period of approximately 3 months **(H)**.

TABLE 2 | Distribution of the patients according to IO-MRI findings.

	IO-MRI/1	IO-MRI/2
Gross total resection	15 patients	7 patients
Subtotal resection (with residue locations)	27 patients *14 patients operation terminated • 4 prepontine cistern • 4 petrous bone • 1 temporobasal • 1 cervical axis *13 patients operation continued • 6 petrous bone • 5 cavernous sinus • 2 pontocerebellar angle	6 patients • 4 petrous bone • 2 pontocerebellar angle

Our study shows that the IO-MRI complements the operative endoscope, thus helping to maximize the degree of resection which is the most important parameter that affects survival.

Limitations

Since all of our case series consisted of patients operated under IO-MRI, we do not have a control group for skull base chordoma that did not go to IO-MRI. Also, we have limitations in evaluating progression-free survival and tumor recurrence rates since our patient follow-up period is relatively short.

CONCLUSIONS

Our study proves that the use of IO-MRI is a safe method that provides the opportunity to show the degree of resection in skull base chordomas and to evaluate the volume and location of the residual tumor intraoperatively. Hence IO-MRI can improve the life expectancy of patients because it provides an opportunity for both gross total resection and maximal safe resection in cases where total resection is not possible. Also, it makes important contributions in evaluating the adequacy of decompression of neural structures, especially the brainstem which is particularly associated with improvement of clinical status. Another important contribution of IO-MRI is that it enables the evaluation of the relation with residual tumor tissue and radiosensitive neural structures for possible radiation treatments in patients in whom gross total resection is not possible.

DATA AVAILABILITY STATEMENT

The raw data supporting the conclusions of this article will be made available by the authors, without undue reservation.

ETHICS STATEMENT

This study was reviewed and approved by Clinical Research Ethics Committee at the Gazi University, School of Medicine, Ankara, Turkey. The patients/participants provided their written informed consent to participate in this study.

AUTHOR CONTRIBUTIONS

BG, ECe, and ECi contributed to conception and design of the study. ECe organized the database. BG performed the statistical analysis. All surgeries were performed by MS and ECe. BG wrote the first draft of the manuscript. MK, HE, and BK wrote sections of the manuscript. All authors contributed to manuscript revision, read, and approved the submitted version.

REFERENCES

1. Chambers KJ, Lin DT, Meier J, Remenschneider A, Herr M, Gray ST. Incidence and Survival Patterns of Cranial Chordoma in the United States. *Laryngoscope* (2014) 124(5):1097–102. doi: 10.1002/lary.24420
2. Samii A, Gerganov VM, Herold C, Hayashi N, Naka T, Mirzayan MJ, et al. Chordomas of the Skull Base: Surgical Management and Outcome. *J Neurosurg* (2007) 107(2):319–24. doi: 10.3171/JNS-07/08/0319
3. Almefty K, Pravdenkova S, Colli BO, Al-Mefty O, Gokden M. Chordoma and Chondrosarcoma: Similar, But Quite Different, Skull Base Tumors. *Cancer* (2007) 110(11):2467–77. doi: 10.1002/cncr.23073
4. Metwali H, Samii A, Gerganov V, Giordano M, Fahlbusch R, Samii M. The Significance of Intraoperative Magnetic Resonance Imaging in Resection of Skull Base Chordomas. *World Neurosurg* (2019) 128:e185–94. doi: 10.1016/j.wneu.2019.04.086
5. di Maio S, Temkin N, Ramanathan D, Sekhar LN. Current Comprehensive Management of Cranial Base Chordomas: 10-Year Meta-Analysis of Observational Studies: Clinical Article. *J Neurosurg* (2011) 115(6):1094–105. doi: 10.3171/2011.7.JNS11355
6. Ceylan S, Emengen A, Caklili M, Ergen A, Yılmaz E, Uzuner A, et al. Operative Nuances and Surgical Limits of the Endoscopic Approach to Clival Chordomas and Chondrosarcomas: A Single-Center Experience of 72 Patients. *Clin Neurol Neurosurg* (2021) 208:1–9. doi: 10.1016/j.clineuro.2021.106875
7. Bai J, Li M, Shi J, Jing L, Zhai Y, Zhang S, et al. Mid-Term Follow-Up Surgical Results in 284 Cases of Clival Chordomas: The Risk Factors for Outcome and Tumor Recurrence. *Neurosurg Rev* (2021) 44:1–12. doi: 10.1007/s10143-021-01576-4. Published online.
8. Bai J, Li M, Xiong Y, Shen Y, Liu C, Zhao P, et al. Endoscopic Endonasal Surgical Strategy for Skull Base Chordomas Based on Tumor Growth Directions: Surgical Outcomes of 167 Patients During 3 Years. *Front Oncol* (2021) 11:724972. doi: 10.3389/fonc.2021.724972
9. Giordano M, Samii A, Lawson McLean AC, Bertalanffy H, Fahlbusch R, Samii M, et al. Intraoperative Magnetic Resonance Imaging in Pediatric Neurosurgery: Safety and Utility. *J Neurosurg Pediatr* (2017) 19(1):77–84. doi: 10.3171/2016.8.PEDS15708
10. Sen C, Triana AI, Berglind N, Godbold J, Shrivastava RK. Clival Chordomas: Clinical Management, Results, and Complications in 71 Patients Clinical Article. *J Neurosurg* (2010) 113(5):1059–71. doi: 10.3171/2009.9.JNS08596
11. Zenonos GA, Fernandez-Miranda JC, Mukherjee D, Chang YF, Panayidou K, Snyderman CH, et al. Prospective Validation of a Molecular Prognostication Panel for Clival Chordoma. *J Neurosurg* (2019) 130(5):1528–37. doi: 10.3171/2018.3.JNS172321
12. Dort JC, Sutherland GR. Intraoperative Magnetic Resonance Imaging for Skull Base Surgery. *Laryngoscope* (2001) 111(9):1570–5. doi: 10.1097/00005537-200109000-00014
13. Bisdas S, Roder C, Ernemann U, Tatagiba MS. Intraoperative MR Imaging in Neurosurgery. *Clin Neuroradiol* (2015) 25:237–44. doi: 10.1007/s00062-015-0443-6
14. Schwartz TH, Stieg PE, Anand VK. Endoscopic Transsphenoidal Pituitary Surgery With Intraoperative Magnetic Resonance Imaging. *Neurosurgery* (2006) 58(SUPPL. 1):44–51. doi: 10.1227/01.NEU.0000193927.49862.B6
15. Pamir MN, Peker S, Dinçer A. *Intraoperative MR Imaging: Preliminary Results With 3 Tesla MR System*. Ankara, Turkey: Springer-Verlag (2006).
16. Ngu CYV, Tang IP, Ng BHK, Wong ASIIH, Liew DNS. Endoscopic Endonasal Approach in Clival Chordoma Surgery: Case Series. *Indian J Otolaryngol Head Neck Surg* (2021) 73(2):226–32. doi: 10.1007/s12070-021-02455-6
17. Alan O, Akin Telli T, Ercelep O, Tanrikulu Simsek E, Basoglu Tuylu T, Mutis A, et al. Chordoma: A Case Series and Review of the Literature. *J Med Case Rep* (2018) 12(1):1–5. doi: 10.1186/s13256-018-1784-y
18. Ogawa Y, Jokura H, Tominaga T. Midterm Prognosis and Surgical Implication for Clival Chordomas After Extended Transsphenoidal Tumor Removal and Gamma Knife Radiosurgery. *BMC Neurol* (2021) 21(1):1–7. doi: 10.1186/s12883-021-02234-4
19. Zhang HK, Sun XC, Hu L, Wang JJ, Wang DH. Endonasal Endoscopic Resection and Radiotherapy in Skull Base Chordomas. *J Craniofac Surg* (2016) 27(7):E709–13. doi: 10.1097/SCS.0000000000003031
20. Taniguchi M, Kohmura E. Endoscopic Endonasal Removal of Laterally Extended Clival Chordoma Using Side-Viewing Scopes. *Acta Neurochir* (2012) 154(4):627–32. doi: 10.1007/s00701-011-1225-9

21. Theodosopoulos PV, Leach J, Kerr RG, Zimmer LA, Denny AM, Guthikonda B, et al. Maximizing the Extent of Tumor Resection During Transsphenoidal Surgery for Pituitary Macroadenomas: Can Endoscopy Replace Intraoperative Magnetic Resonance Imaging? *J Neurosurg* (2010) 112(4):736–43. doi: 10.3171/2009.6.JNS08916
22. Holzmann D, Reisch R, Krayenbühl N, Hug E, Bernays RL. The Transnasal Transclival Approach for Clivus Chordoma. *Minim Invasive Neurosurg* (2010) 53(5-6):211–7. doi: 10.1055/s-0030-1267929

Conflict of Interest: The authors declare that the research was conducted in the absence of any commercial or financial relationships that could be construed as a potential conflict of interest.

Advantages of publishing in Frontiers

OPEN ACCESS
Articles are free to read for greatest visibility and readership

FAST PUBLICATION
Around 90 days from submission to decision

HIGH QUALITY PEER-REVIEW
Rigorous, collaborative, and constructive peer-review

TRANSPARENT PEER-REVIEW
Editors and reviewers acknowledged by name on published articles

Frontiers
Avenue du Tribunal-Fédéral 34
1005 Lausanne | Switzerland

Visit us: www.frontiersin.org
Contact us: frontiersin.org/about/contact

REPRODUCIBILITY OF RESEARCH
Support open data and methods to enhance research reproducibility

DIGITAL PUBLISHING
Articles designed for optimal readership across devices

FOLLOW US
@frontiersin

IMPACT METRICS
Advanced article metrics track visibility across digital media

EXTENSIVE PROMOTION
Marketing and promotion of impactful research

LOOP RESEARCH NETWORK
Our network increases your article's readership